Variability and Trend in Alberta Climate and Streamflow with a Focus on the North Saskatchewan River Basin

2011-12 Final Report
Water Theme, Prairies RAC
31 March 2012

Dave Sauchyn, Jeannine St. Jacques, Elaine Barrow, Suzan Lapp, Cesar Perez Valdivia and Jessica Vanstone
Prairie Adaptation Research Collaborative (PARC), University of Regina

The North Saskatchewan River above Lake Abraham (Source: D.J. Sauchyn)

TABLE OF CONTENTS

TABLES

FIGURES

Introduction

This report documents the results of technical work conducted at the Prairie Adaptation Research Collaborative (PARC) from April 2011 to March 2012 under the Water Theme of the Prairies Regional Adaptation Collaborative (RAC). The Prairies RAC is a three-year federal-provincial program to advance adaptation to climate change. Water is one of the three major themes of the Prairie RAC and it is a significant component of the other two themes: Drought and Excess Moisture, and Terrestrial Ecosystems.

A shift in the distribution of water resources between seasons, years and watersheds is the major risk from climate change in the Prairies region (Sauchyn and Kulshreshtha, 2008). Adaptation to avoid or reduce adverse impacts on communities, economies, and managed ecosystems requires knowledge of past and future trends and variability in surface and soil water balances. Nearly all of the existing information on future climate and water supplies is in the form of change scenarios, that is, the expected shift in mean conditions from the recent past (usually 1961-90) to a future 30-year period, typically 2040-69. The major challenge from climate change in our region is not a shift in average conditions but rather a change in the frequency and severity of climate extremes and departures from average conditions; in particular, excessive moisture and drought. Without a knowledge of the future tendencies in the distribution of water among years, decades and watersheds, most decision makers will have limited technical capacity to address adaptive management practices and appropriate policy for planned adaptation to climate change.

The work reported in this report is the culmination of a three-year technical investigation of the climate and hydrology (hydroclimate) of the Prairie Provinces based on the statistical analysis of instrumental, proxy and climate model data. The geographic focus has been primarily, although not exclusively, Alberta river basins and gauges. The focus in Year 3 (April 2011 to March 2012) was the North Saskatchewan River Basin (NSRB), although to provide a broader context much of the analysis extended into adjacent river basins and, in come cases, across the Prairie Provinces. The climate forcing of hydrologic

systems is large scale and thus an understanding of trends and variability must extend over large areas, among river basins, and over long time frames including the pre-instrumental hydroclimate. The technical details of these analyses, and the results obtained over a larger area than the NSRB, are given in series of papers appended in Appendices B to F.

In the following section of this report, we summarize the results our analysis of climate and streamflow for the NSRB. Increasing reliance on water from the North Saskatchewan River assumes a certain reliability of the source: mostly snowmelt runoff from the eastern slopes of the Rocky Mountains (Figure 1). Beyond the mountains, the main tributary is the Battle River, which originates in aspen parkland in west-central Alberta. In March and April snowmelt in the parkland and prairie produces an initial rise in the annual hydrograph. The major peak is from mountain snowmelt in July. While the net effect of glacier meltwater runoff on the annual flow of the North Saskatchewan River is small, it does sustain higher river levels in late summer and fall and during drought conditions. Most of the allocation from the North Saskatchewan River (NSR) is for industrial (83%) and municipal (8%) use (North Saskatchewan Watershed Alliance, 2007). The petroleum sector, which currently is allocated about 5% of the water from the NSR, is projected to account for most of the increase in withdrawals over the next 20 years largely for the processing heavy oil at a series of new or expanded facilities in the Edmonton Industrial Heartland. This water use could be as high as about 10 times the current allocation for the city of Edmonton.

Figure 1: The NSRB in Alberta; the sub-basins are identified (Source: NSWA, 2005)

Trends and Variability in Observed and Reconstructed Streamflow

Water level gauges are the principal source of data for our analysis of hydroclimatic variability. Streamflow and lake levels integrate the effective precipitation across a watershed and over days to months. There is a relatively dense network of water level gauges in the southern Prairies since precipitation and the raw surface water supply is a limiting factor for agriculture and most other economic activities. This network was originally established in the early 20th century not for the scientific study of hydrology or climate, but rather to identify supplies of water initially for steam locomotives and irrigation (Greg McCullough, Water Survey of Canada, personal communication, June 2011). Therefore just a few gauges have operated continuously for more than 50 years. Fortunately some of these long records are from Alberta gauges including the North Saskatchewan River (NSR) at Edmonton (Figure 2).

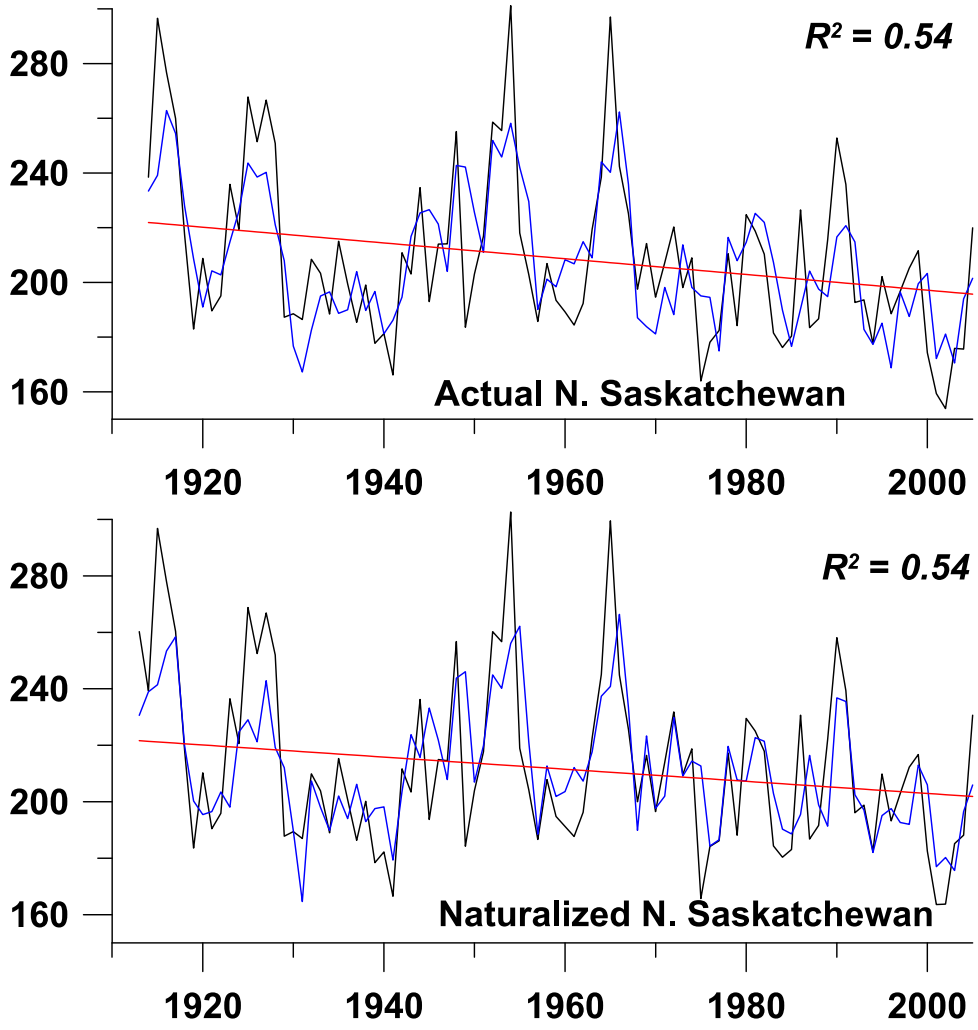

Figure 2: The recorded (top) and naturalized (bottom) annual flow (black curve) of the North Saskatchewan River at Edmonton, 1912-2007 (Source: Alberta Environment). A regression model (blue curve) based on natural drivers (PDO, ENSO, NAO) of hydroclimatic variability captures 54% of the variability of the flow (St Jacques, et al., 2010). In addition to this inter-annual to inter-decadal variability there is significant declining trend over the length of the record as shown with solid red line.

Another constraint on the use of stream gauge data for climate studies is the widespread regulation of river flow, specifically the diversion and storage of surface water for irrigation and flood control. Fortunately Alberta Environment has a program to produce naturalized streamflow records; we have made extensive use of this database. In Figure 3, naturalized annual and March flow is plotted for the Battle River, the major prairie/parkland tributary of the NSR (Figure 1). These flows were computed at the provincial boundary for the period 1912-2009 (Source: Alberta Environment). The best

(least squares) linear fits indicate no trend in annual flow, but significantly increasing flow in March (according to a Mann Kendall test). The latter trend is consistent with well-documented increases in spring flow in snow-dominated watersheds; as the climate warms, snowmelt runoff begins and peaks earlier in the year.

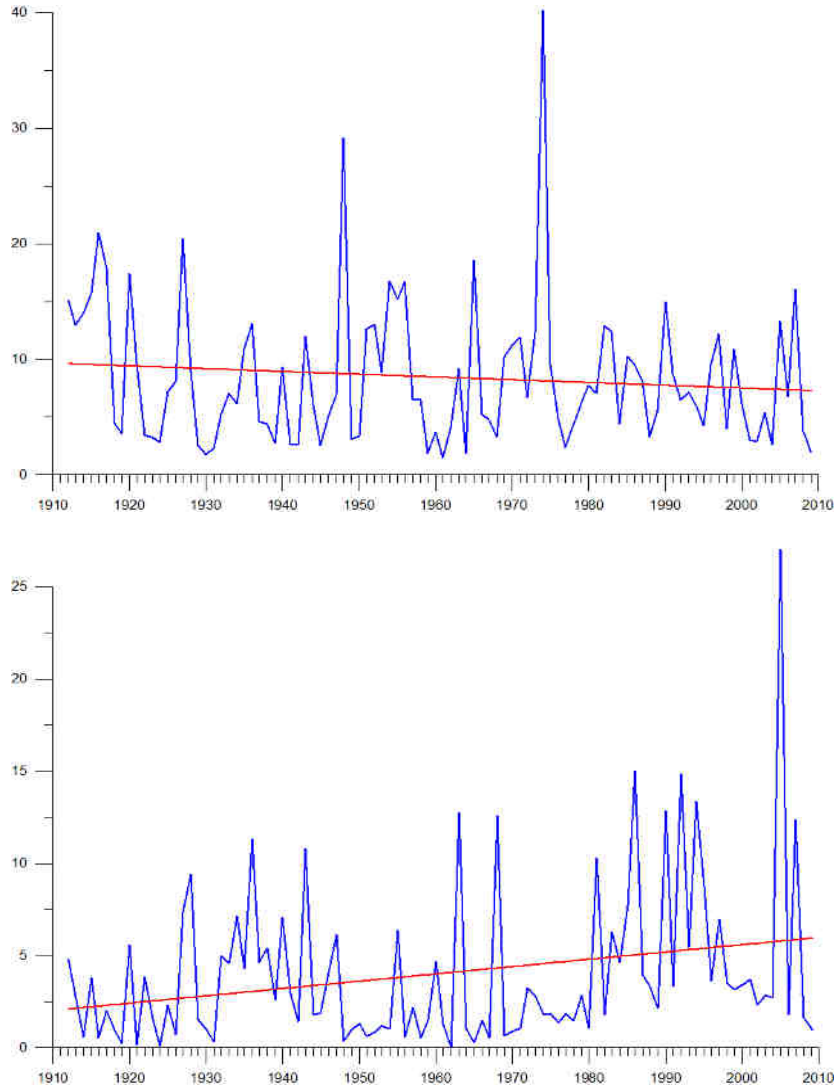

Figure 3: Naturalized Annual (top) and March Flow (m^3/sec), Battle River at the provincial border, 1912-2009 (Source: Alberta Environment). The best linear fit (least squares) indicates no trend in annual flow, but significantly increasing flow in March.

Various studies have concluded that surface water levels have declined in Alberta over the past several decades. Some of these studies, however, have not used the most robust methods of trend detection; transient trends can be an artifact of short record length and

low-frequency variability. We analyzed trends and variability in the observed and naturalized flow of the major streams in southern and central Alberta (St Jacques, et al., 2010). A Generalized Least Squares (GLS) regression model was derived for each gauge using, as predictors, trend plus natural large-scale climatic drivers of hydroclimatic variability: the Pacific Decadal Oscillation (PDO), El Niño Southern Oscillation (ENSO) and North Atlantic Oscillation (NAO). The results for the North Saskatchewan River at Edmonton are plotted in Figure 2. The black curves are the recorded (top) and naturalized (bottom) annual flow from 1912 to 2007 and the blue curves are the flows predicted by the GLS models. The regression models capture 54% of the variability in both recorded and reconstructed flow. (The two annual hydrographs are not dramatically different at Edmonton; flow regulation upstream consists mostly of seasonal storage of runoff behind two dams.) Also shown as a solid red line are declining trends in recorded and naturalized flow of 0.14% and 0.10% per year, respectively, over the length of the record. The statistical significance of the trend coefficients was tested using the Neyman-Pearson statistic as described in St Jacques, et al. (2010). This decline has been documented previously and attributed to a loss of glacier mass in the upper reaches of the watershed (Demuth and Pietroniro, 2003), resulting in significant declines in mid-summer and autumn flows.

The fact that more than half the variance in annual flow can be modeled primarily on the basis of large-scale climate patterns demonstrates the strong influence of these teleconnections on Alberta's surface water supply, and specifically the inter-annual to inter-decadal variability (Gobena and Gan, 2006; Shabbar and Skinner, 2004; Lapp et al., 2011; St. Jacques, et al., 2012). The lower-frequency variability is clearly evident in the Edmonton gauge record, because it is one of longest in western Canada, approaching 100 years in length. In the entire country, only about 40 continuous hydrometric records exceed 50 years (Greg McCullough, Water Survey of Canada, personal communication, June 2011), which is less than the length of a full multi-decadal climate cycle. Therefore, an understanding of the long-term variability of streamflow requires information about pre-instrumental (paleo) hydrology. Tree-rings are the preferred proxy for the study of annual fluctuations in water levels over past centuries to millennia (Meko and

Woodhouse, 2010). They are the source of both hydroclimatic data and a chronology with absolute annual resolution. Tree rings are an especially good indicator of drought; dry years consistently produce narrow rings. Paleohydrologic data can provide water resource planners and engineers with (Sauchyn *et al.,* 2011; St. George and Sauchyn 2006):

- a historical context for reference hydrology to evaluate baseline conditions and water allocations,
- worst-case scenarios: what is possible in terms of severity of flooding and drought
- long-term probability of hydroclimate conditions exceeding specific thresholds,
- a historical context for scenarios of water supply under climate change,
- a much broader perspective on the variability of water levels to assess the reliability of water supply systems under a wider range of flows than recorded by a gauge, and
- probabilities of simultaneous drought in different river basins.

In recent years, researchers at the University of Regina PARC Tree-Ring Lab (www.parc.ca/urtreelab) have built an extensive network of tree-ring chronologies, extending from the island forests of northeastern Montana and northern North Dakota through the forested regions of Alberta and Saskatchewan and across the southern Northwest Territories. At most of these sites, tree growth is limited by available soil moisture and therefore it is a proxy of summer and annual precipitation, soil moisture and runoff (Sauchyn *et al*., 2003, 2011; Axelson *et al*., 2009; Perez-Valdivia and Sauchyn, 2010). Reconstructions of stream flow are possible because annual tree growth, like stream discharge, captures and integrates a regional moisture signal. Climatic conditions that result in reduced runoff (*i.e*. low precipitation and high evapotranspiration) are expressed in trees as low water potential and suppressed growth. There is a growth response to winter precipitation at sites where spring snowmelt water recharges the soil moisture balance immediately prior to the growing season.

Concurrent with our work on the Water Theme of the Prairies RAC, EPCOR Water Services Inc. and NSERC funded the project ‘Past, Recent and Future Hydroclimate of

the Upper North Saskatchewan River Basin" (Sauchyn, Byrne and Kienzle, 2011). Our investigation of the past hydroclimate of the upper NSRB included a reconstruction of the annual flow of the NSR derived from tree rings from seven sites. At all sites but one (WIP), naturalized summer (JJA) and water year (Oct – Sep) streamflow is significantly correlated with indices of annual (RW), early (EW) and late (LW) tree-ring width (Figure 4). If the watershed is dry (wet), both tree growth and runoff are suppressed (enhanced). Streamflow is most highly correlated with latewood width, since water is most limited late in growing season.

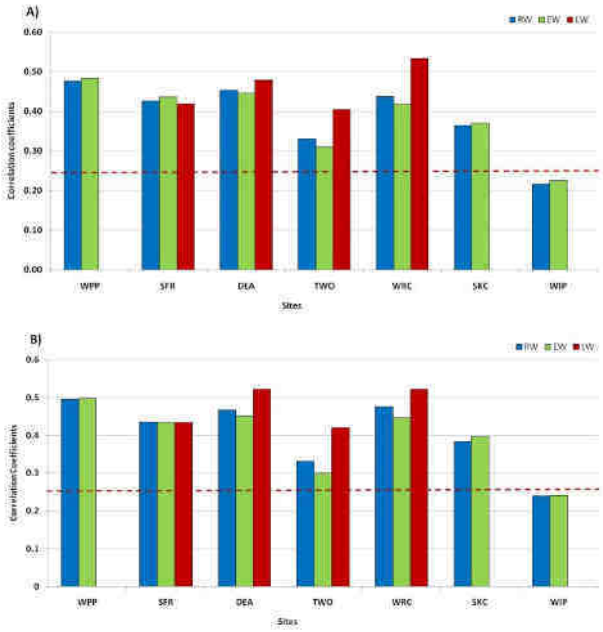

Figure 4: Degree or correlation between naturalized streamflow and indices of annual (RW), early (EW) and late (LW) tree-ring width. Top: water year (Oct – Sep) flow; bottom: summer (JJA) flow. The red dashed lines indicate 95% confidence limits.

To create a tree-ring model of water year streamflow, the data for all the sites (except WIP) was entered in a stepwise linear regression. The correlation between this pool of predictors and annual streamflow was about 0.7 and thus the regression model accounts for approximately 50% (R^2) of the variance in observed streamflow. A plot (Figure 5) of recorded (naturalized) and reconstructed water year flow for the calibration period, 1912-2007, shows that most of the unexplained variance is the underestimation of high flows. Otherwise the tree-rings capture much of the inter-annual to decadal variability in the

gauge record. Using the full length of the tree-ring record, and the optimal tree-ring model, we reconstructed the water year (Oct – Sep) flow of the North Saskatchewan River at Edmonton for the period 1063 to 2006 (Figure 6). The annual flows are plotted as positive (blue) and negative (red) departures from the mean reconstructed flow for the calibration period (1912-2007). A visual scan reveals the tendency for consecutive years of above or below average streamflow, and the reoccurrence of wet and dry intervals with quasi-periodicity. In Figure 7, the results of a spectral (wavelet) analysis of the tree-ring reconstruction, periodicity plotted in red has the highest power (Torrence and Compo, 1998). The black contour indicates statistically significant (95%) power; corresponding mostly to variability in the ENSO band (4-8 years). Periodicity is consistent, although not statistically significant, at ~ 60 years. The 60-year running average reconstructed flow shows sustained periods of relatively higher and lower water levels.

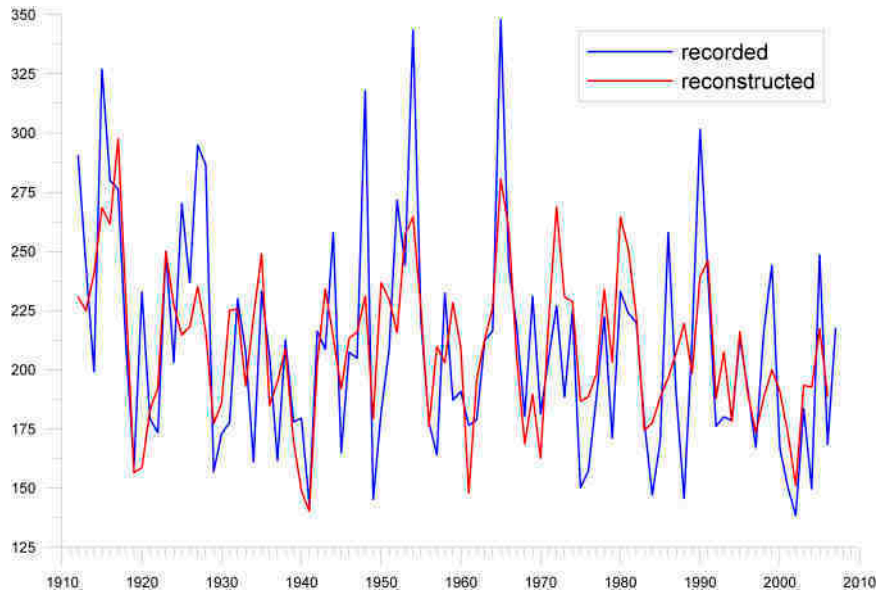

Figure 5: Recorded (naturalized) and reconstructed water year flow for the calibration period, 1912-2007. The variance in streamflow explained by the tree-rings is approximately 50%; most of the unexplained variance is the underestimation of high flows.

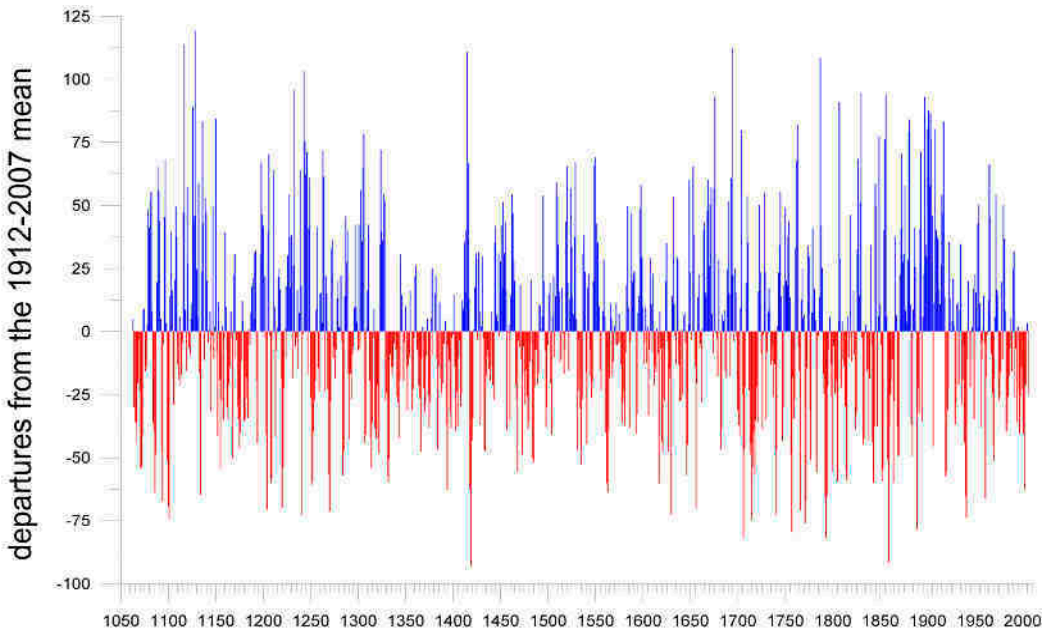

Figure 6: Reconstructed water year (Oct – Sep) flow of the North Saskatchewan River at Edmonton. The annual flows are plotted as positive (blue) and negative (red) departures from the mean flow for the calibration period (1912-2007).

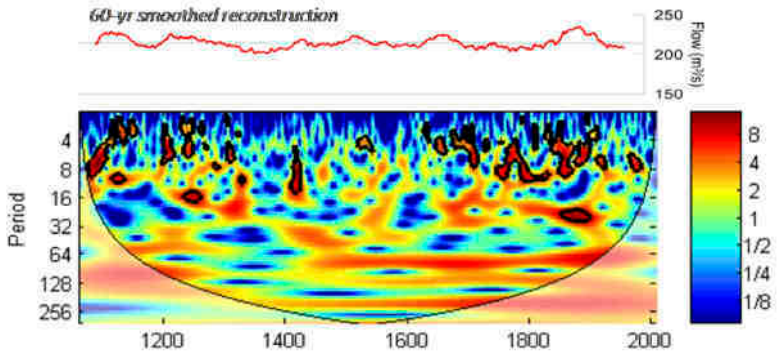

Figure 7: Spectral (wavelet) analysis of the tree-ring reconstruction of water-year flows of the North Saskatchewan River.
Periodicity plotted in red has the highest power. The black contour indicates statistically significant (95%) power; corresponding mostly to variability in the ENSO band (4-8 years). Periodicity is consistent, although not statistically significant, at ~ 60 years. The 60-year running average reconstructed flow shows sustained periods of relatively higher and lower water levels.

The annual flow back to 1063 shows a larger range of water levels than the gauge record including some extended periods of low flow in the pre-instrumental period. Low flow represents hydrological drought. Table 1 lists the most severe and sustained droughts in

the NSRB tree-ring record since 1063. The 20 most intense single-year droughts include two from the 20th century: 1941 (4th) and 1961 (17th). The lowest flow in the 944-year record was in 1859, in the midst of the drought of the 1850s, when Captain John Palliser explored the region and declared it "forever comparatively useless". Arguably the critical attribute of drought, in term of impacts on natural and social systems, is duration, since sustained low water levels have cumulative impacts. Duration can be defined as consecutive years of low water levels or periods lacking above average precipitation and runoff.

In Table 2, there are two operational definitions of prolonged drought: 1) consecutive years (three / five) of low streamflow (20th / 40th percentiles), and 2) decades or longer without streamflow above the 60th percentile. Using these criteria the most prolonged intense droughts of the past millennium in the NSRB occurred from 1714 to 1919. In a tree-ring reconstruction of the Palmer Drought Severity Index for the northwestern Great Plains, Lapp et al. (2012) labeled the drought of the 1710s as the most severe of the sustained droughts of the past 600 years. They attribute the severity of this multi-year drought to the coincidence of a positive phase PDO and high ENSO variability. The 1710s also were relatively warm according to an independent tree-ring reconstruction of summer temperatures. There were 25 intervals with low flow (20th percentile) in three consecutive years, although four of these overlapping three-year droughts were in the period 1714-1719. Since the period 1063-2006 consists of 942 overlapping three-year intervals, the probability of a three-year drought was 25/942 = 0.03. In the instrumental period since 1912, there were two three-year droughts ending in 1921 and 1941. By relaxing the definition of drought to include low flows in the 40th percentile, there were 22 five-year periods of consistent low flow. Two of these fall in the six-year dry period 1935-41. Five-year periods ending in 1987 and 2004 also qualify. Thus the gauge record does encompass some long dry spells, however, the events of longest duration are in preceding centuries. This is most apparent using the alternative operational definition of drought, that is, long intervals during which no annual flows exceeded the 60th percentile. According to this criterion, the longest dry spell is 17 years ending in 1806. In the midst of this period, in May 1796, Hudson Bay Company records reported that furs could not

be transported from Fort Edmonton, "there being no water in the river". The last column in Table 1 lists 10 of the decade or longer dry spells, that is, one per century. Although they did not occur in all centuries, 1935-47 was the 20th century sustained dry spell. The PDO shifted from positive to negative in 1947 and the next long dry spell was not until the 1980s after the PDO shifted back to positive in 1976-77.

Table 1: The most severe and sustained droughts in the NSRB since 1063

Rank [1]	Single-yr	20th_3yr [2]	20th_5yr [2]	40th_5yr [2]	60th (# of yrs) [3]
1	1859	1087	1718	1184	1073 (11)
2	1419	1101	1719	1254	1322 (11)
3	1793	1176		1255	1344 (16)
4	1941	1253		1322	1376 (15)
5	1656	1315		1333	1400 (14)
6	1889	1332		1334	1443 (12)
7	1706	1333		1335	1582 (10)
8	1771	1343		1336	1721 (10)
9	1715	1420		1565	1806 (17)
10	1101	1421		1581	1947 (12)
11	1766	1487		1716	
12	1241	1563		1717	
13	1418	1564		1741	
14	1630	1708		1760	
15	1270	1716		1802	
16	1220	1717		1803	
17	1961	1718		1804	
18	1100	1719		1805	
19	1204	1794		1940	
20	1772	1815		1941	
21	1094	1839		1987	
22	1940	1844		2004	
23	1332	1870			
24	1086	1921			
25	1134	1941			

[1] applies only to single-year droughts; other droughts are listed in chronological order
[2] final year of 3 or 5 consecutive years of low flow (20th or 40th percentile)
[3] at least 10 years of low flow, i.e., no flows above the 60th percentile

Projections of Future Hydroclimate

From the stream gauge records, we identified emerging water level trends and high-frequency variability. The tree-ring records revealed longer-term hydroclimatic variability of lower frequency and extremes that exceed those in those in the gauge record. However, while the gauge and proxy records can inform our understanding of the future hydroclimate, these times series cannot be extrapolated, given the non-stationarity of the recent climate (revealed by the tree-ring record) and therefore changes in rates of hydrologic processes with a warming climate. The only reliable sources of future projections are climate models that simulate the response of ocean-atmosphere circulation to external drivers, including increasing concentrations of greenhouse gases.

Previous work under the Prairies RAC examined future hydroclimatic over the Prairie region using recently released global and regional climate model (GCM and RCM) output (Barrow, 2010). In this report, the climate scenario work is taken a step further and we determine the probabilities of exceeding medians and extremes in hydroclimatic variables, using simple methods of probabilistic analysis including bootstrap resampling of GCM and RCM output. The results presented here are for southern Alberta, that is, the Alberta portion of the Saskatchewan River Basin. The GCM and RCM data were averaged over this region.

A wealth of GCM output is now available mainly from the IPCC Data Distribution Centre (IPCC-DDC; www.ippc-data.org) and the Coupled Model Intercomparison Project (CMIP3; www-pcmdi.llnl.gov/ipcc/about_ipcc.php; Meehl *et al*., 2007). RCM data are becoming available through the North American Regional Climate Change Assessment Program (NARCCAP; www.narccap.ucar.edu) and the Canadian Centre for Climate Modelling and Analysis (CCCma; www.cccma.ec.gc.ca). Sufficient GCM data are available to use in probabilistic analyses, but given the limited number of RCM experiments, RCM projections may be used only as single point values, but expressed in

the context of the GCM results. Tables 2 and 3 provide details of the available GCM experiments; similar information for RCMs is given in Tables 4 and 5.

Table 2: Global Climate Modelling Centres

GCM	Modelling Centre(s)
BCCR-BCM2.0	Bjerknes Centre for Climate Research, Norway
CGCM3.1(T47)	Canadian Centre for Climate Modelling and Analysis, Canada
CGCM3.1(T63)	
CNRM-CM3	Météo-France/Centre National de Recherches Météorologiques, France
CSIRO-MK3.0	Commonwealth Scientific and Industrial Research Organisation (CSIRO) Atmospheric Research, Australia
CSIRO-MK3.5	
ECHAM5/MPI-OM	Max Planck Institute for Meteorology, Germany
ECHO-G	Meteorological Institute of the University of Bonn, Meteorological Research Institute of the Korea Meteorological Administration (KMA), and Model and Data Group, Germany/Korea
FGOALS-g1.0	National Key Laboratory of Numerical Modeling for Atmospheric Sciences and Geophysical Fluid Dynamics (LASG)/Institute of Atmospheric Physics, China
GFDL-CM2.0	U.S. Department of Commerce/National Oceanic and Atmospheric Administration (NOAA)/Geophysical Fluid Dynamics Laboratory (GFDL), USA
GFDL-CM2.1	
GISS-AOM	National Aeronautics and Space Administration (NASA)/Goddard Institute for Space Studies (GISS), USA
GISS-EH	
GISS-ER	
INGV-SXG	National Institute of Geophysics and Volcanology, Italy
INM-CM3.0	Institute for Numerical Mathematics, Russia
IPSL-CM4	Institut Pierre Simon Laplace, France
MIROC3.2(hires),	Center for Climate System Research (University of Tokyo), National Institute for Environmental Studies, and Frontier Research Center for Global Change (JAMSTEC), Japan
MIROC3.2(medres),	
NCAR (CCSM3)	National Center for Atmospheric Research, USA
NCAR (PCM)	
UKMO (HadCM3)	UK Meteorological Office, Hadley Centre for Climate Prediction and Research, UK
UKMO (HadGEM1)	

Table 3: GCM details, including the number of experiments available for each emissions scenario

GCM	20C3M	SRA2	SRA1B	SRB1	Latitude boxes	Longitude boxes	Variables
BCCR-BCM2.0	1	1	1	1	64	128	pr, tas, tasmax, tasmin
CGCM3.1_T47	5	5	5	5	48	96	pr, tas, mrros
CGCM3.1_T63	1	1	1	1	64	128	pr, tas, mrros
CNRM-CM3	1	1	1	1	64	128	pr, tas, mrros
CSIROMk3.0	1	1	1	1	96	192	pr, tas, mrros, tasmax, tasmin
CSIROMk3.5	1	1	1	1	96	192	pr, tas, mrros, tasmax, tasmin
ECHAM5	4	3	4	3	96	192	pr, tas, mrros
ECHO-G	3	3	3	3	48	96	pr, tas
FGOALS	3		3	3	60	128	pr, tas, mrros
GFDL-CM2.0	1	1	1	1	90	144	pr, tas
GFDL-CM2.1	1	1	1	1	90	144	pr, tas
GISS-AOM	2		2	2	60	90	pr, tas, mrros, tasmax, tasmin
GISS-EH	3		3		46	72	pr, tas, mrros
GISS-ER (run numbers)	3 (1, 2, 4)	1 (1)	2 (2, 4)	1 (1)	46	72	pr, tas, mrros
INGV-SXG	1	1	1		160	320	pr, tas
INM-CM3.0	1	1	1	1	45	72	pr, tas, mrros, tasmax, tasmin
IPSL-CM4	1	1	1	1	72	96	pr, tas, mrros
MIROC3.2-hires	1		1	1	160	320	pr, tas, mrros, tasmax, tasmin
MIROC3.2-medres	3	3	3	3	64	128	pr, tas, mrros, tasmax, tasmin
CGCM2.3.2	5	5	5	5	64	128	pr, tas, mrros
NCAR-CCSM (run numbers)	8 (1, 2, 3,	4 (1, 2,	7 (1, 2, 3,	8 (1, 2,	128	256	pr, tas, mrros

	4, 5, 6, 7, 9)	3, 4)	5, 6, 7, 9)	3, 4, 5, 6, 7, 9)			
NCAR-PCM	4	4	4	3	64	128	pr, tas, mrros
UKMO-HadCM3	1	1	1	1	73	96	pr, tas
UKMO-HadGEM1	1	1	1		145	192	pr, tas, mrros
		∑=40	∑=54	∑=48			

Variables: pr – precipitation; tas – mean surface air temperature; mrros – surface runoff; tasmax – mean maximum surface air temperature; tasmin – mean minimum surface air temperature

Table 4: Regional – Global Climate Model Combinations available from NARCCAP
Check marks indicate experiments that are currently available (green) or planned and not yet available (red).

Driving GCM / RCM	GFDL	CGCM3	HadCM3	CCSM	NCEP
CRCM		✓		✓	✓
ECPC	✓		✓		✓
HRM3	✓		✓		✓
MM5I			✓	✓	✓
RCM3	✓	✓			✓
WRFP		✓		✓	✓

Table 5: Regional Climate Model Characteristics			
RCM	Driving GCM	Variables Available	Time series length
Canadian Regional Climate Model (CRCM) OURANOS, UQAM	1. CGCM3 T47, run 4; Flato (2005)[@] 2. NCAR-CCSM	T, T_{max}, T_{min}, P*	12/1960 – 11/2100
Regional Climate Model version 3 (RCM3)** UC Santa Cruz	1. CGCM3, run 4; Flato (2005) 2. GFDL	T, P	12/1970 – 11/2000 12/2040 – 11/2070
		T_{max}, T_{min}	12/1970 – 12/1995 11/2040 – 12/2065
Hadley Regional Model 3 (HRM3)** Hadley Centre for Climate Prediction and Research	1. HadCM3 (custom run for NARCCAP)	T, T_{max}, T_{min}, P	12/1970 – 11/2000 12/2040 – 11/2070
Weather Research and Forecasting Model (WRFP) Pacific Northwest National Laboratory	NCAR-CCSM		
MM5-PSU/NCAR mesoscale model	1. NCAR-CCSM		

(MM5I) Iowa State University			

[@]Two experiments were available for CRCM with CGCM3 T47 as the driving GCM.
*T – mean temperature; T_{max} – maximum temperature; T_{min} – minimum temperature; P – precipitation.
** Monthly data for these two RCMs were calculated from the original 3-hourly files, with a day corresponding to 06 UTC – 06 UTC.

After downloading and pre-processing the GCM data, they were interpolated onto a common grid using MATLAB®'s two-dimensional linear interpolation routine (interp2). A grid resolution of approximately 2.8° longitude by 2.8° latitude was selected so that as many GCMs as possible would remain on their original grid. The RCM data were maintained on their original grids. Grid-box values were averaged over the study area for the baseline period, 1971-2000, and the future time period, 2040-2069. These data sets were then resampled 5000 times using the bootstrap resampling function available in MATLAB®. Cumulative distribution functions (cdf) were constructed using the kernel smoothing density estimate function, also available in MATLAB®. This is a nonparametric alternative to the fitting of a parametric density function (Wilks, 2011). Because there were insufficient RCM data available (eight experiments only) to carry out resampling, RCM results are indicated as solid squares on the cdf plots.

Mean surface air temperature (°C) shows a distinct shift to the right on the cdf plots in Figure 8 with increases of between 3 and 4°C by 2050. Cooler temperatures become less frequent, with annual mean temperature less than -15°C, and summer mean temperatures of less than 4°C, becoming unlikely. RCM results indicate that annual mean temperatures are warmer than those derived from the GCMs, although summer mean temperatures are generally within the range of the GCM results. The cdf plots in Figure 9 illustrate that both annual and summer precipitation generally increase over time (shift to the right in the cdfs). Annual precipitation totals derived from the RCM experiments are higher than any annual totals from the GCMs. For the summer season, there is some overlap between RCM and GCM values, although some of the RCM totals are greater than those of the GCMs.

Annual (Jan-Dec)	Summer (JJA)
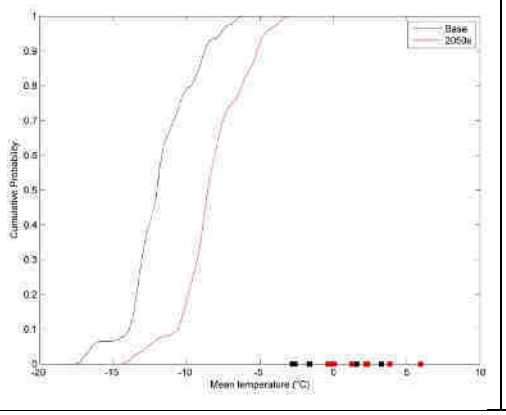	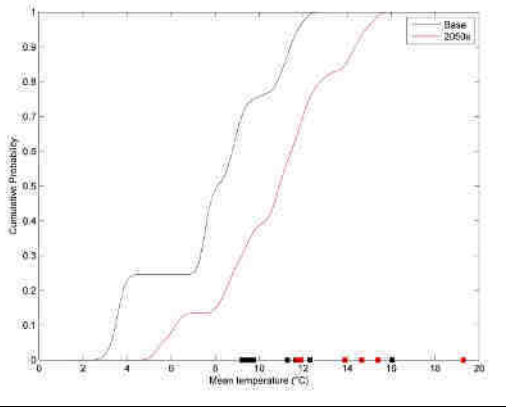

Figure 8: Cumulative distribution functions for mean annual (left) and summer (right) temperature (°C) for Southern Alberta, all GCM experiments pooled. RCM results are represented as black squares for the baseline period and as red squares for the 2050s.

Annual (Jan-Dec)	Summer (JJA)
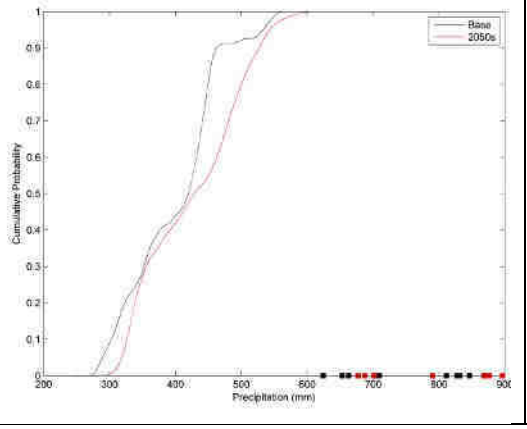	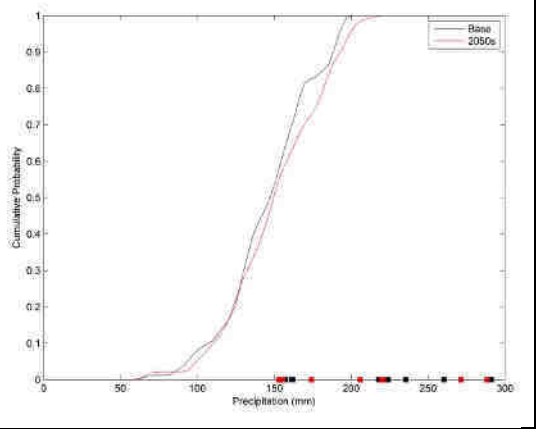

Figure 9: Cumulative distribution functions for annual (left) and summer (right) precipitation for Southern Alberta, all GCM experiments pooled. RCM results are represented as black squares for the baseline period and as red squares for the 2050s.

While temperature and precipitation are the most commonly measured and modeled climate variables, and controls on raw surface water supplies, a more meaningful hydrological variable is the precipitation that is effective in restoring surface and soil water balances. The climate moisture index (CMI; Hogg, 1994, 1997) is a relatively simple expression of a regional water balance. It is a measure of effective precipitation in excess of water loss by evapotranspiration, i.e., P – PET. This index is meaningful

biogeographically, with a CMI value of zero (i.e., P = PET) defining the southern boundary of the boreal forest and a value of -15 corresponding to the aspen parkland – grassland boundary in western Canada (based on 1951-1980 climate data; Hogg, 1994). Here, the CMI has been calculated for the water year (October to the following September) and also over the three-month period May, June and July. There are a number of different methods for calculating potential evapotranspiration, but the Thornthwaite and simplified Penman-Monteith methods (see Appendix A) were chosen for their relative simplicity and basic climate data requirements.

CMI, using both Thornthwaite and Penman-Monteith methods, was calculated for southern Alberta for the 1971-2000 and 2040-2069 time periods and for all GCM and RCM experiments where the required data existed; only 27 out of the 142 GCM experiments had the necessary maximum and minimum temperature data to calculate CMI using Penman-Monteith. Figure 10 presents the CMI cdfs for both PET methods and for the water year and May-June-July. Over the water year, CMI values generally increase in the future, regardless of which method is used to calculate PET; return periods increase for a given level of CMI, i.e., 'drier' events become less likely. For May-June-July, however, CMI values decrease in the future, shown by the shift to the left in the cdf plot, with shorter return periods, i.e., 'drier' events become more likely. The exception is at higher CMI values (> 75mm) calculated using the Penman-Monteith method, where there are slight increases. This implies, therefore, that although annual CMI values are projected to increase, at the time when water is required for crop growth and other water uses, the effective precipitation is projected to decrease compared to the 1971-2000 baseline.

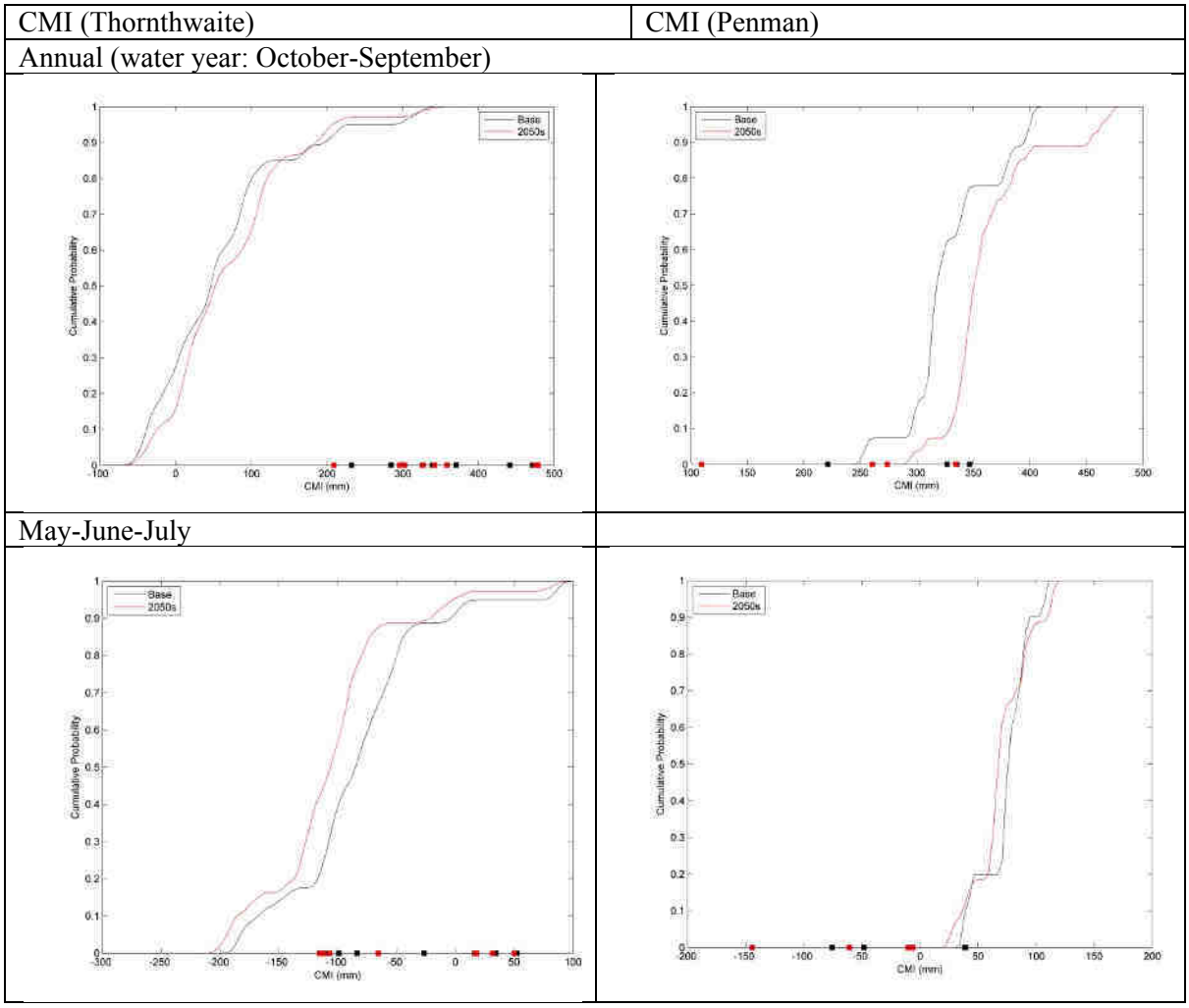

Figure 10: CMI cumulative distribution functions for the water year (top) and summer (bottom), with CMI calculated using Thornthwaite (left) and simplified Penman-Monteith (right) methods.

These climate change scenarios for the Saskatchewan River basin imply more water in winter and spring, and less water in summer and perhaps fall. The impact of these regional climate changes on streamflow can be estimated by coupling the climate change projections and a hydrological model. As part of a large study of climate change and runoff in the NSRB (Sauchyn, Byrne and Kienzle, 2011), Dr. Stefan Kienzle (University of Lethbridge) used the physical-conceptual ACRU agro-hydrological modelling system to simulate the hydrological regime of the upper NSRB, above the confluence of the

Brazeau and North Saskatchewan Rivers. The ACRU model was parameterized and validated using gauge data, and then driven with GCM projections to generate future scenarios of the watershed hydrology.

Figure 11 shows projected changes in streamflow for the 2050s for the upper NSRB for five climate change scenarios. Streamflow is plotted as the percentage change between the baseline of 1961-90 and the future thirty-year period 2049-60 (the '2050s'). These results clearly reflect the dominant climate change scenarios of a warming climate, especially in winter and spring, increased precipitation but mostly in winter, and decreasing effective precipitation in summer. In Figure 11, streamflow of 100% is equivalent to the1961-90 baseline and thus no change into the future. Flow in mid to late summer could fall by as much as 50%, with significantly higher runoff in winter.

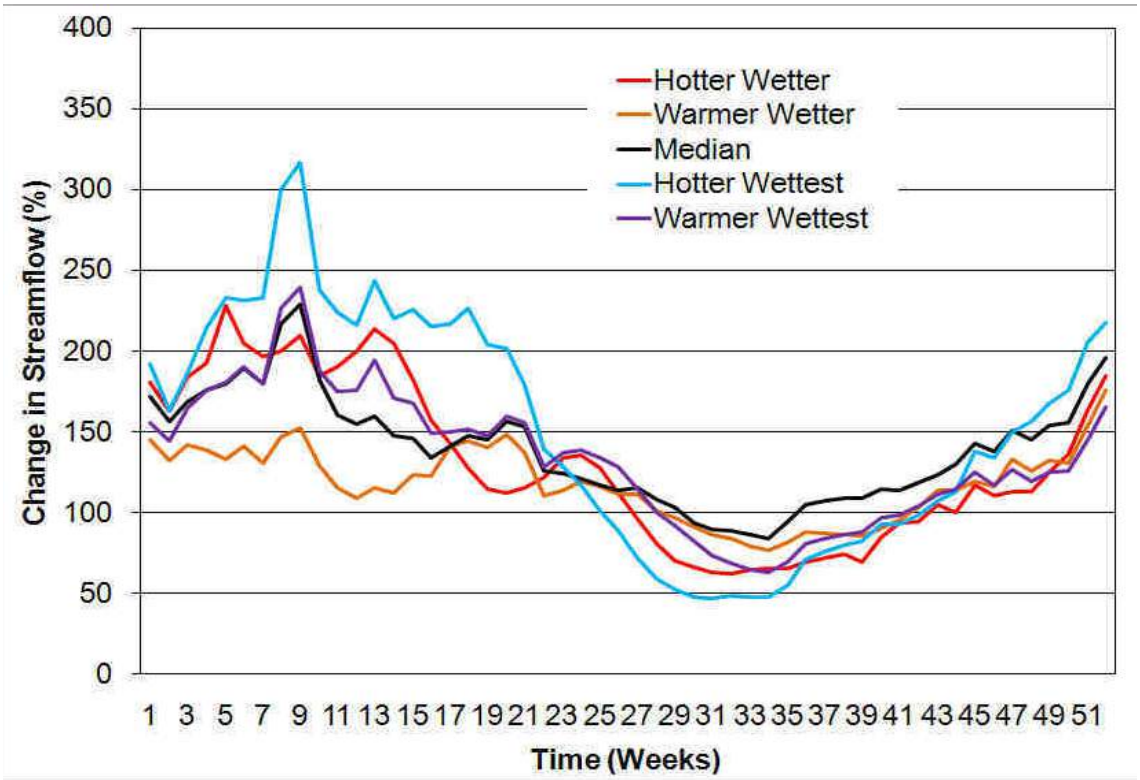

Figure 11: Simulated changes in streamflow for the 2050s for the upper NSRB for five climate change scenarios (Sauchyn, Byrne and Kienzle, 2011). Streamflow of 100% represents the 1961-90 baseline and thus no change into the future. Flow in mid to late summer could fall by as much as 50%, with significantly higher runoff in winter.

There are some limitations to these projections of future water supplies. Even though the hydrological model simulates very well the statistical characteristics of observed flow, it assumes stationary land cover and inter-annual variation (the 61-90 variability). We know that the climate models do not simulate the climate oscillations (for example, El Niño – Southern Oscillation) that drive the inter-annual to decadal variability of precipitation and streamflow. Therefore we are able to provide mean monthly flows for 30-year periods but more analysis of variability and extremes would be necessary to develop scenarios of the variability that will underlie the trends. These scenarios represent the shift in average water levels based on the difference in average daily temperature and precipitation for two 30-year periods. This so-called 'delta approach' does not account for change in the variability of the climate system; it assumes the variability of the baseline period 1961-90. Thus this simulation of future mean weekly water levels should be augmented with the results of our analysis of the variability in the gauge and tree-ring records, and the probability analysis of GCM output which suggested a shorter return period for summer drought.

Conclusions

This report describes the use of innovative scientific methods to augment the more conventional analysis of streamflow records for the NSRB. Our analysis of river flows extended from the mid 11th century (1063) to mid 21st century. This long perspective on past and future flows is an important context for an interpretation of the emerging trends in water levels, natural cycles in the regional hydroclimate, and the impacts of global warming on the hydrology of the eastern slopes of the Rocky Mountains. The flows from 1063 to 2007 were reconstructed from seven new moisture-sensitive tree-ring chronologies derived from samples of old trees and dead wood (limber pine and Douglas fir) collected in the upper reaches of the NSRB. The future flows were simulated by coupling output from global climate models with a model of the watershed hydrology. Extending the reference hydrology from decades to centuries alters perceptions of the reliability of the water supply and understanding of the variability; longer periods of low flow have occurred in the past than have been recorded in the instrumental record and the

future hydrology departs from the recent past in terms of the timing of peak annual runoff and declining summer flows.

From the long proxy hydrometric record, we were able to determine the frequency and duration of periods of sustained low flow over the past millennium, the association between hydroclimatic variability and large-scale climate drivers of the regional hydrology, and whether the envelope of variability recorded by the gauge at Edmonton since 1912 is representative of the variability and extremes captured by the tree rings since 1063. The paleohydrology is characterized by significant periodic behavior including dominant high-frequency (3-9 year) and lower-frequency (60-year) modes associated with periodic fluctuations in Pacific Ocean sea surface temperatures: the El Niño – Southern Oscillation (ENSO) and the Pacific Decadal Oscillation (PDO). The ENSO and PDO have a profound influence on the climate of the western hemisphere, and thus these oscillations confound the detection of trends emerging in the past several decades and imposed by global warming.

Changes in annual and summer temperature, precipitation and the climate moisture index (P-PET), from 1961-90 to the 2050s (2049-60), were derived from142 global climate model (GCM) experiments. The resampling of these data enabled us to construct cumulative distribution functions and determine probabilities for median and extreme hydroclimatic conditions. A number of RCM experiments, available for the first time, were analyzed and the results included, although the number of experiments was insufficient for probabilistic analyses. These climate scenarios show that, although mean temperature and precipitation are projected to increase in the future, moisture is projected to decline in summer, when there is the greatest demand for water.

An increasing reliance on water from the North Saskatchewan River assumes a certain reliability of the source: mostly snowmelt and rainfall runoff from the Rocky Mountains. The average annual basin yield and interannual variability are known, at least if the gauge record is assumed to be stationary, that is, there is no systematic change in either mean or variance of the time series. The assumption of stationarity, “a foundational concept that

permeates training and practice in water-resource engineering" (Milly, et al., 2008), is undermined by observations from before the instrumental period and by projections of future hydroclimate (Sauchyn et al., 2008). Extending the reference hydrology from decades to centuries alters perceptions of the reliability and stationarity of the water supply. From our extensive analysis of the paleohydrology, future climate and watershed hydrology of the NSRB, we conclude that:

- Global climate change, as projected by global circulation models (GCM), will produce a shift in water resources from summer to winter, with higher mean and low flows winter and reduced flows in summer.
- The total annual yield may not be significantly different from present but the scenarios range from a modest increase to decreased annual flow depending on the GCM and especially the greenhouse gas emission scenario.
- Therefore a major risk to water supplies in the NSRB from climate change is lower summer flows, and the associated degraded water quality.
- The most challenging climate change scenario is hydrological drought superimposed on lower mean summer flows, since the negative departure (deficit) will be relative to a lower mean condition.
- Storage behind the Big Horn and Brazeau dams will mitigate these impacts since low flows can be managed will the release of stored water. However, stored water will not be available to enhance summer flows if there is a dramatically reduced snowpack and/or drought in consecutive years that has cumulative impacts on basin water yield and reservoir storage. Therefore the worst-case scenario would be a prolonged drought, such as those that are apparent in the pre-gauge segment of our tree-ring reconstructions of the natural flows. Since these droughts occurred in the past, they are likely to reoccur in the future and a warming atmosphere and oceans amplifies this probability.
- This study demonstrated that expanding the reference hydrology from a century to a millennium, including the future, changes our understanding of the variability and consistency of supplies. It suggests that water resource agencies and managers must

consider adaptations that accommodate a lesser degree of determinacy, certainty and stationarity in water supplies.

Acknowledgements

Financial support for the work described in this report was primarily from the Prairie RAC, which in 2011-12 consisting of funding from Alberta and Environment Natural Resources Canada. Alberta Environment also provided naturalized streamflow data. The paleohydrology of the North Saskatchewan River was research sponsored by EPCOR Water Services with matching funds from NSERC. All GCM data were obtained from the IPCC Data Distribution Centre (www.ipcc-ddc.org) or from the Program for Climate Model Diagnosis and Intercomparison (PCMDI) Coupled Model Intercomparison Project 3 (CMIP3; www-pcmdi.llnl.gov/ipcc/about_ipcc.php). Data from UKMO HadCM3 and UKMO HadGEM1 were supplied to these centres by the UK Met. Office Hadley Centre for Climate Prediction and Research and are © Crown copyright 2005. RCM data were obtained from the Canadian Centre for Climate Modelling and Analysis (CCCma; www.cccma.ec.gc.ca) and the North American Regional Climate Change Assessment Program (NARCCAP; www.narccap.ucar.edu).

References

Axelson J., Sauchyn, D. And Barichivich J. 2009. New reconstructions of streamflow variability in the South Saskatchewan River Basin from a network of tree ring chronologies, Alberta, Canada. Water Resources Research doi:10.1029/2008WR007639.

Barrow, E.M. (2010): Hydroclimate Data for the Prairies: An Analysis of Probabilities. A Report Prepared for PARC, May 2010. 34pp.

Demuth, M. and A. Pietroniro. 2003. The impact of climate change on the glaciers of the Canadian Rocky Mountain eastern slopes and implications for water resource-related adaptation in the Canadian Prairies: Phase I – Headwaters of the North Saskatchewan River Basin. Prairie Adaptation Research Collaborative Project P55.

Gobena, A., and Gan, T. 2006. Low-frequency variability in southwestern Canadian streamflow: Links with large scale climate anomalies. International Journal of Climatology 26, 1843-1869.

Hogg, E.H. (1994): Climate and the southern limit of the western Canadian boreal forest. Canadian Journal of Forest Research 24, 1835-1845.

Hogg, E.H. (1997): Temporal scaling of moisture and forest-grassland boundary in western Canada. Agricultural and Forest Meteorology 84, 115-122.

Lapp, SL; DJ Sauchyn; J-M St. Jacques; JR Vanstone. 2012. Forcing of Hydroclimatic Variability in the Northwestern Great Plains since 1406. Quaternary International.

Lapp, Suzan; St. Jacques, Jeannine-Marie; Barrow, Elaine M.; and Sauchyn, David J. 2011. GCM projections for the Pacific Decadal Oscillation under greenhouse forcing for the early 21st century. International Journal of Climatology, DOI: 10.1002/joc.2364

Meehl, G.A., Covey, C., Delworth, T., Latif, M., McAvaney, B., Mitchell, J.F.B., Stouffer, R. & Taylor, K.E. (2007): The WCRP CMIP3 Multimodel Dataset: A New Era in Climate Change Research. Bulletin of the American Meteorological Society, 88(9), 1383-1394.

Meko, D. M. and Woodhouse, C.A. 2012. Dendroclimatology, dendrohydrology, and water resources management, In: Hughes, M. et al. (eds).Tree Rings and Climate. Kluwer/Springer.

Milly, et al., 2008. Climate change: stationarity is dead: whither water management. Science.

North Saskatchewan Watershed Alliance. 2005. State of the North Saskatchewan Watershed Report 2005 - A Foundation for Collaborative Watershed Management. North Saskatchewan Watershed Alliance, Edmonton, Alberta. 202 pgs.

North Saskatchewan Watershed Alliance. 2007. Current and Future Water Use in the North Saskatchewan River Basin.

Perez-Valdivia, C., Sauchyn, D., (2010) Tree-ring reconstruction of groundwater levels in Alberta, Canada: Long term hydroclimatic variability. Dendrochronologia, doi:10.1016/j.dendro.2010.09.001

Sauchyn, D.J., Stroich, J. and Beriault, A. 2003. A paleoclimatic context for the drought of 1999-2001 in the northern Great Plains. The Geographical Journal, 169(2): 158-167.

Sauchyn, D., and Kulshreshtha, S. 2008. The Prairies, in From Impacts to Adaptation: Canada in a Changing Climate 2007, edited by D. S. Lemmen et al. Chapter 7, pp. 275-328. Government of Canada, Ottawa.

Sauchyn, Dave, Jim Byrne and Stefan Kienzle (2011) Past, Recent and Future Hydroclimatic Variability, North Saskatchewan River. Final Report on an EPCOR – NSERC Collaborative Research and Development Project, January 2011

Sauchyn, David; Vanstone, Jessica and Perez-Valdivia, Cesar. 2011. Modes and Forcing of Hydroclimatic Variability in the Upper North Saskatchewan River Basin Since 1063. Canadian Water Resources Journal, 36(3): 205_218.

Sauchyn, Demuth, and Pietroniro, 2008. Canada's Rocky Mountains and western plains. Upland watershed management and global change

Shabbar A. and Skinner, W. 2004. Summer drought patterns in Canada and the relationship to global sea surface temperatures. Journal of Climatology 17:2866-2880.

St. George, Scott and Sauchyn, Dave. 2006.Paleoenvironmental Perspectives on Drought in Western Canada. Canadian Water Resources Journal 31(4): 197-204.

St. Jacques, J.M. Sauchyn, D.J. and Yang Zhao. 2010. Northern Rocky Mountain streamflow records: Global warming trends, human impacts or natural variability? Geophysical Research Letters, Vol. 37, L06407, doi:10.1029/2009GL042045, 2010.

St. Jacques, Jeannine-Marie; Suzan L Lapp, Yang Zhao, Elaine M Barrow, and David J Sauchyn. 2012. Twenty-first Century Northern Rocky Mountain River Discharge Scenarios under Greenhouse Forcing. Quaternary International.

Torrence, C., and Compo, G. 1998. A practical guide to wavelet analysis. Bulletin of the American Meteorological Society 79, 61-78.

Wilks, D.S. (2011): Statistical Methods in the Atmospheric Sciences (3rd Ed.). Academic Press, 676pp.

Appendices

Appendix A: Calculation of Potential Evapotranspiration

Calculation of potential evapotranspiration (PET) is dependent upon which climate variables are available. The two methods used here require climate variables that are generally readily available – mean, minimum and maximum temperature. The Thornthwaite method is the least data intensive, requiring only mean temperature, but it tends to exaggerate PET and this is particularly marked in the summer months when high temperatures have a dominant effect in the calculation.

1. Thornthwaite method

The Thornthwaite method is based mainly on mean temperature with an adjustment being made for the number of daylight hours. An estimate of the PET (Shaw, 1994), calculated on a monthly basis, is given by:

$$PE_m = 16N_m\left(\frac{10\overline{T_m}}{I}\right)^a$$

where m is the months 1, 2, 3, …12, N_m is the monthly adjustment factor related to the hours of daylight, $\overline{T_m}$ is the monthly mean temperature (°C), I is the heat index for the year, given by:

$$I = \sum i_m = \sum\left(\frac{\overline{T_m}}{5}\right)^{1.5} \quad \text{for } m = 1 \ldots 12$$

and $a = 6.7 \times 10^{-7}I^3 - 7.7 \times 10^{-5}I^2 + 1.8 \times 10^{-2}I + 0.49$

The heat index, I, requires a full year's data for its calculation and missing data in any month therefore means that it cannot be calculated for that particular year.

2. Simplified Penman-Monteith method

Hogg (1997) simplified the Penman-Monteith method of estimating potential evapotranspiration so that the only input required is the altitude of the station and the mean maximum and minimum temperature for each month. The monthly PET is calculated as:

PET = 93 D exp(A/9300) for T > 10°C
PET = (6.2T+31)Dexp(A/9300) for 10°C > T > -5°C
PET = 0 for T < -5°C

where PET is potential evapotranspiration (mm/month), T is mean temperature (°C), D is vapour pressure deficit (kPa; $D=0.5(e_{Tmax} + e_{Tmin}) - e_{Tdew}$), A is station altitude (m) and e_{Tdew} is equivalent to the saturation vapour pressure at 2.5°C below mean minimum temperature.

Appendix B: Sauchyn, Vanstone and Perez-Valdivia (2011) Modes and Forcing of Hydroclimatic Variability in the Upper North Saskatchewan River Basin Since 1063

Appendix C: Lapp, Sauchyn, St. Jacques and Vanstone (2012) Forcing of Hydroclimatic Variability in the Northwestern Great Plains since 1406

Appendix D: St. Jacques, Lapp, Zhao, Barrow, and Sauchyn (2011) Twenty-first Century Northern Rocky Mountain River Discharge Scenarios under Greenhouse Forcing

Appendix E: St. Jacques, Huang, Zhao, Lapp and Sauchyn (2012) Detection and Attribution of Variability and Trends in Canadian Prairie Provinces Streamflow

Appendix F: Perez-Valdivia, Sauchyn and Vanstone (2012) Groundwater levels and teleconnection patterns in the Canadian Prairies

Modes and Forcing of Hydroclimatic Variability in the Upper North Saskatchewan River Basin Since 1063

David Sauchyn, Jessica Vanstone and Cesar Perez-Valdivia

Abstract: In this paper the mean water year (October through September) flow of the North Saskatchewan River (NSR) at Edmonton, Alberta is reconstructed back to 1063 A.D. using a new network of moisture-sensitive tree-ring chronologies from limber pine and Douglas fir at seven sites in the headwater sub-basins of the North Saskatchewan River Basin (NSRB). Over the full extent of the proxy hydrometric record (1063–2007), we examined 1) the duration and severity of low flow, 2) the dominant frequencies of periodic variability and 3) the correlation between these significant periodicities in proxy streamflow and climate indices, specifically sea surface temperature oscillations, which are known drivers of regional hydroclimatic variability. This new record of the paleohydrology of the NSRB is compared to previous tree-ring reconstructions of the annul flow of the North and South Saskatchewan Rivers. Extending the reference hydrology for the basin from decades to centuries changes perceptions of the reliability of the water supply and understanding of the hydroclimatic variability. The gauge record not does represent the full extent of interannual to multidecadal variability in the tree-ring data; there are periods of low flow in the pre-instrumental record that are longer and more severe than those recorded by the gauge.

Résumé: Dans la présente communication, le débit moyen de l'année hydrologique (d'octobre à septembre) de la riviaère Saskatchewan Nord (RSN) à Edmonton, en Alberta est reconstitué jusqu'à 1063 de notre ére à l'aide d'un nouveau réseau de dendrochronologies sensibles à l'humidité, grâce au pin flexible et au douglas de Menzies, à sept sites dans les sous-bassins du cours supérieur du bassin de la rivière Saskatchewan Nord (BRSN). Pour la durée compléte des relevés hydrométriques indirects (de 1063 à 2007), nous avons examiné 1) la durée et l'intensité des débits d'étiage, 2) les fréquences dominantes de la variabilité périodique et 3) la corrálation entre les périodicités importantes dans les indices climatiques et d'écoulement fluvial substitutifs, plus particulièrement les oscillations de température de surface de la mer, qui sont des facteurs connus de la variabilité hydroclimatique régionale. Ce nouveau relevé de la paléohydrologie du BRSN est comparé aux reconstitutions dendrométriques antérieures du débit annuel des riviéres Saskatchewan Nord et Sud. Le fait d'ètendre

David Sauchyn, Jessica Vanstone and Cesar Perez-Valdivia

Prairie Adaptation Research Collaborative, University of Regina, Regina, SK S4S 7H9

Submitted February 2011; accepted June 2011. Written comments on this paper will be accepted until March 2012

l'hydrologie de référence pour le bassin d'une période allant de décennies à des siècles change les perceptions de la fiabilité des réserves d'eau et la compréhension de la variabilité hydroclimatique. Le relevé ne représente pas l'étendue complète des données dendrométriques de variabilité interannuelle à multidécennale; certaines périodes de basses eaux dans le relevé pré-instrumental sont plus longues et plus intenses que celles enregistrées par la jauge.

Introduction

A growing demand for the surface water resources of the Canadian Prairie Provinces has resulted in increasing vulnerability to hydrological drought (Wheaton *et al.,* 2008; Schindler and Donahue, 2006). This vulnerability will be intensified by further growth in the population and economy and by a warming climate (Barrow, 2010). A shift in the amount and timing of streamflow represents the most serious risk from recent and projected climate warming in western Canada (Sauchyn *et al.,* 2010). Water resource management will be challenged by reduced mean flows in the summer season of peak demand, resulting from earlier spring snowmelt, declining contributions from glacier runoff, and a longer period of net evaporative water loss (Sauchyn *et al*., 2008).

The Saskatchewan River Basin is among Canada's most vulnerable watersheds, in terms of projected climate changes and impacts, and the sensitivity of natural systems and economic activities to Canada's most variable hydroclimate. The South Saskatchewan River (SSR) has been declared Canada's most threatened river (World Wildlife Fund, 2009). Whereas irrigation is the dominant use of water from the SSR (more than 70% of licensed withdrawals), most of the allocation from the North Saskatchewan River (NSR) is for industrial (83%) and municipal (8%) use (North Saskatchewan Watershed Alliance, 2007). The petroleum sector is allocated about 5% but is expected to account for most of the increase in withdrawals over the next 20 years (North Saskatchewan Watershed Alliance, 2007), largely for the processing of heavy oil at a series of new or expanded facilities in the Edmonton Industrial Heartland. This water use could be as high as about 10 times the current allocation for the city of Edmonton. The North Saskatchewan River Basin (NSRB; Figure 1) also is the potential location of a nuclear power generating station in west-central Saskatchewan. According to the proponent Bruce Power "The operation of a nuclear facility also requires water for cooling. An assessment was conducted of all viable water sources in the province near sufficient infrastructure to support a facility. The North and South Saskatchewan Rivers were identified as viable water sources for a new nuclear plant in the province." (Bruce Power, 2008).

This greater reliance on the North Saskatchewan River assumes a certain reliability of the source: mostly snowmelt and rainfall runoff from the Rocky Mountains. The average annual basin yield and interannual variability are known, at least if the gauge record is assumed to be stationary, that is, characterized by no systematic change in either mean or variance. This assumption of stationarity, "a foundational concept that permeates training and practice in water-resource engineering" (Milly *et al.,* 2008), is undermined by observations from before the instrumental period and by projections of future hydroclimate. For example, in May 1796, when Edmonton House was a Hudson Bay Company post, the winter catch of furs could not be exported: "there being no water in the [North Saskatchewan] river" (Sauchyn *et al.,* 2003), an extreme state that is outside the range of flows recorded by the gauge. Model projections of future water levels include significantly reduced summer flows (North Saskatchewan Watershed Alliance, 2008).

In this paper we present a 945-year reconstruction of the annual flow of the NSR derived from tree-rings collected at seven sites in the runoff generating upper basin. From this proxy hydrometric record, we determine 1) the frequency and duration of periods of sustained low flow over the past millennium, 2) the dominant modes of hydroclimatic variability, 3) the degree of correlation between these natural cycles and known drivers of regional hydroclimatic variability, and 4) whether the envelope of variability recorded by the gauge at Edmonton since 1912 is representative of the interannual to interdecadal variability captured by the tree rings since 1063.

The inference of hydroclimate from tree-ring proxies is a common approach to paleohydrology, the study of pre-instrumental water levels (Meko and Woodhouse, 2010). This application of dendrochro-

nology has advanced in recent decades from inferring water levels from tree rings at one or a few sites to the modeling and analysis of hydroclimatic variability across networks of moisture-sensitive tree-ring chronologies. This progress is typified, for example, by the series of papers that document successively more robust reconstructions of the flow of the Colorado River (Woodhouse *et al.*, 2006). Similarly, our work is preceded by a prior tree-ring reconstruction of the flow of the NSR, based on tree rings from one site in the basin and two sites from beyond the NSRB in southern Alberta near the Bow and Crowsnest Rivers (Case and Macdonald, 2003). The tree-ring chronology located in the basin spanned 1113 years but explained only 34% of the variance in the gauge record, an estimation of the naturalized flow at the Alberta – Saskatchewan boundary. Introducing tree rings from outside the basin raised the explained variance to 49% but reduced the reconstructed length to 522 years (Case and Macdonald, 2003). Edwards *et al.* (2008) used the Case and Macdonald (2003) NSR reconstruction, combined with the isotope dendrochronology of some temperature-sensitive treeline sites in the Columbia Icefields area, to infer regional climatic and hydrologic variability over the past millennium. Our new tree-ring reconstruction, extending to 1063, is derived from tree rings from seven sites, all located in the upper NSRB. This improved streamflow reconstruction is the basis for an analysis of the long-term variability in the regional hydrologic regime.

Tree-Ring and Streamflow Data

A network of seven new tree-ring chronologies was established in the upper runoff-generating sub-basins of the NSRB (Figure 1). At low to mid elevations in the Front Ranges of the Rocky Mountains, the montane forest includes open canopy stands of long-lived and moisture-sensitive coniferous trees. Limber pine (*Pinus flexilis*) grows at dry windy sites. They reach their northern limit in North America in the North Saskatchewan River valley. Douglas fir (*Pseudotsuga menziesii*) has a wider ecological amplitude that includes south to southwest facing slopes where soil moisture is limited. Both species are long lived, with 800-year-old limber pine and 700-year-old Douglas fir known to occur in western Alberta (Case and MacDonald, 2003; Watson and Luckman, 2006). During July 2008 and August 2009, we collected cores from living trees and cross sections of dead wood at the seven field sites (Table 1).

In the PARC Tree-Ring Lab at the University of Regina, high-resolution (1200+ dpi) images of sanded samples were captured using an Epson Expression 10000XL flatbed scanner. WinDendro Density (ver 2009b), a semi-automated image analysis system designed for tree rings, was used for visual and statistical crossdating of the tree-ring series and for measuring the annual growth increments to within 0.001 mm. The crossdating, which ensures that proper calendar years are assigned to each tree ring, was verified with the program COFECHA (Holmes, 1983). The program ARSTAN (Cook, 1985) was used to standardize the measured tree-ring series using conservative detrending methods: a negative exponential curve, which removes the juvenile biological growth trends in the tree-ring series; or a cubic smoothing spline, a low-pass digital filter with a 50% frequency response cutoff, the frequency at which 50% of the amplitude of the signal is retained (Cook *et al.,* 1990). The standardized ring-width series of various lengths were averaged for each site, using a mean value function that minimizes the effect of outliers (Cook *et al.,* 1990), producing dimensionless stationary index data with a defined mean of 1.0 and a relatively constant variance. In addition to this standard index chronology, ARSTAN produces a residual chronology by modeling and removing the first-order autocorrelation, and then an ARSTAN chronology by restoring the autocorrelation that is shared by the time series at a site (Cook, 1985). Site chronology statistics are given in Table 1. Record length ranges from 438 to 945 years. The coefficients of inter-series correlation and mean sensitivity indicate a strong common response to an external factor, very likely inter-annual variability in hydroclimate.

Naturalized weekly streamflow data for the North Saskatchewan River at Edmonton, AB were provided by Alberta Environment for the period 1912 – 2002. These naturalized flow data were derived from streamflow records, reservoir data, recorded and estimated irrigation withdrawals, and climate data using the Streamflow Synthesis and Reservoir Regulation (SSARR) model. The annual streamflow has a Gaussian frequency distribution according to a robust nonparametric Lilliefors test of normality. No significant autocorrelation was found in either the annual or water year streamflow records.

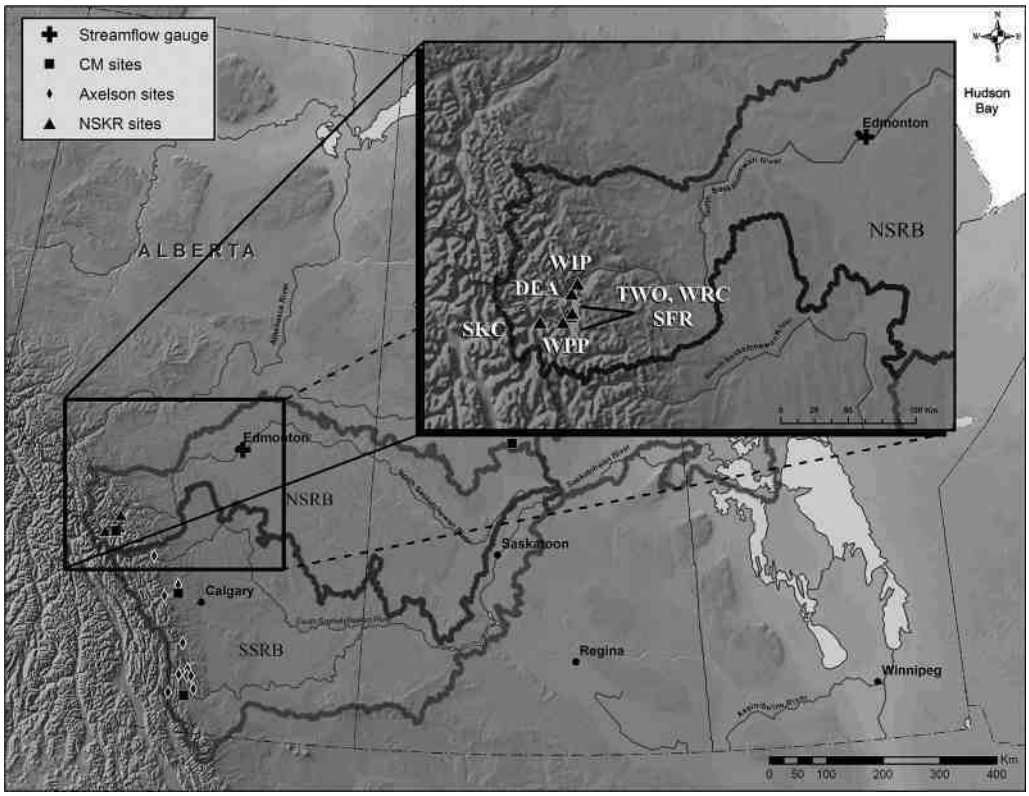

Figure 1. The North Saskatchewan River Basin, Alberta, Canada, and locations of tree-ring chronologies and streamflow gauges. CM sites – Case and MacDonald, 2003; Axelson sites: Axelson *et al*., 2009; inset map: the new tree-ring sites introduced here.

Streamflow Reconstructions

The tree-ring modeling of surface water levels is based on the principles and methods of dendrohydrology, which are well documented, for example by Loaiciga *et al*. (1993) and Meko and Woodhouse (2010). A consistent statistical relationship between mean (annual and seasonal) water levels and tree growth at dry sites is physically based on the direct link between the soil water balance and both rates of tree

Table 1. Properties of tree-ring chronologies sampled in the North Saskatchewan River Basin, Alberta, Canada. Species code: PSME, Douglas fir (*Pseudotsuga menziesii)*; PIFL, Limber pine (*Pinus flexilis*).

Site Name	Code	Species	# Trees	Years	Type	Mean Sensitivity	Series Intercorrelation	Year EPS > 0.85
Douglas Fir Ecological Area	DEA	PSME	25	1471–2007	RW	0.389	0.802	1471
Siffleur Ridge	SFR	PIFL	33	1018–2008	RW	0.383	0.776	1280
Saskatchewan Crossing	SKC	PIFL	33	1109–2007	RW	0.286	0.667	1640
Two O'clock Creek	TWO	PSME	20	1496–2007	RW	0.428	0.787	1496
Windy Point	WIP	PIFL	11	1569–2007	RW	0.307	0.562	1790
Whirlpool Point	WPP	PIFL	17	1062–2007	RW	0.463	0.751	1063
Whiterabbit Creek	WRC	PSME	22	1555–2008	RW	0.414	0.836	1600

growth and watershed runoff. To ensure that our tree-ring width data from the NSRB are suitable predictors of streamflow, and to investigate the response of tree growth to seasonal climate, the standardized tree-ring chronologies were examined for the degree of correlation with monthly climatic and hydrometric data. Correlation coefficients were calculated between the residual index chronologies and mean monthly temperature and total monthly precipitation at Edmonton, Alberta (1880–2005), and between the standard, residual and ARSTAN chronologies and average monthly, annual and water year (October–September) naturalized flow for the period 1912 to 2002. The results (not shown) include significant ($p < 0.05$) correlations between the standard and residual tree-ring indices and summer and water year precipitation and streamflow for the current and previous year. Given the absence of significant autocorrelation in the annual flow series, the residual tree-ring chronologies were chosen as the potential predictors of water year flow.

A series of tree-ring models of average water year flow were constructed by forward stepwise regression. The pool of potential predictors consisted of the seven residual index chronologies for the growth year and at forward lags of one and two years. The lagged predictors account for an offset of up to two years between climate conditions in a given year and the response of tree growth and/or streamflow. The models were optimized according to a set of statistical measures of model quality and predictive capacity. The expressed population signal (EPS) is a ratio of signal to noise as a function of the correlation among trees at a site and sample depth. The length of the individual predictor chronologies was limited to the segment with an EPS ≥ 0.85, minimizing the inflation of variance associated with decreasing sample size (Briffa and Jones, 1990). Regression models of varying length were validated using a leave-*n*-out method, where observations are left out sequentially throughout the length of the streamflow record allowing maximum use of the data (Hughes *et al.*, 1982). For the calibration period (1912–2006) the strength of the regression models was expressed using the adjusted R^2, which quantifies the explanatory power of the regression while accounting for lost degrees of freedom with an increasing number of predictors (Fritts, 1976). For the verification period we used the reduction of error (RE) statistic, a rigorous measure of association between a series of actual values and their estimates. The theoretical limits of the RE range from a maximum of +1 to negative infinity. Any positive value indicates that the model has some predictive capacity (Fritts, 1976; Fritts *et al.*, 1990). The F values for the regression models are a goodness-of-fit statistic. The standard error (SE) and root-mean-square error of validation ($RMSE_v$) are measures of the uncertainty in predicted values over the calibration and validation periods, respectively. Regression residuals were tested for autocorrelation using the Durbin-Watson test (Ostrom, 1990). The mean variance inflation factor (VIF) was calculated to detect multicollinearity in the matrix of predictor values (Haan, 2002).

We were able to extend the annual hydrograph at Edmonton, Alberta, back to 1063 (Figure 2) by nesting a series of reconstructions of varying length (Meko, 1997). Calibration and verification statistics for the models indicate skillful reconstruction of the water year flow (Table 2). The models accounted for up to $\sim 46\%$ of the instrumental variance and had significant skill when subjected to cross validation, according to consistently positive values of RE and significant ($p < 0.01$) F statistics. In every case, the standard error and root-mean-square error of validation have similar magnitude and are relatively small ($< 20\%$ of the reconstruction mean). The VIF values are near one, indicating little or no multicollinearity, with the exception of model 2, where a VIF of 4.6 indicates some inflation of the explained variance. The reconstruction replicates well the interannual variability in streamflow (Figure 2), however, it is generally better at capturing the magnitude of the low flows, while underestimating the high flows throughout the calibration period. Underestimation of peak flows is a common limitation of tree-ring reconstructions; there is a biological limit to the response of tree growth to high precipitation and low evapotranspiration during wet years (Fritts, 1976).

Interpretation of Hydroclimatic Variability

Given the uncertainty in estimating streamflow from tree rings, and especially the high flows, our interpretation of the proxy hydrograph is based initially on a ranking of the annual flows and assigning them to percentile classes. The most severe droughts are defined as flows in the lowest 10^{th} percentile. Figure 3 and Table 3 show that our reconstruction,

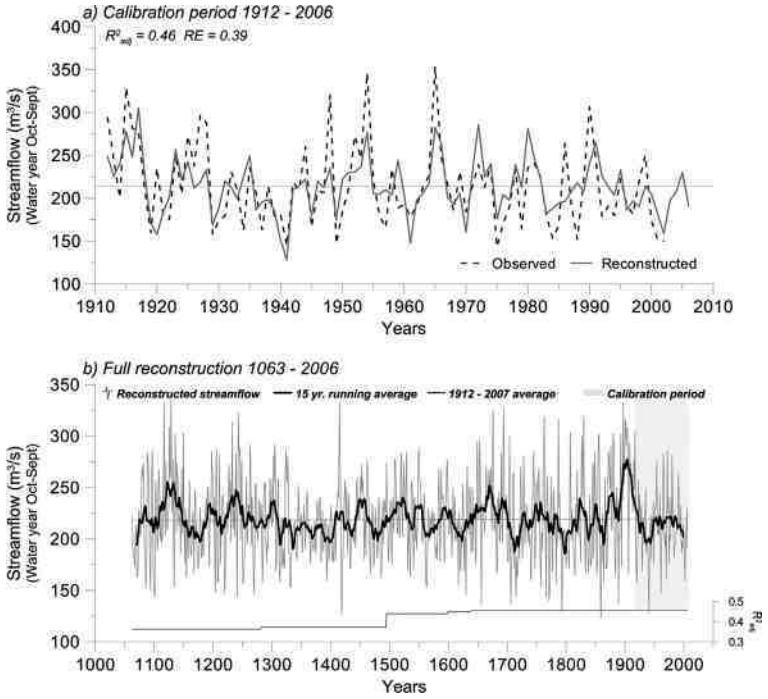

Figure 2. Top: North Saskatchewan River observed and reconstructed water year (October to September) flow for the calibration period 1912–2006. Bottom: The full reconstruction of water year flow for the period 1063 – 2006. The adjusted R-squared values for the length of the reconstruction are shown along the bottom of the plot.

and the prior reconstructions for the North and South Saskatchewan Rivers (Case and MacDonald, 2003, and Axelson *et al.*, 2009, respectively), have a similar sequence ($\pm$ 1 or 2 years) of extreme single and multi-year droughts. Slight discrepancies between the NSRB and SSRB likely reflect differences in hydroclimate, such that the severity and timing of drought can differ between these large basins even though they are adjacent and both shed runoff from the Rocky Mountains. Discrepancies between the two NSR reconstructions, on the other hand, are attributable to different sets of predictor tree-ring chronologies. We argue the newer reconstruction presented here is more likely to represent the timing and severity

Table 2. Calibration and verification statistics for the tree-ring reconstruction models of water year flow. The predictand for each of the five models is water year (October to September) flow at Edmonton. The predictors, the tree-ring chronologies, are labeled using the codes from Table 1 and Figure 1. The subscripts indicates whether the tree-ring data are for the current year (0 lag) or lagged by 1 or 2 years.

Nest	Period	Predictors	R^2	Adjusted R^2	RE	F Ratio	SE	$RMSE_v$	DW	VIF
1	1639–2006	$WPP_{0,-1}$, TWO_{+1}, WRC_{+1}, SKC_{+1}	0.479	0.455	0.39	15.65	34.75	36.45	H_0	1.9
2	1599–1638	$WPP_{0,-1}$, DEA, TWO_{+1}, WRC_{+1}	0.473	0.468	0.37	15.23	34.97	36.82	H_0	4.6
3	1495–1598	$WPP_{0,-1}$, $DEA_{0,-1}$, TWO_{+1}	0.464	0.439	0.37	14.74	35.24	36.91	H_0	1.1
4	1282–1494	$WPP_{0,-1}$, $SFR_{+1,-2}$	0.393	0.372	0.32	13.94	37.29	38.50	H_0	1.0
5	1063–1281	$WPP_{0,-1}$	0.369	0.362	0.33	25.75	37.59	38.18	H_0	1.0

DW: Durbin-Watson statistic: H_0-no first order autocorrelation in residuals

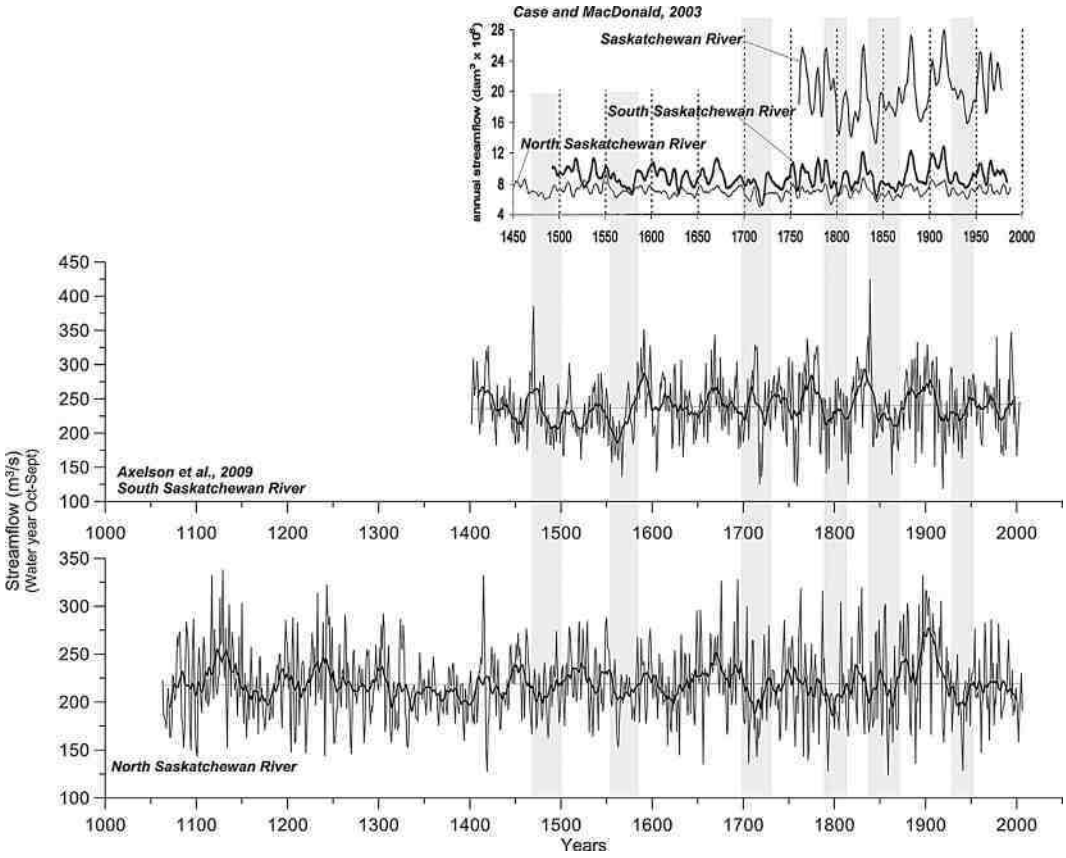

Figure 3. Reconstructions of a) total annual streamflow of the North Saskatchewan River at the provincial boundary (Case and MacDonald, 2003), b) water year streamflow (October – September) for of the South Saskatchewan River at Medicine Hat (Axelson *et al.,* 2009), and c) water year flow of the NSR at Edmonton (from Figure 2). Reconstructions are smoothed with a 15-year running average.

of drought given that it is derived from a network of tree-ring chronologies that capture the drought signal at seven sites in the basin (versus one) and for two species (versus one).

The lower frequency variability in hydroclimate can be characterized by the sequence of reconstructed flows in the 75th and 25th percentiles (wet and dry conditions, respectively; Figure 4). The most sustained wet period, or pluvial, in the entire proxy record, is during the late 19th century and early 20th century, when the Saskatchewan River basin was transformed by an influx of settlers. Whereas this best case scenario (i.e. in terms of consistently high water supply), occurred recently, the longest and most severe droughts pre-date Euro-Canadian settlement of the region. These multidecadal or 'mega' droughts include about ~30 years in the early 1700s. This sustained drought also is recorded in a high-resolution pollen record from Lake Mina, Minnesota (St. Jacques *et al.,* 2008) and a tree-ring record from southern Manitoba (St. George and Nielsen, 2002). Another ~30 year drought during the mid 1100s also appears in many other proxy records from central North America (Laird *et al.,* 2003; Sridhar *et al.,* 2006; Tian *et al.,* 2006). The most prominent mega-droughts, lasting for most of the 14th century, and occurring again in the late 15th century, are the so-called Mississippian droughts, originating in the Mississippi Valley and extending northwest (to the NSRB), and eventually on a northeast tangent up into parts of eastern Canada (Szeicz and MacDonald, 1996; Stahle *et al.*, 1998, 2000; Cook *et al.,* 2007).

The re-occurrence of low and high water levels at more or less regular intervals in Figure 4 suggests some quasi-cyclical behavior in the hydroclimatic regime of the past millennium. The main modes of periodic variability were identified using spectral

Table 3. Top 10 worst single year droughts for the North and South Saskatchewan River Basins, listed by descending severity. Underlined drought years occur in all the reconstructions (NSR 2010 – this paper; NSR 2003-Case and MacDonald, 2003; Oldman and SSR-Axelson *et al.,* 2009).

Top 10 Worst Drought Years: NSRB		SSRB	
NSR 2010	NSR 2003	Oldman	SSR
1859	**1793**	1985	1567
1419	1030	1863	1720
1941	1251	1872	1863
1793	906	**1794**	1522
1656	1084	**1657**	1563
1889	1269	1720	1919
1706	965	1721	1759
1771	1042	1759	1761
1715	1238	**1717**	1721
1101	**1716**	**1718**	1568

analysis: the multitaper method (MTM) of Mann and Lees (1996) and a continuous wavelet transform (CWT; Grinsted *et al.,* 2004). The MTM is a powerful and widely used nonparametric method of spectral estimation providing high resolution while minimizing spectral leakage and reducing the variance of spectral estimates by using orthogonal tapers (Ghil, 2002). It is particularly well suited for short and noisy time series. With a frequency resolution suitable for resolving distinct climate signals, and improved spectral estimation properties over classical methods, the MTM has been widely applied to instrumental records of atmospheric and oceanic variables. We implemented MTM using the SSA-MTM Toolkit available at http://www.atmos.ucla.edu/tcd/ssa/. The CWT analysis is a powerful tool for the identification of non-stationary signals because it decomposes the time series into frequency components. Most traditional mathematical methods that examine periodicities in the frequency domain, such as Fourier analysis, have implicitly assumed that the underlying processes are stationary in time. Wavelet transforms expand time series into time frequency space and can therefore find localized intermittent periodicities (Grinsted *et al.,* 2004).

Results of the single-spectrum MTM analysis (Figure 5, bottom) show a highly significant component of variability at interannual time scales in the El Niño-Southern Oscillation (ENSO) band (2–6 years). Various peaks in this frequency band extend above the 99% confidence level. Wavelet analysis (Figure 6, bottom) mirrors the MTM spectrum, but with the additional context of the time domain. The dark shade (highest power) and black contours (statistical significance at $p < 0.05$) indicate dominant modes of periodicity at high frequencies (2–8 years). There is also significant periodicity during

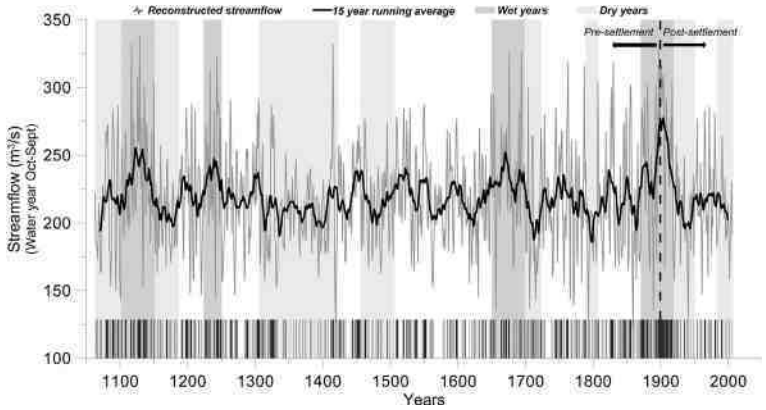

Figure 4. Wet and dry years and intervals for the water year streamflow reconstruction for the North Saskatchewan River, 1063–2006. The bars and shading symbolize years and intervals, respectively, of low flows (25th percentile) and high flows (75th percentile). The reconstruction is smoothed with a 15-year running average (heavy line).

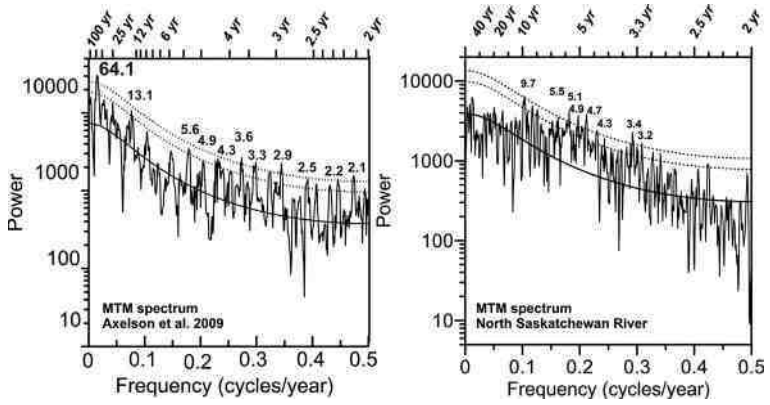

Figure 5. Results of the single-spectrum MTM analysis of the SSR (left) and NSR (right) reconstructions. The spectral peaks are labeled where they exceed the 99% confidence level.

18th and 19th centuries at about 32 and 64 years. For comparison, Figures 5 and 6 include the MTM and Wavelet analyses of the Axelson *et al.* (2009) SSR reconstruction. The strong interannual variability in the flow of the NSR and SSR conforms to the results of previous studies of sea surface temperature (SST) forcing, specifically ENSO, on the hydroclimate of western Canada (Shabbar and Skinner, 2004; Gobena

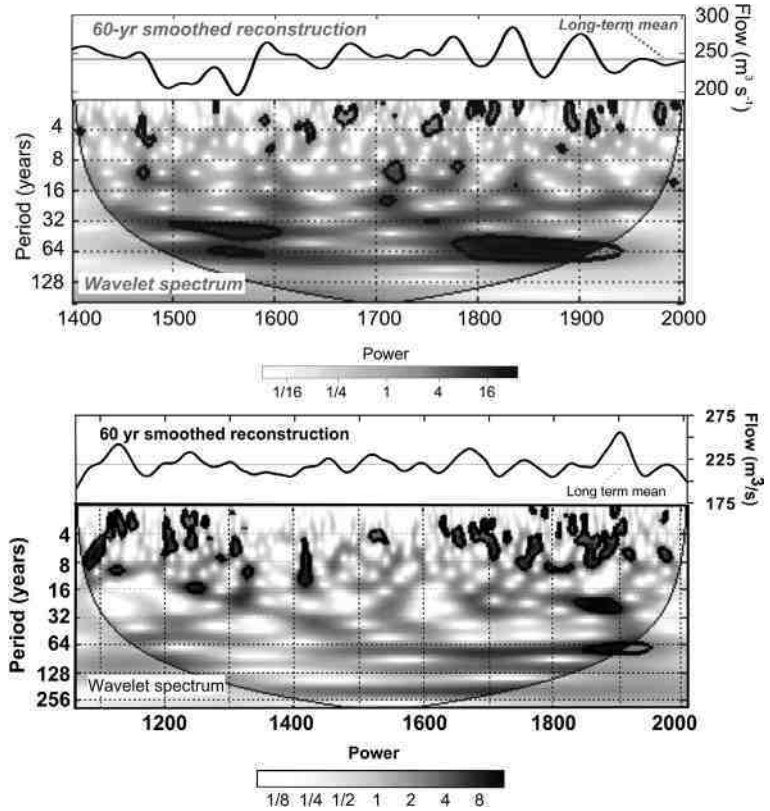

Figure 6. Wavelet power spectrums and a 60-year smoothed reconstruction for the NSR (bottom) and SSR (top). The darkest tones represent the highest spectral power. The heavy black line enclosing a dark shade indicates significance at the 95% level.

and Gan, 2006). Lower frequency variability, reflecting the influence of the Pacific Decadal Oscillation (PDO; Gedalof and Smith, 2001; Gray *et al.,* 2003) is evident in our NSR record but it accounts for a larger proportion of the variance in the SSR reconstruction (Axelson *et al.,* 2009).

Conclusions

By developing a network of new moisture-sensitive tree-ring chronologies in the headwaters of the North Saskatchewan River, we were able to produce a robust reconstruction of streamflow since 1063. Our results are not directly comparable to previous studies of long-term hydrologic variability in the Saskatchewan River Basin (Case and MacDonald, 2003; Axelson *et al.,* 2009), because we used somewhat different methods to create, calibrate, and validate the tree-ring models; however, the timing of severe low flow years and multidecadal mega-droughts are generally similar among the proxy records. They also are similar in terms of the amount of instrumental streamflow variance explained by the tree rings, about 50%, although according to other measures of model skill and validation and signal strength, our new reconstruction, based on tree-ring data from seven sites and two species, provides better estimation of the past annual flows than the prior reconstruction from tree-rings from one site in the watershed. Because much of the unexplained variance is related to the underestimation of high flows, we have more confidence in the interpretation of the low flows, which consistently correspond to narrow tree rings, capturing the timing and duration of drought. Spectral analyses provided evidence that streamflow variability in the upper NSRB is driven primarily by interannual oscillation patterns at 4–8 year frequencies (ENSO), rather than by multidecadal/low frequency forcing such as the PDO, which is more highly correlated with hydrometric records from southern Alberta (St. Jacques *et al.,* 2010). However, oceanic-atmospheric circulation anomalies tend to influence hydroclimate at certain times of the year, so future work on the reconstruction of seasonal flow might produce different results in terms of the modes of variability in summer versus winter. This study of seasonal paleohydroclimate will require sub-annual tree-ring proxies, such as the width and density of the early- and late-wood components of the annual growth increment.

This 945-year reconstruction of the flow of the North Saskatchewan River provides an important context for water managers and policy makers. Research on the consequences of global warming for Canada's western interior suggests a shift in the distribution of runoff between seasons and years, such that there is an expanded range of hydroclimatic variability. These changes are all in relation to the known historical hydrology. If we assume stationarity, and that the historical record captures the envelope of natural variability, future departures from this recorded variability can be ascribed to the impacts of climate change. If we hypothesize, however, that the gauge record, despite its 98-year length, does not capture the full range of natural variability, then future extreme fluctuations partly represent natural variability that exceeds the range measured over the instrumental period. The study described here was able to address this hypothesis by comparing statistical properties, and specifically modes of variability, between the gauge record and a tree-ring reconstruction of the annual flow extending to 1063. The results indicate that the gauge record is comparable to the proxy record in terms of interannual variability, and the frequency of low flows. There is a significant discrepancy at lower frequencies, however, with proxy records displaying more and longer sustained departures from average flow. This interdecadal variability is associated with the most catastrophic climate event, prolonged drought. It also can lead to detection and interpretation of transient streamflow trends, especially in gauge records that are only decades in length. This study demonstrated that expanding the reference hydrology from a century to a millennium changes our understanding of the variability and consistency of water supplies. This longer perspective suggests that there is less certainty and stationarity in western water supplies than implied by the instrumental record, the conventional basis for water resource management and planning.

Acknowledgements

This research was funded by EPCOR Water Services Inc., the Natural Sciences and Engineering Research Council and the Prairie Adaptation Research Collaborative. For field and lab assistance, we thank

Jonathan Barichivich, Michael Felgate, Sarah Ludlow, Golden Gooding, Nataliia Prytula, and Jeannine St. Jacques. We extend a further thank you to Dr. Scott St. George for suggestions and help in the field. Naturalized streamflow data were provided by Alberta Environment.s

References

Axelson, J., D. Sauchyn, and J. Barichivich. 2009. New reconstructions of streamflow variability in the South Saskatchewan River Basin from a network of tree ring chronologies, Alberta, Canada. *Water Resources Research* doi:10.1029/2008WR007639.

Barrow, E. 2010. Climate Change Scenarios for the Prairie Provinces. Chapter 4 in *The New Normal: The Canadian Prairies in a Changing Climate*, ed. D. Sauchyn, H. Diaz, and S. Kulshreshtha, 41–58. Regina: CPRC Press.

Briffa, K. and P. Jones. 1990. Tree-ring standardization and growth-trend estimation. In *Methods of Dendrochronology:Applications in the Environmental Sciences*, ed. E.R. Cook and L.A. Kairiukstis, 137–152. Dordrecht, Netherlands: Kluwer Academic.

Bruce Power. 2008. *Saskatchewan 2020: Clean energy. New opportunity*. Report on Bruce Power's Feasibility Study. Tiverton, ON: Bruce Power, 24 pp.

Case, R., and G. MacDonald. 2003. Tree ring reconstructions of streamflow for three Canadian prairie rivers. *Journal of the American Water Resources Association* 39: 703–716.

Cook, E.R. 1985. *A time series analysis approach to tree-ring standardization*. PhD. Dissertation, University of Arizona, Tucson. 171 pp.

Cook, E. R., K. Briffa, S. hiyatov, and V. Mazepa. 1990. Tree-ring standardization and growth-trend estimation. In *Methods of Dendrochronology: Applications in the Environmental Sciences*, ed. E.R. Cook and L.A. Kairiukstis, 104–123. Dordrecht, Netherlands: Kluwer Academic.

Cook, E., R. Seager, M. Cane, and D. Stahle. 2007. North American drought: Reconstructions, causes and consequences. *Earth-Science Reviews* 81: 93–134.

Edwards, T.W.D., S.J. Birks, B.H. Luckman, and G.M. Macdonald. 2008. Climatic and hydrologic variability during the past millennium in the eastern Rocky Mountains and northern Great Plains of western Canada. *Quaternary Research* 70: 188–197.

Fritts, H.C. 1976. *Tree Rings and Climate*. London: Academic. 567 pp.

Fritts, H.C., J. Guiot, and G.A. Gordon. 1990. Tree -ring standardization and growth-trend estimation. In *Methods of Dendrochronology: Applications in the Environmental Sciences*, ed. E.R. Cook and L.A. Kairiukstis, 178–185. Dordrecht, Netherlands: Kluwer Academic.

Gedalof, Z., and D. Smith. 2001. Interdecadal climate variability and regime scale shifts in Pacific North America. *Geophysical Research Letters* 28: 1515–1518.

Ghil, M. 2002. Advanced spectral methods for climatic time series. *Reviews of Geophysics* 40: 1003, 41 pp., doi:10.1029/2000RG000092

Gobena, A., and T. Gan. 2006. Low-frequency variability in southwestern Canadian streamflow: Links with large-scale climate anomalies. *International Journal of Climatology* 26: 1843–1869.

Gray, S., J. Betancourt, C. Fastie, and S. Jackson. 2003. Patterns and sources of multidecadal oscillations in drought-sensitive tree-ring records from the central and southern Rocky Mountains. *Geophysical Research Letters* 30: doi:10.1029/2002GL016154.

Grinsted, A., J. Moore, and S. Jevrejeva. 2004. Application of the cross wavelet tranform and wavelet coherence to geophysical time series. *Nonlinear Processes in Geophysiology* 11: 561–566.

Haan, C.T. 2002. *Statistical Methods in Hydrology*, 2nd ed. Ames: Iowa State University Press. 378 pp.

Holmes, R. 1983. Computer-assisted quality control in tree-ring dating and measurement. *Tree Ring Bulletin* 44: 69–75.

Hughes, M.K., P.M. Kelly, J.R. Pilcher, and V.C. Lamarche Jr. (Eds.) 1982. *Climate From Tree Rings*. Cambridge, U.K.: Cambridge University Press. 223 pp.

Loaiciga, H.A., L. Haston, and J. Michaelsen. 1993. Dendrohydrology and long-term hydrologic phenomena. *Reviews of Geophysics* 31: 151–171.

Laird, K.R., B.F. Cumming, S. Wunsam, J.A. Rusak, R.J. Oglesby, S.C. Fritz, and P.R. Leavitt. 2003. Lake sediments record large-scale shifts in moisture regimes across the northern prairies of North America during the past two millennia. *Proceedings of National Academy of Sciences* 100: 2483–2488.

Mann, M.E., and J.M. Lees. 1996. Robust estimation of background noise and signal detection in climatic time series. *Climate Change* 33: 409–445, doi: 10.1007/BF00142586.

Meko, D. M. 1997. Dendroclimatic reconstruction with time varying subsets of tree indices. *Journal of Climate* 10: 687–696.

Meko D.M., and C.A. Woodhouse. 2010. Dendroclimatology, dendrohydrology, and water resources management. In *Tree Rings and Climate*, ed. M. Hughes, T. Swetnam, and H. Diaz, 231–262. New York: Springer.

Milly, P. C. D., J. Betancourt, M. Falkenmark, R.M. Hirsch, Z.W. Kundzewicz, D.P. Lettenmaier, and R.J. Stouffer. 2008. Climate change: stationarity is dead: whither water management. *Science* 319: 573–574.

North Saskatchewan Watershed Alliance. 2007. *Current and Future Water Use in the North Saskatchewan River Basin*. Edmonton: NSWA, 30 pp.

North Saskatchewan Watershed Alliance. 2008. *Assessment of Climate Change Effects on Water Yield from the North Saskatchewan River Basin*. Edmonton: NSWA, 57 pp.

Ostrom, C. 1990. *Time Series Analysis: Regression Techniques*. Quantitative Applications in the Social Sciences 07- 009, 2nd ed. Newbury Park, CA: Sage, 96 pp.

Sauchyn, D.J., J. Stroich, and A. Beriault. 2003. A paleoclimatic context for the drought of 1999-2001 in the northern Great Plains. *The Geographical Journal* 169: 158–167.

Sauchyn, D., H. Diaz, and S. Kulshreshtha. 2010. *The New Normal: The Canadian Prairies in a Changing Climate*. Regina: CPRC Press, 400 pp.

Sauchyn, D., M. Demuth, and A. Pietroniro, 2008. Upland Watershed Management and Global Change: Canada's Rocky Mountains and Western Plains. Chapter 3 in *Managing Water Resources in a Time of Global Change: Mountains, Valleys and Flood Plains*, ed. A. Garrido and A. Dinar, 32–49. London: Routledge.

Shabbar, A., and W. Skinner. 2004. Summer drought patterns in Canada and the relationship to global sea surface temperatures. *Journal of Climatology* 17: 2866–2880.

Schindler, D.W., and W.F. Donahue. 2006. An impending water crisis in Canada's western prairie provinces. *Proceedings of the National Academy of Sciences* 103: 7210–7216.

Sridhar, V., D.B. Loope, J.B. Swinehart, J.A. Mason, R.J. Oglesby, and C.M. Rowe. 2006. Large wind shift on the Great Plains during the Medieval Warm Period. *Science* 313: 345–347.

Stahle, D., M. Cleaveland, D. Blanton, M. Therell, and D. Gay. 1998. The lost ecology and Jamestown droughts. *Science* 280: 564–567.

Stahle, D., E. Cook, M. Cleaveland, M. Therrel, D. Meko, H. Grissino-Mayer, E. Watson, and B. Luckman. 2000. Tree-ring data document 16th century megadrought over North America. *Eos* 81: 12, 121.

St. George, S., and E. Nielsen. 2002. Hydroclimatic change in southern Manitoba since A.D. 1409 inferred from tree rings. *Quaternary Research* 58: 103–111.

St. Jacques, J.M., B.F. Cumming, and J.P. Smol. 2008. A 900-year pollen-inferred temperature and effective moisture record from varved Lake Mina, west-central Minnesota, USA. *Quaternary Science Review* 27: 781–796.

St. Jacques, J.M., D.J. Sauchyn, and Yang Zhao. 2010. Northern Rocky Mountain streamflow records: Global warming trends, human impacts or natural variability? *Geophysical Research Letters* 37: L06407, doi:10.1029/2009GL042045.

Szeicz, J., and G. MacDonald. 1996. A 930-year ring-width chronology from moisture-sensitive white spruce (*Picea glauca* Moench) in northwestern Canada. *Holocene* 6: 345–351.

Tian, J., Q. Yang, X. Liang, L. Xie, D. Hu, F. Wang, and T. Qu. 2006. Observation of Luzon Strait transport. *Geophysical Research Letters* 33: L19607, doi:10.1029/2006GL026272.

Watson, E., and B.H. Luckman. 2006. Long hydroclimate records from tree-rings in western Canada: Potential problems and prospects. *Canadian Water Resources Journal* 31(4): 205–228.

Wheaton, E., S. Kulshreshtha, V. Wittrock, and G. Koshida. 2008. Dry times: hard lessons from the Canadian drought of 2001 and 2002. *Canadian Geographer* 52: 241–262.

Woodhouse, C.A., S.T. Gray, and D.M. Meko. 2006. Updated streamflow reconstructions for the Upper Colorado River basin. *Water Resources Research* 42(5): W05415, doi: 10.1029/2005WR004455.

World Wildlife Fund. 2009. *Canada's Rivers at Risk: Environmental Flows and Canada's Freshwater Future*. Toronto: WWF Canada, 17 pp.

Elsevier Editorial System(tm) for Quaternary International
Manuscript Draft

Manuscript Number:

Title: Forcing of Hydroclimatic Variability in the Northwestern Great Plains since 1406

Article Type: PACLIM 4

Keywords: Dendrochronology; El Niño-Southern Oscillation (ENSO); Pacific Decadal Oscillation (PDO); Palmer Drought Severity Index (PDSI); 500 hPa Geopotential Heights

Corresponding Author: Ms. Suzan Lapp,

Corresponding Author's Institution:

First Author: Suzan L Lapp

Order of Authors: Suzan L Lapp; David J Sauchyn; Jeannine-Marie St. Jacques; Jessica R Vanstone

Abstract: The 20th century hydroclimatology of northwestern North America has been linked to naturally recurring large-scale climate patterns such as the Pacific Decadal Oscillation (PDO) and the El Niño-Southern Oscillation (ENSO). Few hydroclimatic records from this region exceed in length the ~60-year periodicity of the lower frequency oscillations; however, tree-ring proxy data from semiarid western North America document natural hydroclimate variation over centennial to millennial scales. A reconstruction of the summer Palmer Drought Severity Index (PDSI) over the northwestern Great Plains provides a record of drought for the past 600 years. We examine these long reconstructions for embedded information about the severity, intensity, and duration of positive (wet) and negative (dry) summer moisture anomalies during the different phases of the PDO and the ENSO, as reconstructed from independent proxy datasets. As well, by comparing our moisture reconstructions to other researchers' independent regional summer temperature reconstructions, we were able to identify warm/cool drought/pluvial periods. The reconstruction is also compared to 500 hPa geopotential heights; these results further imply that summer moisture conditions are associated with the North Pacific Ocean and the Tropical Pacific Ocean variability. Summer drought events have frequently been coupled with the positive PDO signature phase pattern; however, ENSO conditions have varied between the El Niño and the La Niña phases. The most severe droughts, such as the 1858-1872 and 1930-1941 events, were commonly associated with higher summer temperatures, the positive phase of the PDO, and increased ENSO variability.

August 21, 2011

Dear Dr. Starratt,

Please receive our manuscript, "Forcing of Hydroclimatic Variability in the Northwestern Great Plains since 1406", for consideration for the 2011 PACLIM issue of Quaternary International. The hydroclimate variability of the Pacific North America is influenced by large-scale climate patterns, particularly the Pacific Decadal Oscillation (PDO) and the El Niño-Southern Oscillation (ENSO). These hydroclimatic fluctuations, at inter-annual to multi-decadal timescales, have been associated with severe floods and droughts causing extreme damage and economic hardship throughout the 20th century instrumental record. Water managers in the northern Prairies have great interest in extreme drought and pluvial climatology given the historical impacts of these events, and projections of increased frequency and severity associated with human induced climate change. In this manuscript, we reconstruct summer moisture conditions for the past six centuries using tree-ring data from the eastern Rocky Mountains of Alberta and Montana. Extreme drought and pluvial events were identified by exploring the frequency, severity, intensity, and duration of positive (wet) and negative (dry) moisture anomalies. We were particularly interested in the relation between the summer moisture anomalies and the PDO phase and the ENSO phase and variability. We believe that our manuscript will be a useful contribution to the pre-instrumental natural hydroclimatic variability and provide insight into water management decision-making and adaptation.

Thank you,

Suzan Lapp
Prairie Adaptation Research Collaborative
University of Regina
Regina, Saskatchewan

Forcing of Hydroclimatic Variability in the Northwestern Great Plains since 1406

Suzan L. Lapp[1*], David J. Sauchyn[1], Jeannine-Marie St. Jacques[1] and Jessica R. Vanstone[1]

[1] Prairie Adaptation Research Collaborative (P.A.R.C.), Room 120, 2 Research Drive, University of Regina, Regina, Saskatchewan, Canada, S4S 7H9

*Corresponding author: lapp200s@uregina.ca.

Abstract

The 20th century hydroclimatology of northwestern North America has been linked to naturally recurring large-scale climate patterns such as the Pacific Decadal Oscillation (PDO) and the El Niño-Southern Oscillation (ENSO). Few hydroclimatic records from this region exceed in length the ~60-year periodicity of the lower frequency oscillations; however, tree-ring proxy data from semiarid western North America document natural hydroclimate variation over centennial to millennial scales. A reconstruction of the summer Palmer Drought Severity Index (PDSI) over the northwestern Great Plains provides a record of drought for the past 600 years. We examine these long reconstructions for embedded information about the severity, intensity, and duration of positive (wet) and negative (dry) summer moisture anomalies during the different phases of the PDO and the ENSO, as reconstructed from independent proxy datasets. As well, by comparing our moisture reconstructions to other–researchers'–independent regional summer temperature reconstructions, we were able to identify warm/cool drought/pluvial periods. The reconstruction is also compared to 500 hPa geopotential heights; these results further imply that summer moisture conditions are associated with the North Pacific Ocean and the Tropical Pacific Ocean variability. Summer drought events have frequently been coupled with the positive PDO signature phase pattern; however, ENSO conditions have varied between the El Niño and the La Niña phases. The most severe droughts, such as the 1858-1872 and 1930-1941 events, were commonly associated with higher summer temperatures, the positive phase of the PDO, and increased ENSO variability.

Keywords: Dendrochronology, El Niño-Southern Oscillation (ENSO), Pacific Decadal Oscillation (PDO), Palmer Drought Severity Index (PDSI), 500 hPa Geopotential Heights

1 Introduction

Numerous studies have shown significant associations between teleconnections, specifically the Pacific Decadal Oscillation (PDO), the El Niño-Southern Oscillation (ENSO), and the North Atlantic Oscillation (NAO) and variations in the 20th century Pacific North American hydroclimate (Mantua and Hare, 2002; MacDonald and Case, 2005; Bonsal et al., 2006; Nyenzi and Lefale, 2006; Ault et al., 2010; St. Jacques et al., 2010). These hydroclimatic fluctuations at inter-annual to multi-decadal timescales have been associated with severe floods and droughts causing extreme damage and economic hardship throughout western North America (Wheaton et al., 2005; Garnett, 2006; Cook et al., 2007; Gan et al., 2007; Bonsal et al., 2011). The single year extreme drought/pluvial events are damaging but are not necessarily good indicators of the cumulative environmental and socioeconomic impacts. The critical indicator is duration, since recovery from the cumulative damage from an extreme multi-year event is more challenging than from a single-year event (Wheaton et al., 2005; Cook et al., 2007; Marchildon et al., 2008). Extreme drought and pluvial climatology are of substantial relevance in the northern Prairies given the historical impacts of these events, and projections of increased frequency and severity associated with human induced climate change (Bonsal et al., 2011).

The PDO is a re-occurring sea surface temperature (SST) anomaly pattern that describes a large amount of the extra-tropical North Pacific Ocean variability (Mantua et al., 1997; Zhang et al., 1997; Mantua and Hare, 2002). The positive (negative) PDO phase has anomalously warm (cold) SSTs off the west coast of North America and a deepened (weakened) Aleutian Low, resulting in decreased (increased) winter precipitation throughout the Pacific Northwest (Mantau et al., 1997; St. Jacques et al., 2010; Bonsal et al., 2011). The ENSO is defined by two metrics 1) the Southern Oscillation Index (SOI) (*i.e.*, the normalized difference between monthly mean sea level pressure (SLP) at Tahiti and Darwin) (Ropelewski and Jones, 1987), and 2) the SST anomalies throughout the tropical Pacific Niño region (5°N-10°S, 170°W-80°W) (Smith and Reynolds, 1998). The El Niño (La Niña) phase of ENSO typically has the same association with winter climate in the Pacific Northwest as the positive (negative) phase of the PDO (Cayan et al., 1999; St. Jacques et al., 2010; Bonsal et al., 2011). Typically there are more occurrences of El Niño (La Niña) events during the positive (negative) phase of the PDO. The atmospheric planetary-scale waves determine the variations of these interactions between the atmosphere and ocean on large scales (i.e., teleconnections) (Trenberth and Hurrell, 1994); rather than using the PDO as the only metric for measuring the Pacific climate variability, the ENSO and the North Pacific Index (NPI; Aleutian Low) should also be considered as other key physical variables (IPCC4, 2007). The strength of the Aleutian Low pressure system co-varies with the North Pacific SST anomalies (IPCC4, 2007) by shifting the storm track and impacting the downstream climate (Trenbeth and Hurrell, 1994); the deepened (weakened) Aleutian Low shifts the storm track to the north (south). The interaction between the pentadecadal (50-70 years) and the bidecadal (15-25 years) variations modulate the winter and spring variability of the Aleutian Low, with the pentadecadal variability controlling the basin regime timescale shifts and the bidecadal variability controlling the rate of transition between the regimes (Minobe, 1999). There is a close link between the extra-tropical North Pacific Ocean changes at the decadal time scale to those at the inter-annual time scale in the tropical Pacific and Indian Ocean, via an 'atmospheric bridge' (Vimont et al., 2001), that impacts climate in North America, particularly around the North Pacific basin (Trenberth and Hurrel, 1994; Power et al., 1999; Salinger et al., 2001; McGregor et al., 2010).

The teleconnections between ENSO and the climate of the Pacific Northwest are well established for the instrumental period. Similarly, the influence of the PDO is also documented, but the instrumental period encompasses only about 1.5 full cycles of this low-frequency oscillation and therefore, is unable to provide a robust assessment of the variability at the lower frequency oscillations (IPCC4, 2007). Tree-ring proxy data from the semiarid, western North America record natural hydroclimate variation over centuries to millennia (Biondi et al., 2001; Gedalof et al., 2002; MacDonald and Case, 2005; Axelson et al., 2009). Tree-rings provide both climate information and an absolute annual chronology. At dry sites tree growth is limited by the available soil moisture, enabling the reconstruction of hydroclimatic variables: precipitation (Watson and Luckman, 2004, 2005a), streamflow (Case and MacDonald, 2003; Watson and Luckman, 2005b; Axelson et al., 2009), forest fire frequency and area burned (Giardin and Sauchyn, 2008), and drought (Sauchyn and Skinner, 2001; Sauchyn et al., 2003; Giardin et al., 2006; Cook et al., 2007; St. George et al., 2009). Multi-year megadroughts of the 12th and 13th century, identified in paleoclimatic records (Woodhouse, 2004; Cook et al., 2007), are of greater magnitude and sustained duration compared to the recent 20th century events that lasted at most a decade. Dendroclimatology has also contributed to the study of the inter-annual to multi-decadal natural climate variations associated with the large-scale teleconnections (Woodhouse, 1997; Gedalof and Smith, 2001; Hughes, 2002; Mantua and Hare, 2002). These proxy records reflect: 1) the inter-annual to multi-decadal variability of frequency and amplitude in summer/annual moisture captured by moisture sensitive tree-rings over the past millennium; 2) the correlation between periodicity in the tree-ring records and known large-scale drivers of climatic variability; and, 3) the frequency, severity, and duration of periods of sustained low and high moisture conditions.

Because recurrent drought excludes trees from the northern Great Plains (with the exception of a few island forests), the tree-ring record of hydroclimate is mostly inferred from sites along the forested margins of this region. St. George et al. (2009) drew conclusions about the history and forcing of drought from a collection of sites that border the northern plains, from the dry eastern slopes of the Rocky Mountains, to the humid eastern boreal forest. Tree-rings in the northern Prairie region are best for reconstructing spring/summer moisture conditions (St. George et al., 2009; St. George et al., 2010); however, antecedent winter precipitation has a significant impact on the spring/summer moisture conditions in these northern latitudes (Hamlet et al., 2007). St. George et al. (2009) found no apparent relationship between the regional tree-ring chronologies and the ENSO or the PDO, most likely due to their insensitivity to the winter precipitation signals associated with these teleconnections; however, we explore this in further detail. In this paper, we examine the hydroclimatic variability (drought and pluvials) of the past 600 years over the northwestern Great Plains region, by reconstructing the June-July-August (JJA or summer) Palmer Drought Severity Index (PDSI) using a network of moisture-sensitive tree-ring chronologies. This study's multi-centennial reconstruction of the regional hydroclimate complements the recent work by St. George et al. (2009), who developed a tree-ring record of drought across the three Canadian Prairie Provinces, by exploring the frequency, severity, intensity, and duration of positive (wet) and negative (dry) moisture anomalies in greater detail. We focused on the western margin of their study region, where: 1) the tree-ring chronologies have the greatest length, approaching 1000 years (Sauchyn et al., *in press*); 2) the signal of SST forcing is most evident (St. Jacques et al., 2010); and, 3) the water supply for majority of the population of the Prairie Provinces is generated. We were interested in the relation between the summer moisture anomalies and the Pacific Ocean teleconnection patterns, in particular the PDO

phase and the ENSO phase and variability. By comparing our moisture reconstruction to an independent mean summer temperature reconstruction, based on maximum latewood density and ring width (Luckman and Wilson, 2005), we also identified warm/cool drought/pluvial periods.

2 Methods

2.1 Palmer Drought Severity Index

The Palmer Drought Severity Index (PDSI) is a index of meteorological drought widely used in North America. It is calculated using monthly temperature and precipitation data and the soil Available Water Content (AWC) to express the cumulative departure of moisture supply (Palmer, 1965; Keyantash and Dracup, 2002). It is a standardized index that allows comparisons between different geographical locations and months (Palmer, 1965). This index is preferred to indices based solely on precipitation, as it has considerable month-to-month persistence and better represents the basic terms of the water balance, including evapotranspiration, soil recharge, runoff, and surface moisture loss (Alley, 1984). Long-term drought (pluvial) is cumulative, so the intensity during the current month is dependent on the current weather patterns plus the antecedent conditions of previous months. PDSI is derived by including one third of the current month's precipitation deficit (surplus) and almost nine-tenths of the previous month's value (Guttman, 1998). For this reason, the PDSI is effective in capturing the cumulative effect of long-term drought or pluvial events. The index typically varies between -4.0 and 4.0, with values below -0.49 but greater than -1.0 (above 0.49 but less than 1.0) considered an "incipient dry spell" ("incipient wet spell"); -1.0 (1) is the threshold value of an actual drought (pluvial) event (Table 1).

JJA PDSI was calculated for the 1901-2005 period using the observed monthly baseline historical gridded (0.5^{o}) precipitation and temperature climate data generated by the Canadian Forest Service (McKenney et al., 2006). Global AWC was available, on 0.5^{o} grid in millimetres (mm) of water per one metre soil depth, from the Oak Ridge National Laboratory Distributed Active Archive Center (ORNL DAAC) (Batjes, 2000) (http://daac.ornl.gov).

2.2 Tree-ring data and study area

Researchers at the University of Regina Tree-Ring Laboratory have established a network of tree-ring chronologies that extends across the montane forest of the northern Rocky Mountains, and the island forests of the northern Great Plains (i.e., Alberta, Saskatchewan, and Montana; Figure 1). Because the western interior of North America has a semiarid climate and the sampled trees are growing on dry sites (south- and west-facing slopes, sandy soils, and ridge crests), there is a strong correlation between the moisture-sensitive tree-ring chronologies and the PDSI. We used chronologies located along the eastern slopes of the southern Canadian Rocky Mountains, which are the oldest in our collection, and this region is the headwaters of the Saskatchewan and Missouri Rivers.

In total 28 chronologies were either within or near the study region ($46\text{-}52^{o}$N and $105\text{-}116^{o}$W) and significantly correlated ($p \leq 0.05$) with the JJA PDSI regional average (Table A.1 and Figure 1). Residual and standard tree-ring chronologies were included initially; however, the highest correlations were found using the standard chronologies. The chronologies were

detrended using the program ARSTAN (Cook, 1985) and standardized using a 100-year cubic spine (50% cutoff) to maintain low frequency variability (Cook, 1985; St. George et al., 2009). Subsample Signal Strength (SSS) was computed as a function of mean inter-tree correlation and sample size (Briffa and Jones, 1990). A SSS equal to or greater than 0.85 was used as the threshold for truncating the time series at a sample depth for a reliable chronology (Cook and Kairiukstis, 1990). The chronologies ranged in length from 116 to 990 years.

Principal Component Analysis (PCA) of the covariance matrix yielded an orthogonal set of new variables (Meko et al., 2007; St. George et al., 2009) derived from the 28 standard chronologies over the common period of 1901-2005. Any chronologies that did not span to 2005 were extended using the mean value from the remaining chronologies (Kim and North, 1993). This produced a first principal component (PC1) that explained 58% of the variance over the common period. Then we removed the next shortest chronology, repeated the PCA on the remaining chronologies, and compared that PC1 to the common period PC1. This procedure was repeated until PC1 no longer shared the same signal as the common period PC1 (i.e., the Pearson correlation coefficient $r < 0.9$). The final reduced PC1 consisted of five chronologies (Table 2) and was highly correlated ($r = 0.93$) to the common period PC1. Using PCA produced the longest possible reconstruction with the least number of chronologies, yet maintained the same key information as the initial 28 sites. This PC1 spanned the years 1406-2005 AD and explained 52.5% of the total variance. PC2 explained 25.4% of the variance and correlated with the common period PC2 ($r = 0.85$). Throughout the rest of this manuscript PC1 and PC2 refer to the 1406-2005 AD tree-ring chronologies.

Two other study regions were defined by including the JJA PDSI gridcells (1901-2005) that significantly ($p \leq 0.01$) correlated with the 1901-2005 AD interval of PC1 and PC2. The PC1 study region coincided with the North and South Saskatchewan River Basins, and Milk River sub-basin of the Missouri River Basin (Figure 1a). The PC2 study region included areas of southern Alberta, southeastern Montana, and western North and South Dakota (Figure 1b). A regional average was then calculated using those gridcells that significantly correlated with PC1 and PC2 for the 1901-2005 period. Each study region average was reconstructed using linear regression: PC1 JJA PDSI = (PC1 * 0.6944 - 0.5306) ($r = 0.70$; S.E. = 1.26; RE = 0.47) (Figure 2a), and PC2 JJA PDSI = (PC2 * 0.8103 + 0.0096) ($r = 0.44$; S.E. = 1.78; RE = 0.17) (Figure 2b). The labels PC1 JJA PDSI and PC2 JJA PDSI will refer to the reconstructed regional averages correlated with PC1 and PC2, respectively, from 1406-2005 AD.

2.3 Additional Proxy and instrumental climate data

The latest Luckman and Wilson (2005) mean summer (May-August) temperature reconstruction for the south/central Canadian Rockies utilized new and multiple tree-ring sites spanning 950-1994 AD. This updated reconstruction remains the longest from the Canadian Rockies, providing a more regional representation than previously developed essentially from a single site. They also identified the most extreme warm and cool, non-overlapping, 20-year intervals as calculated from the mean summer temperature reconstruction relative to the 1900-1980 period. This temperature reconstruction was used to define sustained warm and cool periods in relation to drought and pluvial episodes.

There are numerous PDO reconstructions using tree-ring chronologies from the Pacific Northwest and subtropical North America (Biondi et al., 2001; D'Arrigo et al., 2001; Gedalof and Smith, 2001; MacDonald and Case, 2005; D'Arrigo and Wilson, 2006). The MacDonald and Case (2005) PDO index reconstruction was the longest, dating from 993-1996 AD. It also was the only reconstruction significantly ($p \leq 0.05$) correlated with PC1 (results not shown); very likely it was derived from a single chronology (Whirlpool Point) located in our study area. Because our tree-ring data included a chronology from the same site, we also used the Verdon and Franks (2006) Composite PDO Index derived from various PDO proxies and instrumental PDO indices spanning 1662-1998 AD. Step changes in this Composite PDO index signify a switch from a predominately positive to a predominately negative phase period. We also used the observed November-March averaged PDO index for the 1901-2005, as described by Lapp et al. (2011), and following the Mantua et al. (1997) methodology.

Numerous ENSO reconstructions have also been derived from networks of tree-ring chronologies (Cook et al., 2000; Cook et al., 2008) and multi-proxy indicators (Mann et al., 2000) influenced by ENSO. McGregor et al. (2010) has consolidated the common ENSO signal from previously defined proxy reconstructions into a Unified ENSO Proxy (UEP) spanning 1650-1977 AD. These ENSO reconstructions are significantly ($p \leq 0.05$) correlated with each other, therefore, we used the longest (1300-1978 AD) and most up-to-date Cook et al. (2008) Niño 3.4 index reconstruction. We also used the instrumental December-March Niño 3.4 index (5^{o}S-5^{o}N, 120^{o}W-170^{o}W) for the 1872-2005 period (Trenberth and Stepaniak, 2001) (http://www.cgd.ucar.edu/cas/catalog/climind/TNI_N34/index.html) to maintain a consistent ENSO phase sign with the UEP and Cook et al. (2008) reconstruction. El Niño events were defined by a positive UEP and Niño 3.4 index and La Niña events as a negative UEP and Niño 3.4 index. The reconstructed data were obtained from the World Data Center for Paleoclimatology (www.ncdc.noaa.gov/paleo/paleo.html).

To explore the stability of the link between climate forcing and tree-ring response through time, 31-year running correlations were calculated with the PCs' and the reconstructed MacDonald and Case (2005) PDO and Cook et al. (2008) Niño 3.4 indices over the 993-1996 AD and 1406-1978 AD periods, respectively. The instrumental November-March PDO and December-March Niño 3.4 indices were used to extend the running correlations to 2005. All correlation values were adjusted for autocorrelation using the effective sampling size for the correlation coefficient (Dawdy and Matalas, 1964).

Given the relationship between the hydroclimate of the study region and the large-scale teleconnection indices, we also explored the physical dynamics associated with each PC. Correlation maps were derived between PC1 and PC2 and the average December-March (winter) and May-August (summer) gridded 500 hPa geopotential heights, for the 1948-2005 period, using the NCEP Reanalysis Derived data and software (NOAA/OAR/ESRL PSD, Boulder, Colorado, USA, from their Web site at http://www.esrl.noaa.gov/psd/) (Kalnay et al., 1996).

2.4 Runs analysis to define drought events

Typically tree-ring reconstructions of hydroclimate have focused on drought since water shortages are a major and widespread climate hazard. However, extreme pluvial events also have socio-economic and environmental consequences, and therefore, are characterized in this study. We used runs analysis (Dracup et al., 1980; Meko et al., 1995; Biondi et al., 2005) to categorize multi-year drought/pluvial events according to their duration, intensity, and severity. Duration is the number of consecutive years (n) (Biondi et al., 2005) the PDSI remained below (above) a certain threshold value (X_o). The severity of the drought (pluvial) is the run-sum (sum of the deficits below (above) the X_o over the n years), and intensity is the average deviation from X_o (severity/duration). This analysis allowed us to rank events and identify the underlying persistent climate modes associated with extreme hydroclimatic events (Biondi et al., 2005). A PDSI of -0.49 (0.49) was chosen as the drought (pluvial) threshold value. Drought tends to be more prolonged than periods of excess water (Bonsal et al., 2011); therefore, drought (pluvial) events were considered extreme if they persisted for five (three) years or longer. If a drought of five years or longer included one or more non-successive year(s) with a PDSI greater than -0.49 but less than 0, then these were still considered drought years and were included in the total run-sum (severity) calculation. This same method was applied to pluvial events exceeding the three year baseline. The PDO phase and ENSO phase and variability were characterised for each drought/pluvial event. The MacDonald and Case (2005) PDO and the Composite PDO indices were compared and used to identify the dominant PDO phase for their period of record up to 1900, and the observed November-March PDO index was used for the 1901-2005 period. The ENSO phase was characterized for the preceding year and each year of the event using a threshold level of 0.4^{o}C to define strong ENSO events (Trenberth, 1997). For their period of record up to 1871, both the Cook et al. (2008) Niño 3.4 index and the UEP reconstructions were used to ensure consistency, and the December-March Niño 3.4 index was used for the 1872-2005 observed period. To assess changes in ENSO variability the variance was calculated using a sliding 17-year window of the Cook et al. (2008) index.

2.4 Spectral analysis methods

Multi-taper method (MTM) spectral analysis (Thomson, 1982; Ghil et al., 2002) and Morlet Wavelet Analysis (Grinsted et al., 2004) were applied to the PCs to identify dominant modes of variability. In the SSA-MTM Toolkit for MTM Spectral Analysis (http://www.atmos.ucla.edu/tcd/ssa/), we used Adaptively weighted spectra with a red noise background (three tapers) (Mann and Lees, 1996). The Wavelet Analysis was conducted in MATLAB® (http://www.pol.ac.uk/home/research/waveletcoherence/). We were primarily interested in the frequency variability at periodicities characteristic of the PDO (~20 and ~60 years) (Minobe, 1997, 1999; Chao et al., 2000) and the ENSO (2-7 years) (Rasmussen and Carpenter, 1982; Trenberth, 1997). The North Atlantic Oscillation (NAO) (Wallace and Gutzler, 1981) also influences the hydroclimate of northwestern North America (Bonsal et al., 2001; St. Jacques et al., 2010); however, to differentiate its frequency (2-10 years) (Hurrell and Deser, 2009) from the ENSO frequency is problematic. MTM analysis was also conducted on the 28 individual tree-ring chronologies to explore their capacity to capture the PDO- and ENSO-like spectrum and to confirm the regional hydroclimatic impact associated with the large-scale circulation patterns.

3 Results

Runs analysis of the PC1 JJA PDSI over the past six centuries detected droughts that were more extreme in severity, intensity, and duration than those recorded during the instrumental period (Table 3). The 1858-1872 drought was the most severe, followed by 1930-1941, and the 1483-1494 events (Table 3 and Figure 3). The drought of the 1720's (1717-1721) ranks seventh in severity but was the most intense (-2.4); thus, the longest sustained drought was not the most severe. Recent drought intervals in the instrumental period include 1918-1926, 1930-1941, 1956-1963, 1983-1989 and 2000-2004. The dominant PDO phase was consistent between the MacDonald and Case (2005) and the Composite PDO reconstructions for all droughts except the 1755-1761 and 1858-1872 events. Of the 24 drought events in the full proxy record, eighteen (six) occurred during the positive (negative) PDO phase based on the MacDonald and Case (2005) reconstruction. The 2000-2004 drought was unique, as it was not predominantly in the positive PDO phase, rather, the PDO index waxed and waned between the positive and negative phases during the event. The 1717-1721 drought was the only event where the Cook et al. (2008) and the UEP index reconstructions disagreed (results not shown); the Cook et al. (2008) reconstruction defined this event as having more occurrences of La Niña than El Niño. The most severe drought and longest in duration (1858-1872), occurred during the positive PDO phase (MacDonald and Case, 2005) and had more occurrences of La Niña than El Niño. However, the next three droughts, ranked by severity, occurred during the positive PDO phase and had more occurrences of El Niño than La Niña. Droughts were more likely to be preceded with a La Niña or neutral phase rather than an El Niño phase and there was no precedence for which ENSO phase initiated the drought. During the period of the instrumental Niño 3.4 index there were six droughts, five of which had an equal or greater number of occurrences of La Niña or neutral phase events than El Niño's. The pre-instrumental period had 18 droughts, of which 14 had an equal or greater number of La Niña or neutral phase events than the number of El Niño's. High (low) ENSO variability coincided with 15 (9) drought events; the five most severe droughts occurred during periods of high ENSO variability (1483-1494, 1717-1721, 1791-1800, and 1930-1940).

The 18th and 20th centuries each had four pluvial events, constituting them as the wettest centuries of the entire reconstruction (Table 4). The most severe pluvial occurred from 1826-1830, the second from 1668-1676, and the third from 1900-1905; the next fourth through sixth ranked extreme events occurred during the 18th century. The PDO reconstructions were coherent for all pluvials except the 1826-1830 event. In total there were seven (eight) events that occurred during the positive (negative) phase of the PDO, based on the MacDonald and Case (2005) reconstruction. Pluvial events typically had more occurrences of the La Niña or neutral phases than El Niño phases. However, the frequency of El Niño was higher during the positive PDO phase events of 1550-1554 and 1993-1996, and the negative PDO phase events of 1826-1830 (severest pluvial), 1900-1905, and 1953-1955. There was no prevailing ENSO phase that preceded the pluvials; five events were preceded with a La Niña, three with a neutral, and seven with an El Niño phase. Also, there was no consistent ENSO phase that initiated the first year of the pluvial events. ENSO variability appears to have little impact; eight pluvials were associated with low variability, including the two most extreme events, and seven events with high variability.

The majority of the droughts occurred during warm periods (e.g. 1559-1583, 1717-1721, and 1858-1872), although not always during an extreme warm interval (Figure 3). All of the 20th century droughts occurred during, or partially overlapped, an extreme warm interval. The droughts of the mid-to-late 1400's and early 1500's, and the 1811-1815 event occurred during three of the most extreme cool intervals of 1456-1475, 1481-1500, and 1799-1818, respectively, and coincide within the Spörer and Dalton solar minima's. Overall, the pluvial periods occurred during cool periods; four (1469-1471, 1668-1676, 1693-1695, and 1826-1830) occurred during extreme cool intervals and the 1709-1711 event followed the Maunder Minima. Although the 1724-1750 period did not include three consecutive wet years (PDSI > 0.49), it was wet and occurred during the 1727-1746 extreme cool interval. The early 20th century (1900-1910) pluvial period was relatively warm compared to the entire time series mean; however, it was relatively cool compared to the 1900-1980 mean, reflecting the increasing average temperature since the 1850's. The 1953-1956 pluvial was the only event that occurred during an extreme warm interval (Luckman and Wilson, 2005).

PC1 captured the characteristic spectrum of the PDO: the lowest frequency pentadecadal periodicity, the low-frequency bidecadal periodicity, and the higher frequency variability in the ENSO band of 2-7 years (Minobe, 1999) (Figure 4). Low frequency variability was reduced around the latter half of the 1700's when temperatures alternated between cool and warm decades (Luckman and Wilson, 2005). PC2 also captured some of the low frequency pentadecadal (~50 year) and bidecadal (22-35 years) periodicity, but more of the high frequency variability in the ENSO bands than PC1. Both PC's captured a significant 13-year band of variability. From MTM spectral analysis conducted on each of the 28 tree-ring chronologies, we concluded that those with sufficient length (>150years) detected all three frequency bands and the short chronologies (<150 years) detected the ENSO and the higher PDO frequency bands (results not shown).

The spatial correlation of PC1 and PC2 with the average gridded December-March (winter) and May-August (summer) seasonal 500 hPa heights are shown in Figure 5. Negative (positive) correlations imply high (low) 500 hPa heights associated with drought events; the opposite correlations would be associated with pluvial events. During the winter season the PC1 drought conditions are associated with a ridge of high pressure originating off the west coast of North America that extends over the Pacific Northwest and south over the southeastern United States. Low pressure is located over the North Pacific Ocean and off the west coast of Mexico. During the summer season, the PC1 drought conditions are associated with high pressure located over western North America, that encompasses the study region; low pressure is located in the eastern North Pacific Ocean and continues north of the high pressure system and then south along the east coast of North America. The PC2 drought conditions are associated with high pressure off the west coast of North America and over the Gulf of Mexico; low pressure is found over northern Canada, off the east coast of Canada, and over the tropics during the winter season (Figure 5). During the summer season the high/low pressure areas are shifted westward relative to their winter positions, with the regions over eastern Canada and the tropics heightened in amplitude and the others weakened in amplitude.

The strength and sign of the running correlations vary throughout the reconstruction according to the phases of ocean-atmosphere oscillation (Figure 6). The running correlations of the PCs' with the PDO are inconsistent (Figure 6a). PC1 predominantly has a negative

relationship with the PDO and weak positive correlations dispersed throughout the reconstructed time period. Significant ($p \leq 0.10$) correlations occurred during 1650-1700, 1850-1880, 1920-1930, and ~1950. PC2 overall has a weak positive correlation with the PDO index and interspersed periods of weak negative correlations. The running correlations of PC1 and PC2 with the ENSO index also oscillationed between periods of significantly positive correlations and significantly negative correlations (Figure 6b). PC1 and PC2 have similar correlations with ENSO during 1700-1740, shifting from a slightly positive to a significantly negative and back to a slightly positive correlation, and during 1825-1910 the correlations shifted from significantly positive to virtually no relationship. Opposite correlations existed during: 1675-1700 when PC1 (PC2) had a negative (positive) correlation; 1740-1825 when PC1 (PC2) had a significant negative correlation (no correlation to positive correlation); and, 1910-1960 when PC1 (PC2) shifted towards a significantly negative (positive) correlation with ENSO.

4 Discussion

In this paper we reconstructed the annual hydroclimate (PDSI) in the northwestern Great Plains over the last six centuries using the first two-leading PC's, from the five longest tree-ring chronologies. This study's in-depth analysis of drought and pluvial periods demonstrates the complexity of the linkages between the large-scale teleconnections, specifically the PDO and the ENSO, and the associated hydroclimate variability in the eastern Rocky Mountains of southern Alberta and northern Montana (Figure 1). These results are consistent with the shorter eastern Rockies summer PDSI reconstruction (St. George et al., 2009) and a South Saskatchewan River reconstruction (Axelson et al., 2009). Our summer PDSI reconstruction also closely corresponds to the growth season atmospheric relative humidity (RH) reconstructions from the Columbia Icefield area in the eastern Rocky Mountains, by Edwards et al. (2008), over the past 1000 years. Using this RH reconstruction and previous temperature and streamflow reconstructions they determined glacial expansion occurred during the periods of ~1450-1500 (Wolfe et al., 2008), ~1590-1610, ~1700-1710, and ~1810-1860 AD. These glacial expansions also coincided with cool mean summer temperatures (Luckman and Wilson, 2005). The decline in RH in the ~1450-1500 and ~ 1810-1860 periods align with our summer PDSI reconstruction (Figure 3); the onset of each period is pluvial, corresponding with higher RH, and progressed to drought conditions, corresponding with lower RH. The spike ~1600 and dip ~1700-1710 in RH also corresponded to our pluvial and drought events. The relatively cold and dry atmospheric conditions of the Little Ice Age (LIA) (~1530-1980 AD) were caused by an intensified meridional circulation and strengthened Aleutian Low (Edwards et al., 2008), resulting in a lack of warm Pacific air masses in relation to cool Arctic air masses, as suggested by the suppressed PDO variability (MacDonald and Case, 2005) and negative NAO index (Cook et al., 2002). Outbreaks of the warm Pacific air masses and enhanced North Pacific Ocean variability (Macdonald and Case, 2005) are connected to the pluvial events during this period. The most recent drought of 2000-2004 has also been considered anomalously cool compared to other droughts in the instrumental period (Bonsal et al., 2011); however, in the reconstructed context it was common.

Spectral and wavelet analysis revealed dominant modes of variability in the tree-ring series at the pentadecadal and bidecadal periodicities characteristic of the PDO and the ENSO (2-7 years) (Figure 4). The lack of low frequency variability between 1700 and 1850, as shown in the wavelet analysis, corresponds to a northward migration of the Inter-tropical Convergence Zone (Sachs et al., 2009). Temperatures around the latter half of the 1700's alternated between

cool and warm decades (Luckman and Wilson, 2005), and also may have contributed to the lack of low-frequency variability.

The winter 500 hPa heights associated with drought resembles the positive phase of the NPI, with a deepened Aleutian low and a stronger northward flow (Trenberth and Hurrell, 1994; Bonsal et al., 2001) and El Niño like atmospheric circulation (Lau, 1997; Yu and Zwiers, 2007) (Figure 5). The tree-ring chronologies capture the lower frequency winter precipitation variability associated with the North Pacific Ocean. The summer meridional circulation pattern concurrent with dry periods (Figure 5) is associated with an amplified mid-tropospheric ridge and trough pattern, resulting in the western directed flow northward of the Prairie region (Bonsal et al., 1999). One weakness in using NCEP Reanalysis derived data is the short period of record (1948-2005), as shown by the varied temporal correlations with the reconstructed PDO index (Figure 6) demonstrating the inconsistent modulation of the summer hydroclimate by this teleconnection. During the periods of significant correlation the hydroclimatic impact of the PDO is carried over from winter to spring/summer. The periods of weak and positive correlation are thus explained by the lack of carryover from the winter season hydroclimatic signal, particularly if opposite correlations occurred during the following growing season. An example would be during the negative PDO or weakened Aleutian Low when precipitation is higher in winter but unable to sustain the spring/summer precipitation required during the growth season, or if warm temperatures result in enhanced evapotranspiration and produce drought conditions. The chronologies may therefore be best at reconstructing the positive phase of the PDO and enhanced Aleutian Low conditions.

The general lack of a growth response to winter precipitation (snowpack) (St. George et al., 2009; St. George et al., 2010) is highlighted by the Pederson et al. (2011) northern Rocky Mountains April 1 snow water equivalence (SWE) reconstruction. In our reconstruction the late 19th century was the severest summer drought on record, whereas, they reconstruct above average SWE. The early 20th century also indicates contrasting conditions; the summer PDSI is predominantly high and the SWE is predominantly low. SWE and summer moisture conditions are coherent during the 1512-1518 and 1717-1721 drought periods, and the 1588-1592 and 1609-1614 wet periods. This divergence between the winter and summer moisture reconstructions explains the non-coherent PDO signals in our chronologies. We also found that the drought of 2000-20001 did not exhibit as pronounced of a negative anomaly, relative to other 20th century droughts, such as 1936-37 or 1961 (St. George et al., 2009), even though this event was deemed as the most intense drought in the western prairies during the last 100 years (Sauchyn et al., 2003; Liu et al., 2004). The absence of an extremely narrow 2001 tree ring may be explained by the previous year's carry-over of moisture (Fritts, 1976); the 2000-01 drought was preceded with eight wet years compared to 1936-1937 and 1961 events, both which occurred during the midst of prolonged dry periods.

El Niño is primarily associated with winter season drought in the northern Prairies (Shabbar et al., 1997; Bonsal and Lawford, 1999; Bonsal et al., 2006; Shabbar, 2006); however, the connection between La Niña events and summer drought may not be as uncommon as originally speculated. Previous wheat yield research over the Canadian Prairies found that the El Niño years brought favourable and the La Niña years brought unfavourable conditions (Garnett and Khandekar, 1992; Shabbar et al., 1997; Garnett et al., 1998; Hsieh et al., 1999; Garnett et al., 2006). The winter 500 hPa heights centres-of-action pattern associated with PC2 drought

conditions (Figure 5) is a distinct feature of La Niña (Diaz et al., 2001), along with the depressed 500 hPa heights at longitudes in the tropical and subtropical latitudes linked with tropospheric cooling. During the summer these centres-of-action are westward shifted, with weaker amplitudes, relative to their winter positions (Figure 5), and explain only 25% of the seasonal variance of the mean surface temperature and precipitation (Diaz et al., 2001). PC2 is capturing a relatively small portion of the overall hydroclimatic variability of the study region; however, it does highlight the non-stationary relationship with ENSO. The non-stationary temporal relationship and spatial variability between the hydroclimate and ENSO (Figure 6) also exists over western Montana (Wise, 2010). The weak ENSO signal in the tree-rings is explained by the sporadic occurrence of ENSO events or by other dominant hydroclimatic sources of variability (Diaz et al., 2001), such as the spatial inconsistency or the North Pacific Ocean variability. Since the onset of SST observations, six multi-year mid-latitude drought events in North America (1856-1865, 1870's, 1890's, 1930's, 1950's and most of the early 21st century) have been accompanied by persistent La Niña-like SST conditions (Fye et al., 2003; Herwijer et al., 2006; Seager, 2007); the 1950's drought was the only event that did not incorporate our study region.

The scientific basis for adapting current water infrastructure, policy, and management involves an understanding of the contribution of historical climate variability to uncertainty in the future climate system and the variability and drivers of climatic extremes (Biondi et al., 2005). Future patterns of SST anomalies in the extratropical ocean will likely include a shift to the decadal time-scale variability of the North Pacific Ocean, impacting oceanic processes by changing the gyre evolution and the associated change in storm tracks, and anomalous transient eddy flux feedbacks on the mean flow anomalies (Trenberth, 1990; IPCC4, 2007). The increased ENSO variance experienced within the past century roughly coincides with an increase in Western Pacific Ocean warm-pool temperature (Newton et al., 2006). Assuming that the warm-pool SSTs can be attributed to global warming, supporting the view that anthropogenic global warming tends to strengthen the ENSO variability (Sun, 2003), we conclude that drought and flood severity and variability may surpass the instrumental and the reconstructed records.

5 Conclusions

This reconstruction of the JJA PDSI extends the length, analysis, and interpretation of the previous work, by St. George et al. (2009), to 1406 for the northwestern Great Plains region. The connection between the PDO and the ENSO and summer moisture conditions in the northern Prairie region is complex, as identified through this study. Runs-analysis identified periods of both extended drought and pluvial events over the study region of greater duration, frequency, severity, and intensity than experienced during the 20th century instrumental period. The severest droughts (pluvials) are associated with the positive (negative) phase of the PDO. Pluvial events typically had more occurrences of La Niña events and extreme drought was associated with increased ENSO variance. The mechanisms that are controlling the summer drought and pluvial events over the northern Prairie Region of North America are more akin to those of the Great Plains of the USA, and the ENSO association. The reconstructed wet periods aligned with cool summer temperatures (Luckman and Wilson, 2005) and the dry periods typically occurred during warm periods, however, cold droughts were not uncommon. Although the tree-rings are primarily capturing the summer moisture conditions there is an underlying signal associated with

the winter Pacific atmosphere-ocean climate variations. Exploring the early/late wood and analyzing each chronology for the dominate moisture signal may differentiate this mixed winter and summer season signal (Vanstone and Sauchyn, 2010). Further research into the 21st century projections of the PDO and the ENSO requires exploration into the full range of possible scenarios, including the variability, using the most up-to-date suite of GCMs, and their ability to accurately reproduce the observed hydroclimate. Multi-year droughts are, and will continue to prove challenging and improved adaptation to these extreme events are needed (Marchildon et al., 2008).

6 Acknowledgements

We appreciate the World Data Center for Paleoclimatology for collecting and archiving their data. The NCEP Reanalysis data was provided by the NOAA/OAR/ESRL PSD, Boulder, Colorado, USA, from their Web site at http://www.esrl.noaa.gov/psd/. This research was funded by the Natural Sciences and Engineering Research Council of Canada.

References

Alley, W.M., 1984. The Palmer Drought Severity Index, Limitations and assumptions. Journal of Climate and Applied Meteorology 23, 1100–1109.

Ault, T.R., St. George, S., 2010. The Magnitude of Decadal and Multidecadal Variability in North American Precipitation. Journal of Climate 23, 842–850.

Axelson, J.N., Sauchyn, D.J., Barichivich, J., 2009. New reconstructions of streamflow variability in the South Saskatchewan River Basin from a network of tree ring chronologies, Alberta, Canada. Water Resources Research 45, W09422.

Batjes, N.H., (ed.). 2000. Global Data Set of Derived Soil Properties, 0.5-Degree Grid (ISRIC-WISE). [Global Data Set of Derived Soil Properties, 0.5-Degree Grid (International Soil Reference and Information Centre - World Inventory of Soil Emission Potentials)].Data set. Available on-line [http,//www.daac.ornl.gov] from Oak Ridge National Laboratory Distributed Active Archive Center, Oak Ridge, Tennessee, U.S.A.

Biondi, F., Gershunov, A., Cayan, D.R., 2001. North Pacific decadal climate variability since 1661. Journal of Climate 14, 5-10.

Biondi, F., Kozubowski, T.J., Panorska., AK., 2005. A new model for Quantifying Climate Episodes. International Journal of Climate 25, 1253-1264.

Bonsal, B.R., Lawford, R.G., 1999. Teleconnections between El Niño and La Niña events and summer extended dry spells on the Canadian Prairies. International Journal of Climatology 19, 1445-1458.

Bonsal, B.R., Zhang, X., Hogg, W.D., 1999. Canadian Prairie growing season precipitation variability and associated atmospheric circulation. *Climate Research* 11, 191-208.

Bonsal, B.R., Shabbar, A., Higuchi, K., 2001. Impact of low frequency variability modes on Canadian winter temperature. International Journal of Climatology 21, 95-108.

Bonsal, B.R., Prowse, T.D., Duguay, C.R., Lacroix M.P., 2006. Impacts of large-scale teleconnections on freshwater-ice break/freeze-up dates over Canada. Journal of Hydrology 330(1-2), 340-353.

Bonsal, B.R., *Wheaton, E.E., Chipanshi, A., Lin, C., Sauchyn, D.J., Wen, L., 2011. Drought Research in Canada, A Review. Atmosphere-Ocean,* 2011.555103.

Briffa, K., Jones, P.D., 1990. Basic chronology statistics and assessment, in Cook, E.R., and Kairiukstis L., eds, Applications in the Environmental Science. Kluver, Dordrecht, 137-152.

Case, R.A., MacDonald, G.M., 2003. Tree ring reconstructions of streamflow for three Canadian prairie rivers. Journal of American Water Resources Association 39, 703-716.

Cayan, D.R., Redmond, K.T., Riddle, L.G., 1999. ENSO and Hydrologic Extremes in the Western United States. Journal of Climate 12, 2881-2893.

Chao, Y., Ghil, M., McWilliams, J.C., 2000. Pacific interdecadal variability in this century's sea surface temperatures. Geophysical Research Letters 27, 2261-2264.

Cook, E.R., 1985. A time series analysis approach to tree-ring standardization. Ph.D. dissertation, The University of Arizona, Tuscon, pp. 171.

Cook, ER., 2000. El Nino 3 Index Reconstruction, in, International Tree-Ring Data Bank, IGBP PAGES/World Data Center-A for Paleoclimatology Data Contribution Series.

Cook, E.R., D'Arrigo, R., Mann, M.E., 2002. A Well-Verified, Multiproxy Reconstruction of the Winter North Atlantic Oscillation Index since A.D. 1400. Journal of Climate 15, 1754-1764.

Cook, E.R., Kairiukstis, L.A,. (Eds). 1990. Methods of Dendrochronology, Applications in the Environmental Sciences, Klumer Academic Publishers, Dordrech, pp. 98-105.

Cook, E.R., Seager, R., Cane, M.A., Stahle, D.W., 2007. North American Drought, Reconstructions, Causes, and Consequences. Earth Science Reviews 81, 93-134.

Cook, E.R., D'Arrigo, R., Anchukaitis, K.J., 2008. ENSO reconstructions from long tree-ring chronologies, Unifying the differences, in, Talk presented at a special workshop on Reconciling ENSO Chronologies for the Past 500 Years, held in Moorea, French Polynesia on 2-3 April 2008,

D'Arrigo, R., Villalba, R., Wiles, G., 2001. Tree-ring estimates of Pacific decadal climate variability. Climate Dynamics 18, 219-224.

D'Arrigo, R., Wilson, R., 2006. On the Asian Expression of the PDO. International Journal of Climatology 26, 1607-1617.

Dawdy, D.R., Matalas, N.C., 1964. Statistical and probability analysis of hydrologic data, part III, Analysis of variance, covariance and time series, in Ven Te Chow, ed., Handbook of applied hydrology, a compendium of water-resources technology, New York, McGraw-Hill Book Company, pp. 8.68-8.90.

Diaz, H.F., Hoerling, M.P., Eischeid, J.K., 2001. ENSO variability, teleconnections and climate change. International Journal of Climatology 21(15), 1845-1862.

Dracup, J.A., Lee, K.S., Paulson, E.G., 1980. On the statistical characteristics of drought events. Water Resources Research 16, 289–296.

Edwards, T.W.D., Birks, S.J., Luckman, B.H., MacDonald, G.M., 2008. Climatic and hydrologic variability during the past millennium in the eastern Rocky Mountains and northern Great Plains of western Canada. Quaternary Research 70, 188-197.

Fritts, H.C., 1976. Tree Rings and Climate. Academic Press, New York.

Fye, F.K., Stahle, D.W., Cook, E.R., 2003. Paleoclimatic analogs to twentieth- century moisture regimes across the United States. Bulletin of the *American* Meteorological *Society* 84, 901-909.

Gan, T.Y., Gobena, A.K., Wang, Q., 2007. Precipitation of southwestern Canada , Wavelet, scaling, multifractal analysis, and teleconnection to climate anomalies. Journal of Geophysical Research 112, 2006JD007157

Garnett, E.R., Khandekar, M.L., 1992. The impact of large-scale atmospheric circulation and anomalies on Indian monsoon droughts and floods and on world grain yields - statistical analysis. Journal of Agriculture and Forest Meteorology 61, 113-128.

Garnett, E.R., Khandekar, M.L., Babb, J.C., 1998. On the Utility of ENSO and PNA Indices for the Long Lead Forecasting of Summer Weather over the Crop Growing Region of the Canadian Prairies. Journal of Theoretical and Applied Climatology 60, 37-45.

Garnett, E.R., Nirupama, N., Haque, C.E., Murty, T.S., 2006. Correlates of Canadian Prairie summer rainfall, implications for crop yields. Climate Research 32, 25-33.

Gedalof, Z., Smith, D.J., 2001. Interdecadal climate variability and regime-scale shifts in Pacific North America. Geophysical Research Letters 28(8) , 1515-1518.

Gedalof, Z., Mantua, N.J., Peterson, D.L., 2002. A multi-century perspective of variability in the Pacific Decadal Oscillation, new insights from tree rings and coral. Geophysical Research Letters 29(24), 57.1-57.4

Ghil, M., Allen, R.M., Dettinger, M.D., Ide, K., Kondrashov, D., Mann, M.E., Robertson, A., Saunders, A., Tian, Y., Varadi, F., Yiou, P., 2002. Advanced spectral methods for climatic time series," Review of Geophysics 40(1), 3.1-3.41.

Girardin, M.P., Tardif, J.C., Flannigan, M.D., Bergeron, Y., 2006. Synoptic-Scale Atmospheric Circulation and Boreal Canada Summer Drought Variability of the Past Three Centuries. Journal of Climate 19, 1922-1947.

Girardin, M.P., Sauchyn, D.J., 2008. Three centuries of annual area burned variability in northwestern North America inferred from tree rings. The Holocene 18(2), 205-214.

Grinsted, A., Moore, J.C., Jevrejeva, S., 2004.Application of the cross wavelet transform and wavelet coherence to geophysical time series. *Nonlinear Processes* in *Geophysics* 11, 561-566.

Guttmann, N.B., 1998. Comparing the Palmer drought index and the standardized precipitation index. Journal of American Water Resources Association 34, 113-121.

Hamlet, A.F., Mote, P.W., Clark, M.P., Lettenmaier, D.P., 2007. Twentieth-Century Trends in Runoff, Evapotranspiration, and Soil Moisture in the Western United States. Journal of Climate 20, 1468–1486.

Herweijer, C., Seager, R., Cook, E.R., 2006. North American droughts of the mid to late Nineteenth Century, History, simulation and implications for Medieval drought. Holocene 16, 159-171.

Hsieh, W.W., Tang, B., Garnett, E.R., 1999. Teleconnections between Pacific sea surface temperatures and Canadian prairie wheat yield. Agriculture Forest Meteorology 96, 209-217.

Hughes, M.K., 2002. Dendrochronology in climatology - the state of the art. Dendrochronologia 20(1-2), 95-116.

Hurrell, J.W., Deser, C., 2009. North Atlantic climate variability, The role of the North Atlantic Oscillation. Journal of Marine Systems 78(1), 28-41.

IPCC4., 2007. Climate Change 2007, The Physical Science Basis. Contribution of Working Group I to the Fourth Assessment Report of the Intergovernmental Panel on Climate Change (Solomon, S., D. Qin, M. Manning, Z. Chen, M. Marquis, K.B. Avery, M. Tignor and H.L. Miller (eds.)), Cambridge University Press, Cambridge, UK.

Jones, P.D., Briffa, K.R., Barnett, T.P., Tett, S.F.B., 1998. High-resolution palaeoclimatic records for the last millennium , interpretation, integration and comparison with General Circulation Model control-run temperatures. The Holocene 8(4), 455-471.

Kalnay, E., Kanamitsu, M., Kistler, R., Collins, W., Deaven, D., Gandin, L., Iredell, M., Saha, S., White, G., Woollen, J., Zhu, Y., Leetmaa, A., Reynolds, R., Chelliah, M., Ebisuzaki, W., Higgins, W., Janowiak, J., Mo, K.C., Ropelewski, C., Wang, J., Jenne, R., Joseph, D., 1996. The NCEP/NCAR 40-year reanalysis project. Bulletin of the American Meteorological Society 77(3), 437-471.

Kim, K.W., North, G.R., 1993. EOF analysis of surface temperature field in a stochastic noise model. Journal of Climate 6, 1681-1690.

Keyantash, J., Dracup, J.A., 2002. The Quantification of Drought, An Analysis of Drought Indices. Bulletin of the American Meteorological Society 83(8),1167-1180.

Lau, N.C., 1997. Interactions between global SST anomalies and the midlatitude atmospheric circulation. Bulletin of the American Meteorological Society 78, 21-33.

Luckman, B.H., Wilson, R.J.S., 2005. Summer Temperature in the Canadian Rockies During the last Millennium, a Revised Record. Climate Dynamics 24, 131-144.

Lui, J., Stewart, R.E., Szeto, K.K., 2004. Moisture transport and other hydrometeorological features associated with the severe 2000/01 drought over the Western and Central Canadian prairies. Journal of Climate 17, 305–319.

MacDonald, G.M., Case, R.A., 2005. Variations in the Pacific Decadal Oscillation over the past millennium. Geophysical Research Letters 32, 2005GL022478.

Mann, M.E., Lees, J.M., 1996. Robust estimation of background noise and signal detection in climatic time series. Climatic Change 33, 409-445.

Mann, M.E., Bradley, R.S., Hughes, M.K., 2000. Multi-scale Variability and Global and Regional Impacts, chap. Long-term variability in the El Nino-Southern Oscillation and associated teleconnections, Cambridge University Press, 357–412.

Mantua, N.J., Hare, S.R., Zhang, Y., Wallace, J.M., Francis, R.C., 1997. A Pacific interdecadal climate oscillation with impacts on salmon production. Bulletin of the American Meteorological Society 78, 1069-1079.

Mantua, N.J., Hare, S.R., 2002. The Pacific Decadal Oscillation. Journal of Oceanography 58(1), 35-44.

Marchildon, G.P., Kulshreshtha, S., Wheaton, E., Sauchyn, D., 2008. Drought and Institutional Adaptation in the Great Plains of Alberta and Saskatchewan, 1914-1939. Natural Hazards 3(3), 391-411.

McGregor, S., Timmerman, A., Timm, O.A., 2010. Unified Proxy for ENSO and PDO Variability Since 1650. Climate of the Past 6, 1-17.

McKenney, D.W., Pedlar, J.H., Papadopol, P., Hutchinson, M.F., 2006. The Development of 1901-2000 Historical Monthly Climate Models for Canada and the United States. Agricultural and Forest Meteorology 138, 69-81.

Meko, D., Stockton, C.W., Boggess, W.R., 1995. The Tree-Ring Record of Severe Sustained Drought. Water Resources Bulletin 31, 789-801.

Meko, D.M., Woodhouse, C.A., Baisan, C.A., Knight, T., Lukas, J.J., Hughes, M.K., Salzer, M.W., 2007. Medieval Drought in the Upper Colorado River Bain. Geophysical Research Letters 34, 2007GL029988.

Minobe, S., 1997. A 50-70 year climatic oscillation over the North Pacific and North America. Geophysical Research Letters 24, 683-686.

Minobe, S., 1999. Resonance in bidecadal and pentadecadal climate oscillations over the North Pacific, role in climatic regime shifts. Geophysical Research Letters 26(7), 1999GL900119.

Newton, A., Thunell, R., Stott, L., 2006.Climate and hydrographic variability in the Indo-Pacific Warm Pool During the last Millenium. Geophysical Research Letters 33, 2006GL027234

Nyenzi, B., Lefale, P.F., 2006. El Niño Southern Oscillation (ENSO) and global warming. Advances in Geosciences 6, 95-101.

Palmer, W.C., 1965. Meteorological drought. Research Paper No. 45, U.S. Department of Commerce Weather Bureau, Washington, D.C.

Pederson, G.T., Gray, S.T., Woodhouse, C.A., Betancourt, J.L., Fagre, D.B., Littell, J.S., Watson, E., Luckman, B.H., Graumlich, L.J., 2011. The Unusual Nature of Recent Snowpack Declines in the North American Cordillera. Science 9 June 2011, 1201570 Published online 9 June 2011.

Power, S., Casey, T., Folland, C., Colman, A., Mehta, V., 1999. Interdecadal modulation of the impact of ENSO on Australia. Climate Dynamics 15, 319-324.

Rasmussen, E.M., Carpenter, T.H., 1982, Variations in tropical sea surface temperature and surface wind fields associated with the Southern Oscillation/El Nino. Monthly Weather Review 110, 354-384.

Ropelewski, C.F., Jones, P.D., 1987. An extension of the Tahiti-Darwin Southern Oscillation Index. Monthly Weather Review 115, 2161-2165.

Sachs, J.P., Sachse, D., Smittenberg, R.H., Zhang, Z., Battisti, D.S., Golubic, S., 2009. Southward movement of the Pacific intertropical convergence zone AD 1400-1850. Nature Geoscience, 2, 519–525.

Salinger, M.J., Renwick, J.A., Mullan, A.B., 2001. Interdecadal Pacific Oscillation and South Pacific climate. International Journal of Climatology 21(14), 1705-1721.

Sauchyn, D.J., Skinner, W.R., 2001. A proxy PDSI record for the southwestern Canadian plains. Canadian Water Resource Journal 26(2), 253-272.

Sauchyn, D.J., Stroich, J., Beriault, A., 2003. A paleoclimatic context for the drought of 1999-2001 in the northern Great Plains. The Geographical Journal 169, 158-167.

Sauchyn, D., Vanstone, J., Perez-Valdivia, C., In press. Modes and Forcing of Hydroclimatic Variability in the Upper North Saskatchewan River Basin Since 1063. Canadian Water Resources Journal.

Seager, R., 2007. The Turn of the Century drought across North America, global context, dynamics and past analogues. Journal of Climate 20, 5527-5552.

Shabbar, A., Bonsal, B., Khandekar, M.L., 1997, Canadian Precipitation Patterns Associated with the Southern Oscillation Journal of Climate. Journal of Climate 10, 3016-3027.

Shabbar, A., 2006. The impact of El Niño-Southern Oscillation on the Canadian climate. Advances in Geosciences 6, 149-153.

Smith, T.M., Reynolds, R.W., 1998. A high-resolution global sea surface temperature climatology for the 1961-90 base period. Journal of Climate 11, 3320-3323.

St. George, S., Meko, D.M., Girardin, M.P., MacDonald, G.M., Nielsen, E., Pederson, G.T., Sauchyn, D.J., Tardif, J.C., Watson, E., 2009. The tree-ring record of drought on the Canadian Prairies. Journal of Climate 22, 689-710.

St. George, S., Meko, D.M., Cook, ER., 2010. The seasonality of precipitation signals embedded within the North American Drought Atlas. The Holocene 20(6), doi, 10.1177/0959683610365937

St. Jacques, J-M., Sauchyn, D.J., Zhao, Y., 2010. Northern Rocky Mountain streamflow records, global warming trends, human impacts or natural variability? Geophysical Research Letters 37, 2009GL042045.

Sun, D-Z., 2003. A possible effect of an increase in the warm-pool SST on the magnitude of El Niño warming. Journal of Climate 16, 185–205.

Thomson, D.J., 1982. Spectrum estimation and harmonic analysis, Proceedings IEEE, 70, 1055-1096.

Trenberth, K.E., 1990. Recent observed interdecadal climate changes in the northern hemisphere. Bulletin of the American Meteorological Society 71, 988-993.

Trenberth, K.E., Hurrell, J.W., 1994. Decadal atmosphere-ocean variations in the Pacific. Climate Dynamics 9, 303-319.

Trenberth, K.E., 1997. The Definition of El Niño. Bulletin of the American Meteorological Society 78, 2771-2777.

Trenberth, K.E., Stepaniak, D.P., 2001. Indices of El Niño evolution. Journal of Climate 14, 1697-1701.

Vanstone, J.R., Sauchyn, D.J., 2010. Q. macrocarpa annual, early- and late-wood widths as hydroclimatic proxies, southeastern Saskatchewan, Canada. IOP Conference Series, Earth and Environmental Science 9.

Verdon, D.C., Franks, S.W., 2006. Long-term behavior of ENSO, Interactions with the PDO over the past 400 years Inferred from Paleoclimate Records. Geophysical Research Letters 33, 2005GL025052

Vimont, D.J., Battisti, D.S., Hirst, A.C., 2001. Footprinting, A seasonal connection between the tropics and mid-latitudes. Geophysical Research Letters 28(20), 3923-3926.

Wallace, J.M., Gutzler, D.S., 1981. Teleconnections in the geopotential height field during the Northern Hemisphere winter. Monthly Weather Review 109, 784-812.

Watson, E., Luckman, B.H., 2004. Tree-Ring Based Reconstructions of Precipitation for the Southern Canadian Cordillera. Climatic Change 65, 209-241

Watson, E, Luckman, BH., 2005a. Spatial patterns of preinstrumental moisture variability in the southern Canadian Cordillera. Journal of Climate 18(15), 2847-2863.

Watson E., Luckman B.H., 2005b. An exploration of the controls of pre-instrumental streamflow using multiple tree-ring proxies. Dendrochronologia 22, 225–234.

Wheaton, E., Wittrock, V., Kulshreshtha, S., Koshida, G., Grant, C., Chipanshi, A., Bonsal, B.R., 2005. Lessons Learned from the Canadian Drought Years of 2001 and 2002, Synthesis Report, Agriculture and Agri-Food Canada, Saskatchewan Research Council Publication No. 11602-46E03, Saskatoon, SK.

Wise, E.K., 2010. Spatiotemporal variability of the precipitation dipole transition zone in the western United States. Geophysical Research Letters 37, 2009GL042193.

Wolfe, B.B., Hall, R.I., Edwards, T.W.D., Jarvis, S.R., Sinnatamby, R.N., Yi, Y., Johnston, J.W., 2008. Climate-driven shifts in quantity and seasonality of river discharge over the past 1000 years from the hydrographic apex of North America. Geophysical Research Letters 35, 2008GL036125

Woodhouse, C.A., 1997. Winter climate and atmospheric circulation patterns in the Sonoran Desert region, USA. International Journal of Climatology 17(8), 859-873.

Woodhouse ,C.A., 2004. A Paleo Perspective on Hydroclimatic Variability in the Western United States. Aquatic Sciences, 66, 346-356.

Yu, B., Zwiers, F.W., 2007. The impact of combined ENSO and PDO on the PNA climate, a 1,000-year climate modeling study. Climate Dynamics 29, 837-851.

Zhang, Y., Wallace, J.M., Battisti, D.S., 1997. ENSO-like interdecadal variability, 1900-1993. Journal of Climate 10, 1004-1020.

Table 1. The Palmer Drought Severity Index (PDSI) of moisture classifications (Palmer, 1965).

Classification	PDSI
Extreme Drought	≤ -4.0
Severe Drought	> -4.0 to -3.0
Moderate Drought	> -3.0 to -2.0
Mild Drought	> -2.0 to -1.0
Incipient Dry Spell	> -1.0 to -0.5
Near Normal	> -0.5 to < 0.5
Incipient Wet Spell	0.5 to < 1.0
Mildly Wet	1.0 to < 2.0
Moderately Wet	2.0 to < 3.0
Severely Wet	3.0 to < 4.0
Extremely Wet	≥ 4.0

Table 2. The longest five standard tree-ring chronologies used to construct PC1 and PC2 for 1406-2005 AD. SSS > 0.85 is the earliest year that the chronology is able to estimate at least 85% of the original signal derived from all trees within the stand. See Appendix Table A.1 for more details about the chronologies.

Code	Species	Lat (°N)	Long (°W)	Elev (m)	Median	SSS>0.85	Last Yr	First Yr
Cabin Creek	PSME	49.7	114.0	1375	406	1406	2004	1375
Oldman River	PIFL	49.8	114.2	1447	284	1364	2007	1203
Siffleur Ridge	PIFL	52.5	116.4	1390	244	1028	2008	1018
Wildcat Hills	PSME	51.3	114.7	1351	300	1351	2006	1341
Ward Creek	PIFL	52.0	116.5	1356	261	1160	2007	1062

Table 3. Drought events and their associated severity, rank based on severity, and intensity (severity/duration). The ENSO phase for each year the event (beginning with the year preceding the event) and variance, calculated using a 17-year window (see text and Figure 3), were based on the Cook et al., 2008 Niño 3.4 index reconstruction for the 1300-1871 and 1300-2005 AD periods, respectively. The average December-March Niño 3.4 Index was used to determine the annual ENSO phase during the observed period of 1872-2005 AD. The average PDO phase of the event was based on the MacDonald and Case (2005) PDO for the 1406-1900 period, the Composite PDO Index (Verdon and Franks, 2006) for the 1662-1900 AD period (phase shown in brackets), and the November-March PDO index for the observed period of 1901-2005 AD. E = El Niño, L = La Niña, N = neutral, (LV) = low variance, (HV) = high variance. A strong to moderate ENSO event was defined as |Niño 3.4| > 0.5. + denotes a Positive PDO phase; – denotes a Negative PDO phase.

Drought	Severity	Severity Rank	Intensity	ENSO Phase (Variance)	PDO Phase
1472-1481	-7.6	14	-0.8	LELLLLEENNN (HV)	+
1483-1494	-14.2	3	-1.2	ENEEELLENNELN (HV)	+
1498-1508	-8.2	11	-0.7	LEENNLNEELNL (HV)	+
1512-1518	-5.8	18	-0.8	LLLLNE (LV)	+
1559-1570	-12.3	5	-1.0	ENLLNNNELLLLL (HV)	+
1576-1583	-6.7	16	-0.8	NLNNLLNEE (LV)	+
1618-1623	-4.3	19	-0.7	ELENLL (LV)	–
1626-1630	-6.7	17	-1.3	LLNEEE (LV)	–
1645-1654	-7.4	15	-0.8	NELNLEEENLL (HV)	–
1682-1688	-3.3	24	-0.5	EENLLEEL (LV)	+
1701-1708	-7.9	12	-1.0	NNELLLNLN (LV)	–
1717-1721	-11.8	7	-2.4	LNENNN (HV)	+
1755-1761	-8.8	9	-1.3	LNNLNNLN (HV)	+ (–)
1791-1800	-12.7	4	-1.3	LEEENLNNLEE (HV)	+
1811-1815	-3.7	23	-0.7	NNLLEE (HV)	–
1842-1847	-12.1	6	-2.0	LLLNENN (LV)	+
1850-1854	-4.2	21	-0.8	NELENN (LV)	+
1858-1872	-19.7	1	-1.3	LELLNLLLNLNNELLL (HV)	+ (–)
1889-1897	-7.8	13	-0.9	EELNNLLLEE (HV)	+
1918-1926	-9.5	8	-1.1	LLEENNLELE (HV)	+
1930-1941	-15.6	2	-1.3	NEENNLNEENLEE (HV)	+
1956-1963	-4.2	22	-0.6	LLNEENNNN (LV)	–
1983-1989	-8.4	10	-1.2	NELLLEEL (HV)	+
2000-2004	-4.3	20	-0.9	LLLNEE (HV)	+

Table 4. Pluvial events and their associated severity, rank based on severity, and intensity (severity/duration). The ENSO phase for each year the event (beginning with the year preceding the event) and variance, calculated using a 17-year window (see text and Figure 3), were based on the Cook et al., 2008 Niño 3.4 index reconstruction for the 1300-1871 and 1300-2005 AD periods, respectively. The average December-March Niño 3.4 Index was used to determine the annual ENSO phase during the observed period of 1872-2005 AD. The average PDO phase of the event was based on the MacDonald and Case (2005) PDO for the 1406-1900 period, the Composite PDO Index (Verdon and Franks, 2006) for the 1662-1900 AD period (phase shown in brackets), and the November-March PDO index for the observed period of 1901-2005 AD. E = El Niño, L = La Niña, N = neutral, (LV) = low variance, (HV) = high variance. A strong to moderate ENSO event was defined as |Niño 3.4| > 0.5. + denotes a Positive PDO phase; – denotes a Negative PDO phase.

Pluvial	Severity	Severity Rank	Intensity	ENSO Phase (Variance)	PDO Phase
1469-1471	1.2	13	0.4	LELL (HV)	+
1550-1554	1.8	9	0.4	EEENEE (HV)	+
1588-1592	0.7	14	0.1	NNLNEL (LV)	–
1598-1600	1.5	12	0.5	ENNL (LV)	+
1609-1614	1.5	11	0.3	ENENNLN (LV)	+
1668-1676	6.9	2	0.6	LLNLELLLNL (LV)	–
1709-1711	0.1	15	0.0	NLEN (LV)	–
1752-1754	2.6	6	0.9	NLLL (HV)	–
1778-1782	3.3	4	0.7	LLNELL (LV)	–
1786-1790	2.9	5	0.7	LLNELL (HV)	–
1826-1830	7.0	1	1.4	ELEENL (LV)	– (+)
1900-1905	4.9	3	0.8	LEENELE (HV)	+
1907-1909	1.7	10	0.6	ELNL (HV)	+
1953-1955	1.8	8	0.6	EEEL (LV)	–
1993-1996	2.0	7	0.5	EENEL (HV)	+

Table A.1. The 28 standard tree-ring chronologies used in this study and their details. The chronologies were collected by the University of Regina Tree-Ring Laboratory. The expressed population signal (EPS) measures the ability of each record to represent the ideal population signal and the between-tree correlation (R_bar) is the mean correlation between all ring width records within a site. SSS>0.85 is the earliest year that the chronology is able to estimate at least 85% of the original signal, derived from all trees within the stand. Median series length is the median number of annual rings contained by the tree-ring samples from an individual site; Sens is mean sensitivity of the residual chronology. Not available is denoted by *na*. *Picea glauca* (PCGL); *Pinus contorta* (PICO); *Pinus flexilis* (PIFL); *Picea glauca* (PIGL); *Pseudotsuga menziesii* (PSME). * denotes the five longest chronologies used in the reconstructions.

Site Name	Species	Lat (°N)	Long (°W)	Elev (m)	EPS	R_bar	Median	Cores	First Yr	Last Yr	SSS >0.85	Sens
Beaver Creek, AB	PSME	49.8	-113.9	1592	0.93	0.56	275	23	1592	2006	1624	0.237
Beaver Dam Creek, AB	PSME	49.9	-114.2	1661	0.97	0.55	345	42	1482	2004	1526	0.279
Buhrman, AB	PIFL	49.1	-113.6	1297	0.93	0.31	83	34	1796	2007	1896	0.270
Boundary, AB	PSME	49.1	-114.0	1297	0.95	0.41	198	45	1759	2005	1780	0.200
Burles Ridge, AB	PSME	49.7	-114.1	1320	0.88	0.57	163	7	1768	2004	1830	0.319
Beauvais Lk, AB.	PSME / PIFL	49.4	-114.1	1427	0.96	0.40	257	34	1627	2003	1701	0.219
Cabin Creek, AB *	PSME	49.7	-114.0	1375	0.99	0.67	406	40	1375	2004	1406	0.369
Callum Creek, AB	PSME	50.0	-114.2	1677	0.97	0.56	288	35	1572	2004	1634	0.250
Cypress Hills, SK	PICO	49.7	-110.0	1000	0.92	0.26	99	40	1872	2001	1885	0.152
Crandell Mountain, AB	PSME	49.1	-113.9	1284	0.89	0.40	227	30	1450	2005	1457	0.175
Dutch Creek, AB	PSME	49.9	-114.4	1680	0.98	0.64	244	42	1618	2004	1620	0.310
Douglas Fir Ecological Area, AB	PSME	52.2	-116.4	1320	0.983	0.601	294	49	1472	2007	1587	0.332
Emerald Lake, AB	PIFL	49.6	-114.6	1384	0.93	0.29	270	39	1450	2004	1591	0.215
Hawkeye Mesa, AB	PIFL	49.7	-113.8	1308	0.94	0.41	171	59	1542	2007	1641	0.245
Little Bob Creek, AB	PSME	49.9	-114.2	1602	0.98	0.63	307	45	1509	2004	1579	0.322
Oldman River, AB	PSME	49.9	-114.2	1331	0.94	0.57	202	26	1534	2003	1597	0.374
Oldman River, AB *	PIFL	49.8	-114.2	1447	0.98	0.50	284	90	1203	2007	1364	0.329

Ridge Crest, AB	PSME	49.9	-114.3	1667	0.93	0.54	167	10	1797	2003	1810	0.209
Siffleur Ridge, AB *	PIFL	52.0	-116.4	1390	0.978	0.556	244	62	1018	2008	1028	0.355
Stoney Indian Park, AB	PSME	51.1	-115.0	*na*	0.98	0.68	270	22	1597	2003	1637	0.296
South Milk River, MT	PIFL	48.7	-113.3	1718	0.82	0.23	79	13	1892	2007	1926	0.183
Tower Ridge, AB	PCGL	51.1	-114.4	1250	0.98	0.41	131	93	1315	1992	1602	0.267
Two O'Clock Creek, AB	PSME	52.1	-116.4	1560	0.976	0.564	411	38	1496	2007	1500	0.338
Wildcat Hills, AB *	PSME	51.3	-114.7	1351	0.98	0.72	300	48	1341	2006	1351	0.419
Ward Creek, AB	PSME	50.1	-114.2	*na*	0.97	0.55	169	32	1708	2005	1724	0.165
Whirlpool Point, AB *	PIFL	52.0	-116.5	1356	0.959	0.594	261	32	1062	2007	1160	0.395
White Rabbit Creek, AB	PIFL	52.1	-116.4	1420	0.981	0.678	266	38	1555	2008	1559	0.366
West Sharples Creek, AB	PSME	49.9	-114.1	1520	0.99	0.55	360	63	1525	2004	1562	0.291

Figure Captions

Figure 1. Pearson's correlation maps of (a) PC1 and (b) PC2, with the June-July-August Palmer Drought Severity Index (JJA PDSI), for the 1901-2005 period, used to identify the study region of the northwestern Great plains. The white box outlines the initial study region (46-52^{o}N and 105-116^{o}W) and the thick black line identifies the positive correlation at the 99% significance level with the corresponding PC. The green triangles represent the five longest tree-ring chronologies used to construct PC1 and PC2, and the black triangles represent the remaining 23 tree-ring chronologies used for the common period principal component analysis. Significance values were adjusted for autocorrelation.

Figure 2. The reconstructed June-July-August Palmer Drought Severity Index (JJA PDSI) region average, using linear regression, for the region significantly correlated with (a) PC1 and (b) PC2, as identified in Figure 1. The solid line represents the observed JJA PDSI region average and the dashed line represents the reconstruction inferred from each PC, (a) PC1 JJA PDSI and (b) PC2 JJA PDSI. Pearson's correlations significant at the 95% confidence level.

Figure 3. Runs analysis of the PC1 June-July-August Palmer Drought Severity Index (PC1 JJA PDSI) reconstruction compared to the Luckman and Wilson (2005) summer temperature reconstruction. (a) PC1 JJA PDSI (solid black line) smoothed with a 9-year running average. The grey bars are the drought / pluvial severity (run-sum), and the light yellow panels represent approximate timing and duration of solar minima's (Spörer, Maunder, and Dalton, respectively). (b) The reconstructed summer temperature anomalies (^{o}C), inverted, relative to the 1900-1980 mean (Luckman and Wilson, 2005) (grey line) and the PC1 JJA PDSI (black line), smoothed with a 9-year running average. The red (blue) bars represent extreme 20 year periods (inverted) of warm (cool) intervals, relative to 1900-1980 mean. (c) Sliding 17-year variance of Cook et al. (2008) reconstructed Niño 3.4 Index (assigned to centre year of the window). The solid black line represents the average variance (0.6) over the entire reconstruction length (1300-1979).

Figure 4. Reconstruction of (a) PC1 June-July-August Palmer Drought Severity Index (PC1 JJA PDSI) (left panel) and PC2 JJA PDSI (right panel) spanning 1406-2005, smoothed with a 9-year running average. (b) Shows results of the MTM spectral analysis using three tapers and the significance levels (smoothed dotted curves). (c) Shows results of the Morlet wavelet analysis with the heavy black line showing significance at the $p \leq 0.1$ level.

Figure 5. Correlation maps of PC1 and PC2 with the observed 500 hPa geopotential heights (Kalnay, et al., 1996) averaged over the previous December- current March and current May-August season, for the 1947-2004 period. Image produced by the software provided by the NOAA/ESRL Physical Sciences Division, Boulder Colorado website at http://www.esrl.noaa.gov/psd/.

Figure 6. The 31-year running correlations (assigned to centre year of the window) with PC1 (black line) and PC2 (grey line) and (a) the MacDonald and Case (2005) reconstructed PDO index, and (b) the Cook et al. (2008) reconstructed Niño 3.4 index. The horizontal dashed line corresponds to $p \leq 0.1$. The instrumental December-March Niño 3.4 index and November-March PDO indices extended the reconstructed indices to 2005.

Figure 1

Click here to download high resolution image

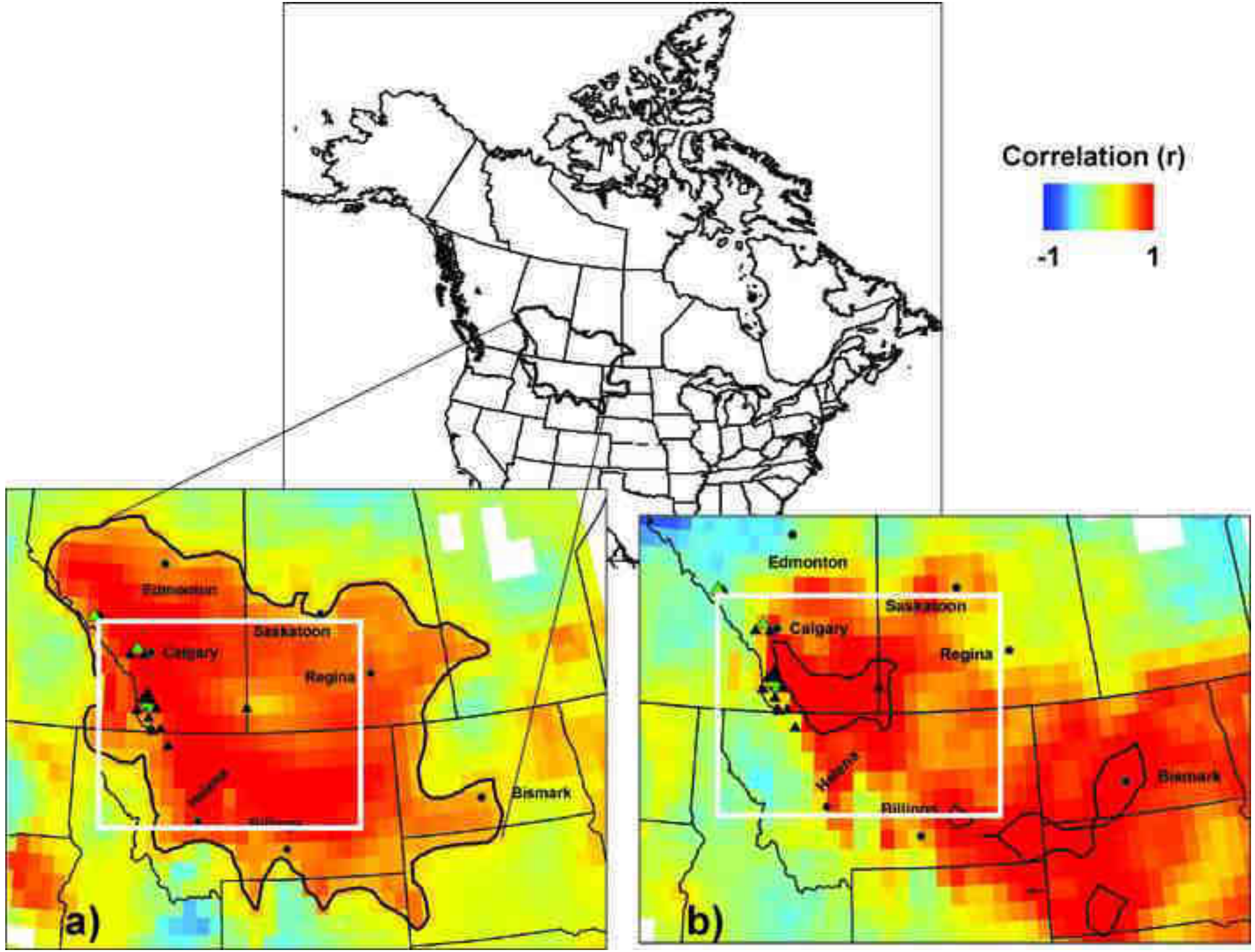

Figure 2

Click here to download high resolution image

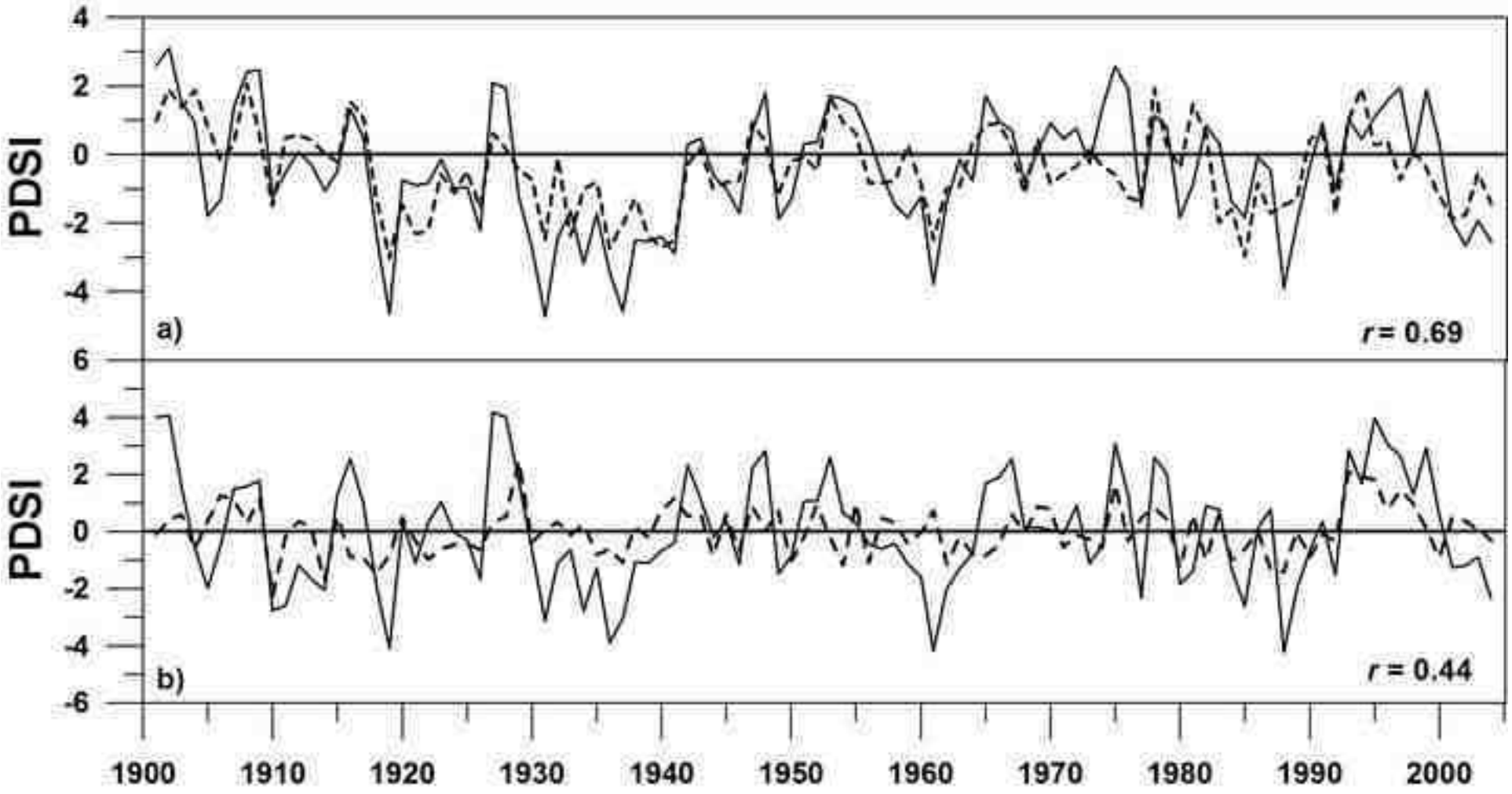

Figure 3

Click here to download high resolution image

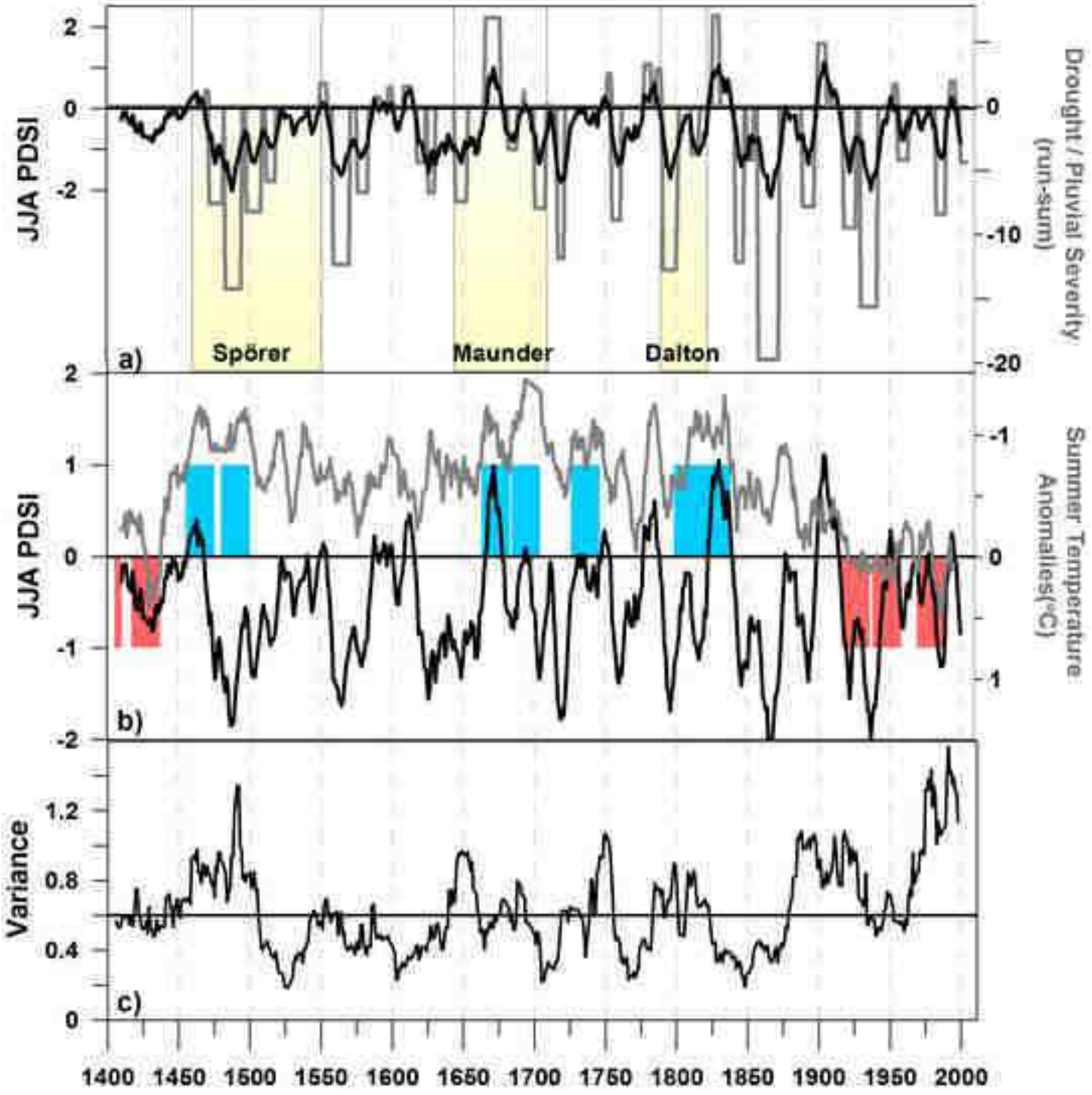

Figure 4

Click here to download high resolution image

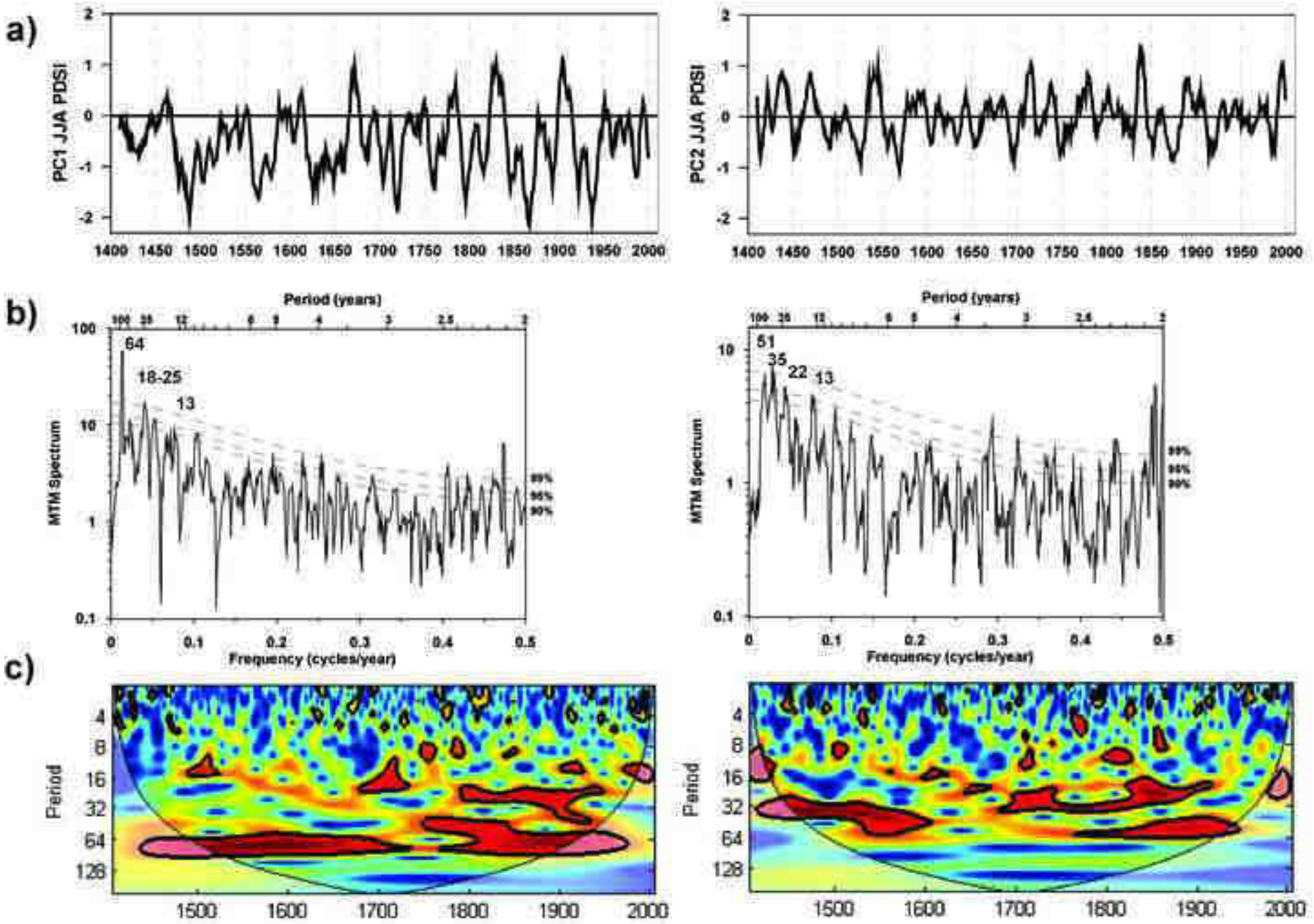

Figure 5

Click here to download high resolution image

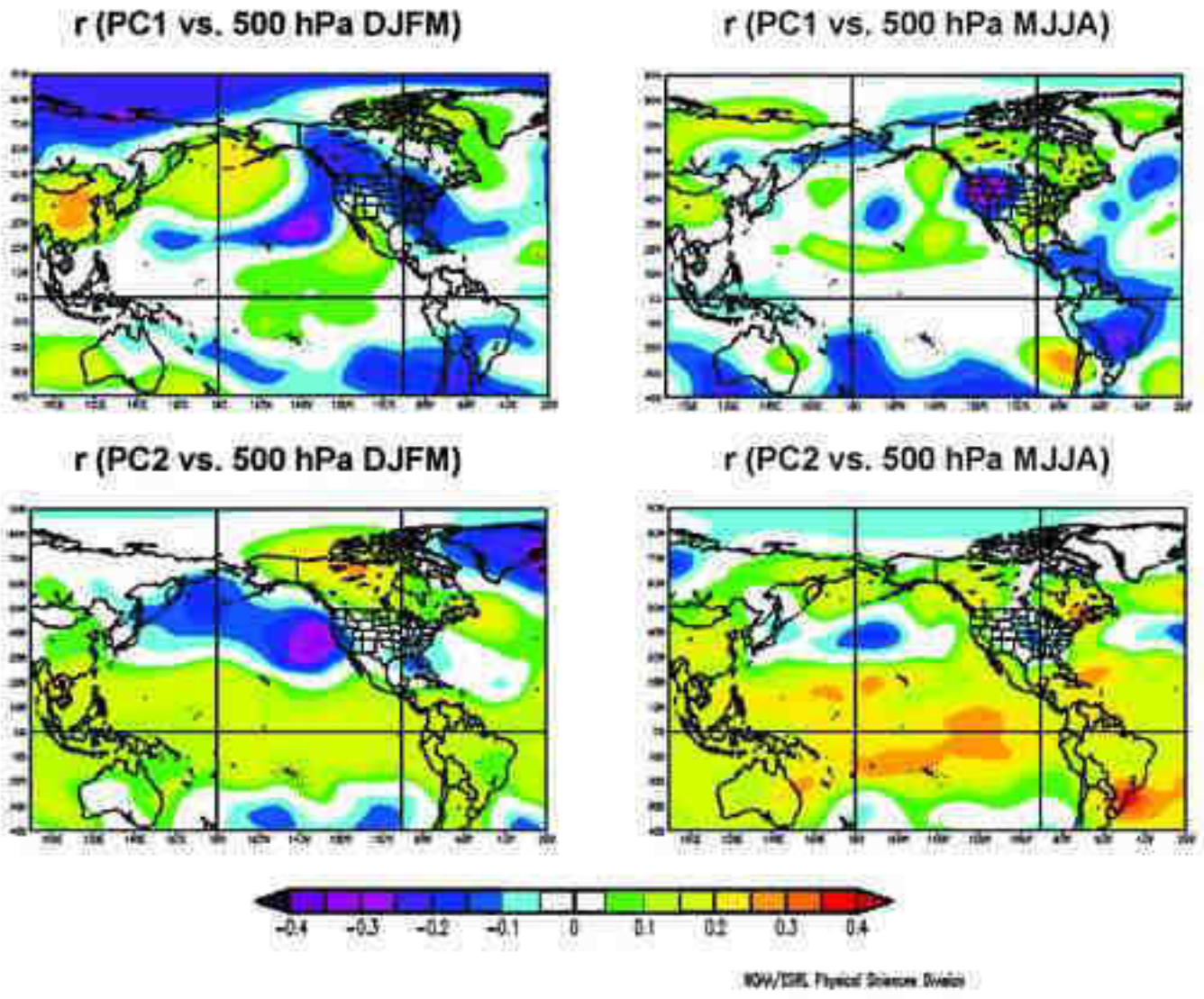

Figure 6

Click here to download high resolution image

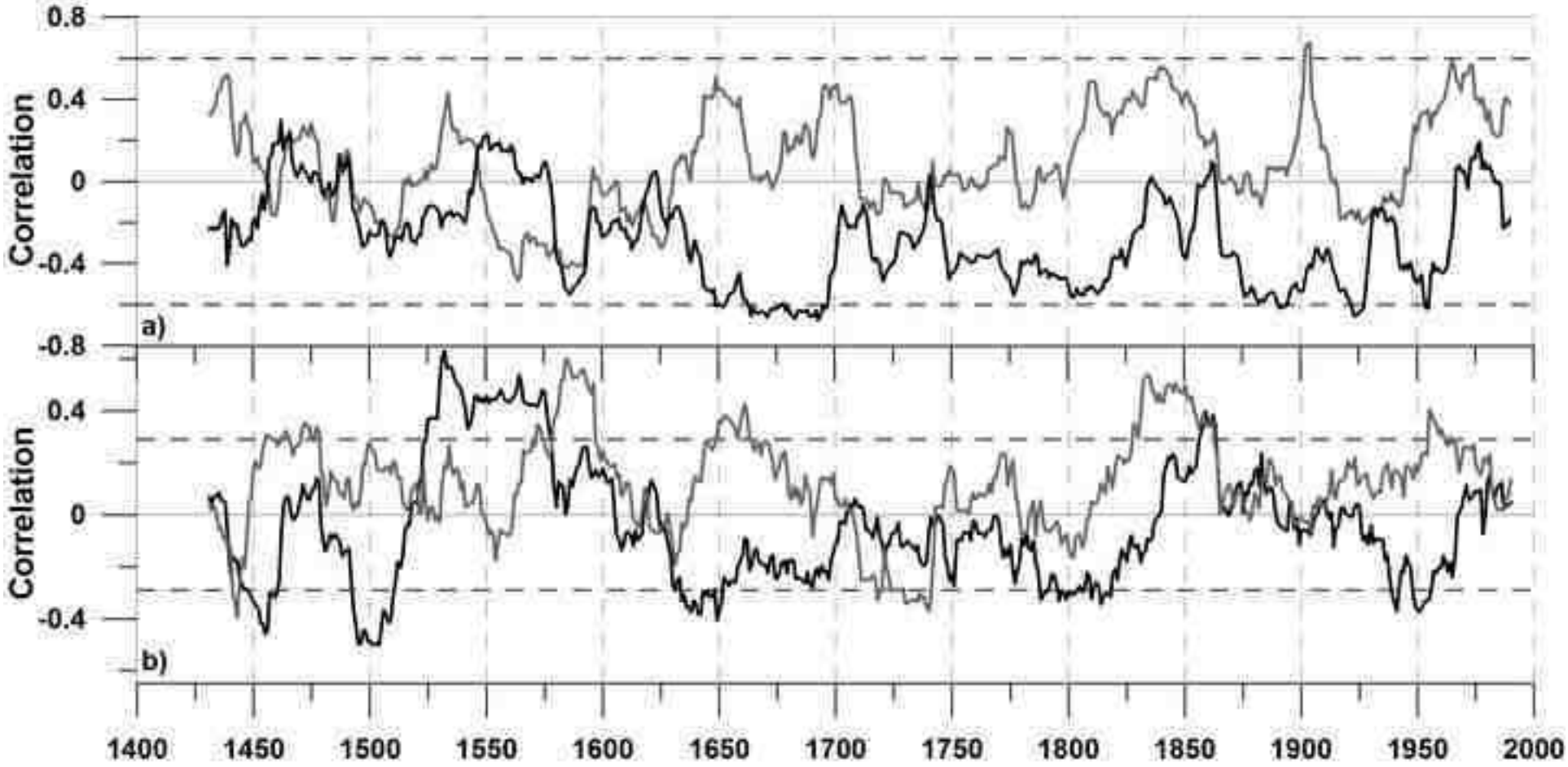

Elsevier Editorial System(tm) for Quaternary International
Manuscript Draft

Manuscript Number: QUATINT-D-11-00350

Title: Twenty-first Century Northern Rocky Mountain River Discharge Scenarios under Greenhouse Forcing

Article Type: PACLIM 4

Keywords: El Niño-Southern Oscillation (ENSO); Generalized Least Squares (GLS) regression models; North Atlantic Oscillation (NAO); Pacific Decadal Oscillation (PDO); projected river discharge; northern Rocky Mountains

Corresponding Author: Dr. Jeannine-Marie St. Jacques, Ph.D.

Corresponding Author's Institution: University of Regina

First Author: Jeannine-Marie St. Jacques, Ph.D.

Order of Authors: Jeannine-Marie St. Jacques, Ph.D.; Suzan L Lapp, M.Sc.; Yang Zhao, Ph.D.; Elaine M Barrow, Ph.D.; David J Sauchyn, Ph.D.

Abstract: The 20th century hydroclimatology of the northern Rocky Mountains is heavily influenced by recurring large-scale climate patterns: the Pacific Decadal Oscillation (PDO), the El Niño-Southern Oscillation (ENSO), and the Arctic Oscillation/North Atlantic Oscillation (AO/NAO). Hence, low frequency northern Rocky Mountain river discharge variability can be successfully modeled by regression techniques using these climate indices as predictors. We developed Generalized Least Squares (GLS) regression equations which captured a large portion of streamflow variability at the hydrological apex of North America. Using archived runs from global climate models from the IPCC Fourth Assessment Report (AR4) (Phase 3 of the Coupled Model Intercomparison Project - CMIP3), we projected the PDO, ENSO and the NAO for the 21st century for the B1, A1B and A2 Special Report on Emission Scenarios (SRES). These projected climate indices were used as inputs into the GLS regression equations, giving projected northern Rocky Mountains river discharges. These projections showed generally declining trends in northern Rocky Mountains surface water availability for 2006-2050 and 2006-2096.

*Cover Letter

July 12, 2011

Dear Dr. Starratt

Please receive our manuscript, "Twenty-first Century Northern Rocky Mountain River Discharge Scenarios under Greenhouse Forcing", for consideration for the 2011 PACLIM issue of Quaternary International. The northern Rocky Mountains are a region that is already experiencing surface water deficits; hence, there is great concern about what impacts anthropogenic global warming will have on these already scarce supplies. Understandably, water managers have great interest in regional river discharge projections for the 21st century. The regional hydroclimatology is heavily influenced by recurring large-scale climate patterns: the Pacific Decadal Oscillation (PDO), the El Niño-Southern Oscillation (ENSO), and the North Atlantic Oscillation (NAO). In this manuscript, we use 21st century projections of these climate oscillations as inputs into Generalized Least Squares regression models to produce projected northern Rocky Mountain river discharges for 2000-2096. We believe that our manuscript will be a useful contribution to water management decision-making.

Thank you,

Jeannine-Marie St. Jacques

Prairie Adaptation Research Collaborative

University of Regina

Regina, Saskatchewan

Twenty-first Century Northern Rocky Mountain River Discharge Scenarios under Greenhouse Forcing

Jeannine-Marie St. Jacques[1*], Suzan L. Lapp[1], Yang Zhao[2], Elaine M. Barrow[1] and David J. Sauchyn[1]

[1] Prairie Adaptation Research Collaborative (P.A.R.C.), Room 120, 2 Research Drive, University of Regina, Regina, Saskatchewan, Canada, S4S 7H9

[2] Department of Mathematics and Statistics, University of Regina, Regina, Saskatchewan, Canada, S4S 0A2

*Corresponding author: stjacqje@uregina.ca, office: 306-337-2293, fax: 306-337-2301.

Abstract

The 20th century hydroclimatology of the northern Rocky Mountains is heavily influenced by recurring large-scale climate patterns: the Pacific Decadal Oscillation (PDO), the El Niño-Southern Oscillation (ENSO), and the Arctic Oscillation/North Atlantic Oscillation (AO/NAO). Hence, low frequency northern Rocky Mountain river discharge variability can be successfully modeled by regression techniques using these climate indices as predictors. We developed Generalized Least Squares (GLS) regression equations which captured a large portion of streamflow variability at the hydrological apex of North America. Using archived runs from global climate models from the IPCC Fourth Assessment Report (AR4) (Phase 3 of the Coupled Model Intercomparison Project - CMIP3), we projected the PDO, ENSO and the NAO for the 21st century for the B1, A1B and A2 Special Report on Emission Scenarios (SRES). These projected climate indices were used as inputs into the GLS regression equations, giving projected northern Rocky Mountains river discharges. These projections showed generally declining trends in northern Rocky Mountains surface water availability for 2006-2050 and 2006-2096.

Keywords: El Niño-Southern Oscillation (ENSO), Generalized Least Squares (GLS) regression models, North Atlantic Oscillation (NAO), Pacific Decadal Oscillation (PDO), projected river discharge, northern Rocky Mountains.

1 Introduction

Northern Rocky Mountain hydroclimatology is heavily influenced by recurring large-scale climate patterns: the Pacific Decadal Oscillation (PDO), the El Niño-Southern Oscillation (ENSO), and the Arctic Oscillation (AO). Strong periodic cycles associated with the low-frequency Pacific Decadal Oscillation (PDO) are manifested in much of the western North American hydroclimate, including that of the northern Rocky Mountains (Mantua et al., 1997; Stewart et al., 2005; St. Jacques et al., 2010). The PDO is an integrated measure of North Pacific oceanic and atmospheric variability that shifts phases on an inter-decadal time scale, usually ~30 years (Minobe, 1997; Mantua and Hare, 2002). In the northern Rocky Mountains, a strong negative relationship exists between the PDO and winter precipitation, and subsequently between the PDO and streamflow (Mantua et al., 1997; Comeau et al., 2009; Wise, 2010). In 1890, the PDO entered into a negative or cool phase, which lasted until 1925 when a positive or warm phase began. In 1947, the PDO shifted back into a negative phase, which continued until 1977, whereupon a positive phase began, which possibly terminated in its turn in 2008. The higher frequency ENSO also affects the hydroclimatology of this region as precipitation and streamflow are decreased during El Niño events and increased during La Niña events (Shabbar and Khandekar, 1996; Shabbar et al., 1997; Bonsal and Lawford, 1999; Bonsal et al., 2001; Shabbar and Skinner, 2004; Bonsal and Shabbar, 2008). The AO is a measure of the intensity of the polar vortex and is closely related to (if not the same as) the North Atlantic Oscillation (NAO) (Wallace and Gutzler, 1981). A negative relationship exists between northern Prairie winter precipitation and the NAO, as the positive NAO (and AO) allows more frequent outbreaks of cold, dry Arctic air to this region (Bonsal and Shabbar, 2008).

Under anthropogenic global warming scenarios, decreased streamflow is projected in the northern Rocky Mountains (see Fig. 10.12, IPCC4, 2007, for multi-model mean run-off changes). St. Jacques et al. (2010) analyzed southern Alberta, and adjacent British Columbia and Montana streamflow records for any significant existing trends attributable to global warming, while explicitly including the possible effects of the PDO and interannual regional circulation anomalies (i.e., ENSO, NAO) to account for naturally-occurring hydroclimatic variability. They concluded that streamflows are declining at most gauges due to hydroclimatic changes (probably from global warming) and, in some cases, intensive use of surface water resources, which were of the same order of magnitude as the changes in the hydrologic regime, if not greater. In the process, they developed Generalized Least Squares (GLS) regression models which explained a large amount of the variance in regional river discharge as a function of the PDO, ENSO and the NAO. In this paper, we take their best-fitting river discharge models, add more models from additional gauges and use these empirical models to project northern Rocky Mountain river discharges for the 21st century. Lapp et al. (2011) developed 21st century projections of the PDO, ENSO and NAO from archived runs of global climate models (GCMs) from the IPCC Fourth Assessment Report (AR4) (Phase 3 of the Coupled Model Intercomparison Project - CMIP3). We used these climate oscillation projections as inputs into the GLS regression equations to produce projected northern Rocky Mountain river discharges for 2000-2096. These projections should be regarded as scenarios or as a thought-experiment, since these extrapolations assume no change in the regional physical hydrology and water management practices, but are useful explorations of the consequences of global warming, including the future status of teleconnections, and of current trends and water management practices.

2 Methods

2.1 *River discharge modeling and projection*

Five actual (recorded) stream discharge records and three naturalized discharge records in the northern Rocky Mountains analyzed by St. Jacques et al. (2010), together with two additional actual stream discharge records, were chosen based on the large amount of variance of observed 20th century discharge (i.e., high R^2) explained by the GLS models (Figure 1, Tables 1 and 2). Four of the gauges, on the Waterton, Elk, Marias and North Fork of the Flathead Rivers, are on unregulated or slightly regulated reaches of these rivers. Three of the gauges measure regulated flows, on the Oldman, St. Mary and Belly Rivers, and in these cases, both the observed actual flows and the reconstructed naturalized flows were separately analyzed, providing an additional six records. Four of the gauges are located in southern Alberta, one in southern British Columbia, and two in adjacent Montana. All records span at least 73 years. The gauges are located at the hydrographic apex of North America, with headwater streams flowing to the Arctic, Atlantic, and Pacific Oceans (Rood et al., 2005).

We extracted the streamflow records from the databases of the Water Survey of Canada (HYDAT; http://www.wsc.ec.gc.ca/applications/H2O/index-eng.cfm, July 12, 2011) and the U.S. National Water Information System (http://waterdata.usgs.gov/nwis/sw, July 12, 2011). In addition to gauge records from unregulated streams, a streamflow database produced by Alberta Environment provided naturalized daily flows and void-filled records to overcome the effects of human impacts and gaps in the time series, respectively (Alberta Environmental Protection, 1998). Mean daily flows averaged over the year were used, because annual averaging normalizes the data by the Central Limit Theorem (Wilks, 2006), thus enabling the use of more powerful parametric statistics. Shapiro-Wilks tests confirmed that most records were normally distributed, and that departures from normality were mild. Low-frequency variability (i.e., slightly smoothed data) was analyzed because of the associated severe socio-economic and ecological impacts of prolonged drought (Figure 2). High-frequency variability in precipitation and streamflow can be accommodated via conventional hazard mitigation strategies (insurance, reservoir storage, etc.), but not low frequency variability (i.e., sustained drought), which is a much more challenging climate hazard. The region has reservoir capacity for a drought of a year or two, but not longer (*pers. comm.* Michael Senaka, Alberta Environment).

Following St. Jacques et al. (2010), we included as predictors in our models a linear trend and three climate indices: the PDO, ENSO, and the NAO, as a proxy for the AO record. The winter averaged (November-March) PDO was computed from the HadSST2 dataset of sea surface temperatures (SST) (Rayner et al., 2003) following the method outlined in Lapp et al. (2011), which closely followed the methodology of Mantua et al. (1997), Zhang et al. (1997), and Mantua and Hare (2002). The annually averaged Southern Oscillation Index (SOI) (used as an ENSO metric) and the winter averaged (December-March) NAO were obtained from the Earth Systems Research Laboratory (National Oceanic and Atmospheric Administration, www.cdc.noaa.gov/ClimateIndices/, July 12, 2011). Since streamflow is naturally lagged and smoothed from precipitation by surface and subsurface hydrology, and large-scale climatic phenomena act most prominently at inter-annual time scales, the stream observations were lagged relative to the climate indices by 0, ±1, and +2 years, and a binomial smoother of five

years was applied to both the stream and climate data. The climate indices and their lags showed only minor collinearity.

Generalized Least Squares (GLS) computes time series regression with serially correlated residuals and is therefore suitable for hydrological data (Brockwell and Davis, 2002). Autoregressive-moving-average (ARMA(p,q)) models were fit to the residuals using a Maximum Likelihood Estimator. Open-source software from the R statistical programming language (version 2.9.1) was used (R Development Core Team, 2008).

The statistical model used in this study is

$$Q_t = \mu + \lambda T_t + \beta_1 x_{1,t} + \ldots + \beta_k x_{k,t} + \varepsilon_t, \qquad t = 1, \ldots, L,$$

where $\{Q_t\}$ is mean daily streamflow for year t, index t runs over L years; μ is the mean streamflow over all L of these years; T_t is a linear trend with coefficient λ representing the trend to be detected; $\{x_{i,t}, i = 1, \ldots, L\}$ is the i^{th} explanatory variable; k is the number of explanatory variables; β_i is the coefficient for the i^{th} explanatory variable; and $\{\varepsilon_t\}$ is the residual time series, which is an autoregressive-moving average process of order (p,q) (ARMA(p,q)). An optimum minimal subset of significant predictors and an optimum minimal ARMA(p,q) residual model was chosen using the corrected Akaike Information Criterion (AIC_c) goodness-of-fit statistic (Brockwell and Davis, 2002) applied to all predictor subsets of size ≤ 6, and for all $p \leq 8$ and $q \leq 5$. Simulation results by Hurvich and Tsai (1989) suggest that the AIC_c outperforms many other model selection criteria, including the AIC and the BIC, when the number of total estimated parameters is more than 10% of the sample size. When the optimum minimal ARMA(p,q) residual model had $p + q > 5$, the model was examined for overfitting using the methods described in *sec. 8.2* of Cryer and Chan (2008) and adjusted accordingly to the ARMA(p,q) residual model with the next smallest AIC_c, if appropriate. Because in GLS regression an ARMA(p,q) model is fit to the residual error, an estimate of the error can be projected into the future and added to the extrapolated future value derived from the regression equation alone, improving the projection (Cryer and Chan, 2008). We projected the residual errors for all regression models, until the projected errors' absolute value were less than 0.05.

We used ARMA processes, rather than the more general integrated autoregressive moving average (ARIMA) processes (Brockwell and Davis, 2002). If $\{Q_t\}$ is modeled with ARMA residuals, but has ARIMA residuals, then erroneous trends may be found (Woodward and Grey, 1993). If a process actually is ARIMA($p,1,q$) and an ARMA($p+1, q$) model is fitted to the series, its characteristic autoregressive equation is likely to have a near-unit root x (i.e., $|x - 1| < 0.2$) (Zheng et al., 1997; Zheng and Basher, 1999; Brockwell and Davis, 2002). We therefore examined the characteristic autoregressive roots of our fitted models to verify that our ARMA modeling was appropriate. The non-zero significance of the trend coefficient λ was tested by the Neyman-Pearson statistic (RP) (Zheng et al., 1997) using the null model of the optimum set of explanatory variables (minus the trend variable if included in the optimum set) versus the alternative model of the optimum set of explanatory variables together with the linear trend (if not already added). The RP is asymptotically distributed as a chi-square distribution with one degree of freedom. If the estimated RP is greater than the 0.10 percentile of $\chi^2_{(1)}$, the trend is significant at the 90% level.

2.2 *How the climate indices were calculated and projected*

2.2.1 *Choice of GCMs*

As part of the IPCC Fourth Assessment Report (AR4) Phase 3 of the Coupled Model Intercomparison Project (CMIP3), international modeling centers submitted their projections for the 21st century under different emissions scenarios, together with their simulations of 20th century climate and pre-industrial control runs to scrutiny by the wider scientific community (Meehl et al., 2007). These data from 23 GCMs are archived by the Program for Climate Model Diagnosis and Intercomparison (PCMDI) of Lawrence Livermore National Laboratory (http://www-pcmdi.llnl.gov/ipcc/about_ipcc.php, July 12, 2011). Details of the GCMs are found in IPCC4 (2007), Table 8.1. Because of the importance of recurring large-scale climate patterns (i.e., the PDO, ENSO, NAO) on surface climate, these CMIP3 runs have been critically examined for their ability to model these atmosphere-ocean climate oscillations (e.g., Muller and Roeckner, 2006; Overland and Wang, 2007; Yu and Zwiers, 2007; Oshima and Tanimoto, 2009; Stoner et al., 2009; Wang et al., 2010; IPCC4, 2007; Lapp et al., 2011). Lapp et al. (2011) were the first to explicitly project the PDO, as calculated by EOF analysis of North Pacific SST residuals, as defined by Mantua et al. (1997) and Zhang et al. (1997). From the 23 GCMs with archived data, Lapp et al. (2011) chose the models best able to simulate the PDO, ENSO, and NAO, using comparisons among the 20th century observed records and the 20th century simulation runs. As well, they specifically examined the GCM's capacity to simulate the low-frequency variability of the PDO using the multi-century pre-industrial control runs. They selected model runs under the low B1, moderate A1B and high A2 emissions scenarios (Nakicenovic et al., 2000). Lapp et al. (2011)'s final set of ten GCMs was CGCM3.1 (T47) (Flato, 2005), CGCM3.1 (T63) (Flato, 2005), ECHAM5/MPI-OM (Roeckner et al., 2003), GDFL-CM2.1 (Delworth et al., 2006), MIROC3.2 (hires) (Hasumi and Emori, 2004), MIROC3.2 (medres) (Hasumi and Emori, 2004), MRI-CGCM2.3.2 (Yukimoto et al., 2001; Yukimoto and Noda, 2003), NCAR-CCSM3 (Collins et al., 2006), NCAR-PCM (Washington et al., 2000) and UKMO-HadCM3 (Gordon et al., 2000; Pope et al., 2000) (Table 3).

2.2.2 *Calculation of the PDO for 1900-2099 from observed and GCM data*

For the calculation of the PDO from the observed instrumental data, Lapp et al. (2011) followed the method described in Mantua et al. (1997), Zhang et al. (1997), and Mantua and Hare (2002). Their PDO index was the leading Principal Component (PC) time series from an un-rotated EOF analysis of monthly, "residual" North Pacific SST anomalies, poleward of 20° N for the 1900-1993 time period. "Residuals" are the difference between the observed SST anomalies and the monthly mean global average SST anomaly (Zhang et al., 1997). The PDO index for 1994-2008 was calculated by projecting the 1994-2008 residual SST anomalies onto the leading eigenvector or loading pattern (EOF 1) from the 1900-1993 SST data. The main methodological divergence of Lapp et al. (2011) from Mantua et al. (1997) lies in their usage of the later and more complete sea surface temperature HadSST2 dataset (Rayner et al., 2003) (http://www.cru.uea.ac.uk/cru/data/temperature/, July 12, 2011), rather than the earlier HadSST1 (Folland and Parker, 1990; 1995) and the Optimally Interpolated SST data (Reynolds and Smith, 1995).

Calculation of the PDO for 1900-2099 from GCM data was computed analogously to the above, simply replacing the observed SST data by GCM SST data. For each chosen GCM and for each of its archived paired 20th and 21st century runs, the GCM SSTs were regridded, using MATLAB®, to the same 5° by 5° grid-cell size as the Hadley Centre SST data set for direct comparison. In particular, the projected PDO indices for 2000-2099 were calculated by projecting the 2000-2099 residual SST anomalies from each of the GCMs onto the leading eigenvector (EOF 1) from the 1900-1993 GCM SST data. Full details concerning the 20th century PDO calculation and its 21st century projection via the GCM runs are in Lapp et al. (2011).

The 21st century winter PDO projections showed a shift towards more occurrences of the negative phase PDO, non-significant for 2000-2050, but significant for 2000-2099, for all three emissions scenarios (Table 4) (Lapp et al., 2011). This can be seen by comparing the all-model 1900-1999 simulation mean to the 2000-2050 and 2000-2099 all-model means (Table 4). Under the more severe A2 emissions scenario, the shift towards more negative phase PDO occurrences was most pronounced. Comparison of the all-model 1900-1999 simulation means to the actual 1900-1999 observed mean PDO index showed that that the GCMs have a slight bias towards the negative PDO phase.

2.2.3 *Calculation and projections of the SOI and NAO*

The annual SOI was calculated as the difference between monthly mean sea level pressure (SLP) at Tahiti, Polynesia (17.5° S, 149.6° W), and Darwin, Australia (12.4° N, 130.9° E), with the difference normalized relative to 1951-1980 (Ropelewski and Jones, 1987). The SOI was projected using the same formula with the station monthly mean SLP data replaced by SLP monthly mean data from the corresponding GCM grid cells. For validation purposes, the SOI was calculated in the same fashion using the corresponding 20th century simulation runs for each GCM and emissions scenario. The early 21st century (2000-2050) SOI projections showed a shift towards a climate with more occurrences of El Niño (negative SOI) and decreases in the occurrences of La Niña (positive SOI) for all emissions scenarios, significantly for the B1 scenario (Table 4). However, the entire 21st century (2000-2099) SOI projections showed a significant shift towards a climate with more occurrences of El Niño for the B1 emissions scenario, but shifts towards more occurrences of La Niña for the A1B and A2 scenarios, non-significantly for the former, and significantly for the latter (Table 4). Comparison of the all-model 1900-1999 simulation means to the actual 1900-1999 observed mean SOI showed that that the GCMs had a bias towards simulating more La Niña events than actually happened.

Likewise, the winter NAO index was calculated as the difference between monthly mean SLP at Gibraltar, Spain (36.1° N, 5.2° W), and Reykjavik, Iceland (64.1° N, 21.6° W), each normalized relative to 1951-1980 before differencing (Jones et al., 1997). The NAO was projected using the same formula with the station monthly mean SLP data replaced by SLP monthly mean data from the corresponding GCM grid cells. For validation purposes, the NAO was calculated in the same fashion using the corresponding 20th century simulation runs for each GCM and emissions scenario. The 21st century NAO projections showed a shift towards a climate with more occurrences of the positive phase of the NAO (positive AO) and decreases in the occurrences of the negative NAO (negative AO) for all three emissions scenarios, a shift significant at the $p \leq 0.05$ level for the A1B and A2 scenarios for both 2000-2050 and 2000-2099

(Table 4). Comparison of the all-model 1900-1999 simulation means to the actual 1900-1999 observed mean NAO index showed that that the GCMs had a problem reproducing the NAO accurately, having a marked bias towards simulating more negative NAO events than actually happened for all emissions scenarios.

2.2.4 *Streamflow projection assessment methods*

In order to determine if significant changes in streamflow were projected for each emissions scenario, GLS trend lines were fit using the R Programming Language to the all-model mean streamflows for the ten mean daily discharge records for two time periods: 2006-2050 and 2006-2096, and the significance of the trend term coefficient β_1 was assessed using the coefficient variance-covariance matrix (i.e., whether or not the interval ($\beta_1 \pm 1.96 * $ standard deviation) contains zero). Extrapolations to mid-century are not unreasonable, given the shortness of the intervening interval; extrapolations to century's end are more speculative, but still worth exploring. A commencement year of 2006 was used because the GLS regressions have the common form of a linear regression equation together with projected ARMA error term in this time period (prior to 2006 there can be no ARMA error term as the GCMs do not explicitly include modeled rivers). Discharge projections end at 2096 (not 2099) because we are using five-year binomially smoothed predictors with leads and lags. In order to compare changes across records, the magnitude of the changes in estimated mean daily flows over the projection periods of 2006-2050 and 2006-2096 were calculated as percentage changes *per annum*: $\Delta/yr = 100*\beta_1/mean(Q)$ (Rood et al., 2005).

Ensembles of climate projections are frequently used to describe prediction uncertainties arising from different GCM constructions, differing initial conditions, and unknown future greenhouse emissions. In this study, each of the ten river discharge records is forecast by an ensemble consisting of a total of 51 GCM streamflow projections drawn from ten GCMs, several of which have multiple runs from different initial conditions, and three emissions scenarios. A typical climate-change ensemble produces a collection of irregular, often tangled, time series or "spaghetti" (Dettinger, 2005). In order to focus on the most likely changes, rather than just the possible changes, a balanced, quantitative assessment of the spaghetti of an ensemble requires an estimation of the underlying projection distribution function (PDF), as the best available approximation of the actual climate-change probability distribution function (Dettinger, 2005; 2006). Smoothed PDFs were estimated by the resampling approach of Dettinger (2005; 2006) based upon principal components analysis (PCA), which generates a large number of additional time series or realizations which share important first- and second-order statistical characteristics with the original ensemble. For each river discharge record, the PCA components were resampled 20,000 times, generating an additional climate-change "projection" realization each time. Following Dettinger (2005, 2006), mixing of the ensemble loading patterns was restricted to only allow intermixing of projections by a single GCM at a time. The realizations were ranked and summarized in histograms to obtain PDFs for 2006, 2050 and 2096. In order to provide flow probabilities for risk analysis and water management, empirical cumulative distribution functions (CDFs) were constructed from the PDFs (Wilks, 2006). All of these calculations were done with MATLAB® Release 2011a.

3 Results

3.1 *GLS river discharge modeling from observed 20th century data*

The GLS regression analysis of the observed streamflow data showed a regional pattern of declining flows in the 20th century (Tables 1 and 2, and Figure 3). Seven of the ten regression models revealed significant declining trends, with the exceptions being the North Fork of the Flathead, the naturalized St. Mary and the naturalized Belly discharge records, which showed no significant trends at the 10% level in the 20th century. Three of the gauge records in relatively undisturbed watersheds, the Elk, Marias and Waterton Rivers, showed significant declines, as did the naturalized Oldman River, which indicates that the declines are not purely due to direct human impact, but also to hydroclimatic causes, presumably global warming. The current year PDO or a lead or lag was the explanatory variable that always appeared in the optimum predictor set (Table 2). Because the predictor variables were standardized to zero mean and unit standard deviation, the relative importance of the predictors can be assessed by comparing the regression coefficients. This showed that the declining trend and the PDO were the most influential predictors. The majority of the 20th century low frequency variance (i.e., that passed by a five-year binomial smoother) was captured by the GLS regression models. The mean R^2_{regular} was 0.56, with R^2_{regular} computed as 1 – (sum-of-squares of simple regression residuals/total-sum-of-squares), i.e., without modeled error adjustment (Table 2). Also shown in Table 2 are the large improvements in the coefficient of determination, $R^2_{\text{innovations}}$, that result from ARMA modeling of the error during the period of record. When $R^2_{\text{innovations}}$ was computed with the modeled error adjustment, its mean was 0.70. During this study, a large number of the longest, naturally-flowing Pacific Northwest and Rocky Mountain rivers were examined for their suitability for similar GLS regression models (Slack and Landwehr, 1992; Harvey et al., 1999; Rood et al., 2005). A large number had very high $R^2_{\text{innovations}}$, but much lower R^2_{regular}, and therefore they were not used for 21st century projections as the ARMA error term can be only projected ~30 years before it decays. Plots of the ten discharge records, together with the fitted regression models, show that the low frequency variance was captured well, with the extreme flows being captured less well (Figure 3). ARMA(p, q) models where $p \geq 2$ and $q \geq 1$ most frequently fitted the error terms, showing the importance of multi-year persistence. All records had no near-unit autoregressive roots, which suggested that ARMA residuals are appropriate.

This study found a greater prevalence of declining significant trends than the earlier study of St. Jacques et al. (2010) using many of the same discharge records (Table 1). We attribute this to our use of the later compiled and more complete HadSST2 dataset in our construction of the PDO index, which we think more accurately represents the historic North Pacific pattern of variability. St. Jacques et al. (2010) used Mantua's PDO index in their analysis which is based upon the earlier and less complete HadSST1 dataset (Mantua et al., 1997).

3.2 *Northern Rocky Mountain projected streamflows to mid- and late-21st century*

Our GLS regression modeling approach based upon GCM projected climate indices indicated generally declining trends in projected northern Rocky Mountain surface water availability for both the first half of the 21st century and over its entirety (Figure 4abc and Table 5). Five of the ten models, those of the Marias, Elk, St. Mary, Oldman and naturalized Oldman discharge records, showed declining trends in the all-model mean projections regardless of the

time period considered for all three emissions scenarios at the 95% significance level. The Waterton record showed significant decreasing trends for all emissions scenarios over the half century; and significant decreasing trends for the B1 and A1B scenarios, and a non-significant decreasing trend for the A2 scenario over the entire century. The actual Belly record showed significant decreasing trends for the B1 and A1B scenarios, and a non-significant decreasing trend for the A2 scenario over the half century; all trends were significantly decreasing for all emissions scenarios over the entire century. The North Fork of the Flathead record showed mainly no significant trends for both time periods, with a decline by 2050 for the A1B scenario, and an increase by 2096 for the A2 scenario. The naturalized St. Mary and naturalized Belly discharge records showed no significant trends for all scenarios for the first half century, which became significantly increasing trends over the entire 21st century for the A2 scenario for the former, and for the A1B and A2 scenarios for the latter. As first observed in the instrumental records, three of the four gauge records in relatively undisturbed watersheds, the Elk, Marias and Waterton Rivers, showed continued projected declines (as did the naturalized Oldman River) which suggests that the declines are not purely due to projected continued direct human impact, but also to global warming. As well, these three projections of records with little direct human impact showed relatively low decline rates compared to those of some of the regulated flows (Table 5). At all three regulated gauges, the all-model mean projections based upon the actual flows showed much steeper declines than the all-model mean projections based upon the naturalized flows. The all-model mean projection based upon the actual flow record for the Oldman River at Lethbridge showed the steepest rate of decline, approaching zero flow at the end of the 21st century. Streamflow trends were broadly similar across all three emissions scenarios, but the A2 emissions scenario showed the most significant increasing trends among the three when considered for the entire century (Figures 4abc).

Time slices of the PDFs of a 20,000-member resampling of the 51-member projection ensemble are shown for 2006, 2050 and 2096 for each of the ten northern Rocky Mountain river records (Figure 5). The PDFs for eight of the discharge records, the Flathead, Marias, Waterton, Elk, St. Mary, Belly, Oldman and naturalized Oldman Rivers, shift from relatively symmetric distributions in 2006 towards broader, left-skewed distributions with modal peaks centered at lower discharges by 2050, with the PDFs for 2096 generally continuing these tendencies. This left-skewness suggests that extreme low flows will become more frequent. Since five-year binomially smoothed data are analyzed, these are conservative estimates. The PDFs for the naturalized St. Mary records show a shift towards having modal peaks centered at lower discharges by 2050, which then reverses by 2096. The PDFs for the naturalized Belly record show a shift towards a modal peak centered at a higher discharge by 2050, a tendency which continues through 2096. The increasing spread over the entire 21st century seen in all ten PDFs is a result of increasing variance in the projected PDO, SOI and NAO indices (i.e., the input variables in the GLS models), and increasing divergence among the GCMs and the emissions scenarios. In a corresponding fashion, the empirical CDFs for seven of the discharge records, the Marias, Waterton, Elk, St. Mary, Belly, Oldman and naturalized Oldman Rivers, shift to the left from 2006 to 2050, and continue to move leftwards through to 2096, with the Oldman River showing a noticeable non-zero probability of negative discharges by 2050, and the Marias, St. Mary, and Oldman Rivers showing negative discharges by 2096 (Figure 6). These negative flows we interpret as demonstrating a significant probability of a dry watercourse, assuming 20th century hydrology and water management practices. For the Oldman River, this probability is

5% by 2050, which grows to 38% by 2096; for the St. Mary River, it is 6% by 2096; and for the Marias River, it is 2% by 2096. The Flathead and naturalized St. Mary CDFs show leftward shifts from 2006 to 2050, and then shift rightward back to their 2006 position by 2096, except for slightly more variance in 2096; whereas the naturalized Belly CDF shows definite right shifts from 2006 to 2050 and then again from 2050 to 2096.

4 Discussion

This study suggests a declining availability of surface water supplies for the northern Rocky Mountains for the 21st century based on river discharges projected using GLS regression models with GCM-derived climate oscillations as predictor variables (Table 2). This study also suggests that any deleterious effects of global warming on surface water supplies are only compounded by the drawdown effects of direct human impacts, which are of at least a similar order of magnitude, as shown by comparison of trends in paired actual and naturalized flow records (Figure 4, Table 5). This is particularly illustrated by the projection of the actual flow of the Oldman River at Lethbridge, an acknowledged over-allocated system (Rood and Vandersteen, 2010), which has a 5% probability of zero flows by 2050, which becomes 38% by the end of the 21st century (Figures 4 and 6). Time slices of the projection distribution functions (PDFs) also suggest a change in the variance of the smoothed flows, from a relatively symmetric equal probability of low versus high flows about the mode and mean in 2006, to a flow pattern with a higher probability of flows less than the mode by 2050, a tendency which generally continues and increases by 2096 (Figure 5).

For the climatological context of these hydrological projections, Barrow (2010) examined Second Coupled Model Intercomparison Project (CMIP2) GCM projections for temperature and precipitation for southern Alberta and Saskatchewan. These projections showed median increases in annual mean temperature of 4° to 6° C by 2070-2099, with maximum annual mean temperature increases of between 6° and 8° C. Minimum annual precipitation changes indicate slight decreases of 0-10% across the southern Prairies throughout the 21st century; however, median and maximum changes suggest annual increases in regional precipitation. There is a projected seasonal shift in precipitation from summer to winter (Barrow, 2010).

This study's results are compatible with the extrapolation of declining trends in the observed centennial-length instrumental records (e.g., Zhang et al., 2001; Rood et al., 2005; 2008; Schindler and Donahue, 2006; St. Jacques et al., 2010; Shepherd et al., 2010). For comparison, the instrumental climate records from 1900-1998 show that the headwater region has experienced increased daily maximum and minimum temperatures and increased annual precipitation (Zhang et al., 2000). This present study is also in accord with Schindler and Donahue (2006) and St. Jacques et al. (2010) that any deleterious effects of global warming on regional surface water supplies are only compounded by the drawdown effects of direct human impacts.

This study used GCM-derived atmosphere-ocean climate indices as predictors in statistical hydrological models (Vicuna and Dracup, 2007). Our statistical model captures the hydroclimatic variability over the entire instrumental record which allows us to include the effects of low frequency climate variability such as that of the PDO. This regression-based projection approach is not without precedent: Stewart et al. (2004) developed a similar ordinary least squares regression-based projection of changes in western North American snowmelt runoff timing, using downscaled GCM-projected temperature and precipitation data as predictors. Regression-based approaches using atmosphere-ocean climate oscillations, such as ENSO, or other oceanic variables, have been used in many regions of the globe to successfully forecast short-term streamflow (e.g., Ruiz et al., 2007; Xu et al., 2007; Lima and Lall, 2010). Because regression models are relatively fast and easy to build, it is feasible to construct many such

models, enabling coverage of a wide geographical area. A limitation of these statistical approaches is that they do not explicitly account for the physical mechanisms and processes that define basin response to climate forcing. The use of GCM temperature and precipitation projections (with or without downscaling) as predictors in physically-based hydrologic models (e.g., Dettinger et al., 2004; Lapp et al., 2009; Shepherd et al., 2010; Kienzle et al., 2011; Larson et al., 2011) is typically labor- and time-intensive, requiring detailed basin physical characteristics and climate data for model parameterization, calibration and validation. The northern Rocky Mountain rivers are largely fed by snowmelt at high elevations. Snowpack accumulation and climate monitoring data are sparse, if they even exist, and are certainly not available at a density to adequately represent spatially this very climatologically heterogeneous region. These data constraints generally limit the calibration data to the period of satellite remote sensing datasets for estimating snowcover, land-use, vegetation extent and type, etc. (Day, 2009). Therefore the full extent of instrumental climatological and hydrological variability, as brief and unrepresentative it is (as shown by proxy-based paleoclimatic records, e.g., Luckman and Wilson, 2005; Axelson et al., 2010), is not applied to the physically-based hydrologic models. Thus, the statistical hydrological models and the physically-based watershed models form two complimentary approaches, each with its own advantages and limitations. If the two approaches converge on a common projected result, this lends confidence to both.

This study's results are broadly consistent with other related work on regional trends in projected streamflow using physically-based hydrologic models (i.e., Lapp et al., 2009; Shepherd et al., 2010; Larson et al., 2011). Lapp et al. (2009) generated scenarios of future flows of the South Saskatchewan River at Lake Diefenbaker and its tributaries, the Bow, Red Deer and Oldman Rivers, under the SRES A2 emissions scenario by coupling the HadCM3 GCM with the hydrological WATFLOOD model. When comparing 2040-2069 mean projected data to 1961-1990 baseline data, Lapp et al. (2009) found projected annual flow decreases in all rivers (an average decline of -7%), and a shift in the dominant flow to earlier in the year in all rivers. Similarly, Shepherd et al. (2010) drove the physical models MTCLIM, SNOPAC and RIVRQ with statistically-downscaled global circulation data from six recent CMIP2 and CMIP3 GCMs to project Rocky Mountain rivers, including the Belly, Waterton, naturalized Oldman, and naturalized St. Mary Rivers, for the first half of the 21st century under the SRES A2 emissions scenario. Shepherd et al. (2010) found that summer flows are projected to decline considerably, while winter and early spring flows are projected to increase, with an overall decline in annual discharge of -3% over 2005-2055. On the other hand, Larson et al. (2011) and MacDonald et al. (2011) projected decreases in spring flows from snowmelt for the 21st century, using delta-method downscaled GCM data over a range of SRES emissions scenarios as inputs into the hydrological models SIMGRID to model spring runoff from snowpack, and GENESYS to model snowpack, respectively, in the fully allocated St. Mary River watershed, Montana and Alberta. Since mountain snowpack provides so much of the total annual discharge in these mountain rivers, the declining spring meltwater volumes projected in these two latter studies would be consistent with our study's projected declines in annual discharge.

The declining trend terms and the PDO terms were the most influential predictors among those examined (Table 2). All of the PDO terms had negative coefficients in the GLS regression models (Table 2) and therefore modeled increasing discharge when the PDO index is negative and decreasing discharge when the PDO index is positive. Lapp et al. (2011) showed a

statistically significant multi-model mean shift towards more occurrences of the negative phase PDO for the time period 2000-2099 for the B1, A1B and A2 emissions scenarios. In particular, the A2 scenario all-model mean PDO index was projected to become significantly more negative which is reflected in the significantly increased discharges for the Flathead, naturalized St. Mary and naturalized Belly records, whose GLS models do not include a declining trend term (Figure 4 and Table 5). More occurrences of the negative phase of the PDO are also consistent with increasing winter precipitation (Barrow, 2010). Hence, it might be expected that the influential PDO terms would only contribute to projected discharges (but see paragraph below). Yet note that in the projected competing effects between the PDO terms' largely contributing to northern Rocky mountain discharge, and the declining trend terms contributing to decreased flows, this study suggests that the declining trend terms dominate in the majority of the modeled river records.

In Lapp et al. (2011) not all the models showed a consistent shift to negative PDO conditions. The GCMs separate between those showing a shift, often significant, towards more negative PDO-like conditions for all three scenarios (i.e., MIROC (medres), MRI and HadCM3), and those showing a contrary shift, also often significant, towards more positive PDO-like conditions for all runs and all three scenarios (i.e., CGCM3.1 (T47) , CGCM3.1 (T63), GDFL2.1, MIROC (hires) and NCAR-PCM). If these latter GCMs are correct and the PDO shifts into a more positive state in the 21st century, then the PDO terms in the GLS models will contribute to discharge deficits, rather than increases. PDO projections from the ongoing AR5 (CMIP5) climate prediction experiments would be valuable for projecting the regional hydroclimatology, especially if they show more consistency in the direction of PDO shift. Overland and Wang (2007) and Wang et al. (2010) examined the closely related question of when the anthropogenic global warming trend will surpass the natural variability of the North Pacific region under the A1B emissions scenario. They suggested circa 2040-2050, leading towards a weaker meridional temperature gradient in the North Pacific Region, and thereby perhaps to a weakening of its effect on the sub-polar jetstream. (The mechanism by which the PDO affects the hydroclimatology of the downstream western North America is through a shift in the position of the sub-polar jet, which brings winter storms and precipitation as it crosses over the edge of the continent (Gershunov and Barnett, 1998; Bonsal et al., 2001; Stahl et al., 2006)). Because of this result, our streamflow projections past 2050 are likely less reliable.

The reliability of our results also depends on the representativeness of the low B1, moderate A1B and severe A2 SRES emission scenarios. Recent research (van Vuuren and Riahi, 2008) compared actual measured emissions to the IPCC Special Report on Emissions Scenarios (SRES) forecast rates and showed that thus far, for 1990-2006, a high emissions scenario has been most appropriate. The growth rate of global emissions after 2000 has been about 3%, whereas the forecast growth rates under SRES had ranged from between 1.4% and 3.4%. Hence, the actual emissions have been well represented by the scenario variability so far.

These GLS model extrapolations are thought-experiments of what could happen if present-day trends in temperature, precipitation, evapotranspiration, water demand and use continue on the same path; together with the current relationships between northern Rocky Mountain hydroclimatology and the atmosphere-ocean climate oscillations (as assessed over the entire centennial-length instrumental record). These projections out to 2050 do not seem

unreasonable, given the shortness of the intervening time interval. They present a sobering picture of probable declines in surface water supplies in a region where water is already highly in demand and tightly allocated. Post-2050, these projections are certainly more speculative, given our assumption of no changes in the physical hydrology, such as those induced by a shift of precipitation from snow to rain, the post-2050 North Pacific Ocean variability shifts (Overland and Wang, 2007; Wang et al., 2010), and the tendency of GCM-based post-2050 PDO projections to divide into those demonstrating strong negative PDO phase shifts and those demonstrating strong positive PDO phase shifts (Lapp et al*.,* 2011). Nevertheless, these entire 21st century projections are a worthwhile exploration of the range of possible scenarios, highlighting probable future surface water deficits and the importance of the future behavior of the PDO upon northern Rocky Mountain river discharges.

5. Acknowledgments

We acknowledge the international modeling groups for providing their data for analysis, the Program for Climate Model Diagnosis and Intercomparison (PCMDI) for collecting and archiving the model data, the WCRP/CLIVAR Working Group on Coupled Models (WGCM), and their Coupled Model Intercomparison Project (CMIP) and Climate Simulation Panels for organizing the model data analysis activity, and the IPCC WG1 TSU for technical support. This research was funded by the Natural Sciences and Engineering Research Council of Canada and Alberta Environment.

References

Alberta Environmental Protection, 1998. South Saskatchewan River basin historical weekly natural flows 1912 to 1995: Main Report and MicrosoftAccess Database. Natural Resources Services, Water Management Division, Water Sciences Branch, Edmonton.

Axelson J., Sauchyn D.J., Barichivich J., 2010. New reconstructions of streamflow variability in the South Saskatchewan River basin from a network of tree-ring chronologies, Alberta, Canada. Water Resources Research 45, W09422.

Barrow, E., 2010. Climate change scenarios for the Prairie Provinces. In: Sauchyn, D.J., H. Diaz, H., Kulshreshtha, S. (Eds.), The New Normal: the Canadian Prairies in a Changing Climate, Canadian Plains Research Center Press, Regina, Saskatchewan, pp. 41-58.

Bonsal, B., Lawford, R.G., 1999. Teleconnections between El Niño and La Niña events and summer extended dry spells on the Canadian prairies. International Journal of Climatology, 19, 1445-1458.

Bonsal, B., Shabbar, A., 2008. Impacts of large-scale circulation variability on low streamflows over Canada: a review. Canadian Water Resources Journal, 33, 137-154.

Bonsal, B., Shabbar, A., Higuchi, K., 2001. Impacts of low frequency variability modes on Canadian winter temperature. International Journal of Climatology, 21, 95-108.

Brockwell, P.J., Davis, R.A., 2002. Introduction to time series and forecasting, 2nd *ed.*, Springer-Verlag, New York.

Collins W.D., Bitz, C.M., Blackmon, M.L., Bonan, G.B., Bretherton, C.S., Carton, J.A., Chang, P., Doney, S.C., Hack, J.J., Henderson, T.B., Kiehl, J.T., Large, W.G., McKenna, D.S., Santer, B.D., Smith, R.D., 2006. The Community Climate System Model Version 3 (CCSM3). Journal of Climate, 19, 2122-2143.

Comeau, L.E.L., Pietroniro, A., Demuth, M.N., 2009. Glacier contribution to the North and South Saskatchewan Rivers. Hydrological Processes, 23, 2640-2653.

Cryer, J.D., Chan, K.-S., 2008. Time series analysis with applications in R, 2nd *ed.,* Springer-Verlag, New York.

Day, C.A., 2009. Modelling impacts of climate change on snowmelt runoff generation and streamflow across western US mountain basins: a review of techniques and applications for water resource management. Progress in Physical Geography 33, 614-633.

Delworth, T.L., Rosati, A., Stouffer, R.J., Dixon, K.W., Dunne, J., Findell, K., Ginoux, P., Gnanadesikan, A., Gordon, C.T., Griffies, S.M., Gudgel, R., Harrison, M.J., Held, I.M., Hemler, R.S., Horowitz, L.W., Klein, S.A., Knutson, T.R., Lin, S.-J., Milly, P.C.D., Ramaswamy, V., Schwarzkopf, M.D., Sirutis, J.J., Stern, W.F., Spelman, M.J., Winton, M., Wittenberg, A.T., Wyman, B., 2006. GDFL's CM2 global coupled climate models. Part I: Formulation and simulation characteristics. Journal of Climate, 19, 643-674.

Dettinger, M.D., 2005. From climate-change spaghetti to climate-change distributions for 21st century California. San Francisco Estuary and Watershed Science, 3(1) Article 4 (http://repositories.cdlib.org/jmie/sfews/vol3/iss1/art4).

Dettinger, M.D., 2006. A component-resampling approach for estimating probability distributions from small forecast ensembles. Climatic Change 76, 149-168.

Dettinger, M.D., Cayan, D.R., Meyer, M.K., Jeton, A.E., 2004. Simulated hydrologic responses to climate variations and change in the Merced, Carson and American River basins, Sierra Nevada, California, 1900-2099. Climatic Change 62, 283-317.

Flato, G.M., 2005. The Third Generation Coupled Global Climate Model (CGCM3). (Available online at http://www.cccma.bc.ec.gc.ca/models/cgcm3.shtml.)

Folland, C.K., Parker, D.E., 1990. Observed variations of sea surface temperature. In: Schlesinger, M.E. (Ed.), Climate-Ocean Interaction, Kluwer, Amsterdam, pp. 21-52.

Folland, C.K., Parker, D.E., 1995. Correction of instrumental biases in historical sea surface temperature data. Quarterly Journal of the Royal Meteorological Society 121, 319-367.

Gershunov, A., Barnett, T.P., 1998. Interdecadal modulation of ENSO teleconnections. Bulletin of the American Meteorological Society 79, 2715-2725.

Gordon, C., Cooper, C., Senior, C.A., Banks, H.T., Gregory, J.M., Johns, T.C., Mitchell, J.F.B., Wood, R.A., 2000. The simulation of SST, sea ice extents and ocean heat transports in a version of the Hadley Centre coupled model without flux adjustments. Climate Dynamics 16, 147–168.

Harvey, K.D., Pilon, P.J., Yuzyk T.R., 1999. Canada's reference hydrometric basin network (RHBN). In: Partnerships in Water Resources Management. Paper presented at Canadian Water Resources Association (CWRA)'s 51st Annual Conference, June 1999, Halifax, Nova Scotia.

Hasumi, H., Emori, S., 2004. K-1 coupled GCM (MIROC) description. K-1 Tech. Rep. 1, Center for Climate System Research, University of Tokyo, 39 pp. (Available online at http://www.ccsr.u-tokyo.ac.jp/kyosei/hasumi/MIROC/tech-repo.pdf.).

Hurvich, C.M., Tsai, C.L., 1989. Regression and time series model selection in small samples. Biometrika 76, 297-307.

IPCC4, 2007. Climate Change 2007: The Physical Science Basis. Contribution of Working Group I to the Fourth Assessment Report of the Intergovernmental Panel on Climate Change (Solomon, S., Qin, D., Manning, M., Chen, Z., Marquis, M., Avery, K.B., Tignor, M., Miller, H.L. (Eds.)), Cambridge University Press, Cambridge, UK.

Jones, P.D., Jonsson, T., Wheeler, D., 1997. Extension to the North Atlantic Oscillation using early instrumental pressure observations from Gibraltar and South-west Iceland. International Journal of Climatology, 17, 1433-1450.

Kienzle, S.W., Nemeth, M.W., Bryne, J.M., McDonald, R.J., 2011. Simulating the hydrological impacts of climate change in the upper North Saskatchewan River basin, Alberta, Canada. Journal of Hydrology, DOI: 10.1016/j.jhydrol.2011.01.058.

Lapp, S., Sauchyn, D.J., Toth, B., 2009. Constructing scenarios of future climate and water supply for the SSRB: Use and limitations for vulnerability assessment. Prairie Forum 34, 153-180.

Lapp, S., St. Jacques, J.M., Barrow, E.M., Sauchyn, D.J., (2011). GCM projections for the Pacific Decadal Oscillation under greenhouse forcing for the early 21st century. International Journal of Climatology. DOI: 10.1002/joc.2364.

Larson, R.P., Byrne, J.M., Johnson, D.L., Kienzle, S.W., Letts, M.G., 2011. Modelling climate change impacts on spring runoff for the Rocky Mountains of Montana and Alberta II: runoff change projections using future scenarios. Canadian Water Resources Journal 36, 35-52.

Lima, C.H.R., Lall, U., 2010. Climate informed monthly streamflow forecasts for the Brazilian hydropower network using a periodic ridge regression model. Journal of Hydrology 380, 438-449.

Luckman B.H., Wilson, R.J.S., 2005. Summer Temperature in the Canadian Rockies During the last Millennium: a Revised Record. Climate Dynamics 24, 131-144.

MacDonald, R.J., Byrne, J.M., Kienzle, S.W., Larson, R.P., 2011. Assessing the potential impacts of climate change on mountain snowpack in the St. Mary River watershed, Montana, Journal of Hydrometeorology 12, 262-273.

Mantua, N.J., Hare, S.R., 2002. The Pacific Decadal Oscillation, Journal of Oceanography 58, 35-44.

Mantua, N.J., Hare, S.R., Zhang, Y., Wallace, J.M., Francis, R.C., 1997. A Pacific interdecadal climate oscillation with impacts on salmon production. Bulletin of the American Meteorological Society 78, 1069-1079.

Meehl, G.A., Covey, C., Delworth, T., Latif, M., McAvaney, B., Mitchell, J.F.B., Stouffer, R.J., Taylor, K.E., 2007. The WCRP CMIP3 multimodel dataset, a new era in climate change research. Bulletin of the American Meteorological Society 88, 1383-1394.

Minobe, S., 1997. A 50-70 year climatic oscillation over the North Pacific and North America, Geophysical Research Letters 24, 683-686.

Muller, W.A., Roeckner, E., 2006. ENSO impact on Midlatitude Circulation Patterns in Future Climate Change Projections. Geophysical Research Letters 33, L05711, DOI:10.1029/2005GL025032.

Nakicenovic N., Alcamo, J., Davis, G., de Vries, B., Fenhann, J., Gaffin, S., Gregory, K., Grübler, A., Jung, T.Y., Kram, T., La Rovere, E.L., Michaelis, L., Mori, S., Morita, T., Pepper, W., Pitcher, H., Price, L., Riahi, K., Roehrl, A., Rogner, H.H., Sankovski, A.,

Schlesinger, M., Shukla, P., Smith, S., Swart, R., van Rooijen, S., Victor, N., Dadi, Z., 2000. IPCC Special Report on Emissions Scenarios, Cambridge University Press, Cambridge, United Kingdom and New York, NY, USA.

Oshima, K., Tanimoto, Y., 2009. An evaluation of reproducibility of the Pacific Decadal Oscillation in the CMIP3 simulations. Journal of the Meteorological Society of Japan 87, 755-770.

Overland, J.E., Wang, M., 2007. Future climate of the North Pacific Ocean. Eos 88, 178, 182.

Pope, V.D., Gallani, M.L., Rowntree, P.R., Stratton, R.A., 2000. The impact of new physical parameterizations in the Hadley Centre climate model: HadAM3. Climate Dynamics 16, 123–146.

R Development Core Team, 2008. R: A language and environment for statistical computing. R Foundation for Statistical Computing, Vienna, Austria. ISBN 3-900051-07-0, (version 2.91. used) URL http://www.R-project.org.

Rayner, N.A., Parker, D.E., Horton, E.B., Folland, C.K., Alexander, L.V., Rowell, D.P., Kent, E.C., Kaplan, A., 2003. Globally complete analyses of sea surface temperature, sea ice and night marine air temperature, 1871-2000. Journal of Geophysical Research 108, 4407, DOI 10.1029/2002JD002670.

Reynolds, R.W., Smith, T.M., 1995. A high-resolution global sea surface temperature climatology. Journal of Climate 8, 1571-1583.

Roeckner E, Bauml, G., Bonaventura, L., Brokopf, R., Esch, M., Giorgetta, M., Hagemann, S., Kornblueh, L., Schlese, U., Schulzweida, U., Kirchner, I., Manzini, E., Rhodin, A., Tompkins, A., 2003. The atmospheric general circulation model ECHAM5. Part I: Model description. Max-Planck-Institute for Meteorology Report, 127 pp. (Available online at http://edoc.mpg.de/175329.)

Rood, S.B., Vandersteen, J.W., 2010. Relaxing the principle of prior appropriation: stored water and sharing the shortage in Alberta, Canada. Water Resources Management 24, 1605-1620.

Rood, S.B., Samuelson, G.M., Weber, J.K., Wywrot, K.A., 2005. Twentieth-century decline in streamflows from the hydrographic apex of North America. Journal of Hydrology 306, 215-233.

Rood, S.B., Pan, J., Gill, K.M., Franks, C.G., Samuelson, G.M., Shepherd, A., 2008. Declining summer flows of Rocky Mountain rivers: changing seasonal hydrology and probable impacts on floodplain forests. Journal of Hydrology 349, 397-410.

Ropelewski, C.F., Jones, P.D., 1987. An extension of the Tahiti-Darwin Southern Oscillation Index. Monthly Weather Review 115, 2161-2165.

Ruiz, J.E., Cordery, I., Sharma, A., 2007. Forecasting streamflows in Australia using the tropical Indo-Pacific thermocline as predictor. Journal of Hydrology 341, 156-164.

St. Jacques, J.M., Sauchyn, D.J., Zhao, Y., 2010. Northern Rocky Mountain streamflow records: global warming trends, human impacts or natural variability? Geophysical Research Letters 37, 2009GL042045.

Schindler, D.W., Donahue, W.F., 2006. An impending water crisis in Canada's western prairie provinces. Proceedings of the National Academy of Sciences 103, 7210-7216.

Shabbar, A., Khandekar, M., 1996. The impact of El Niño-Southern Oscillation on the temperature field over Canada. Atmosphere-Ocean 34, 401-416.

Shabbar, A., Skinner, W., 2004. Summer drought patterns in Canada and the relationship to global sea surface temperatures. Journal of Climate 17, 2866-2880.

Shabbar, A., Bonsal, B., Khandekar, M., 1997. Canadian precipitation patterns associated with the Southern Oscillation. Journal of Climate 10, 3016-3027.

Shepherd, A., Gill, K.M., Rood, S.B., 2010. Climate change and future flows of Rocky Mountain rivers: converging forecast from empirical trend projection and down-scaled global circulation modeling. Hydrological Processes 24, 3864-3877.

Slack, J.R., Landwehr, J.M., 1992. Hydro-climatic data network: a U.S. Geological Survey streamflow data set for the United States for the study of climate variations, 1874-1988, United States Geological Survey Open-File Report 92-129.

Stahl, K., Moore, R.D., McKendry, I.G., 2006. The role of synoptic-scale circulation in the linkage between large-scale ocean-atmosphere indices and winter surface climate in British Columbia, Canada. International Journal of Climatology 26, 541-560.

Stewart, I., Cayan, D.R., Dettinger, M.D., 2004. Changes in snowmelt runoff timing in western North America under a "business as usual" climate change scenario. Climatic Change 62, 217-232.

Stewart, I., Cayan, D.R., Dettinger, M.D., 2005. Changes toward earlier streamflow timing across western North America. Journal of Climate 18, 1136-1155.

Stoner, A.M.K., Hayhoe, K., Wuebbles, D.J., 2009. Assessing general circulation model simulations of atmospheric teleconnection patterns. Journal of Climate 22, 4348-4372.

van Vuuren, D.P., Riahi, K., 2008. Do recent emission trends imply higher emissions forever? Climatic Change 91, 237-248.

Vicuna, S., Dracup, J.A., 2007. The evolution of climate change impact studies on hydrology and water resources in California. Climatic Change 82, 327-350.

Wallace, J.M., Gutzler, D.S., 1981. Teleconnections in the geopotential height field during the Northern Hemisphere winter. Monthly Weather Review 109, 784-812.

Wang, M., Overland, J.E., Bond, N.A., 2010. Climate projections for selected large marine ecosystems. Journal of Marine Systems 79, 258-266.

Washington, W. M., Weatherly, J.W., Meehl, G.A., Semtner Jr., J.A., Bettge, T.W., Craig, A.P., Strand Jr., W.G., Arblaster, J., Wayland, V.B., James, R., Zhang, Y., 2000. Parallel Climate Model (PCM) control and transient simulations. Climate Dynamics 16, 755–774.

Wilks, D.S., 2006. Statistical Methods in the Atmospheric Sciences, *2nd ed.*, Academic Press, New York.

Wise, E.K., 2010. Spatiotemporal variability of the precipitation dipole transition zone in the western United States. Geophysical Research Letters 37, L07706.

Woodward, W.A., Gray, H.L., 1993. Global warming and the problem of testing for trend in time series data. Journal of Climate 6, 953-962.

Xu, K., Brown, C., Kwon, H.-H., Lall, U., Zhang, J., Hayashi, S., Chen, Z., 2007. Climate teleconnections to Yangtze river seasonal streamflow at the Three Gorges Dam, China. International Journal of Climatology 27, 771-780.

Yu, B., Zwiers, F.W., 2007. The impact of combined ENSO and PDO on the PNA climate: a 1,000-year climate modeling study. Climate Dynamics 29, 837-851.

Yukimoto, S., Noda, A., 2003. Improvements of the Meteorological Research Institute Global Ocean-Atmosphere Coupled GCM (MRI-GCM2) and its climate sensitivity. CGER's Supercomputing Activity Report, Vol. 10-2001, National Institute for Environmental Studies, Ibaraki, Japan, 37–44.

Yukimoto, S., Noda, A., Kitoh, A., Sugi, M., Kitamura, Y., Hosaka, M., Shibata, K., Maeda, S., Uchiyama, T., 2001. The new Meteorological Research Institute global ocean-atmosphere coupled GCM (MRICGCM2)–Model climate and variability. Papers in Meteorology and Geophysics 51, 47–88.

Zhang, X., Vincent, L.A., Hogg, W.D., Niitsoo, A., 2000. Temperature and precipitation trends in Canada during the 20th century. Atmosphere-Ocean 38, 395-429.

Zhang, X., Harvey, K.D., Hogg, W.D., Yuzyk, T.R., 2001. Trends in Canadian streamflow. Water Resources Research 37, 987-998.

Zhang, Y., Wallace, J.M., Battisti, D.S., 1997. ENSO-like interdecadal variability: 1900-1993. Journal of Climate 10, 1004-1020.

Zheng, X., Basher, R.E., 1999. Structural time series models and trend detection in global and regional temperature series. Journal of Climate 12, 2347-2358.

Zheng, X., Basher, R.E., Thompson, C.S., 1997. Trend detection in regional-mean temperature series: maximum, minimum, mean, diurnal range, and SST. Journal of Climate 10, 317-326.

Table 1. Details of the ten northern Rocky Mountain discharge records. Significant linear trend as assessed following the methodology of St. Jacques et al. (2010). Low-pass variance is the variance in low-frequency filtered streamflow data as a percentage of the total variability. Mean Q_t is mean daily discharge averaged over the year. The naturalized records are from the same location as the corresponding actual flow gauge.

Flow record (HYDAT or USGS code)	Record period	Flow regime	Significant linear trend?	Low-pass variance	Gross drainage (km^2)	Mean Q_t (m^3/s)
1.North Fork Flathead R., MT (12355500)	1936-2008	natural	none	43.1%	4009.3	83.9
2. Marias R. near Shelby, MT (06099500)	1912-2007	natural	decreasing	45.3%	3242.0	25.0
3. Waterton R. near Waterton Park, AB (05AD003)	1912-2007	natural	decreasing	40.6%	612.7	17.6
4. Elk R. at Phillips Bridge, BC (08NK005)	1933-2008	natural	decreasing	40.7%	4450.0	75.9
5. St. Mary R. at International Boundary, AB (05AE027)	1903-2007	regulated	decreasing	51.6%	1206.4	20.2
6. St. Mary R. at International Boundary	1912-2001	naturalized	none	38.9%	1206.4	25.1
7. Belly R. near Mountain View, AB (05AD005)	1912-2007	regulated	decreasing	38.5%	319.2	8.6
8. Belly R. near Mountain View	1912-2001	naturalized	none	38.6%	319.2	9.1
9. Oldman R. near Lethbridge, AB (05AD007)	1912-2007	regulated	decreasing	52.2%	17,045.6	84.6
10. Oldman R. near Lethbridge	1912-2001	naturalized	decreasing	44.1%	17,045.6	109.6

Table 2. Identification of the optimum Generalized Least Squares (GLS) equations and residual models for the ten northern Rocky Mountain streamflow records. AIC_c: corrected Akaike Information Criterion. Predictor variables are standardized to zero mean and unit standard deviation; discharge Q_t is centered to zero mean. 0, ±1, +2 year lags of climate indices included in analysis. P1: climate leads streamflow 1 year. P2: climate leads streamflow 2 years. N1: climate lags streamflow 1 year. RP: Neyman-Pearson statistic (results significant at the 10% level in bold).

Flow record	R^{2*} (regular)	R^{2**} (innovations)	AIC_c	GLS equation	Residual model	RP (p-level)
1.North Fork Flathead R.	0.53	0.75	464.4	$Q_t = 0.10 - 7.92*PDO - 2.21*NAO_{P1} - 4.18*PDO_{P2} - 3.39*SOI_{P2}$	ARMA(2,1)	1.1 (0.29)
2. Marias R.	0.56	0.74	526.2	$Q_t = 0.21 - 3.0*trend - 2.07*PDO - 1.06*NAO_{P1} - 1.21*PDO_{P1} - 2.06*PDO_{P2} - 2.44*SOI_{P2}$	ARMA(2,3)	30.0 ($4.3xe^{-8}$)
3. Waterton R.	0.57	0.66	359.4	$Q_t = 0.06 - 0.58*trend - 1.06*PDO + 0.57*SOI_{N1} - 1.06*PDO_{P2} - 0.69*SOI_{P2}$	ARMA(1,2)	12.8 (0.0003)
4. Elk R. at Phillips Bridge	0.54	0.71	478.8	$Q_t = 0.05 - 1.75*trend - 6.66*PDO - 1.68*NAO_{N1} - 1.37*NAO_{P1} - 3.09*PDO_{P2} - 3.12*SOI_{P2}$	ARMA(2,1)	18.2 ($2.0xe^{-5}$)
5. Actual St. Mary R.	0.61	0.75	492.6	$Q_t = -0.03 - 3.10*trend - 1.52*PDO + 0.80*NAO_{P2} - 1.31*PDO_{P2} - 1.50*SOI_{P2}$	ARMA(0,3)	22.6 ($2.0xe^{-6}$)
6. Naturalized St. Mary R.	0.51	0.71	393.5	$Q_t = -0.03 - 1.55*PDO + 0.76*SOI - 0.90*NAO_{N1} + 1.09*NAO_{P2} - 0.98*PDO_{P2} - 1.04*SOI_{P2}$	ARMA(3,2)	0.58 (0.45)
7. Actual Belly R.	0.55	0.64	239.1	$Q_t = 0.01 - 0.32*trend - 0.40*PDO + 0.34*SOI_{N1} + 0.31*NAO_{P2} - 0.47*PDO_{P2} - 0.35*SOI_{P2}$	ARMA(1,2)	15.3 ($9.0xe^{-5}$)
8. Naturalized Belly R.	0.57	0.67	214.0	$Q_t = 0.002 - 0.37*PDO + 0.24*SOI + 0.31*SOI_{N1} + 0.24*NAO_{P2} - 0.50*PDO_{P2} - 0.34*SOI_{P2}$	ARMA(2,1)	0.02 (0.89)
9. Actual Oldman R.	0.62	0.73	787.3	$Q_t = 0.11 - 17.17*trend - 9.25*PDO - 9.52*PDO_{P2} - 9.75*SOI_{P2}$	ARMA(2,3)	19.7 ($9.0xe^{-6}$)
10. Naturalized Oldman R.	0.49	0.65	729.0	$Q_t = -0.24 - 5.16*trend - 8.38*PDO - 10.02*PDO_{P2} - 10.19*SOI_{P2}$	ARMA(2,3)	3.6 (0.06)

* $R^2_{regular}$ computed as 1 – (sum-of-squares of regression residuals/total-sum-of-squares), i.e., without modeled error adjustment.
** $R^2_{innovations}$ computed with the modeled error adjustment.

Table 3. List of the ten chosen coupled atmosphere-ocean models which archived the required fields, their details, and number of available 21st century runs per scenario.

#	IPCC4 Model ID	Country	Atmospheric resolution	Oceanic resolution	Number 21st century runs		
					B1	A1B	A2
1	CGCM3.1(T47)	Canada	3.7^{o}x3.7^{o} L31	1.84^{o}x1.85^{o} L29	3	3	3
2	CGCM3.1(T63)	Canada	2.8^{o}x2.8^{o} L31	1.4^{o}x0.9^{o} L29	1	1	0
3	ECHAM5/MPI-OM	Germany	1.875^{o}x1.865^{o} L31	1.5^{o}x1.5^{o} L40	2	2	1
4	GDFL-CM2.1	USA	2.5^{o}x2.0^{o} L24	1.0^{o}x1.0^{o} L50	1	1	1
5	MIROC3.2(hires)	Japan	1.125^{o}x1.12^{o} L56	0.28^{o}x0.188^{o} L47	1	1	0
6	MIROC3.2(medres)	Japan	2.8^{o}x2.8^{o} L20	(0.5-1.4^{o}) x1.4^{o} L43	1	1	1
7	MRI-CGCM2.3.2	Japan	2.8^{o}x2.8^{o} L31	(0.5-2.5^{o}) x2.0^{o} L23	5	5	5
8	NCAR-CCSM3	USA	1.4^{o}x1.4^{o} L26	(0.3-1.0^{o}) x1.0^{o} L40	1	1	1
9	NCAR-PCM	USA	2.8^{o}x2.8^{o} L18	(0.5-0.7^{o}) x0.7^{o} L32	2	2	2
10	UKMO-HadCM3	UK	3.75^{o}x2.5^{o} L15	1.25^{o}x1.25^{o} L20	1	1	1

Table 4. 20th century observed mean climate indices and multi-model mean climate indices for the 20th century simulations and for the 21st century projections under the B1, A1B and A2 emission scenarios. Red values identify a future shift to a positive PDO or negative SOI (El Niño-like) or negative NAO mean state; and blue to the opposite conditions (i.e., negative PDO or positive SOI (La Niña-like) or positive NAO), relative to the 20th century simulation mean. Bold underscore denotes a significant change in a multi-model mean index at the $p \leq 0.05$ level, relative to the 20th century simulation mean, as assessed by a Monte Carlo *t*-test. Bold * denotes significant change at the $0.05 < p \leq 0.10$ level.

	Winter PDO			Annual SOI			Winter NAO		
SRES emission scenario	B1	A1B	A2	B1	A1B	A2	B1	A1B	A2
Observed mean 1900-1999	0.168			-0.098			0.485		
All-model 1900-1999 simulation mean**	-0.109	-0.075	-0.101	0.040	0.049	0.046	-0.059	-0.050	-0.060
All-model 2000-2050 mean	-0.130	-0.095	-0.129	-0.029	0.017	0.025	-0.019	0.115	0.101
All-model 2000-2099 mean	-0.161*	-0.162	-0.321	-0.025	0.068	0.099	-0.040	0.177	0.161

**Not all GCMs had 21st century projected data for all three emission scenarios, therefore their simulation runs were dropped from the multi-model simulation mean where applicable.

Table 5. Significance of trend in the all-model mean projected streamflows for 2006-2050 and 2006-2096 for the B1, A1B and A2 SRES emissions scenarios. Significant declines at the 0.05 level are denoted by a bold red ▼; significant increases at the 0.05 level are denoted by bold blue ▲; and no significant trend by ↔. Projected percentage changes *per annum* (Δ/yr) is defined as $100*\beta_1/mean(Q)$.

Flow record	2006-2050						2006-2096					
	B1		A1B		A2		B1		A1B		A2	
	Trend	**Δ/yr**	Trend	**Δ/yr**	Trend	**Δ/yr**	Trend	**Δ/yr**	Trend	**Δ/yr**	Trend	**Δ/yr**
1.North Fork Flathead R.	↔	-0.06	▼	-0.08	↔	-0.07	↔	-0.01	↔	-0.01	▲	0.07
2. Marias R.	▼	-0.67	▼	-0.74	▼	-0.74	▼	-0.63	▼	-0.71	▼	-0.48
3. Waterton R.	▼	-0.19	▼	-0.16	▼	-0.17	▼	-0.14	▼	-0.11	↔	-0.03
4. Elk R.	▼	-0.16	▼	-0.17	▼	-0.20	▼	-0.11	▼	-0.13	▼	-0.06
5. Actual St. Mary	▼	-0.85	▼	-0.79	▼	-0.82	▼	-1.00	▼	-0.98	▼	-0.79
6. Naturalized St. Mary R.	↔	0.01	↔	-0.03	↔	-0.01	↔	0.01	↔	0.02	▲	0.08
7. Actual Belly R.	▼	-0.16	▼	-0.12	↔	-0.02	▼	-0.16	▼	-0.12	▼	-0.03
8. Nat. Belly R.	↔	-0.01	↔	0.02	↔	0.04	↔	0.003	▲	0.05	▲	0.11
9. Actual Oldman	▼	-1.76	▼	-1.64	▼	-1.78	▼	-2.07	▼	-2.15	▼	-1.74
10. Naturalized Oldman R.	▼	-0.25	▼	-0.24	▼	-0.29	▼	-0.22	▼	-0.22	▼	-0.12

Figure captions

Figure 1. Map of the northern Rocky Mountains showing the seven gauge locations located at the hydrographic apex of North America, after Rood et al. (2005).

Figure 2. Mean daily flows (m^3/s) (averaged over the year) of the ten river discharge records at the seven gauge locations for 1900-2007. Order same as that of Table 1. Black denotes mean daily flows, blue denotes the five-year binomial smoothed flows.

Figure 3. Plots of the ten northern Rocky Mountain flow records, smoothed by five-point binomial filters (black lines), together with fitted multiple linear GLS regressions with ARMA modeled error terms (blue), fitted multiple linear GLS regressions without the error terms (green), and significant trend lines (red). Trend lines only shown where significant. Mean daily flows (m^3/s) averaged over the year are presented.

Figure 4. Northern Rocky Mountain 20^{th} century river simulations (1900-1999) and river projections (2000-2096) (daily mean flows (m^3/s), averaged over the year, smoothed by five-point binomial filters) under the B1 SRES emissions scenario (a), the A1B emissions scenario (b), and the A2 emission scenario (c), together with observed records (1905-2007). The grey lines are the individual model runs, the heavy blue lines are all-model means of the GCM runs, and the heavy red lines are the observed river records.

Figure 5. Projection distributions of projected lightly smoothed annual discharges (five-year binomial smoother) for the ten Northern Rocky Mountain river records in response to 20,000 climate-change realizations based upon 51 GCM streamflow projections, following the methodology of Dettinger (2005, 2006).

Figure 6. Empirical cumulative frequency distributions of projected lightly smoothed annual discharges (five-year binomial smoother) for the ten Northern Rocky Mountain river records in response to 20,000 climate-change realizations based upon 51 GCM streamflow projections, following the methodology of Dettinger (2005, 2006).

Figure

Click here to download high resolution image

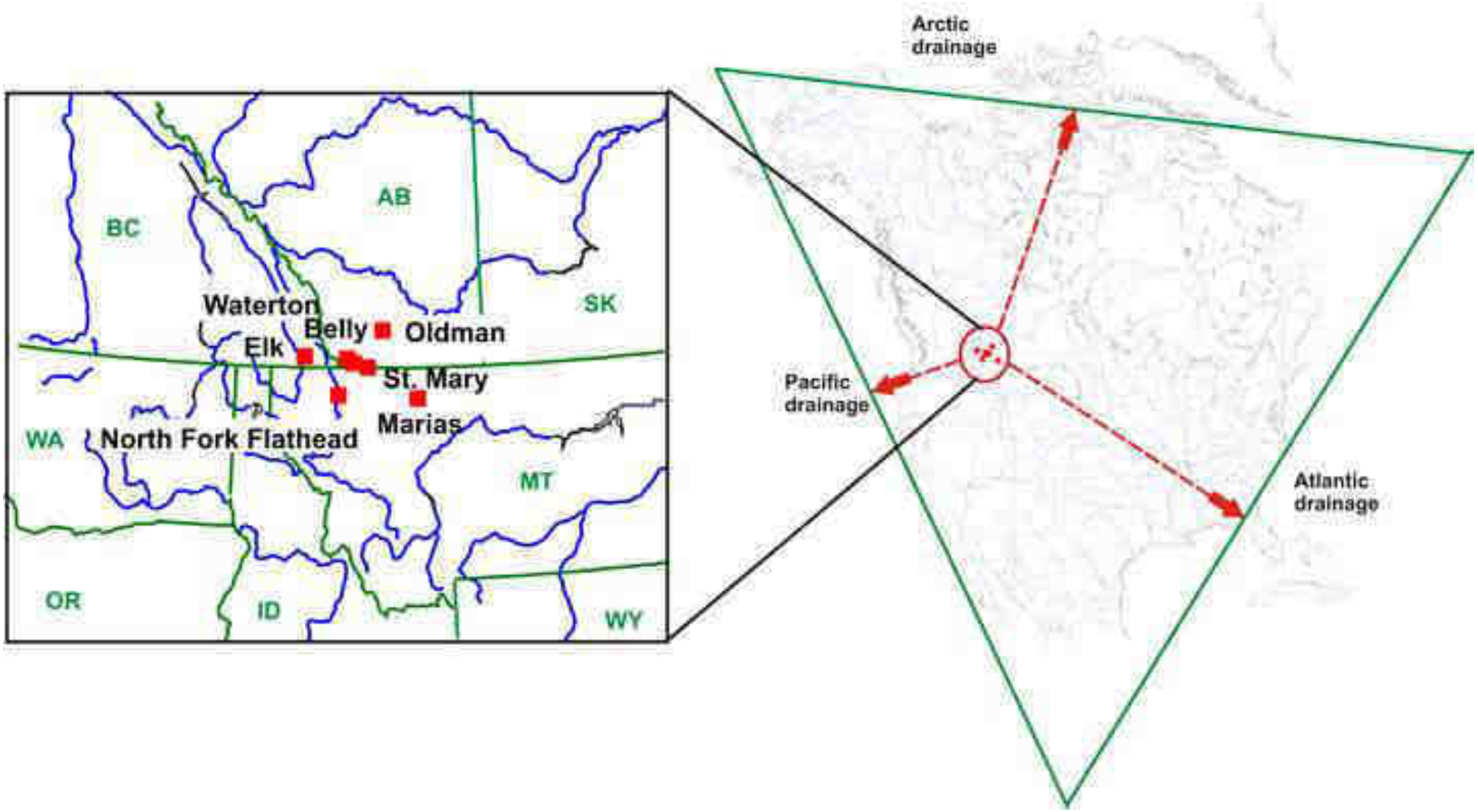

Figure

Click here to download high resolution image

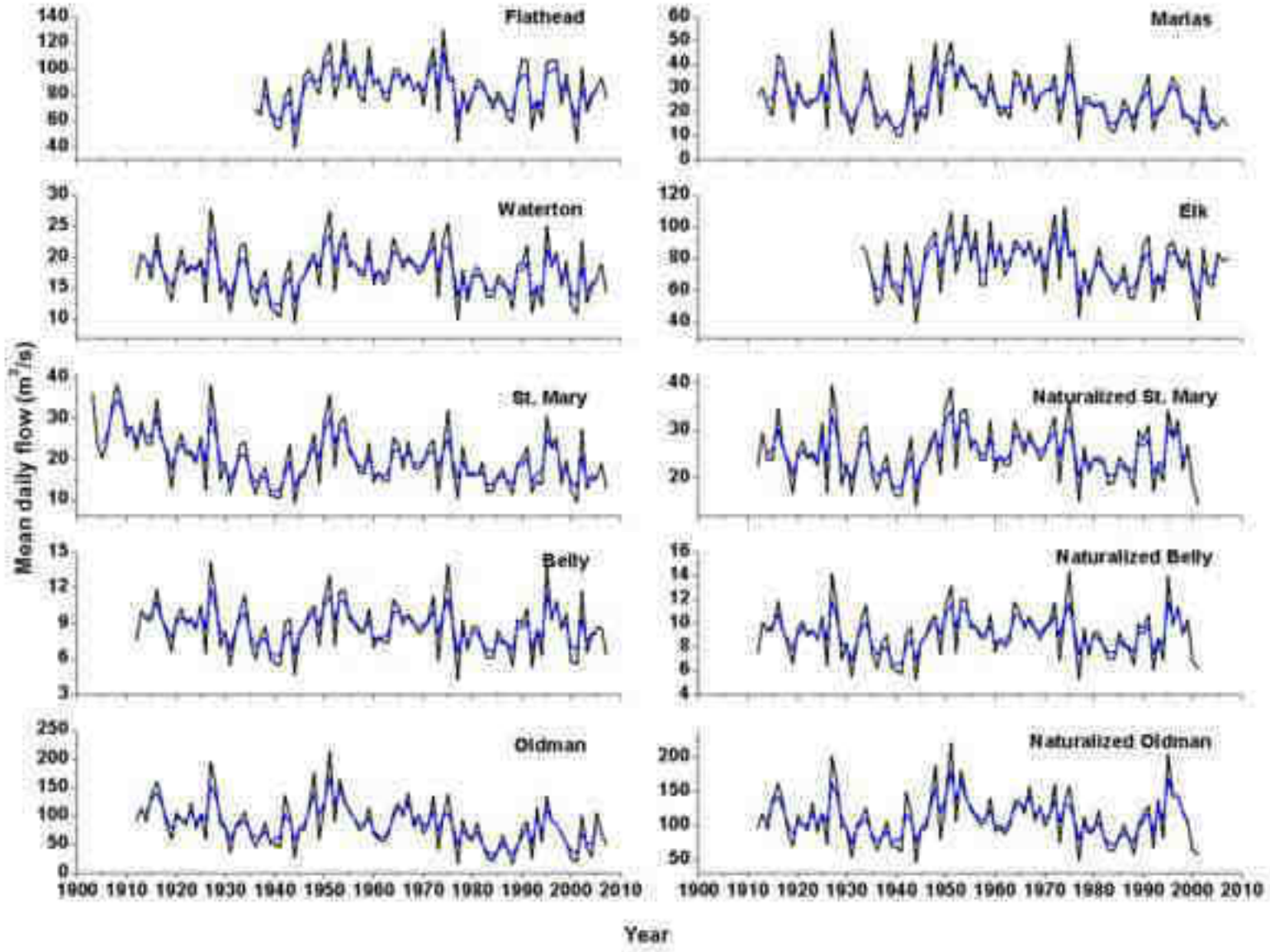

Figure

Click here to download high resolution image

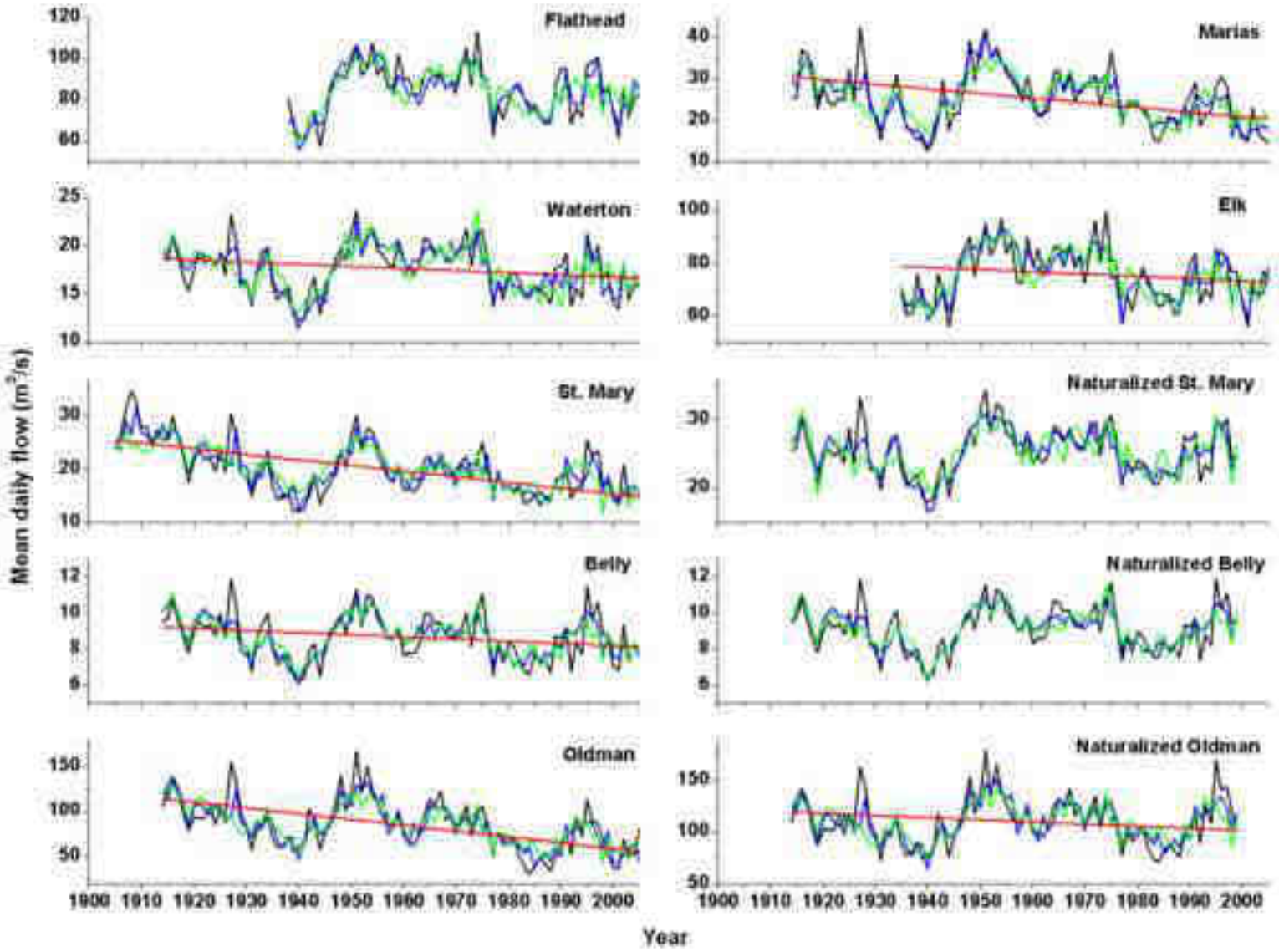

Figure

Click here to download high resolution image

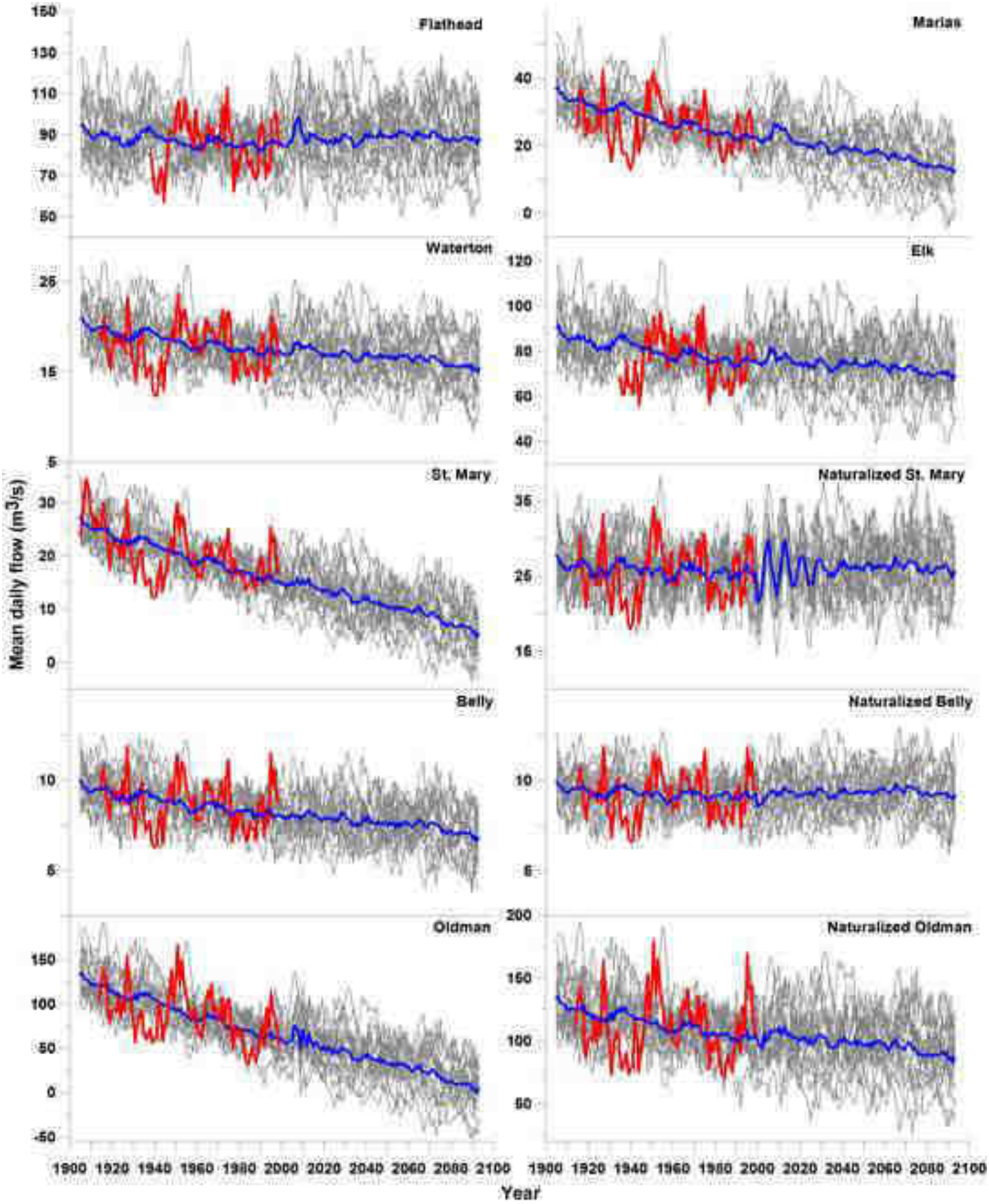

Figure

Click here to download high resolution image

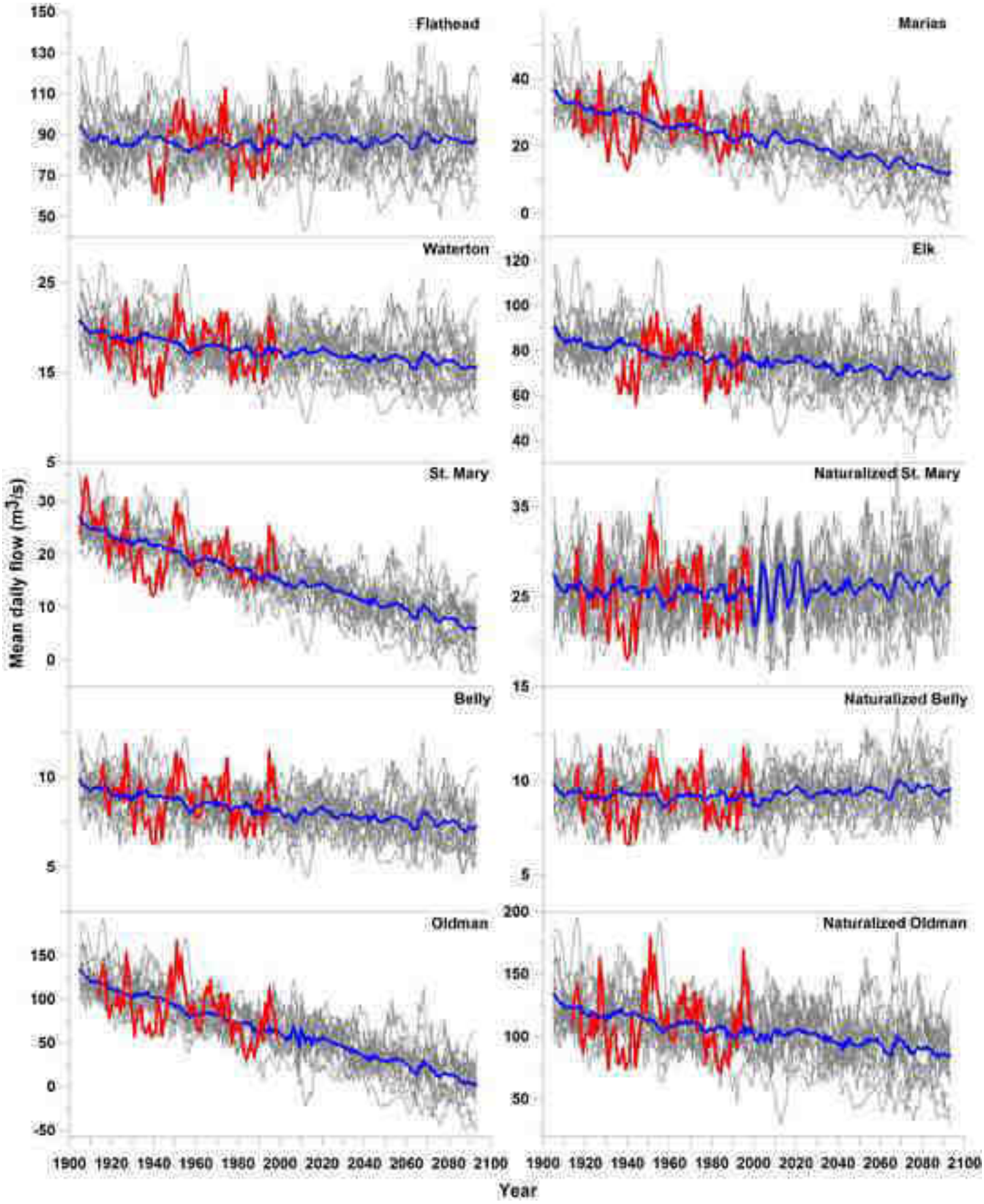

Figure

Click here to download high resolution image

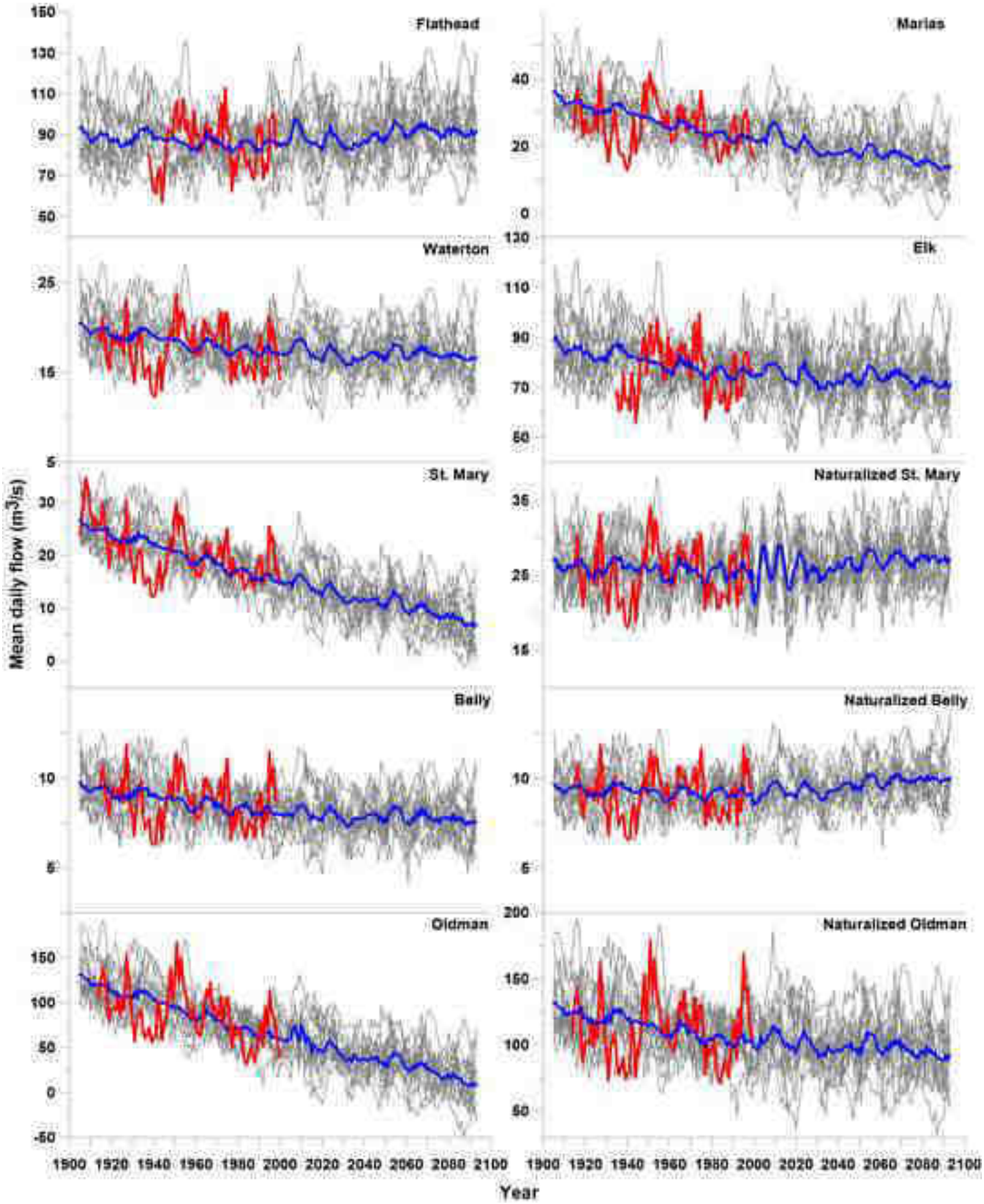

Figure

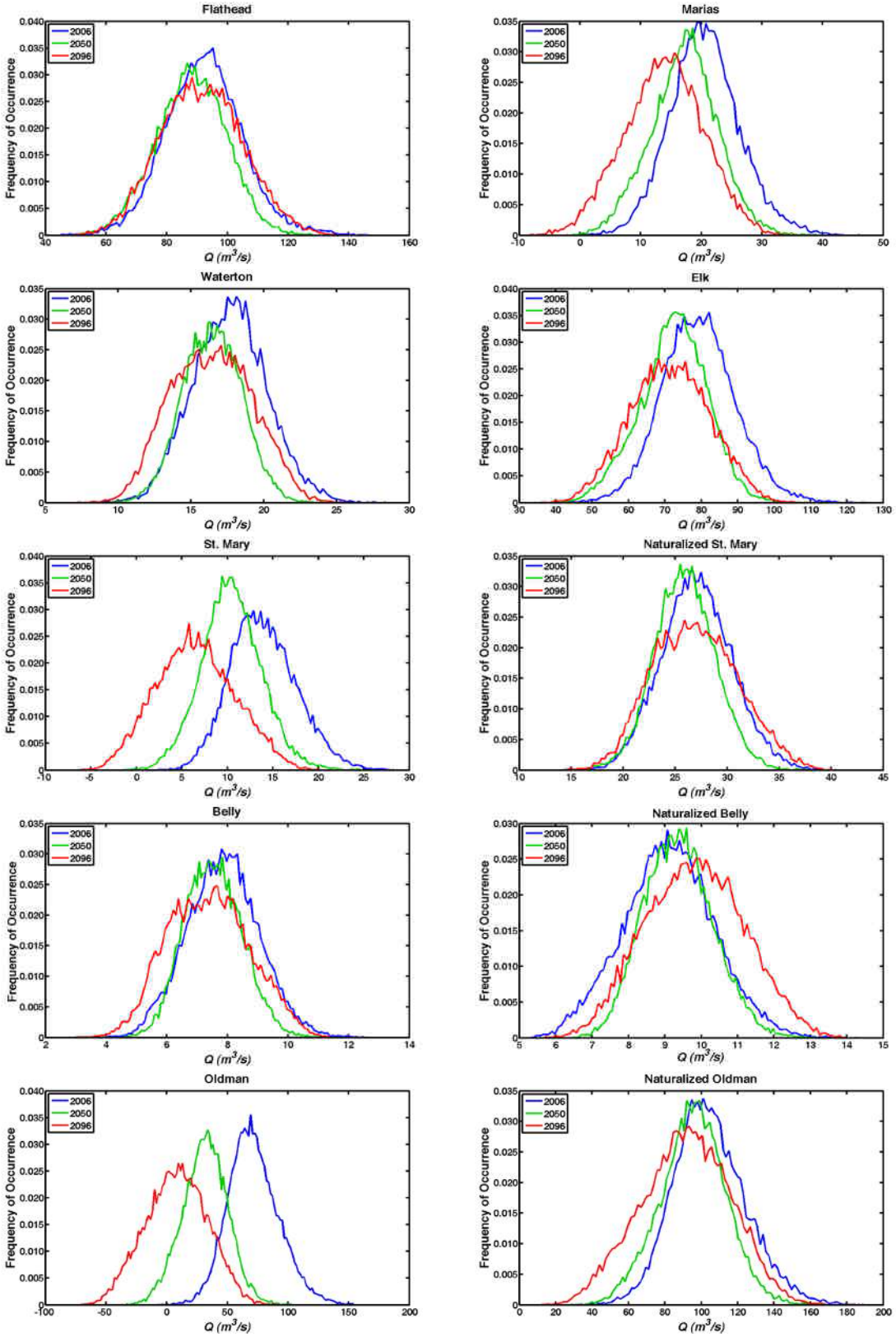
Flathead
Marias
Waterton
Elk
St. Mary
Naturalized St. Mary
Belly
Naturalized Belly
Oldman
Naturalized Oldman
2006
2050
2096
Frequency of Occurrence
Q (m3/s)

Figure

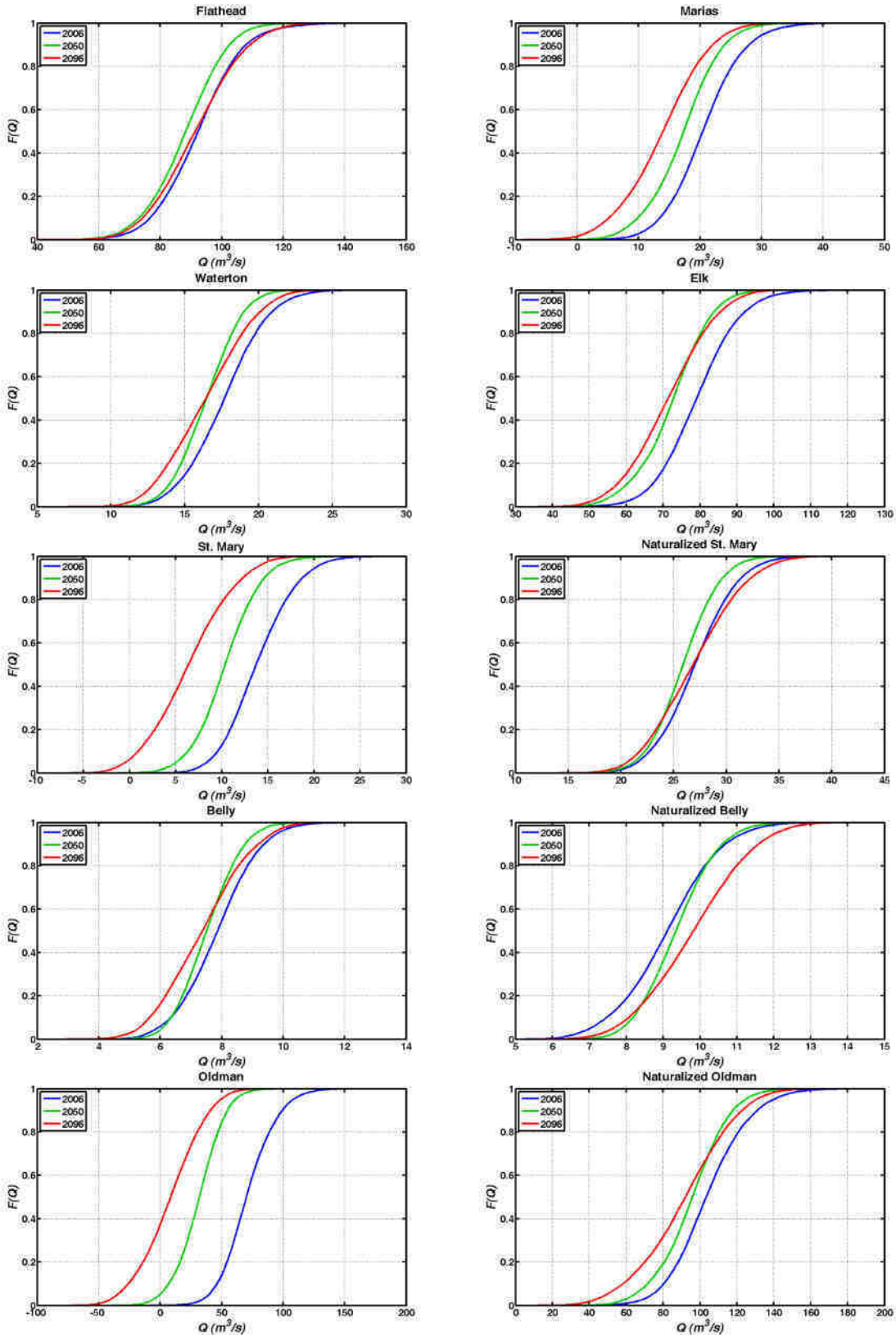
Flathead
Marias
Waterton
Elk
St. Mary
Naturalized St. Mary
Belly
Naturalized Belly
Oldman
Naturalized Oldman
2006
2050
2096
F(Q)
Q (m3/s)

Elsevier Editorial System(tm) for Journal of Hydrology
Manuscript Draft

Manuscript Number:

Title: Detection and attribution of variability and trends in instrumental streamflow records from the Canadian Prairie Provinces

Article Type: Research Paper

Keywords: Prairie Provinces' streamflow; trends; permutation t-tests; Pacific Decadal Oscillation (PDO); North Pacific Index (NPI); El Niño-Southern Oscillation (ENSO); Pacific North American mode (PNA) and Arctic Oscillation (AO)

Corresponding Author: Dr. Jeannine St. Jacques,

Corresponding Author's Institution: University of Regina

First Author: Jeannine St. Jacques

Order of Authors: Jeannine St. Jacques; Yuhui A Huang, M.Sc.; Yang Zhao, Ph.D.; Suzan L Lapp, M.A.; David J Sauchyn, Ph.D.

Suggested Reviewers: Barrie R. Bonsal
Research Scientist, Hydrological Process and Modelling Research, Environment Canada
Barrie.Bonsal@ec.gc.ca
He has published extensively on the hydrology of the Canadian West and are aware of regional surface water availability issues.

Stephan Déry
Professor, Environmental Science and Engineering Program , University of Northern British Columbia
sdery@unbc.ca
He has published extensively on the hydrology of the Canadian West and are aware of regional surface water availability issues.

Stewart Rood
Professor, Biological Sciences Department , University of Lethbridge
rood@uleth.ca
He has published extensively on the hydrology of the Canadian West and are aware of regional surface water availability issues.

Sean Fleming
Senior Hydrologist, Research and Development , Meteorological Service of Canada, Science Division , Environment Canada
Sean.Fleming@ec.gc.ca
He has published extensively on the hydrology of the Canadian West and are aware of regional surface water availability issues.

Stefan Kienzle
Professor, Department of Geography, University of Lethbridge
stefan.kienzle@uleth.ca

He has published extensively on the hydrology of the Canadian West and are aware of regional surface water availability issues.

March 10, 2012

Dear Journal of Hydrology Editor,

Please receive our manuscript "Detection and attribution of variability and trends in instrumental streamflow records from the Canadian Prairie Provinces" for consideration in your journal. The Canadian Prairie Provinces are one of the world's important grain exporting areas. They are semi-arid presently and are already experiencing serious surface water allocation issues. There are understandably great concerns for regional water availability under global warming scenarios. Hence, we feel that our study examining the longest, naturally-flowing streamflow annual discharge records for natural variability associated with climate oscillations, e.g., the Pacific Decadal Oscillation and the El Niño-Southern Oscillation, and emerging trends is both topical and of interest to your journal.

This manuscript has not been published elsewhere; nor is it under consideration for publication elsewhere. All authors contributed significantly to its preparation.

We recommend the following four possible reviewers. All have published extensively on the hydrology of the Canadian West and are aware of regional surface water availability issues.

Prof. Stephan Déry
Environmental Science and Engineering Program
8-414 Teaching Laboratory
University of Northern British Columbia
3333 University Way
Prince George, BC, Canada, V2N 4Z9
Phone: 250-960-5193
Fax: 250-960-5845
sdery@unbc.ca

Prof. Stewart Rood
Biological Sciences Department
Office: WE2058 (Alberta Water & Env Science Bldg)
4401 University Drive
University of Lethbridge
Lethbridge, Alberta, Canada, T1K 3M4
Phone: 403-329-2327
Fax: 403-329-2082

rood@uleth.ca

Dr. Sean Fleming
Senior Hydrologist, Research and Development
Meteorological Service of Canada, Science Division
Environment Canada
Pacific and Yukon Region
201-401 Burrard St.
Vancouver, BC, Canada, V6C 3S5
Phone: 604-664-9245
Fax: 604-664-9004
Sean.Fleming@ec.gc.ca

Prof. Stefan Kienzle
Department of Geography
Alberta Water and Environmental Science Building
4401 University Drive
University of Lethbridge
Lethbridge, Alberta, Canada, T1K 3M4
Phone: 403-380-1875
stefan.kienzle@uleth.ca

Thank you for your consideration,

Jeannine-Marie St. Jacques, Ph.D.
Prairie Adaptation Research Collaborative
University of Regina
Regina, Saskatchewan, Canada
stjacqje@uregina.ca

Highlights

- The PDO, NPI and PNA have a clear impact on Canadian Prairie Province annual mean daily discharge.
- ENSO and the AO have a weaker impact on Canadian Prairie Province annual mean daily discharge.
- Annual discharge is declining in the unregulated streams in N. Alberta and the S.W. prairies.
- There are declines in the regulated flows of the South Saskatchewan River Basin.
- There are increases in annual discharge in the unregulated streams in Manitoba.

Detection and attribution of variability and trends in instrumental streamflow records from the Canadian Prairie Provinces

Jeannine-Marie St. Jacques[1*], Yuhui Althea Huang[2], Yang Zhao[2], Suzan L. Lapp[1] and David J. Sauchyn[1]

[1]Prairie Adaptation Research Collaborative, University of Regina, Saskatchewan, Canada, S4S 7H9

[2]Department of Mathematics and Statistics, University of Regina, Saskatchewan, Canada

*Corresponding author: stjacqje@uregina.ca, phone: (1)306.337.2293, fax: (1)306.337.2301

Abstract

The detection and attribution of past variability and trends in hydrological variables are essential for the understanding of future climate change and prudent water management in the Canadian Prairie Provinces. Canadian western interior precipitation and temperature are heavily influenced by recurring large-scale climate patterns: the Pacific Decadal Oscillation (PDO), the North Pacific Index (NPI), the El Niño-Southern Oscillation (ENSO), the Pacific North American mode (PNA) and the Arctic Oscillation (AO). We examined relationships between 86 Canadian Prairie Provinces naturally-flowing streamflow records and these atmospheric and oceanic climate oscillations, using composite analyses based upon Monte Carlo permutation *t*-tests. These composite analyses demonstrated that the PDO, NPI and PNA have a clear impact on Prairie Province annual mean daily discharge, with higher annual discharges occurring during negative PDO, high NPI and negative PNA years, and lower flows during the positive PDO, low NPI and positive PNA years, except in the far north. Composite analyses also show the impact of ENSO, and the weaker effect of the AO. Because trend analyses of annual discharges are either not based upon the most recent data and/or do not explicitly deal with the problem of autocorrelation biasing the trend test according to the most recent best practice, we examined the same 86 naturally-flowing and 5 regulated annual mean daily flow records using a modified Mann-Kendall test to address autocorrelation. There are declines in annual mean daily flow in the naturally-flowing streams in northern Alberta and the

45 southwestern prairies. There also are significant declines in the regulated flows of the
46 South Saskatchewan River Basin, which propagate all the way downstream to the
47 gauge at The Pas, Manitoba. There are increases in annual mean daily flow in the
48 naturally-flowing streams in Manitoba. The results of this study have implications for
49 water resource management: the recognition of significant natural modes of
50 hydrological variability leads to a more rigorous interpretation of recent trends and
51 fluctuations in raw water supply, and is further indication that conventional methods
52 of water supply forecasting are wrong to assume the stationarity of hydrological time
53 series.

54

55 Keywords: Prairie Provinces' streamflow, trends, permutation *t*-tests, Pacific
56 Decadal Oscillation (PDO), North Pacific Index (NPI), Pacific North American mode
57 (PNA).

1. Introduction

The hydroclimate of Canada's western interior is heavily influenced by recurring large-scale climate patterns: the Pacific Decadal Oscillation (PDO), the North Pacific Index (NPI), the El Niño-Southern Oscillation (ENSO), the Pacific North American mode (PNA) and the Arctic Oscillation (AO). Much of western North America displays strong periodic hydroclimate cycles linked to the low-frequency Pacific Decadal Oscillation (PDO), an integrated or rectified measure of the North Pacific atmosphere-ocean system (Mantua et al., 1997; McCabe and Dettinger, 2002; Stewart et al., 2005; St. Jacques et al., 2010). The PDO is a pattern of North Pacific Ocean variability that shifts phases on an inter-decadal time scale, usually about 20 to 35 years (Minobe 1997, 1999; Mantua and Hare, 2002). Winter precipitation in the northern Rocky Mountains is higher when the PDO is in a negative phase (1890-1924, 1947 to 1976), and lower when the PDO is in a positive phase (1925-1946, 1977-~2008) (Mantua et al., 1997; Comeau et al., 2009; Wise, 2010). Hence, a strong negative relationship exists between the PDO and precipitation and streamflow throughout Alberta, British Columbia and Montana. The NPI is a measure of the intensity of the Aleutian High, which is a possible driving mechanism of the PDO (Trenberth and Hurrell, 1994; Lapp et al., 2012). When the NPI is high (low), the intensity of the Aleutian Low is weak (strong); a state consistent with the negative (positive) phase of the PDO. The tropical Pacific ENSO also affects the hydroclimatology of this region as precipitation and streamflow are

decreased during El Niño events and increased during La Niña events (Shabbar and Khandekar, 1996; Shabbar et al., 1997; Bonsal and Lawford, 1999; Bonsal et al., 2001; Shabbar and Skinner, 2004; Bonsal and Shabbar, 2008). The Pacific North American mode (PNA) is a prominent mode of low-frequency atmospheric variability in the Northern Hemisphere extratropics (Wallace and Gutzler, 1981). The PNA pattern is associated with strong fluctuations in the strength and location of the East Asian jet stream. The positive phase of the PNA pattern is associated with above-average temperatures over western Canada and lower-than-average precipitation anomalies in the Gulf of Alaska, extending into the Pacific Northwest. The Arctic Oscillation (AO) is a measure of the intensity of the polar vortex and is closely related to (if not the same as) the North Atlantic Oscillation (NAO) (Wallace and Gutzler, 1981). A negative relationship exists between winter precipitation in the northern Prairie Provinces and the NAO, as the positive NAO (and AO) allows more frequent outbreaks of cold, dry Arctic air to this region (Bonsal and Shabbar, 2008).

Although the large-scale forcing of the hydrology of British Columbia and southern Alberta has been well-studied recently (*e.g.*, Stewart et al., 2005; Gobena and Gan, 2006, 2009; Fleming et al., 2007; St. Jacques et al*.,* 2010), the hydroclimatology of the Canadian Prairie Provinces as a whole has been examined much less and less recently (*e.g.*, Gan, 1998; Zhang et al., 2001; Woo and Thorne, 2003; Burn et al., 2008). In this manuscript, we examine relationships between Canadian Prairie Provinces' streamflow and the atmospheric and oceanic climate

100 oscillations (*i.e.,* the PDO, NPI, ENSO, PNA and AO) by means of composite
101 analysis with permutation *t*-tests.

102 Also in this manuscript, we examine Canadian Prairie Provinces' annual mean
103 daily streamflow records for trends, and use the results of the composite analysis to
104 interpret any trends. There are many problems with analyzing the instrumental
105 streamflow records simplistically using methods such as ordinary least squares
106 regression techniques. These records can be discontinuous, and short, for instance,
107 having periods of record of ~35-50 years with a few exceptions. The naturally-
108 flowing streams in the southern Prairies can have years of little or no flow, but also
109 outlier years of exceptionally high flows, *i.e*, extremely flashy flows with a very non-
110 normal distribution. There is frequent positive autocorrelation in many river
111 discharge time series, which results in the overestimation of the effective sample size
112 of the residuals in classical linear regression and Mann-Kendall non-parametric
113 methods (Kulkarni and von Storch, 1995; Zheng et al*.*, 1997; Cryer and Chan, 2008).
114 Therefore, these methods will disproportionately reject a null hypothesis of no trend
115 (Zheng et al*.*, 1997; Zhang et al*.*, 2001; Burn and Hag Elnur, 2002; Yue et al*.*, 2002a).
116 Lastly, there is heavy human impact from water consumption, diversion and storage,
117 especially in the southern Prairies, which overlays and obscures the natural
118 hydrology. Because most trend analyses of Prairie streamflow are either not based on
119 recent data (*e.g.*, Westmacott and Burn, 1997; Yulianti and Burn, 1998; Gan, 1998;
120 Zhang et al., 2001) and/or do not deal with the problem of autocorrelation biasing the

121 trend test according to the most recent best practice (Khaliq et al., 2009), we
122 examined streamflow records from throughout the Canadian Prairie Provinces and
123 environs for trends.

124 2. Datasets and methods

125 We extracted the streamflow records from the Water Survey of Canada
126 (HYDAT) (http://www.wsc.ec.gc.ca/) database, augmented with unpublished data
127 supplied by Saskatchewan Watershed Authority, Alberta Environment and Manitoba
128 Hydro (Figure 1 and Table 1). We selected the two longest, most continuous,
129 naturally-flowing streamflow records in each drainage sub-basin, thus giving a
130 reasonable geographical coverage across the Prairies. This was not always possible
131 due to lack of gauges, particularly in the north. In total, 86 naturally- flowing stream
132 discharge records were analyzed by composite and trend analysis: 37 from Alberta
133 and environs, 27 from Saskatchewan, and 22 from Manitoba; most were from active
134 gauges (Table 1 and Figure 1). To provide context for comparison, 5 regulated
135 records were also analyzed for trend only (Table 2). We averaged mean daily flow
136 over January to December (the water year of October-September is inappropriate
137 because there frequently is a second late autumn peak in the far north and Manitoba)
138 or March-October (many of the gauges on the smaller streams do not record in
139 winter) (Appendix Table A.1). This is equivalent to analyzing total annual discharge.
140 In the dry and heavily human modified landscape of the southern Prairies, most
141 naturally flowing streams are relatively small, with correspondingly small watersheds

142 (Table 1, Figure 2). These small streams have high coefficients of variation, as their
143 flows can change dramatically from year to year (Appendix Table A.1). In the
144 relatively unpopulated northern half of the provinces, the naturally flowing rivers are
145 relatively large (Figure 2); and their coefficients of variation are much lower, as year
146 to year flows are steadier (Appendix Table A.1). The average record length was 52
147 years, but the distribution is skewed with a few long records and many relatively
148 short ones (Figure 2).

149 The monthly PDO time series of sea surface temperature (SST) residuals
150 (Mantua et al., 1997; Zhang et al., 1997) was obtained from the Joint Institute for the
151 Study of the Atmosphere and Ocean (http://jisao.washington.edu/pdo/). The
152 November-March averaged NPI index of sea level pressures (SLP) was obtained
153 from James Hurrell at the National Center for Atmospheric Research
154 (http://www.cgd.ucar.edu/cas/jhurrell/indices.html). There are various ENSO metrics
155 available (http://www.cdc.noaa.gov/ClimateIndices/); however, only the SLP-based
156 monthly Southern Oscillation Index (SOI) (*i.e.*, the normalized difference between
157 monthly mean SLP at Tahiti, French Polynesia and Darwin, Australia) starts by 1900
158 (Ropelewski and Jones, 1987). A few of the Prairie streamflow records begin in the
159 1910s. The SOI and the 500 millibar height-based monthly PNA were obtained from
160 Earth Systems Research Laboratory (National Oceanic and Atmospheric
161 Administration, 2009, http://www.cdc.noaa.gov/ClimateIndices/). The SLP-based
162 December-March averaged AO index, also called the Northern Annular Mode

(NAM), was also obtained from James Hurrell. All time series began by 1901, except for the PNA, which commenced by 1950, the year upper atmospheric data became dense enough to produce world-wide coverage (Figure 3).

The relationships between streamflow and the climate oscillations were examined by composite analysis. For each climate oscillation and for each Prairie stream, mean daily discharges are composited into two classes: those corresponding to the strong positive climate oscillation events and those corresponding to the strong negative climate oscillation events. The differences in average discharge between the two classes were then assessed using a Monte Carlo permutation *t*-test. A permutation *t*-test, rather than a regular classical *t*-test was required because of the typical extreme non-normality of the mean daily discharges (Manly, 1998).

The composite analyses required identifying individual strong positive and negative climate oscillation events. Strong positive PDO events are defined as those years in which the winter averaged (November-March) PDO was greater or equal to 0.75 standard deviations from the mean; and, correspondingly, strong negative PDO events are defined as those years in which the winter averaged PDO was less than or equal to -0.75 standard deviations (Table 3). Strong NPI and PNA events are defined analogously using the November-March NPI and December-February PNA (Table 3). Strong AO events are defined using the December-March AO and ± 0.80 standard deviations (Table 3). The winter values of the PDO, NPI, PNA and AO are used because the oscillations are strongest in winter, and their downstream teleconnections

184 are strongly correlated to Prairie winter precipitation (Figures 4A, 5A, 7A, 8A).
185 Winter snowfall is the source of much of the water flowing in the local rivers (Pham
186 et al., 2009). Even if the season of analysis started in November or December, the
187 season was assigned to the year corresponding to the following January, *i.e.*, a strong
188 negative PDO event during November and December 2007, and continuing January
189 through March 2008, was assigned the year 2008; and similarly for the NPI, PNA and
190 AO.

191 The SOI was handled differently. Strong or moderate El Niño events were
192 defined as when the averaged June-November SOI < -0.5, and a La Niña event was
193 when the averaged June-November SOI > 0.5 (Table 2), following Redmond and
194 Koch (1991). These authors found better correlations between the SOI and Pacific
195 Northwest winter climate when the SOI leads by a few months, as the teleconnection
196 between the tropical Pacific Ocean and the downstream Pacific Northwest operates at
197 a definite multi-monthly lag. Therefore, we maintained this relationship by
198 comparing the leading SOI (June-November) event to the following year's
199 streamflow (January-December, or March-October), as it is the immediate winter
200 after an El Niño / La Niña event that is drier / wetter on the Prairies (Figure 5)
201 (Shabbar et al., 1997; Bonsal and Shabbar, 2008; their Figure 2).

202 Both two-sample and one-sample permutation *t*-tests were performed for each
203 of the climate oscillations and for each individual streamflow time series of length n.
204 In the two-sample *t*-tests, the n_1 streamflow magnitudes corresponding to the negative

climate oscillation events were compared to the n_2 streamflow magnitudes corresponding to the positive climate oscillation events, and a regular *t*-statistic between the two was computed, *i.e.*,

$$t = \frac{\bar{x}_1 - \bar{x}_2}{\sqrt{s^2\left(\frac{1}{n_1} + \frac{1}{n_2}\right)}}, \qquad (1)$$

where

$$s^2 = \frac{(n_1 - 1)s_1^2 + (n_2 - 1)s_2^2}{n_1 + n_2 - 2}. \qquad (2)$$

Then, the merged $n_1 + n_2$ streamflow time series corresponding to both strong phases of the climate oscillation was randomly shuffled and divided into an n_1 initial portion and an n_2 latter portion, and a *t*-statistic between the two was computed (R Development Core Team, 2008). This was done 10,000 times. The number of times the actual *t*-statistic exceeded the randomly simulated *t*-statistic was determined, as was the frequency of the converse, and the one-tailed significance was assessed at the 10% level, which is typically used with geophysical data. In the one-sample *t*-tests, the n_1 (n_2) streamflow data corresponding to the negative (positive) climate oscillation events were compared to all the n-n_1 (n-n_2) remaining streamflow data corresponding to both the positive (negative) and neutral climate oscillation events, and a regular a *t*-statistic between the two was computed, and the permutations were done analogously. One-sample *t*-tests were performed in case the effect of the climate

225 oscillation is asymmetric in any given watershed. One-tailed *t*-tests were used
226 because the choice of tail can be justified from correlation plots between the climate
227 oscillations and winter precipitation. To guide the tail choice, correlation plots were
228 constructed between the climate oscillations and ~10 km gridded (1950-2005)
229 precipitation data from the Canadian Forest Service Climate Dataset (McKenney et
230 al., 2006) (http://cfs.nrcan.gc.ca/subsite/glfc-climate/namonthly). For example, when
231 a strong negative correlation exists between winter precipitation falling on a
232 watershed and the PDO, we expect a corresponding significant one-sided result from
233 the permutation *t*-test between streamflow magnitude at a gauge in that watershed and
234 the PDO, with flow higher during the negative PDO years.

235 Because the PDO has a large effect on winter prairie precipitation and the
236 immediate subsequent year streamflow (*e.g.*, Mantua et al., 1997; Mantua and Hare,
237 2002; Whitfield et al., 2010; St. Jacques et al., 2010), we further examined the effect
238 of PDO phase on the probability of two successive years of low or high flows of
239 Saskatchewan River tributaries and adjacent rivers. The reservoir capacity of the
240 Alberta portion of the North and South Saskatchewan Rivers basins is estimated to be
241 two years in case of drought (*personal comm., Michael Seneka, Alberta*
242 *Environment*); hence, the interest in two successive years of low annual discharge.
243 Twenty-five of the longest (centennial-scale length), most continuous mean daily
244 flows (annualized) of Saskatchewan River tributaries or neighboring rivers were
245 examined from the headwaters in Alberta and downstream (Appendix Table A.2).

246 Both actual and naturalized flows were included. Details of 23 of the gauge records
247 are described in St. Jacques et al. (2010); the other two gauges are the North
248 Saskatchewan River at Prince Albert and the Saskatchewan River at The Pas,
249 Manitoba. For each gauge, the mean daily flow magnitudes were ranked into
250 quartiles. The number of two successive years of least quartile streamflows were
251 tallied and examined according to PDO phase. The probability of two successive
252 years of least quartile flow in a given PDO phase is estimated by the number of two
253 successive years of least quartile streamflows strictly occurring in that phase divided
254 by the total number of two successive years occurring in that phase with streamflow
255 data. The highest quartile flow probabilities were similarly estimated. A paired
256 permutation *t*-test was used to determine the significance of the mean basin-wide
257 difference between the probability of two successive years of least quartile flow in a
258 given river during the positive PDO phase versus the probability of two successive
259 years of least quartile flow in the same river during the negative PDO phase (Manly,
260 1998). Likewise, a paired permutation *t*-test was used to determine the significance of
261 the mean basin-wide difference between the probability of two successive years of
262 highest quartile flow in a given river during the positive PDO phase versus the
263 probability of two successive years of highest quartile flow in the same river during
264 the negative PDO phase. The exactRankTests package in the R programming
265 language was used for the paired permutation *t*-tests (R Development Core Team,
266 2008).

Trends in annual (or warm season, as appropriate) mean daily flow (m^3/s) for the 86 naturally-flowing and the 5 regulated flow Prairie streamflows over their individual periods of record were assessed by the non-parametric Mann-Kendall (MK) statistical test (Mann, 1945; Kendall, 1975). The MK test is widely used to assess the significance of trend in hydrological time series (Burn, 1994; Helsel and Hirsch, 2002; Khaliq et al., 2009). The MK test searches for a trend in a time series without specifying whether the trend is linear or nonlinear. It is based on the test statistic S, where Y_i and Y_j are the sequential flow data, N is the length of the time series, $S = \sum_{i=1}^{N-1} \sum_{j=i+1}^{N} signum\ (Y_j - Y_i)$, and

$$signum\ (Y_j - Y_i) = \begin{cases} 1\ if\ (Y_j - Y_i) > 0 \\ 0\ if\ (Y_j - Y_i) = 0 \\ -1\ if\ (Y_j - Y_i) < 0. \end{cases} \quad (3)$$

A positive (negative) value of S demonstrates an increasing (decreasing) trend. For $N \geq 10$, Mann (1945) and Kendall (1975) have proven that S is approximately normally distributed with mean $E(S) = 0$ and

$$Var\ (S) = \frac{[N(N-1)(2N+5) - \sum_{i=1}^{n} t_i i(i-1)(2i+5)]}{18} \quad (4)$$

where t_i is the number of ties of extent i (*i.e.*, the size of the tied group) and n is the number of tied groups. The standardized test statistic Z based upon S follows the standard normal distribution.

$$Z = \begin{cases} \frac{(S-1)}{\sqrt{Var(S)}} & if\ S > 0 \\ 0 & if\ S = 0 \\ \frac{(S+1)}{\sqrt{Var(S)}} & if\ S < 0 \end{cases} \quad (5)$$

At significance level α, the null hypothesis of no trend is rejected if the absolute value of Z is greater than the theoretical value $Z_{(1-\alpha)/2}$.

However, the MK test needs data to be serially independent, a condition often not met with hydrological data (Kulkarni and von Storch, 1995). To remove the effect of serial correlation on the MK test, we use a variance correction approach (VC) (also called an effective sample size (ESS) approach) (Yue and Wang, 2004). As described by Bayley and Hammersley (1946), the VC approach rests upon the fact that N serially correlated observations contain the same information as $N^* < N$ uncorrelated observations. The presence of autocorrelation in a time series changes $Var(S)$, although it does not change $mean(S)$ or alter the asymptotic normality of the MK test statistic S (Hamed and Rao, 1998; Yue et al., 2002a; Yue and Wang, 2004). Yue and Wang (2004) suggest correcting $Var(S)$ by using an effective sample size that reflects the degree of autocorrelation present, *i.e.*, $Var^*(S)$ = correction factor $CF * Var(S)$ where $CF = 1 + 2\sum_{k=1}^{N-1}(1 - \frac{k}{N})r_k$ and r_k is the lag-k serial correlation coefficient of the data. In practice, an AR(1) process is reasonable for much annual mean daily flow data; therefore, we only use r_1, so

$$CF = 1 + 2 \cdot \frac{r_1^{N+1} - N \cdot r_1^2 + (N-1) \cdot r_1}{N\,(r_1 - 1)^2} \quad (6)$$

where if $X_1, X_2, \ldots, X_N$ is a time series, then

$$r_1 = \frac{\frac{1}{N-1}\sum_{t=1}^{N-1}(X_t - \bar{X}_t)(X_{t+1} - \bar{X}_t)}{\frac{1}{N}\sum_{t=1}^{N}(X_t - \bar{X}_t)^2} \quad (7)$$

(Yue and Wang, 2004; Khaliq et al., 2009). Yue and Wang (2004) showed that the existence of a trend in a time series contaminates the estimate of the true serial correlation; and therefore, if the contaminated serial correlation is used to derive CF, then the effect of the true serial correlation on the MK test cannot be properly eliminated. Hence, the trend component is removed first, leaving the detrended residual series of an AR(1) process and noise (Yue and Wang, 2004). The sample lag-one autocorrelation coefficient (r_1) is then computed from this detrended residual series. If a record was discontinuous, r_1 was calculated from the longest continuous segment. Lastly, the modified MK test with VC is then applied to the original time series to assess the trend significance. The trend is removed using a robust, rank-based, non-parametric Sen-Theil line, where β_1 is the estimate of the trend slope and β_0 is the estimate of the intercept (Theil, 1950; Sen, 1968).

$$\beta_1 = median\left(\frac{(Y_j - Y_l)}{j - l}\right) \forall\, l < j \quad (8)$$

$$\beta_0 = median(1,2,\ldots,N) - \beta_1 \cdot median\,(Y_1, Y_2, \ldots, Y_N) \quad (9)$$

Significance levels of $p \leq 0.05$ and $0.05 < p \leq 0.10$ were used in trend detection following standard hydrological practice (Smith et al., 2007). Khaliq et al. (2009) in their evaluation of hydrological trend detection methods considered the modified MK

test with variance correction and an AR(1) assumption to be one of the best performing analysis methods. The magnitude of the changes in estimated mean daily flow over the period of record were calculated by the Sen-Theil line and reported as both total percentage changes from the beginning of record, and *per annum*.

Because of the possibility of finding random significant results when either performing permutation *t*-tests or modified MK trend tests at multiple streamflow gauges across the Canadian Prairies, the field significance, *P*, of obtaining a given fraction of significance results, *f*, at our two significance criteria (α = 0.05, α = 0.10) was tested against a binomial distribution, where

$$P = 1 - \sum_{i=0}^{\lfloor n_{ef} f \rfloor} \binom{\lfloor n_{ef} \rfloor}{i} \alpha^i \, (1-\alpha)^{\lfloor n_{ef} \rfloor - i} \qquad (10)$$

(Livezey and Chen, 1983; Wilks, 2006; Luce and Holden, 2009). Although n = 86 gauges were analyzed, the effective sample size represented by n_{ef} will be lower because streamflow across a geographical area is spatially correlated. Following Bretherton et al. (1999), we first estimated n_{ef}, the effective number of gauges, from the covariance matrix of streamflows, $\mathbf{C}$, as

$$n_{ef} = \frac{(\sum_{i=1}^{n} c_{ii})^2}{\sum_{i,j=1}^{n} c_{ij}^2}. \qquad (11)$$

Secondly, we also estimated n_{ef} to be the number of leading principal components necessary to explain 86% of the variance in the streamflow matrix (Bretherton et al., 1999). We calculated the field significance using n_{ef} from both methods. For each

climate oscillation and each gauge record, three permutation *t*-tests: a two-sample and two one-sample tests were calculated. We considered the permutation *t*-test type which had the greatest proportion f of significant results to be the appropriate test type for that oscillation and this f was used in the binomial test.

3. Results

A clear, strong fingerprint of the extra-tropical oceanic PDO is shown for mean annual discharge of naturally-flowing Prairie streams, with 63% of the gauges having at least one significant permutation *t*-test ($p \leq 0.10$) out of the three calculated at each gauge (Figure 4). There is a negative relationship between the PDO and streamflow throughout the Prairie Provinces, except for northern Saskatchewan where the relationship becomes positive. The fingerprint is clearest in Alberta (70% of the gauges have at least one significant permutation test), next clearest in Saskatchewan (63%), and weakest in Manitoba (50%). The two-sample tests (49%) and the tests of streamflow magnitudes occurring during strong positive PDO events against the remaining streamflow data (45%) were most likely to be significant. Therefore, we assume that the two-sample tests are the most appropriate for detecting the PDO's effects. Using the first estimation method, the effective sample size of these 86 highly correlated streamflow records is $n_{ef} = 2.64$. Four principal components explained 87% of the variance in the streamflow records. Using $f = 0.49$, the binomial distribution specifies a field significance of $P = 0.01$ using the first method to

360 estimate n_{ef} and $P = 0.05$ using the second method. Therefore, it is unlikely that this
361 pattern appears by chance, and therefore the PDO's effect is real.

362 A clear, strong fingerprint of the extra-tropical atmospheric NPI is also shown
363 for mean annual discharge of naturally-flowing Prairie streams, with 53% of the
364 gauges having at least one significant permutation *t*-test ($p \leq 0.10$) (Figure 5). There
365 is a positive relationship between the NPI and streamflow throughout the Prairie
366 Provinces, except for northern Saskatchewan where the relationship becomes
367 negative. Again, the fingerprint is clearest in Alberta (65% of the gauges), next
368 clearest in Saskatchewan (59%), and weakest in Manitoba (27%). Tests of
369 streamflow magnitudes occurring during strong low NPI events against the remaining
370 streamflow magnitudes (48%) or the two-sample tests (37%) were most likely to be
371 significant. Therefore, we assume that the one-sample tests of streamflow magnitudes
372 occurring during strong low NPI events against the remainder are the most
373 appropriate for detecting the NPI's effects. Using $f = 0.48$, the binomial distribution
374 specifies a field significance of $P = 0.01$ using the first method and $P = 0.05$ using the
375 second. Therefore, the NPI's effect is probably real.

376 A weaker fingerprint of the tropical atmospheric SOI is shown for the mean
377 annual discharge of naturally-flowing Prairie streams, with 47% of the gauges having
378 at least one significant permutation *t*-test (Figure 6). There is a positive relationship
379 between the SOI and streamflow throughout the Prairies (that is, more discharge
380 during La Niña events, and decreased flow during El Niño events) except for the far

381 north where the pattern reverses. Again, the fingerprint is clearest in the west (in
382 Alberta 54% of the gauges and in Saskatchewan 44%), and weakest in Manitoba
383 (36%). Tests of streamflow magnitudes occurring during La Niña events against the
384 remaining streamflow data (44%) or the two-sample tests (34%) were most likely to
385 be significant. Therefore, we assume that the one-sample tests of streamflow
386 magnitudes occurring during strong La Niña events against the remainder are the
387 most appropriate for detecting the SOI's effects. Using $f = 0.44$, the binomial
388 distribution specifies a field significance of $P = 0.01$ using the first method and $P =$
389 0.05 using the second. Therefore, the SOI's effect is probably real.

390 A strong fingerprint of the extra-tropical atmospheric PNA is shown for the
391 mean annual discharge of naturally-flowing Prairie streams, with 51% of the gauges
392 having at least one significant permutation *t*-test (Figure 7). There is a negative
393 relationship between the PNA and streamflow throughout the Prairies (that is, more
394 discharge during negative PNA events, and decreased flow during positive PNA
395 events) except for the far north. Again, the fingerprint is clearest in the west (in
396 Alberta 59% of the gauges and in Saskatchewan 56%), and weakest in Manitoba
397 (32%). Tests of streamflow magnitudes occurring during positive PNA events against
398 the remaining streamflow magnitudes (40%) or the two-sample tests (40%) were
399 most likely to be significant. Therefore, we assume that the two-sample tests are the
400 most appropriate for detecting the PNA's effects. Using $f = 0.40$, the binomial

401 distribution specifies a field significance of $P = 0.01$ using the first method and $P =$
402 0.05 using the second. Therefore, the PNA's effect is probably real.

403 A weak fingerprint of the polar atmospheric AO is shown for the mean annual
404 discharge of naturally-flowing Prairie streams, with only 40% of the gauges having a
405 significant permutation *t*-test (Figure 8). The pattern in the precipitation correlation
406 plot is different from those of the other Pacific-based climate oscillations, with
407 negative correlations in the central Prairies and positive correlations in the southern
408 Rocky Mountains of Alberta, southern Saskatchewan and Manitoba and northern
409 Saskatchewan and northern Manitoba. The AO fingerprint on streamflow is weakest
410 in the west (in Alberta 30% of the gauges), and strongest in the east (in Saskatchewan
411 48% of the gauges and likewise in Manitoba 45%). Tests of streamflow during
412 negative AO events against the remaining streamflow magnitudes (33%) or the two-
413 sample tests (22%) were most likely to be significant. Therefore, we assume that
414 these one-sample tests of streamflow magnitudes occurring during negative AO
415 events against the remainder are the most appropriate for detecting the AO's effects.
416 Using $f = 0.33$, the binomial distribution specifies a field significance of $P = 0.19$
417 using the first method, but $P = 0.05$ using the second. Therefore, it is ambiguous as to
418 whether this pattern appears by chance or not.

419 Our examination of the effect of PDO phase on the probability of two years of
420 successive least (or highest) quartile flows of Saskatchewan River tributaries
421 confirms the above fingerprint of the PDO, with higher flows during the negative

422 phase and lower flows during the positive phase (Figure 9 and Appendix Table A.2).
423 The mean probability of two years of successive least quartile flows is 0.149 during
424 the positive phase of the PDO; this probability drops to a negligible 0.015 during the
425 negative phase of the PDO. This difference is shown to be highly significant by a
426 paired permutation *t*-test ($p = 6.0 \times 10^{-8}$). Conversely, the mean probability of two
427 years of successive highest quartile flows is a small 0.043 during the positive phase
428 of the PDO; this probability increases to 0.135 during the negative phase. Again, this
429 difference is shown to be highly significant by a paired permutation *t*-test ($p = 1.5 \times$
430 10^{-7}). This pattern in the least quartile flows is seen at 24 of the 25 examined
431 discharge records; the Red Deer River at Red Deer (a regulated gauge) is the
432 exception. This pattern in the highest quartile flows is seen at 23 of the examined
433 discharge records; the Bow River at Banff and the Columbia River at Nicholson (both
434 naturally-flowing records) are the exceptions.

435 The modified Mann-Kendall trend tests demonstrate a distinct geographical
436 pattern with significant declines in the west and significant increases in the east
437 (Figure 10 and Appendix Table A.3). There are 12 declining trends (10 significant at
438 the $p \leq 0.05$ level) throughout Alberta, which extend into western Saskatchewan as
439 three further declining trends (two significant at the $p \leq 0.05$ level). On the other
440 hand, there are three significant increasing trends ($p \leq 0.05$) in southern Manitoba,
441 and one increasing trend ($p \leq 0.05$) at Seal River, and one decreasing trend ($p \leq 0.10$)
442 at Gods River, both in northern Manitoba. The binomial test showed lack of field

443 significance over all the 86 records for both $\alpha = 0.05$ and $\alpha = 0.10$. Significant
444 declines ($p \leq 0.05$) were also detected at regulated gauges: the North Saskatchewan
445 River at Edmonton, the South Saskatchewan River at Medicine Hat and the
446 Saskatchewan River at The Pas. No significant trends were detected at the Red Deer
447 River at Red Deer and the North Saskatchewan at Prince Albert.

448 ## 4. Discussion

449 Composite analyses based upon Monte Carlo permutation *t*-tests show that the
450 PDO, NPI and PNA have a clear impact on Prairie annual mean daily discharge, with
451 higher annual discharges occurring during negative PDO, high NPI and negative
452 PNA years, and lower flows during the positive PDO, low NPI and positive PNA
453 years throughout most of the Prairie Provinces (Figures 4, 5 and 7). Composite
454 analyses also show the weaker impact of ENSO, and the weaker still effect of the
455 AO, again with usually higher flows during La Niña and the negative AO years
456 throughout the region, and usually lower flows during El Niño and the positive AO
457 years (Figures 6 and 8). The phase relationships are reversed in the very far north for
458 the Pacific Ocean-based climate patterns. Unlike the Pacific-based climate
459 oscillations, the AO's fingerprint on streamflow is weakest in the west and strongest
460 in the east and shows a negative relationship in the central Prairies, which reverses in
461 the periphery. As expected, there are similar patterns of streamflow and precipitation
462 variation according to climate oscillation phases (Figures 4-8).

463 This study is the most comprehensive, in terms of prairie-wide extent and
464 numbers of gauges and climate oscillation examined, to demonstrate relationships
465 between the climate oscillations and Prairie Provinces' streamflow. Burn et al. (2008)
466 undertook a similar study on small prairie streams and found that no such
467 relationships existed. However, their study included only a quarter of the streamflow
468 gauges examined here, was based upon shorter streamflow and climate oscillation
469 records, and used a lower threshold of climate oscillation events and a regular *t*-test
470 with its normality assumptions that are inappropriate for small streams (Gobena and
471 Gan, 2006). Using the non-parametric Mann-Whitney test and data ending in 2001,
472 Gobena and Gan (2006) found that river discharge is higher during negative PDO, La
473 Niña and negative PNA years, and lower in the positive phase years in streamflow
474 records concentrated in British Columbia and southern Alberta mountain headwaters,
475 but they included only three gauge records each from Saskatchewan and Manitoba.
476 Woo and Thorne (2003) demonstrated significant relationships between western
477 Canadian annual and spring peak flows and the SOI and PNA, using Spearman's r^2
478 and 1968-1998 data.

479 How exactly the upstream North Pacific Ocean is linked to the overlying
480 atmosphere, and how these linkages affect the precipitation, temperature and
481 hydrology of the Canadian Prairies, and how the various atmosphere-ocean climate
482 oscillations are mechanistically generated and how they interact with and affect each
483 other are active areas of research. The PDO's zonal dipole in North Pacific SSTs

484 affects the downstream western North America hydroclimatology by a shift in the
485 position of the sub-polar jet, which brings winter storms and precipitation as it passes
486 over the continental margin (Gershunov and Barnett, 1998; Bonsal et al., 2001; Stahl
487 et al., 2006). A low (high) NPI winter, *i.e.*, a strong (weak) Aleutian Low, is
488 consistent with a positive (negative) PDO winter (Gershunov and Barnett, 1998); and
489 the winter PDO and the winter NPI are strongly correlated to each other (r = -0.56, df
490 = 109, p = 1.2 x 10^{-10}). Davis (1976), Trenberth and Hurrell (1994), Lau (1997) and
491 Kushnir et al. (2002), among others, suggest that the North Pacific atmospheric
492 circulation forces the underlying mixed-layer oceanic variability, observing that the
493 correlations between North Pacific SSTs and SLPs are strongest when the atmosphere
494 leads the ocean by several months. Whether or not the PDO is independent of ENSO
495 is unclear. Newman et al. (2003), Schneider and Cornuelle (2005) and Newman
496 (2007) have suggested that ENSO forces the PDO, *i.e.*, that El Niño (La Niña) forces
497 the positive (negative) phase of the PDO. However, other researchers (*e.g.*, Zhang et
498 al., 1996; Yu et al., 2007; Zhang and Delworth, 2007) have deemed the PDO, or
499 portions of its variability, to be independent of ENSO, but that reinforcing
500 interactions can occur between the two oscillations. Gershunov and Barnett (1998),
501 Yu et al. (2007) and Wise (2010) found that there occurred an enhanced response of
502 the PNA when the PDO and ENSO were in the same phase; that is, when a negative
503 (positive) PDO phase and a La Niña (El Niño) both occurred, the Pacific Northwest
504 and western interior experienced cooler and wetter (warmer and drier) conditions than
505 normal in a negative (positive) PDO alone. In winter, a positive AO is consistent with

506 a negative PDO, as a more positive AO suggests a weaker Aleutian Low which is
507 more consistent with the negative phase of the PDO (Gershunov and Barnett, 1998).

508 The southwestern prairies are distinct in their great sensitivity of streamflow to
509 Pacific Ocean SSTs (Rood et al., 2005; St. Jacques et al., 2010; St. Jacques et al., *in*
510 *review*). A majority of the slightly low-pass filtered streamflow variance is explained
511 by simple generalized-least-squares regression models using the PDO, SOI and North
512 Atlantic Oscillation as predictors. This almost certainly reflects the high sensitivity
513 of Rocky Mountain snowpack to these climate oscillations.

514 Any analysis of the Canadian Prairie hydroclimatology is limited by the
515 available streamflow data. In our study, the Saskatchewan hydrometric records are
516 the shortest, with a mean period of record of 48 years, followed by those from
517 Manitoba (51 years) and Alberta (53 years). Because of this short length, only one
518 low-frequency positive phase (1977-2007) of the PDO is well represented in the
519 period of record. Therefore very few annual mean daily discharges from negative
520 PDO years are available for analysis in the shorter periods of record, which lessens
521 the probability of detecting significantly different streamflows in the different phases.
522 This also means that there are relatively few annual mean daily discharges from high
523 NPI years, La Niña years and negative PNA years in the short records, as high NPI,
524 La Niña and negative PNA events are more likely to occur during the negative phase
525 of the PDO (Figure 3 and Table 2). Similarly, discharge data from negative AO years
526 are underrepresented post-1975, as the AO has had a positive bias during these most

527 recent 35 years. On the other hand, discharges from positive PDO, low NPI, El Niño,
528 positive PNA, and positive AO years are well represented in the hydrological record.
529 This data artifact justifies in part this study's use of one-sample permutation *t*-tests.
530 Other justifications arise because only one phase of a climate oscillation may
531 consistently affect streamflow, but not the other phase (*e.g.*, the southward
532 displacement of the winter sub-polar jet in a positive PDO event may result in low
533 flows, but the more northward position of the jet in a negative PDO event may not in
534 itself be sufficient to guarantee high flows), and individual watershed effects (*e.g.*,
535 nivial versus glacial catchments, upstream lakes buffering flow). Furthermore, there
536 are few moderately-sized naturally-flowing rivers in the southern halves of the Prairie
537 Provinces, where because of extensive agriculture, an accurate portrait of the
538 hydroclimatology is highly desired for water management. From a
539 hydroclimatological perspective, this is a serious limitation as moderately sized rivers
540 are more likely to reflect the impact of the atmosphere-ocean climate oscillations
541 much more strongly than small, flashy streams do, as the later are more impacted by
542 small-scale, local, stochastic processes. Moderately-sized rivers have large enough
543 watersheds to average the patchily distributed precipitation events, small streams do
544 not.

545 Typically, hydrologists assume that the probability of extreme high or low
546 flows is independently and identically distributed from year to year (Franks and
547 Kuczera, 2002; Kiem et al., 2003). The application of this assumption to the

548 Saskatchewan River Basin must be critically examined in light of this study's result
549 that there is a definite asymmetry in the effect of PDO phase on the probability of two
550 years of successive least (or highest) quartile flows of Saskatchewan River tributaries.
551 As well, given that the probability of two years of successive least quartile flow is
552 higher in the positive phase of the PDO, the probability of more than two years of
553 low flow must be considered and the estimated basin reservoir capacity of at most
554 two years should be re-evaluated. This is especially true in the light of the multi-
555 centennial tree-ring records reconstructed for the South and North Saskatchewan
556 Rivers, which shows periods of multi-decadal low flows in the past millennium
557 (Axelson et al., 2009; Sauchyn et al., 2011).

558 There are declines in annual mean daily flow in the naturally-flowing streams
559 throughout Alberta and southwest Saskatchewan, no significant trends in the central
560 region and increased flows in Manitoba in both the far north and south (Figure 10).
561 Although there is no overall field significance to the trends, for this pattern to be
562 purely due to chance; one would expect there to be no geographical pattern in the
563 trends, and no geographical consistency of trend sign. Therefore, the individual
564 regional patterns could be emerging and real, particularly the drying trends in
565 southern Alberta and southwest Saskatchewan, which are consistent with global
566 warming scenarios. The non-parametric Mann-Kendall test used in the analysis is a
567 relatively low-powered test, *i.e.,* a large change must occur before the MK test is able
568 to detect it (Sokal and Rohlf, 1995; Yue et al., 2002b). There could be further

declines or increases present that a more powerful test could detect. To provide climatological context for these trend results, Zhang et al. (2000) showed that the Prairie provinces have become significantly warmer over the past century, as well as wetter (significantly wetter in the Rocky Mountains, in the far north and in eastern Manitoba) in their MK-based analysis of Adjusted Historical Canadian Climate Data.

The declining trends should be interpreted with care in Alberta and southwestern Saskatchewan as the composite analysis shows that this area's streamflow is strongly affected by the PDO (Figures 4 and 10). The ~60 year low frequency cycle of the PDO can potentially generate a declining linear trend in short instrumental streamflow records. Many western North American instrumental streamflow records begin in the 1950s or 1960s (a period of negative PDO, hence high prairie streamflow), or omit the 1930s and 1940s (periods of positive PDO, hence low prairie streamflow). Therefore, any trend line fit between this initial high flow period, followed by this subsequent low flow period shows a declining trend. If this influence of the PDO is not taken into account in an analysis of prairie instrumental hydroclimatic records, this could produce detected declines that could be attributed to climate change, while they are actually artifacts of the sampling period and the PDO phase changes (Chen and Grasby, 2009). Very few western streamflow trend analyses have considered the issue of PDO phase (*e.g.*, Rood et al., 2005; Luce and Holden, 2009; St. Jacques et al., 2010 are exceptions). One solution is to weight more heavily records spanning more than one PDO cycle in length. The six declining

590 gauge records in the southwest Prairies are among the longest streamflow records,
591 with five beginning in the 1910s or 1930s, and spanning more than one PDO cycle;
592 therefore, the declines are less likely to be artifacts of the PDO phase. Zhang et al.
593 (2001), using the MK test on prewhitened data, found similar declining annual mean
594 streamflow at naturally-flowing gauges in the southwest Prairies over an earlier
595 period of record. Rood et al. (2005, 2008) and St. Jacques et al. (2010) also detected
596 declining trends in southern Alberta naturally-flowing stream gauge records. Hence,
597 the streamflow declines in the southwestern Prairies are most likely real.

598 There also are significant declines in the regulated flows of the South
599 Saskatchewan River Basin (Figure 10 and Appendix Table A.3). This is in accord
600 with previous Alberta-focused studies (*i.e.,* Rood et al., 2005, 2008; Schindler and
601 Donahue, 2006; St. Jacques et al., 2010). St. Jacques et al. (2010) showed that the
602 basin declines were due to both direct human impact and climatic changes, with these
603 effects being approximately equal in magnitude. The worst of the decline is in the
604 southern Oldman and Bow River Basins, as the downstream gauge at Medicine Hat
605 shows a very significant decline ($p \leq 0.05$), and not in the northern Red Deer River
606 Basin, which shows a non-significant decline. This decline propagates all the way
607 downstream to the gauge at The Pas, Manitoba, which also shows a highly significant
608 decline.

609 In the central Prairie region, annual naturally-flowing hydrological series show
610 no significant trends. Previous studies, Gan (1998) and Burn et al. (2008) also

showed little significant change in annual or warm-season discharge in Saskatchewan. Since Zhang et al. (2000) showed that Saskatchewan's climate has become significantly warmer over the past century, as well as wetter, our streamflow analysis suggests that either increased evaporation from higher temperatures is balanced by increased precipitation throughout much of the province, or that emerging trends in the short hydrological time series are still below the threshold of detection of the weak MK test. However, Burn and Hesch (2006) found no increase in potential and pan evaporation, and even decreases, with increased temperatures. In response to a warming climate, Burn et al. (2008) detected seasonal shifts towards earlier peak flow from snowmelt across the prairies, particularly in western Alberta, as did Rood et al. (2008).

Southern Manitoba exhibits increasing flows in mean annual discharge, similar to emerging trends in adjacent North Dakota (*pers. com.* R.W. Dudley, United States Geological Service). It is uncertain whether this is due to climatological changes and/or to landscape changes (*i.e.*, increased drainage of wetlands, and canal building). Zhang et al. (2000) showed significantly increased annual precipitation for much of Manitoba over the period 1950-1998, which is in accord with projected precipitation increases (Barrow, 2010). Immediately to the north of the Prairie Provinces, rivers in the Northwest Territories are showing increases in annual discharge and winter baseflow due to hydrological cycle intensification and decaying permafrost from anthropogenic global warming (Smith et al., 2007; St. Jacques and Sauchyn, 2009).

632 The increased flow in the Seal River in northern Manitoba where sporadic permafrost
633 is present is likely also due to permafrost decay. There has been a significant 37.1%
634 increase in winter baseflow in the Seal River (estimated by January-March average
635 daily flow) over the 56 years of record as detected by the modified MK test (z = 3.34,
636 p = 0.0008 from two-tailed test).

637 An assessment of any MK trend analysis must be placed in the context of
638 recent advances in hydrological statistics. It has only relatively recently been widely
639 appreciated that the MK test is affected by the serial correlation present in many
640 hydrological time series (Kulkarni and von Storch, 1995). If there is positive
641 (negative) autocorrelation in a time series, the MK test will suggest a significant trend
642 in the series, which is actually random, more (less) often than specified by the
643 significance level. Gan (1998) did not directly address the issue of autocorrelation,
644 but rather analyzed monthly mean flows, assuming autocorrelation was negligible (an
645 assumption that needs testing). There are various methods of dealing with this
646 problem: at the very least, testing to see if autocorrelation is actually present or not
647 (*e.g.*, St. Jacques and Sauchyn, 2009), applying a variance correction or effective
648 sample size correction to the test, such as that used in this study and Yue and Wang
649 (2004), or pre-whitening, that is, removal of the autocorrelation before testing
650 (Kulkarni and von Storch, 1995; Zhang et al., 2000, 2001; Yue et al., 2002a). There
651 are different, often controversial, approaches to prewhitening. One is to estimate the
652 lag-one autocorrelation coefficient r_1 directly from the time series, and then

653 prewhitening the time series ($y_i = x_i - r_1 x_{i-1}, \forall i$) (Kulkarni and von Storch, 1995;
654 Zhang et al., 2001). This was the approach used by Zhang et al. (2001). The problem
655 with this approach is that if a trend is present in the time series, together with
656 positive autocorrelation; it biases the estimation of r_1, affects the magnitude of
657 estimated slope and leads to an increased chance of accepting the null hypothesis of
658 no trend when a trend is actually present (Yue et al., 2002a; Khaliq et al., 2009). As a
659 correction, Yue et al. (2002a) proposed another prewhitening method: for a given
660 time series, detrend it by a Sen-Theil line, estimate the lag-one autocorrelation
661 coefficient r_1 in the detrended time series, prewhiten the detrended time series using
662 r_1, add back in the trend, and then apply the MK test to the final time series. This is
663 the approach followed by Burn et al. (2008). Unfortunately, this complex method
664 leads to an over-rejection of the no trend null hypothesis (Khaliq et al., 2009). Lastly,
665 there is an iterative method based on successive estimation of r_1 and β (the slope
666 coefficient) which seems reasonable, but its performance is unknown. This is the
667 method used by Zhang et al. (2000). In their recent assessment of the different Mann-
668 Kendall methods, Khaliq et al. (2009) concluded that the use of a variance correction
669 method such as that used here or a bootstrapping approach (*e.g.,* Kundzewicz and
670 Robson, 2000) is best practice.

671 ## 5. Conclusions

672 This study detected the fingerprints of the PDO, the NPI and the PNA on
673 annual discharge in Canadian Prairie Provinces streams and rivers, with increased

674 flows during the negative phases of the PDO and the PNA and weak Aleutian lows,
675 and decreased flows during the positive phases and strong Aleutian lows. A lesser
676 fingerprint of ENSO and the AO are also detected. Because of the ~60-year cycle of
677 the PDO, this has important implications for the recognition of emerging trends in
678 streamflow in response to global climate change. Separation of emerging consistent
679 trend from transient trend as an artifact of PDO phase is greatly facilitated by
680 streamflow time series that span more than one PDO cycle, especially in the small
681 prairie streams where parametric statistical methods are inappropriate. This highlights
682 the continued importance of the stream gauge monitoring programs maintained by the
683 Water Survey of Canada and the various provincial water authorities. A modified MK
684 trend analysis of Prairie Provinces rivers and streams shows decreasing flows in
685 Alberta and in southwestern Saskatchewan, no significant trends in the naturally-
686 flowing streams in the central Prairies and increased mean annual flows in Manitoba.

687 The results of this study have important implications for water resource
688 management in the Canadian Prairie Provinces. The recognition of significant natural
689 modes of hydroclimatic variability leads to a more rigorous interpretation of recent
690 trends and fluctuations in raw water supply. We have been able to attribute much of
691 the variability in the annual flow records, including emerging trends, to the influence
692 of large-scale ocean-atmosphere circulation patterns. At the same time, there are
693 significant trends in some gauge records that span shifts in the phases of these

694 teleconnections. These consistent trends most likely represent a fundamental change
695 in hydrologic regime in response to regional climate and land use change.

696 Acknowledgments

697 We thank Jeremy Pittman and Ron Woodvine (Agriculture and Agri-Food
698 Canada); Michele Williamson (Environment Canada); Stephanie Pow, Jeff
699 Woodward, Bart Oegema, Curtis Hallburg, Dwayne Siba, Clinton Molde, Whit
700 Wyatt, Richard Hammer, Cameron Macdonald (all with the Saskatchewan Watershed
701 Authority); Mike Seneka (Alberta Environment); Bill Girling, John Crawford, Mike
702 Baldaro and Efrem Teklemariam (all with Manitoba Hydro) for their help in
703 compiling streamflow data. This study was a component of the Prairies Regional
704 Adaptation Collaborative, a program initiated and funded by Natural Resources
705 Canada.

706

707 ## References

708 Axelson, J., Sauchyn, D.J., Barichivich, J., 2009. New reconstructions of streamflow
709 variability in the South Saskatchewan River basin from a network of tree-ring
710 chronologies, Alberta, Canada. Water Resour. Res. 45, W09422.
711 Bayley, G.V., Hammersley, J.M., 1946. The effective number of independent
712 observations in an autocorrelated time series. J. Roy. Stat. Soc. 8, 184-197.
713 Bonsal, B., Lawford, R.G., 1999. Teleconnections between El Niño and La Niña
714 events and summer extended dry spells on the Canadian prairies. Int. J.
715 Climatol. 19, 1445-1458.
716 Bonsal, B., Shabbar, A., Higuchi, K., 2001. Impacts of low frequency variability
717 modes on Canadian winter temperature. Int. J. Climatol. 21, 95-108.
718 Bonsal, B., Shabbar, A., 2008. Impacts of large-scale circulation variability on low
719 streamflows over Canada, a review. Can. Water Resour. J. 33, 137-154.
720 Bretherton, C.S., Widmann, M., Dymnikov, V.P., Wallace, J.M., Bladé. I., 1999. The
721 effective number of spatial degrees of freedom of a time-varying field. J.
722 Climate 12, 1990-2009.
723 Burn, D.H., 1994. Hydrological effects of climatic change in west-central Canada. J.
724 Hydrol. 160, 53-70.
725 Burn, D.H., Hag Elnur, M.A., 2002. Detection of hydrologic trends and variability. J.
726 Hydrol. 255, 107-122.
727 Burn, D.H., Hesch, N.M., 2006. A comparison of trends in potential and pan
728 evaporation for the Canadian Prairies. Can. Water Resour. J. 31, 173-184.
729 Burn, D.H., Fan, L., Bell, G., 2008. Identification and qualification of streamflow
730 trends on the Canadian Prairies. Hydrol. Sci. 53, 538-548.
731 Chen, Z., Grasby, S.E., 2009. Impact of decadal and century-scale oscillations on
732 hydroclimate trend analyses. J. Hydrol. 365, 122-133.
733 Comeau, L.E.L., Pietroniro, A., Demuth, M.N., 2009. Glacier contribution to the
734 North and South Saskatchewan Rivers. Hydrol. Process. 23, 2640-2653.
735 Cryer, J.D., Chan, K.-S., 2008. Time series analysis with applications in R, second
736 ed. Springer-Verlag, New York.
737 Davis, R.E., 1976. Predictability of sea surface temperature and sea level pressure
738 anomalies over the North Pacific Ocean. J. Phys. Oceanog. 6, 249-266.
739 Fleming, S.W., Whitfield, P.H., Moore, R.D., Quilty, E.J., 2007. Regime-dependent
740 streamflow sensitivities to Pacific climate modes cross the Georgia-Puget
741 transboundary ecoregion. Hydrol. Process. 21, 3264-3287.
742 Franks, S.W., Kuczera, G., 2002. Flood frequency analysis, evidence and
743 implications of secular climate variability, New South Wales. Water Resour.
744 Res. 38, 20.1-20.

745 Gan, T.Y., 1998. Hydrocllimatic trends and possible climatic warming in the
746 Canadian Prairies. Water Resour. Res. 34, 3009-3015.
747 Gobena, A.K., Gan, T.Y., 2006. Low-frequency variability in southwestern Canadian
748 streamflow: links with large-scale climate anomalies. Int. J. Climatol. 26, 1843-
749 1869.
750 Gobena, A.K., Gan, T.Y., 2009. The role of Pacific climate on low-frequency
751 hydroclimatic variability and predictability in southern Alberta, Canada. J.
752 Hydrometeor. 10, 1465-1478.
753 Gershunov, A., Barnett, T.P., 1998. Interdecadal modulation of ENSO
754 teleconnections. Bull. Amer. Meteor. Soc. 79, 2715-2725.
755 Hamed, K.H., Rao, A.R., 1998. A modified Mann-Kendall trend test for
756 autocorrelated data. J. Hydrol. 204, 219-246.
757 Harvey, K.D., Pilon, P.J., Yuzyk, T.R., 1999. Canada's reference hydrometric basin
758 network (RHBN). In: Partnerships in Water Ressources Management. Paper
759 presented at Canadain Water Resources Association (CWRA)'s 51st Annual
760 Conference, June 1999, Halifax, Nova Scotia.
761 Helsel, D.R., Hirsch, R.M., 2002. Statistical Methods in Water Resources. U.S.
762 Geological Society.
763 Kendall, M.G., 1975. Rank Correlation Methods. Charles Griffin, London.
764 Khaliq, M.N., Ouarda, T.B.M.J., Gachon, P., Sushama, L., St-Hilaire, A., 2009.
765 Identification of hydrological trends in the presence of serial and cross
766 correlations: a review of selected methods and their application to annual flow
767 regimes of Canadian rivers. J. Hydrol. 368, 117-130.
768 Kiem, A.S., Franks, S.W., Kuczera, G., 2003. Multi-decadal variability of flood risk.
769 Geophys. Res. Lett. 30, 7.1-7.4.
770 Kulkarni, A., von Storch, H., 1995. Monte Carlo experiments on the effect of serial
771 correlation on the Mann-Kendal test of trend. Meteorol. Z. 4, 82-85.
772 Kundzewicz, Z.W., Robson, A.J., 2000. Detecting Trend and Other Changes in
773 Hydrological Data. World Climate Program-Data and Monitoring. World
774 Meteorological Organization, Geneva (WMO/TD-no. 1013).
775 Kushnir, Y., Robinson, W.A., Bladé, I., Hall, N.M.J., Peng, S., Sutton, R., 2002.
776 Atmospheric GCM response to extratropical SST anomalies, synthesis and
777 evaluation. J. Climate 15, 2233-2256.
778 Lapp, S.L., St. Jacques, J.M., Barrow, E.M., Sauchyn, D.J., 2012. GCM projections
779 for the Pacific Decadal Oscillation under greenhouse forcing for the early 21st
780 century, Int. J. Climatol. DOI: 10.1002/joc.2364.
781 Lau, N.C., 1997. Interactions between global SST anomalies and the midlatitude
782 atmospheric circulation. Bull. Amer. Meteorol. Soc. 78, 21-33.
783 Livezey, R.E., Chen, W.Y., 1983. Statistical field significance and its determination
784 by Monte Carlo techniques. Mon. Weather Rev. 111, 46-59.
785 Luce, C.H., Holden, Z.A., 2009. Declining annual streamflow distributions in the
786 Pacific Northwest United States, 1948-2006. Geophys. Res. Lett. 36, L16401.

787 Manly, B.F.J., 1998. Randomization, bootstrap and Monte Carlo methods in biology,
788 second ed. Chapman and Hall, London.
789 Mann, H.B., 1945. Non-parametric tests against trend. Econometrica 13, 245-259.
790 Mantua, N.J., Hare, S.R., Zhang, Y., Wallace, J.M., Francis, R.C., 1997. A Pacific
791 interdecadal climate oscillation with impacts on salmon production. Bull.
792 Amer. Meteorol. Soc. 78, 1069-1079.
793 Mantua, N.J., Hare, S.R., 2002. The Pacific Decadal Oscillation. J. Oceanog. 58, 35-
794 44.
795 McCabe, G.J., Dettinger, M.J., 2002. Primary modes and predictability of year-to-
796 year snowpack variations in the western United States from teleconnections
797 with Pacific Ocean climate. J. Hydrometeorol. 3, 13-25.
798 McKenney, D.W., Pedlar, J.H., Papadopol, P., Hutchinson, M.F., 2006. The
799 development of 1901-2000 historical monthly climate models for Canada and
800 the United States. Agri. For. Meteorol. 138, 69-81.
801 Minobe, S., 1997. A 50-70 year climatic oscillation over the North Pacific and North
802 America. Geophys. Res. Lett. 24, 683-686.
803 Minobe, S., 1999. Resonance in bidecadal and pentadecadal climate oscillations over
804 the North Pacific: role in climatic regime shifts. Geophys. Res. Lett. 26, 855-
805 858.
806 Newman, M., Compo, G.P., Alexander, M.A., 2003. ENSO-forced variability of the
807 Pacific Decadal Oscillation. J. Climate 16, 3853-3857.
808 Newman, M., 2007. Interannual to decadal predictability of tropical and North Pacific
809 sea surface temperatures. J. Climate 20, 2333-2356.
810 Pham, S.V., Leavitt, P.R., McGowan, S., Wissel, B., Wassenaar, L.I., 2009. Spatial
811 and temporal variability of prairie lake hydrology as revealed using stable
812 isotopes of hydrogen and oxygen. Limnol. Oceanogr. 54, 101-118.
813 R Development Core Team, 2008. R: A language and environment for statistical
814 computing. R Foundation for Statistical Computing, Vienna, Austria. ISBN 3-
815 900051-07-0, URL http://www.R-project.org.
816 Redmond, K.T., Koch, R.W., 1991. Surface climate and streamflow variability in the
817 western United States and their relationship to large-scale circulation indices.
818 Water Resour. Res. 9, 2381-2399.
819 Rood, S.B., Samuelson, G.M., Weber, J.K., Wywrot, K.A., 2005. Twentieth-century
820 decline in streamflows from the hydrographic apex of North America. J.
821 Hydrol. 306, 215-233.
822 Rood, S.B., Pan, J., Gill, K.M., Franks, C.G., Samuelson, G.M., Shepherd, A., 2008.
823 Declining summer flows of Rocky Mountain rivers: changing seasonal
824 hydrology and probable impacts on floodplain forests. J. Hydrol. 349, 397-410.
825 Ropelewski, C.F., Jones, P.D., 1987. An extension of the Tahiti-Darwin Southern
826 Oscillation Index. Mon. Weather Rev. 115, 2161-2165.
827 Sauchyn, D.J., Vanstone, J., Perez-Valdivia, C., 2011. Modes and forcing of
828 hydroclimatic variability in the upper North Saskatchewan River Basin Since
829 1063. Can. Water Resour. J. 36, 205-218.

St. Jacques, J.M., Sauchyn, D.J., 2009. Increasing winter baseflow discharge and mean annual streamflow from possible permafrost thawing in the Northwest Territories, Canada. Geophys. Res. Lett. 36, L01401, doi:10.1029/2008GL035822.

St. Jacques, J.M., Sauchyn, D.J., Zhao, Y., 2010. Northern Rocky Mountain streamflow records: global warming trends, human impacts or natural variability? Geophys. Res. Lett. 37, L06407, DOI:10.1029/2009GL042045.

St. Jacques, J.M., Lapp, S.L., Zhao, Y., Barrow, E.M., Sauchyn, D.J., in review. Twenty-first century northern Rocky Mountain river discharge scenarios under greenhouse forcing. Submitted to Quaternary International, conditionally accepted pending revision, Dec. 27, 2011.

Schindler, D.W., Donahue, W.F., 2006. An impending water crisis in Canada's western prairie provinces. Proc. Natl. Ac. Sci. 103, 7210-7216.

Schneider, N., Cornuelle, B.D., 2005. The forcing of the Pacific Decadal Oscillation. J. Climate 18, 4355-4373.

Sen, P.K., 1968. Estimates of the regression coefficient based on Kendall's tau. J. Amer. Stat. Assoc. 63, 1379-1389.

Shabbar, A., Khandekar, M., 1996. The impact of El Nino-Southern Oscillation on the temperature field over Canada. Atmos.-Ocean 34, 401-416.

Shabbar, A., Bonsal, B., Khandekar, M., 1997. Canadian precipitation patterns associated with the Southern Oscillation. J. Climate 10, 3016-3027.

Shabbar, A., Skinner, W., 2004. Summer drought patterns in Canada and the relationship to global sea surface temperatures. J. Climate 17, 2866-2880.

Smith, L.C., Pavelsky, T.M., MacDonald, G.M., Shiklomanov, A.I., Lammers, R.B., 2007. Rising minimum daily flows in northern Eurasian rivers: a growing influence of groundwater in the high-latitude hydrologic cycle. J. Geophys. Res. 112, G04S47, doi:10.1029/2006JG000327.

Sokal, R.R., Rohlf, F.J., 1995. Biometry, third ed. W.H. Freeman and Company, New York.

Stahl, K., Moore, R.D., McKendry, I.G., 2006. The role of synoptic-scale circulation in the linkage between large-scale ocean-atmosphere indices and winter surface climate in British Columbia, Canada. Int. J. Climatol. 26, 541-560.

Stewart, I., Cayan, D.R., Dettinger, M.D., 2005. Changes toward earlier streamflow timing across western North America. J. Climate 18, 1136-1155.

Theil, H., 1950. A rank-invariant method of linear and polynomial regression analysis, I, II, III. Nederl. Akad. Wetensch. Proc. 53, 386-392, 512-525, 1397-1412.

Trenberth, K.E., Hurrell, J.W., 1994. Decadal atmosphere-ocean variations in the Pacific. Clim. Dyn. 9, 303-319.

Wallace, J.M,, Gutzler, D.S., 1981. Teleconnections in the geopotential height field during the Northern Hemisphere winter. Mon. Weather Rev. 109, 784-812.

Westmacott, J.R., Burn, D.H., 1997. Climate change effects on the hydrologic regime within the Churchill-Nelson River Basin. J. Hydrol. 202, 263-279.

873 Whitfield, P.H., Moore, R.D., Fleming, S.W., Zawadzki, A., 2010. Pacific Decadal
874 Oscillation and the hydroclimatology of Western Canada – reviews and
875 propects. Can. Water Resour. J. 35, 1-28.
876 Wilks, D.S., 2006. Statistical Methods in the Atmospheric Sciences, second ed.
877 Elsevier Academic Press, New York.
878 Wise, E.K., 2010. Spatiotemporal variability of the precipitation dipole transition
879 zone in the western United States. Geophys. Res. Lett. 37, L07706.
880 Woo, M.K., Thorne, R., 2003. Comment on 'Detection of hydrologic trends and
881 variability' by Burn, D.H. and Hag Elnur, M.A., 2002. Journal of Hydrology
882 255, 107-122. J. Hydrol. 277, 150-160.
883 Yu, B., Shabbar, A., Zwiers, F.W., 2007. The enhanced PNA-like climate response to
884 Pacific interannual and decadal variability. J. Climate 20, 5285-5300.
885 Yue, S., Pilon, P., Phinney, B., Cavadias, G., 2002a. The influence of autocorrelation
886 on the ability to detect trend in hydrological series. Hydrol. Proc. 16, 1807-
887 1829.
888 Yue, S., Pilon, P., Cavadias, G., 2002b. Power of the Mann-Kendall and Spearman's
889 rho tests for detecting monotonic trends in hydrological series. J. Hydrol. 259,
890 254-271.
891 Yue, S., Wang, C., 2004. The Mann-Kendall test modified by effective sample size to
892 detect trend in serially correlated hydrological series. Water Resour. Man. 18,
893 201-218.
894 Yulianti, J., Burn, D.H., 1998. Investigating links between climatic warming and low
895 streamflow in the Prairies regions of Canada. Can. Water Resour. J. 23, 45-60.
896 Zhang, R., Delworth, T.L., 2007. Impact of the Atlantic Multidecadal Oscillation on
897 North Pacific climate variability. Geophys. Res. Lett. 34, L23708.
898 Zhang, Y., Wallace, J.M., Iwasaka, N., 1996. Is climate variability over the North
899 Pacific a linear response to ENSO? J. Climate 9, 1468-1478.
900 Zhang, Y., Wallace, J.M., Battisti, D.S., 1997. ENSO-like interdecadal variability:
901 1900-1993. J. Climate 10, 1004-1020.
902 Zhang, X., Vincent, L.A., Hogg, W.D., Niitsoo, A., 2000. Temperature and
903 precipitation trends in Canada during the 20th century. Atmos.-Ocean 38, 395-
904 429.
905 Zhang, X.., Harvey, K.D., Hogg, W.D., Yuzyk, T.R., 2001. Trends in Canadian
906 streamflow. Water Resour. Res. 37, 987-998.
907 Zheng, X., Basher, R.E., Thompson, C.S., 1997. Trend detection in regional-mean
908 temperature series: maximum, minimum, mean, diurnal range, and SST. J.
909 Climate 10, 317-326.

910 Table 1. Eighty-six naturally-flowing river discharge records from the Prairie Provinces, including Water Survey of Canada gauge
911 names, station codes, period of record, number of years of record analyzed, effective drainage area, mean daily flow and location.
912 Records ordered by province from west to east, and within province by south to north. If period of record is not equal to the number of
913 years of record analyzed, it is because of missing years from unavailable gauge records.

Station name	WSC station code	Period of record	# yrs	Drainage area (km^2)	Mean daily flow (m^3/s)	Latitude (N)	Longitude (W)
Sage Creek at Q Ranch	11AA026	1935-2010	76	504	0.35	49°06'27"	110°13'25"
Waterton River near Waterton Park	05AD003	1912-2010	99	613	17.55	49°06'49"	113°50'22"
Rolph Creek near Kimball	05AE005	1936-2010	75	187	0.35	49°07'30"	113°08'33"
Manyberries Creek	05AF010	1913-1930, 1957-2010	71	335	0.31	49°21'27"	110°43'30"
Pincher Creek at Pincher Creek	05AA004	1919-1930, 1966-2010	57	158	1.56	49°29'11"	113°56'51"
Prairie Blood Coulee	05AD035	1970-2010	41	224	0.11	49°33'58"	112°57'15"
Trout Creek near Granum	05AB005	1919, 1922-1923, 1978-2010	36	441	0.94	49°58'38"	113°41'09"
Blood Indian Creek near the mouth	05CK001	1964-1974, 1976-2010	46	384	0.07	50°57'29"	111°03'36"
Jumpingpound Creek	05BH009	1966-2005	40	571	2.54	51°09'16"	114°31'42"
Bow River at Banff	05BB001	1911-2010	100	2,210	39.05	51°10'20"	115°34'18"
Rosebud River	05CE006	1959-2010	52	642	0.43	51°24'57"	113°43'40"
Mistaya River	05DA007	1967-2010	44	248	6.34	51°53'03"	116°41'21"
Threehills Creek	05CE018	1971-2010	40	138	0.19	51°59'50"	113°34'06"
Prairie Creek	05DB002	1962-2010	49	844	4.45	52°16'25"	114°55'45"
Bigknife Creek near Gadsby	05FC002	1968-2010	43	194	0.26	52°31'02"	112°21'21"
Buffalo Creek at Highway 41	05FE002	1972-2010	39	147	0.23	53°00'26"	110°52'02"
Athabasca River at Hinton	07AD002	1962-2010	49	9,720	170.94	53°25'27"	117°34'09"
McLeod River above Embarras	07AF002	1955-2010	56	2,550	19.32	53°28'12"	116°37'53"
Pembina River	07BB002	1915-1922, 1955-2010	64	4,330	19.99	53°36'15"	115°00'17"

Waskatenau Creek	05EC002	1967-2010	44	201	0.29	54°07'23"	112°46'58"
Beaver River at Cold Lake Reserve	06AD006	1956-2010	55	11,800	18.44	54°21'18"	110°13'02"
Athabasca River at Athabasca	07BE001	1913-1930, 1938-2010	91	73,300	686.99	54°43'19"	113°17'16"
Little Smoky River near Guy	07GH002	1960-2010	51	11,100	46.63	55°27'22"	117°09'42"
Saddle River near Woking	07FD006	1967-2010	44	538	1.45	55°38'39"	118°42'00"
Smoky River at Watino	07GJ001	1916-1920, 1956-2010	60	49,600	338.68	55°42'52"	117°37'23"
Pine River at East Pine, BC	07FB001	1965-2010	46	12,100	188.67	55°43'12"	121°12'28"
Heart River near Nampa	07HA003	1963-2010	48	1,870	4.43	56°03'20"	117°07'47"
Clearwater River at Draper	07CD001	1958-2010	53	30,800	119.62	56°41'07"	111°15'19"
Athabasca River below McMurray	07DA001	1958-2010	53	130,000	616.93	56°46'49"	111°24'07"
Notikewin River	07HC001	1962-2010	49	4,660	13.28	56°55'12"	117°37'06"
Birch River below Alice Creek	07KE001	1968-2010	43	9,860	45.06	58°19'29"	113°03'54"
Richardson River near the mouth	07DD002	1971-2010	40	2,730	17.45	58°21'37"	111°14'25"
Boyer River near Ft.Vermilion	07JF002	1963-2010	48	6,660	4.68	58°26'56"	116°15'50"
Ponton River above Boyer River	07JF003	1963-2010	48	2,440	15.16	58°27'51"	116°15'22"
Sousa Creek near High Level	07OA001	1971-2010	40	820	2.39	58°35'29"	118°29'27"
Chinchaga River	07OC001	1970-2010	41	10,400	28.99	58°35'49"	118°20'02"
Hay River near Hay River	07OB001	1964-2010	47	51,300	115.32	60°44'34"	115°51'34"
Rock Creek below Horse Creek	11AE009	1916-1926, 1957-2010	65	830	0.76	48°58’10”	106°50’20”
Poplar River at Intern. Bd.	11AE008	1931-2010	80	928	0.68	48°59'25"	105°41'46"
Long Creek at W. Crossing*	05NA003	1912-2010	99	1,210	0.71	49°00’01”	103°21’08”
Lyons Creek at							

International Boundary	11AB075	1927-2010	84	136	0.09	49°00’17”	109°13’48”
Lightning Creek near Carnduff	05NF006	1974-2010	37	393	0.31	49°13’17”	101°43’08”
Antler River near Wauchope	05NF010	1965-2010	46	133	0.14	49°35’03”	101°50’52”
Notukeu Creek above Admiral Reservoir	05JB004	1975-2010	36	328	0.18	49°42’32”	108°07’31”
Swift Current Creek below Rock Creek	05HD036	1955-2010	56	1,090	1.33	49°50’40”	108°28’46”
Bridge Creek at Gull Lake	05HA015	1916-1922, 1963-2010	55	319	0.13	50°05’36”	108°29’38”
Cottonwood Creek near Lumsden	05JF011	1974-2010	37	224	0.34	50°35’26”	104°54’31”
Stony Creek near Kamsack	05MD010	1971-2010	40	116	0.32	51°23’19”	101°50’19”
Opuntia Lake West Inflow	05GC007	1960-2010	51	56.2	0.03	51°47’15”	108°37’30”
Maloneck Creek near Pelly	05LE011	1974-2010	37	171	0.50	51°58’08”	101°54’50”
Quill Creek near Quill Lake	05MA020	1973-2010	38	89.6	0.34	52°00’11”	104°14’50”
Lilian River near Lady Lake	05MC003	1970-2010	41	153	0.44	52°01’22”	102°37’30”
Red Deer River near Erwood	05LC001	1954-2010	57	8,550	23.90	52°51’36”	102°11’39”
Overflowing River near Hudson Bay	05LD003	1975-2010	36	349	1.84	53°01’51”	101°12’31”
Sturgeon River near Prince Albert	05GF002	1967-2010	44	2,560	3.26	53°12’47”	105°53’06”
Shell Brook near Shellbrook	05GF001	1966-2010	45	760	1.23	53°15’10”	106°23’09”
Carrot River near Smoky Burn	05KC001	1955-2010	56	7,120	16.22	53°25’00”	103°08’30”
Beaver River near Dorintosh	06AD001	1963-2010	48	16,900	29.04	54°17’47”	108°36’16”
Churchill River above Otter Rapids	06CD002	1964-2010	47	112,000	277.56	55°38’47”	104°44’05”

Haultain River above Norbert River	06BD001	1969, 1972-2010	40	3,680	18.41	56°14’40”	106°33’40”
Gelkie River below Wheeler River	06DA004	1967-2010	44	7,730	45.35	57°35’20”	104°12’10”
Waterfound River below Theriau Lake	07LB002	1975-1976, 1978-2010	35	3,160	21.31	58°23’10”	104°36’30”
MacFarlane River at Outlet of Davy Lake	07MB001	1968-2010	43	9,120	53.73	58°58’00”	108°10’30”
Fond du Lac River at Outlet of Black Lake**	07LE001, 07LE002	1947-2010	60	50,700	305.25	59°08’50”	105°32’20”
Mowbray Creek near Mowbray	05OB021	1962-2010	49	263	0.60	49°00'01"	98°27'13"
Antler River near Melita	05NF002	1943-2010	68	3,220	1.14	49°03'26"	101°02'57"
Graham Creek near Melita	05NF008	1943-1996, 2010	55	741	0.15	49°15'45"	100°59'53"
Shannon Creek near Morris	05OF014	1960-2010	51	617	1.30	49°21'17"	97°25'20"
S. Tobacco Creek near Miami	05OF017	1964-2010	47	76.4	0.24	49°22'45"	98°14'58"
Whitemouth River	05PH003	1957-2010	54	3,750	14.81	49°56'19"	95°57'24"
Brokenhead River near Beausejour	05SA002	1956-2010	55	1,580	6.58	50°05'24"	96°25'41"
Little Saskatchewan River	05MF001	1915-1929, 1959-2010	67	2,610	5.52	50°21'31"	99°54'27"
Pelican Creek S. Tributary	05LL027	1974-2010	37	9.2	0.04	50°28'36"	99°28'38"
Shell River near Inglis	05MD005	1957-2010	54	1,970	3.11	50°57'48"	101°19'07"
Icelandic River near Riverton	05SC002	1959-1996, 2010	39	1,240	2.59	50°57'53"	97°02'14"
Ochre River at Ochre River	05LJ005	1956-2010	55	348	2.14	51°03'04"	99°47'18"
Fisher River near Dallas	05SD003	1962-1996	35	1,710	1.82	51°21'22"	97°30'44"
Waterhen River near Waterhen	05LH005	1953-2010	58	55,100	82.11	51°50'54"	99°32'46"
Pigeon River at Outlet of Round Lake	05RD008	1958-2010	53	18,400	90.40	52°01'49"	96°23'37"
Overflowing River at Overflowing River	05LD001	1956-2010	55	3,100	12.64	53°08'34"	101°06'09"

Island Lake River	04AC007	1933-1964, 1966-1975, 1977-1979, 1981, 1983-1984, 1986-1993	56	14,000	85.46	54°03'34"	94°39'34"
God's River below Allan Rapids	04AC005	1934, 1937-1944, 1948-1993	54	27,200	159.03	55°01'35"	93°50'10"
Grass River above Standing Stone Falls	05TD001	1960-1984, 1986-1988, 1991-2010	48	15,400	65.26	55°44'26"	97°00'23"
Kettle River near Gillam	05UF004	1966, 1969-1996, 1998, 2000-2010	41	1,090	13.25	56°20'29"	94°41'47"
Little Beaver River near the mouth	06FB002	1974-2010	37	4,270	29.21	57°39'11"	95°39'49"
Seal River below Great Is.	06GD001	1955-1996, 2000-2003, 2005, 2007, 2009	49	48,200	366.59	58°53'28"	96°16'36"

914 *Slightly regulated.
915 **Two nearby gauge records merged by drainage area ratio.

916

Table 2. Five regulated flow river discharge records from the Prairie Provinces, including Water Survey of Canada gauge names, station codes, period of record, number of years of record analyzed, effective drainage area, mean daily flow and location. Records ordered by province from west to east, and within province by south to north.

Station name	WSC station code	Period of record	# yrs	Drainage area (km^2)	Mean daily flow (m^3/s)	Latitude (N)	Longitude (W)
S. Saskatchewan River at Medicine Hat	05AJ001	1912-2010	99	41,400	186.73	50°02'31"	110°40'39"
Red Deer River at Red Deer	05CC002	1912-2010	99	11,100	47.48	52°16'34"	113°49'02"
N. Saskatchewan River at Edmonton	05DF001	1912-2010	99	27,100	209.15	53°32'13"	113°29'07"
N. Saskatchewan River at Prince Albert	05GG001	1912-2010	99	72,300	238.05	53°12'12"	105°46'19"
Saskatchewan River at The Pas	05KJ001	1913-2010	98	389,000	622.77	53°50'17"	101°12'31"

Table 3. Classification of years into strong positive and negative climate oscillation events for the Pacific Decadal Oscillation (PDO), North Pacific Index (NPI), Southern Oscillation Index (SOI), Pacific North American mode (PNA) and Arctic Oscillation (AO) (see section 2 for full definitions).

Climate Oscillation	Phase	Strong event years
PDO	positive	1905, 1906, 1908, 1909, 1922, 1924, 1927, 1931, 1935, 1936, 1937, 1940, 1941, 1942, 1970, 1977, 1981, 1983-1988, 1994, 1998, 2003
	negative	1917, 1918, 1946, 1949, 1950, 1951, 1952, 1954, 1956, 1957, 1962, 1964, 1965, 1969, 1971, 1972, 1974, 1976, 1991, 2000, 2008, 2009
NPI	low	1900, 1926, 1931, 1934, 1936, 1940, 1941, 1945, 1961, 1963, 1970, 1977, 1978, 1981, 1983, 1984, 1986, 1987, 1992, 1998, 2001, 2003, 2010
	high	1903, 1904, 1907, 1908, 1910, 1911, 1916, 1917, 1920, 1922, 1932, 1937, 1943, 1948, 1951, 1952, 1955, 1956, 1966, 1971, 1972, 1989, 1991, 2009, 2011
SOI	negative El Niño	1902, 1904, 1905, 1911, 1912, 1913, 1914, 1918, 1919, 1923, 1925, 1932, 1939, 1940, 1941, 1944, 1946, 1951, 1953, 1957, 1963, 1965, 1969, 1972, 1976, 1977, 1982, 1987, 1991, 1992, 1993, 1994, 1997, 2002, 2004, 2006, 2009
	positive La Niña	1906, 1908, 1909, 1910, 1915, 1916, 1917, 1921, 1924, 1938, 1945, 1947, 1950, 1955, 1956, 1964, 1970, 1971, 1973, 1974, 1975, 1988, 1996, 1998, 2000, 2008
PNA	positive	1953, 1961, 1964, 1970, 1977, 1981, 1983, 1986, 1987, 1988, 1992, 1995, 1998, 2001, 2003, 2004, 2007, 2010
	negative	1950, 1951, 1952, 1955, 1956, 1957, 1965, 1966, 1969, 1971, 1972, 1979, 1982, 1990, 2009
AO	positive	1903,1905, 1907, 1913, 1914, 1920, 1925, 1943, 1948, 1949, 1973, 1975, 1976, 1989, 1990, 1992, 1993, 1995, 1997, 2000, 2002, 2007, 2008
	negative	1900, 1915, 1919, 1931, 1936, 1940, 1941, 1942, 1947, 1951, 1955, 1956, 1958, 1960, 1966, 1969, 1970, 1977, 1979, 1985, 1987, 1996, 2006, 2010

931

932

933 List of Figures

934 Figure 1. Eighty-six naturally-flowing streamflow records (red squares) and five regulated gauge
935 records (purple circles) from the Canadian Prairie Provinces used in this study. A Lambert equal
936 area projection was used.
937
938 Figure 2. (A) Histogram of the 86 Canadian Prairie Provinces naturally-flowing streamflow
939 record lengths (years) from Table 1. (B) Histogram of the drainage areas (km^2) of the 86
940 naturally-flowing streams. The *x*-axis numbers list the potentially largest number in that bin.
941
942 Figure 3. Plots of the November-March Pacific Decadal Oscillation (PDO), negative November-
943 March North Pacific Index (NPI), negative June-November Southern Oscillation Index (SOI),
944 December-February Pacific North American mode (PNA) and December-March Arctic
945 Oscillation (AO) for 1900-2010. The red dotted lines mark the strong positive and strong
946 negative climate oscillation events (see Table 2 and section 2 for details).
947
948 Figure 4. (A) Pearson's (*r*) correlation plot between same year winter (November-March) mean
949 Pacific Decadal Oscillation (PDO) and concurrent Prairie Provinces' precipitation for 1950-
950 2005. (B) Fingerprints of the PDO on 86 Prairie naturally-flowing mean daily discharges as
951 assessed by a Monte Carlo permutation *t*-test at the *0.10* significance level. (or) denotes a
952 significant two-sample *t*-test; (or) denotes a significant one-sample *t*-test of streamflows
953 occurring during strong positive PDO events against the remaining streamflows; (or)
954 denotes a significant one-sample *t*-test of streamflows occurring during strong negative PDO
955 events against the remaining streamflows; overlap to make all possible combinations.
956
957 Figure 5. (A) Pearson's (*r*) correlation plot between same year winter (November-March) mean
958 North Pacific Index (NPI) and concurrent Prairie Provinces' precipitation for 1950-2005. (B)
959 Fingerprints of the NPI on 86 Prairie naturally-flowing mean daily discharges as assessed by
960 Monte Carlo permutation *t*-tests at the *0.10* significance level. (or) denotes a significant two-
961 sample *t*-test; (or) denotes a significant one-sample *t*-test of streamflows occurring during
962 strong low NPI events against the remaining streamflows; (or) denotes a significant one-

963 sample *t*-test of streamflows occurring during strong high NPI events against the remaining
964 streamflows; overlap to make all possible combinations.
965
966 Figure 6. (A) Pearson's (*r*) correlation plot between June-November mean Southern Ocean
967 Index (SOI) and following year winter (December-March) Prairie Provinces' precipitation for
968 1950-2005. (B) Fingerprints of the SOI on Prairie naturally-flowing mean daily discharges as
969 assessed by a Monte Carlo permutation *t*-test at the *0.10* significance level. (or) denotes a
970 significant two-sample *t*-test; (or) denotes a significant one-sample *t*-test of streamflows
971 occurring during strong -SOI (El Niño) events against the remaining streamflows; (or)
972 denotes a significant one-sample *t*-test of streamflows occurring during strong +SOI (La Niña)
973 events against the remaining streamflows; overlap to make all possible combinations.
974
975 Figure 7. (A) Pearson's (*r*) correlation plot between same year winter (December-February)
976 mean Pacific North American mode (PNA) and concurrent Prairie Provinces' precipitation for
977 1950-2005. (B) Fingerprints of the PNA on 86 Prairie naturally-flowing mean daily discharges as
978 assessed by a Monte Carlo permutation *t*-test at the *0.10* significance level. (or) denotes a
979 significant two-sample *t*-test; (or) denotes a significant one-sample *t*-test of streamflows
980 occurring during strong positive PNA events against the remaining streamflows; (or)
981 denotes a significant one-sample *t*-test of streamflows occurring during strong negative PNA
982 events against the remaining streamflows; overlap to make all possible combinations.
983
984 Figure 8. (A) Pearson's (*r*) correlation plot between same year winter (December-March) mean
985 Arctic Oscillation (AO) and concurrent Prairie Provinces' precipitation for 1950-2005. (B)
986 Fingerprints of the AO on Prairie naturally-flowing mean daily discharges as assessed by a
987 Monte Carlo permutation *t*-test at the *0.10* significance level. (or) denotes a significant two-
988 sample *t*-test; (or) denotes a significant one-sample *t*-test of streamflows occurring during
989 strong positive AO events against the remaining streamflows; (or) denotes a significant one-
990 sample *t*-test of streamflows occurring during strong negative AO events against the remaining
991 streamflows; overlap to make all possible combinations.
992

Figure 9. Mean probabilities and standard deviations of two successive years of least quartile and highest quartile flows composited according to Pacific Decadal Oscillation (PDO) phase with standard deviations for the 25 records from the Saskatchewan River Basin. Also shown are the *p*-values from the paired permutation *t*-tests determining the significance of the mean basin-wide difference between the probability of two successive years of least (highest) quartile flow in a given river during the positive PDO phase versus the probability of two successive years of least (highest) quartile flow in the same river during the negative PDO phase.

Figure 10. Geographic pattern of trends in 86 naturally-flowing mean daily streamflow records from the Canadian Prairie Provinces as assessed by a modified Mann-Kendall test. Also shown for context are trend test results from five regulated mean daily streamflow records (see section 3 for details). A red down (blue up) arrow denotes a decreasing (increasing) trend. A purple core in an arrow or square denotes the results from a regulated gauge.

1008

1009 Appendix Table A.1. Further information on the 86 naturally-flowing and 5 regulated flow river
1010 discharge records from the Prairie Provinces, including whether or not the gauge record is in the
1011 Reference Hydrometric Basin Network (RHBN) (Harvey et al., 1999), season of flow used for
1012 analysis, and coefficient of variation (C.V.).

Station name	RHBN	Season analyzed	C.V. (%)
Sage Creek	yes	Mar.-Oct.	95.8
Waterton River	yes	Jan.-Dec.	22.7
Rolph Creek	no	Mar.-Oct.	87.2
Manyberries Creek	no	Mar.-Oct.	85.2
Pincher Creek	no	Mar.-Oct.	59.2
Prairie Blood Coulee	no	Mar.-Oct.	138.7
Trout Creek	no	Mar.-Oct.	108.8
Blood Indian Creek	no	Mar.-Oct.	201.0
Jumpingpound Creek	no	Mar.-Oct.	56.7
Bow River at Banff	yes	Jan.-Dec.	13.5
Rosebud River	no	Mar.-Oct.	114.9
Mistaya River	yes	Jan.-Dec.	9.0
Threehills Creek	no	Mar.-Oct.	83.7
Prairie Creek	no	Jan.-Dec.	37.5
Bigknife Creek	no	Mar.-Oct.	112.4
Buffalo Creek	no	Mar.-Oct.	68.6
Athabasca River at Hinton	no	Jan.-Dec.	12.3
McLeod River	no	Jan.-Dec.	31.5
Pembina River	no	Jan.-Dec.	42.4
Waskatenau Creek	no	Mar.-Oct.	148.7
Beaver River at Cold Lake Reserve	no	Jan.-Dec.	75.7
Athabasca River at Athabasca	no	May-Oct.	55.4
Little Smoky River	no	Jan.-Dec.	44.0
Saddle River	no	Mar.-Oct.	71.8
Smoky River	no	Jan.-Dec.	26.3
Pine River	yes	Jan.-Dec.	19.2
Heart River	no	Mar.-Oct.	84.1
Clearwater River	yes	Jan.-Dec.	28.1
Athabasca River	no	Jan.-Dec.	21.9
Notikewin River	no	Jan.-Dec.	48.3
Birch River	yes	Mar.-Oct.	49.5
Richardson River	yes	Mar.-Oct.	11.3
Boyer River	no	Mar.-Oct.	96.6
Ponton River	no	Mar.-Oct.	36.9
Sousa Creek	no	Mar.-Oct.	66.0
Chinchaga River	no	Jan.-Dec.	50.2
Hay River	yes	Jan.-Dec.	46.5
Rock Creek	no	Mar.-Oct.	79.4

Poplar River	no	Mar.-Oct.	83.1
Long Creek	no	Jan.-Dec.	112.4
Lyons Creek	yes	Mar.-Oct.	157.7
Lightning Creek	yes	Mar.-Oct.	156.8
Antler River near Wauchope	yes	Mar.-Oct.	168.9
Notukeu Creek	yes	Mar.-Oct.	84.4
Swift Current Creek	no	Mar.-Oct.	56.1
Bridge Creek	no	Mar.-Oct.	118.8
Cottonwood Creek	no	Mar.-Oct.	141.7
Stony Creek	no	Mar.-Oct.	72.4
Opuntia Lake West Inflow	no	Mar.-Oct.	116.3
Maloneck Creek	yes	Mar.-Oct.	76.2
Quill Creek	no	Mar.-Oct.	107.9
Lilian River	no	Mar.-Oct.	84.0
Red Deer River near Erwood	no	Mar.-Oct.	85.4
Overflowing River near Hudson Bay	yes	Mar.-Oct.	66.6
Sturgeon River	no	Mar.-Oct.	81.7
Shell Brook	no	Mar.-Oct.	88.0
Carrot River	no	Mar.-Oct.	82.1
Beaver River near Dorintosh	no	Mar.-Oct.	75.4
Churchill River	yes	Jan.-Dec.	38.3
Haultain River	yes	Jan.-Dec.	26.8
Gelkie River	yes	Jan.-Dec.	22.4
Waterfound River	no	Jan.-Dec.	14.5
MacFarlane River	no	Jan.-Dec.	15.9
Fond du Lac River	yes	Jan.-Dec.	16.9
Mowbray Creek	no	Mar.-Oct.	97.1
Antler River near Melita	yes	Mar.-Oct.	130.4
Graham Creek	no	Mar.-Oct.	192.9
Shannon Creek	yes	Mar.-Oct.	89.1
S. Tobacco Creek	yes	Mar.-Oct.	67.3
Whitemouth River	no	Jan.-Dec.	54.7
Brokenhead River	yes	Mar.-Oct.	73.3
Little Saskatchewan River	no	Mar.-Oct.	61.1
Pelican Creek S. Tributary	yes	Mar.-Oct.	65.4
Shell River	no	Jan.-Dec.	43.9
Icelandic River	no	Mar.-Oct.	78.3
Ochre River	yes	Mar.-Oct.	46.9
Fisher River	no	Jan.-Dec.	77.6
Waterhen River	yes	Jan.-Dec.	53.7
Pigeon River	no	Jan.-Dec.	34.9
Overflowing River at Overflowing River	yes	Mar.-Oct.	60.0
Island Lake River	no	Jan.-Dec.	28.8
Gods River	no	Jan.-Dec.	26.2
Grass River	yes	Jan.-Dec.	37.0

Kettle River	no	Jan.-Dec.	40.5
Little Beaver River	yes	Jan.-Dec.	36.0
Seal River	yes	Jan.-Dec.	22.9
S. Saskatchewan River at Medicine Hat	no	Jan.-Dec.	38.4
Red Deer River at Red Deer	no	Jan.-Dec.	42.3
N. Saskatchewan River at Edmonton	no	Jan.-Dec.	22.7
N. Saskatchewan River at Prince Albert	no	Jan.-Dec.	24.7
Saskatchewan River at The Pas	no	Jan.-Dec.	29.5

1013

Appendix Table A.2. Empirical probabilities of two successive years of least quartile and highest quartile flows composited according to Pacific Decadal Oscillation (PDO) phase for the Saskatchewan River and its tributaries in Alberta, Saskatchewan and Manitoba.

Streamflow record [WSC or USGS code]	Prob. 2 successive yrs least 1/4 flow in +PDO phase	Prob. 2 successive yrs least 1/4 flow in –PDO phase	Prob. 2 successive yrs highest 1/4 flow in +PDO phase	Prob. 2 successive yrs highest 1/4 flow in -PDO phase
Marias R. near Shelby, MT [06099500]	0.157	0.000	0.020	0.146
Waterton R. near Waterton Park [05AD003]	0.118	0.000	0.039	0.122
Castle R. near Beaver Mines [05AA022]	0.097	0.034	0.000	0.138
Oldman R. near Waldron's Corner[05AA023]	0.167	0.000	0.033	0.077
Highwood R. at Diebel's Ranch [05BL019]	0.194	0.000	0.033	0.042
Bow R. at Banff [05BB001]	0.115	0.000	0.078	0.071
Columbia R. at Nicholson, BC [08NA002]	0.118	0.000	0.059	0.056
Red Deer R. at Red Deer [05CC002]	0.098	0.122	0.039	0.171
Naturalized St. Mary R. at Int. Boundary	0.133	0.000	0.044	0.098
Actual St. Mary R. at Int. Boundary [05AE027]	0.157	0.020	0.020	0.160
Naturalized Belly R. near Mountain View	0.111	0.000	0.022	0.146
Actual Belly R. near Mountain View [05AD005]	0.098	0.000	0.039	0.122
Naturalized Oldman R. near Lethbridge	0.200	0.000	0.067	0.146
Actual Oldman R. near Lethbridge [05AD007]	0.196	0.000	0.020	0.146
Naturalized S. Saskatchewan R. at Medicine Hat	0.200	0.000	0.022	0.171
Actual S. Saskatchewan R. at Medicine Hat [05AJ001]	0.196	0.000	0.020	0.171

Naturalized Elbow R. below Glenmore Dam	0.200	0.000	0.044	0.146
Actual Elbow R. below Glenmore Dam [05BJ001]	0.176	0.048	0.059	0.190
Naturalized Bow R. at Calgary	0.178	0.000	0.044	0.195
Actual Bow R. at Calgary [05BH004]	0.176	0.024	0.039	0.195
Naturalized Spray R. at Banff	0.133	0.000	0.067	0.122
Naturalized N. Saskatchewan R. at Edmonton	0.118	0.024	0.098	0.119
Actual N. Saskatchewan R. at Edmonton [05DF001]	0.118	0.024	0.078	0.122
Actual N. Saskatchewan R. at Prince Albert, SK [05GG001]	0.137	0.049	0.039	0.122
Actual Saskatchewan R. at the Pas, MB [05KJ001]	0.137	0.025	0.059	0.175
Mean	0.149	0.015	0.043	0.135

016
017

Appendix Table A.3. Modified Mann-Kendall (MK) trend tests on Canadian Prairie provinces mean daily river records. All available data were analyzed, even if discontinuous. The coefficients from the Sen-Theil lines are $\widehat{\beta_0}$ (the intercept) and $\widehat{\beta_1}$ (the slope), where time is calendar year; *Total change* (%) is (*Mean Δ/yr* * length of the entire period of record); *Mean Δ/yr* (%) is $100*\beta_1/mean(Q)$; r_1 is the sample lag-one autocorrelation coefficient from the detrended time series; *Z* is the modified Mann-Kendall z-score; *p*-level is the result of the two-tailed modified MK test on |*Z*| at the *0.1* significance level (bold denotes a significant trend).

Station name	$\widehat{\beta_0}$	$\widehat{\beta_1}$	*Total change(%)*	*Mean Δ/yr(%)*	r_1 **significant*	*CF*	*Z*	*p*-level	Significant trend
Naturally-flowing records									
Sage Creek	6.82	-0.0033	-72.4	-0.95	-0.054	0.898	-2.868	0.004	decreasing
Waterton River	48.04	-0.016	-8.8	-0.09	0.079	1.169	-0.929	0.353	no
Rolph Creek	1.77	-0.00077	-16.5	-0.22	0.232*	1.595	-0.500	0.617	no
Manyberries Creek	4.85	-0.0023	-72.7	-0.74	0.058	1.122	-2.540	0.011	decreasing
Pincher Creek	9.17	-0.0039	-23.3	-0.25	-0.070	0.871	-1.025	0.305	no
Prairie Blood Coulee	-1.91	0.0010	28.4	0.69	0.036	1.073	0.858	0.391	no
Trout Creek	-20.89	0.011	105.8	1.15	0.090	1.192	1.460	0.144	no
Blood Indian Creek	0.40	-0.00020	-13.1	-0.28	0.070	1.146	-2.680	0.007	decreasing
Jumpingpound Creek	-4.30	0.0033	5.1	0.13	0.046	1.093	0.212	0.832	no
Bow River	147.45	-0.055	-14.1	-0.14	-0.014	0.974	-2.973	0.003	decreasing
Rosebud River	1.26	-0.00052	-6.3	-0.12	0.198	1.481	-0.175	0.861	no
Mistaya River	18.90	-0.0063	-4.4	-0.10	0.042	1.085	-1.010	0.312	no
Threehills Creek	-0.99	0.00058	12.4	0.31	0.092	1.198	0.437	0.662	no
Prairie Creek	-6.74	0.0054	6.0	0.12	-0.032	0.939	0.383	0.702	no
Bigknife Creek	5.06	-0.0025	-40.7	-0.95	0.085	1.181	-0.992	0.321	no
Buffalo Creek	1.48	-0.00064	-10.8	-0.28	0.184	1.438	-0.504	0.614	no
Athabasca River at Hinton	887.67	-0.36	-10.4	-0.21	-0.014	0.974	-1.661	0.097	decreasing
McLeod River	111.79	-0.047	-13.6	-0.24	-0.063	0.884	-1.181	0.238	no
Pembina River	15.96	0.00088	0.4	0.004	0.058	1.121	0.027	0.978	no
Waskatenau Creek	13.75	-0.0069	-104.2	-2.37	0.167	1.389	-3.296	0.001	decreasing
Beaver River Cold Lake	618.72	-0.31	-91.0	-1.65	0.254*	1.663	-2.871	0.004	decreasing
Athabasca River Athabasca	2023.42	-0.69	-10.0	-0.10	0.100	1.218	-1.062	0.288	no
Little Smoky River	899.51	-0.43	-47.1	-0.92	0.134	1.302	-2.214	0.027	decreasing
Saddle River	35.49	-0.017	-52.3	-1.19	0.077	1.163	-1.585	0.113	no
Smoky River	2998.02	-1.35	-37.8	-0.40	0.022	1.043	-2.398	0.016	decreasing
Pine River	1333.66	-0.58	-14.1	-0.31	-0.111	0.805	-1.320	0.187	no

Heart River	153.23	-0.075	-81.6	-1.70	0.125	1.279	-1.784	0.074	decreasing
Clearwater River	1064.68	-0.48	-20.8	-0.40	0.324*	1.930	-1.335	0.182	no
Athabasca River McMurray	7903.96	-3.68	-30.9	-0.59	0.297*	1.823	-2.309	0.021	decreasing
Notikewin River	245.22	-0.12	-43.4	-0.88	0.122	1.272	-1.705	0.044	decreasing
Birch River	357.48	-0.16	-15.2	-0.35	0.322*	1.919	-0.468	0.639	no
Richardson River	-45.83	0.032	7.3	0.18	0.242	1.618	0.797	0.797	no
Boyer River	13.47	-0.0051	-5.2	-0.11	0.049	1.101	-0.093	0.926	no
Ponton River	3.87	0.0056	1.8	0.04	0.395*	2.260	0.053	0.958	no
Sousa Creek	11.02	-0.0045	-7.5	-0.19	0.161	1.371	-0.169	0.866	no
Chinchaga River	249.40	-0.11	-16.0	-0.39	-0.043	0.920	-0.703	0.482	no
Hay River	-1732.05	0.92	37.6	0.80	0.341*	2.002	1.257	0.209	no
Rock Creek	13.24	-0.0064	-79.6	-0.84	-0.054	0.899	-2.860	0.004	decreasing
Poplar River	4.62	-0.0021	-24.8	-0.31	0.086	1.185	-1.057	0.290	no
Long Creek	0.66	-0.00011	-1.5	-0.02	0.097	1.213	-0.047	0.963	no
Lyons Creek	0.99	-0.00048	-46.5	-0.55	-0.042	0.920	-2.797	0.005	decreasing
Lightning Creek	0.45	-0.00017	-2.0	-0.05	0.244	1.622	-0.349	0.727	no
Antler River Wauchope	1.87	-0.00092	-31.0	-0.67	0.297*	1.819	-1.320	0.187	no
Notukeu Creek	-2.73	0.0015	28.4	0.79	-0.160	0.731	0.972	0.331	no
Swift Current Creek	11.15	-0.0050	-21.2	-0.38	-0.077	0.860	-0.800	0.424	no
Bridge Creek	1.26	-0.00061	-45.2	-0.48	0.078	1.165	-1.439	0.150	no
Cottonwood Creek	2.45	-0.0012	-13.0	-0.35	0.146	1.331	-0.601	0.548	no
Stony Creek	-6.48	0.0034	43.3	1.08	-0.137	0.764	1.586	0.113	no
Opuntia Lake West Inflow	0.50	-0.00024	-35.6	-0.70	0.250*	1.649	-1.088	0.277	no
Maloneck Creek	-9.36	0.0049	36.6	0.99	0.302*	1.832	0.551	0.582	no
Quill Creek	-9.40	0.0048	54.2	1.43	0.243	1.620	0.948	0.343	no
Lilian River	2.96	-0.0013	-12.6	-0.31	0.163	1.377	-0.316	0.752	no
Red Deer River near Erwood	184.96	-0.084	-20.0	-0.35	0.378*	2.182	-0.461	0.645	no
Overflowing River	-59.29	0.030	59.7	1.66	0.116	1.254	1.521	0.128	no
Sturgeon River	-17.95	0.010	13.8	0.3	0.397*	2.268	0.369	0.712	no
Shell Brook	-9.96	0.0049	18.1	0.4	0.324*	1.926	0.388	0.698	no
Carrot River	233.87	-0.11	-38.8	-0.7	0.366*	2.120	-0.830	0.407	no
Beaver River Dorintosh	947.69	-0.47	-77.1	-1.6	0.327*	1.941	-1.882	0.060	decreasing
Churchill River	1724.11	-0.74	-12.5	-0.27	0.618*	4.059	-0.287	0.774	no
Haultain River	-94.39	0.057	12.9	0.31	0.343*	2.002	0.502	0.615	no
Gelkie River	205.04	-0.081	-7.9	-0.18	0.517*	3.041	-0.418	0.676	no

Waterfound River	75.98	-0.028	-4.7	-0.13	0.195	1.468	-0.223	0.824	no
MacFarlane River	24.29	0.014	1.1	0.03	0.435*	2.476	0.080	0.936	no
Fond du Lac River	-487.16	0.40	8.4	0.13	0.382*	2.201	0.740	0.460	no
Mowbray Creek	-28.32	0.014	117.5	2.40	0.288*	1.787	2.250	0.024	increasing
Antler River Melita	13.22	-0.0063	-37.5	-0.55	0.222*	1.561	-1.471	0.141	no
Graham Creek	1.54	-0.00075	-34.7	-0.51	0.181	1.433	-1.410	0.159	no
Shannon Creek	-23.24	0.012	47.9	0.94	0.179	1.425	1.157	0.247	no
S. Tobacco Creek	-0.74	0.00049	9.5	0.20	0.134	1.303	0.273	0.785	no
Whitemouth River	-271.47	0.14	52.4	0.97	0.303*	1.847	1.493	0.135	no
Brokenhead River	-94.39	0.050	42.2	0.77	0.233	1.593	1.081	0.280	no
Little Saskatchewan River	-31.43	0.018	32.0	0.33	0.211	1.525	1.078	0.281	no
Pelican Creek S. Tributary	-1.07	0.00055	48.3	1.31	0.124	1.274	1.170	0.242	no
Shell River	-67.51	0.036	61.9	1.15	0.250*	1.652	2.485	0.013	increasing
Icelandic River	36.72	-0.018	-35.5	-0.68	0.053	1.110	-1.102	0.270	no
Ochre River	-8.97	0.0056	14.3	0.26	0.213	1.530	0.493	0.622	no
Fisher River	22.52	-0.011	-20.5	-0.59	0.091	1.194	-0.494	0.621	no
Waterhen River	-72.27	0.077	5.5	0.09	0.734*	6.169	0.089	0.929	no
Pigeon River	-1237.81	0.67	39.1	0.74	0.164	1.384	1.832	0.067	increasing
Overflowing River	-23.36	0.017	7.5	0.14	0.179	1.426	0.146	0.884	no
Island Lake River	306.16	-0.12	-8.2	-0.13	0.166	1.391	-0.581	0.561	no
God's River	1794.60	-0.84	-31.6	-0.53	0.293*	1.809	-1.881	0.060	decreasing
Grass River	899.40	-0.42	-32.9	-0.65	0.382*	2.196	-1.158	0.247	no
Kettle River	37.68	-0.013	-4.4	-0.10	-0.146	0.750	-0.195	0.846	no
Little Beaver River	-79.80	0.054	6.9	0.19	-0.248	0.611	0.318	0.750	no
Seal River	-3035.64	1.72	25.8	0.47	-0.194	0.680	2.290	0.022	increasing
Regulated-flow records									
S. Saskatchewan River at Medicine Hat	1703.22	-0.78	-41.2	-0.41	0.231*	1.594	-2.486	0.013	decreasing
Red Deer River at Red Deer	193.30	-0.077	-16.0	0.16	0.345*	2.037	-0.839	0.201	no
N. Saskatchewan River at Prince Albert	860.44	-0.32	-13.5	-0.14	0.171*	1.409	-1.286	0.198	no
N. Saskatchewan River at Edmonton	1009.30	-0.41	-19.5	-0.20	0.113	1.253	-2.456	0.014	decreasing
Saskatchewan River at Le Pas	4477.30	-1.98	-31.2	-0.32	0.391*	2.261	-1.962	0.050	decreasing

Figure1

Click here to download high resolution image

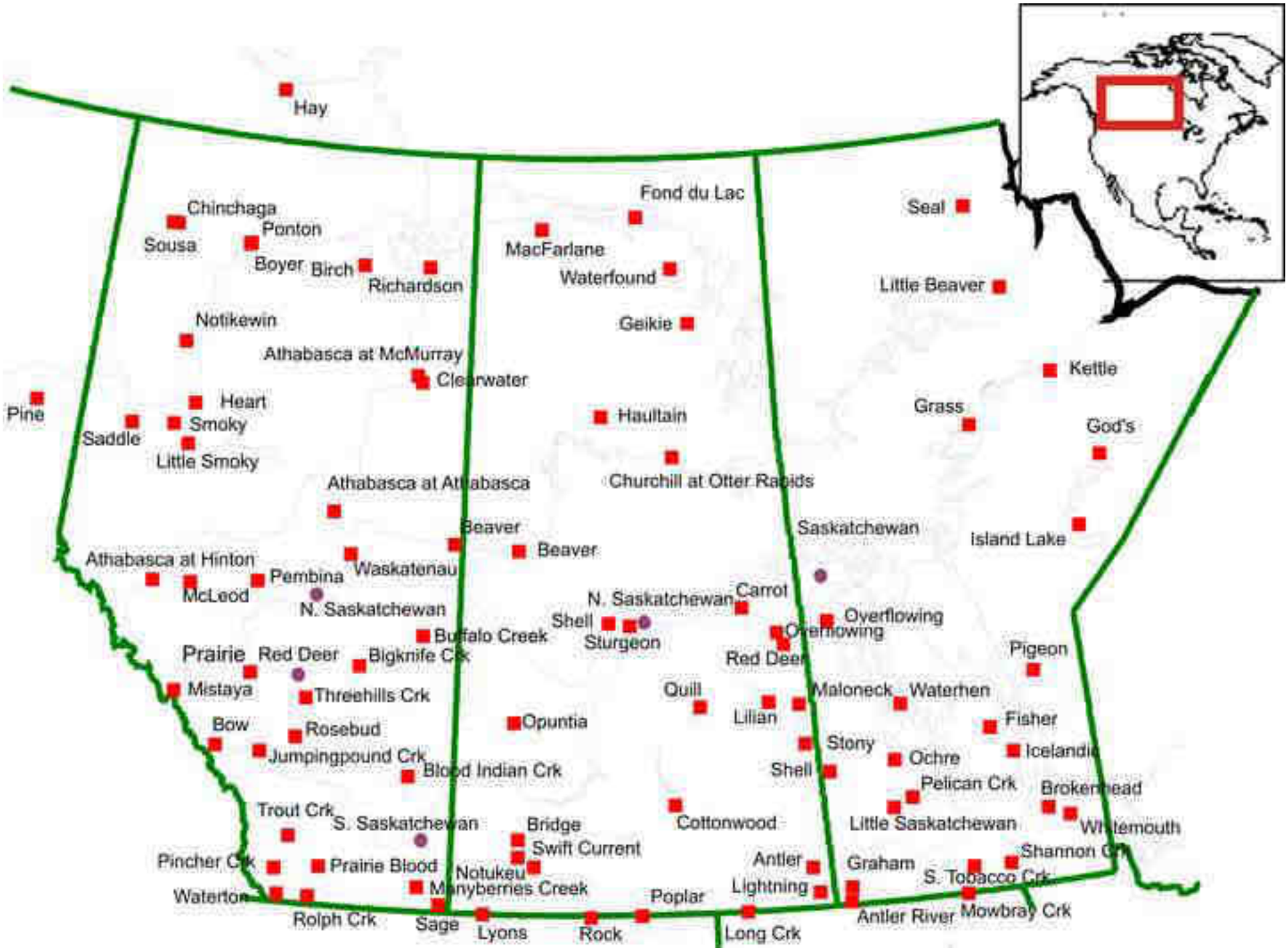

Figure2

Click here to download high resolution image

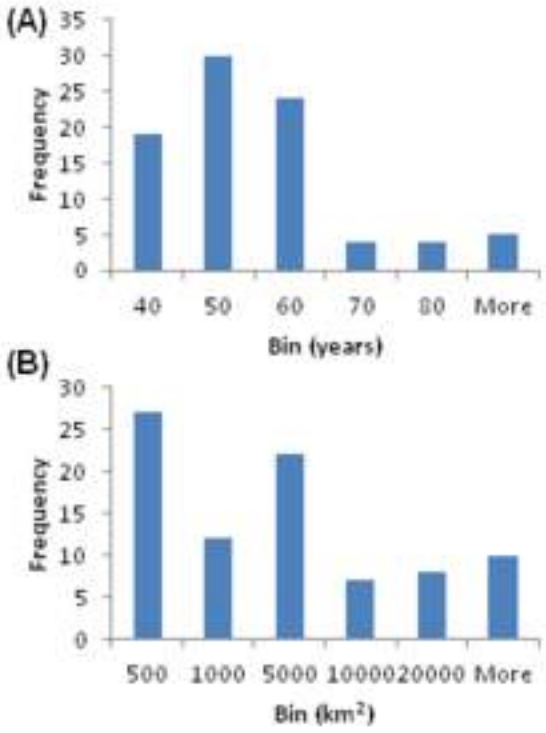

Figure3
Click here to download high resolution image

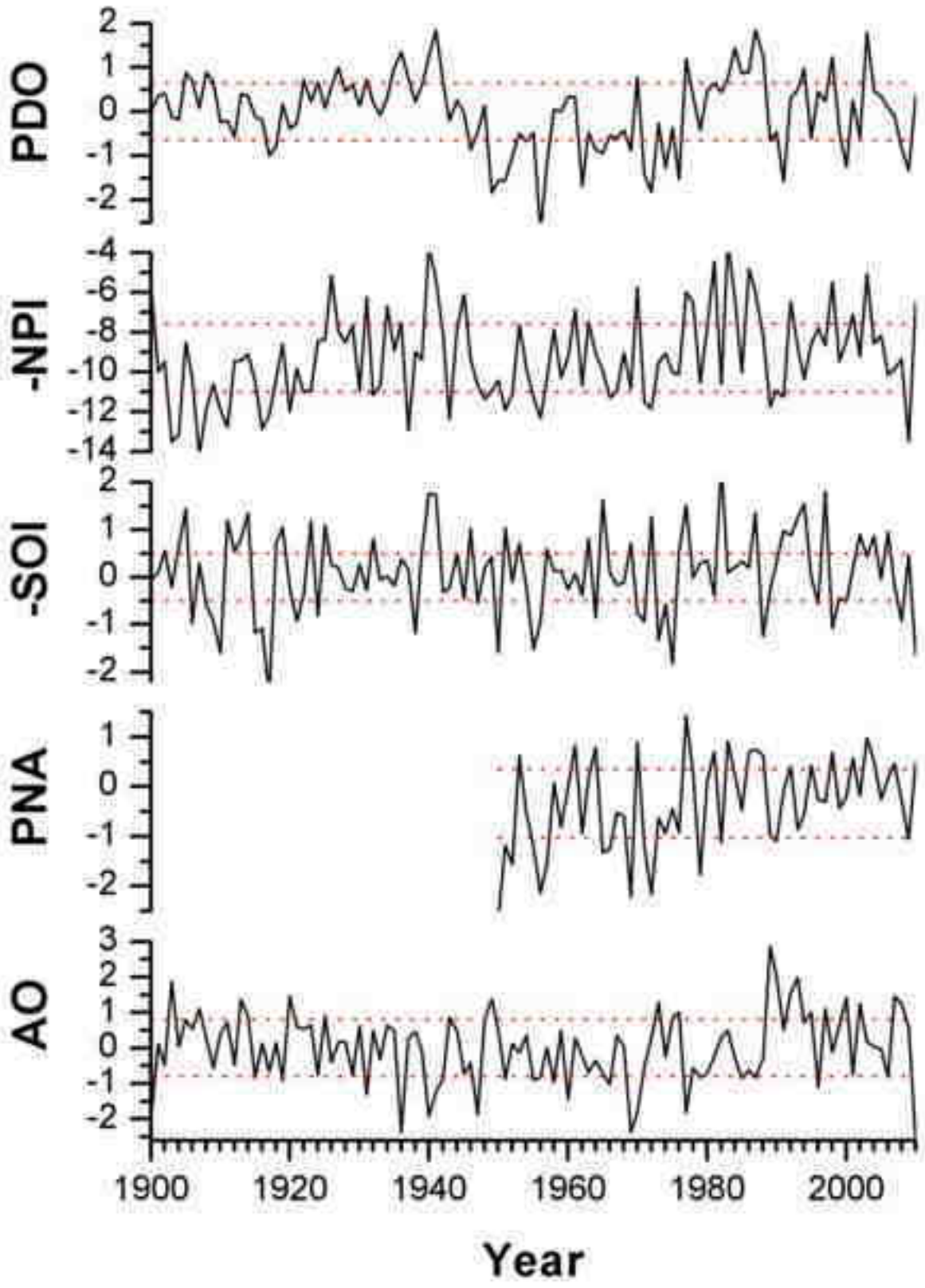

Figure4

Click here to download high resolution image

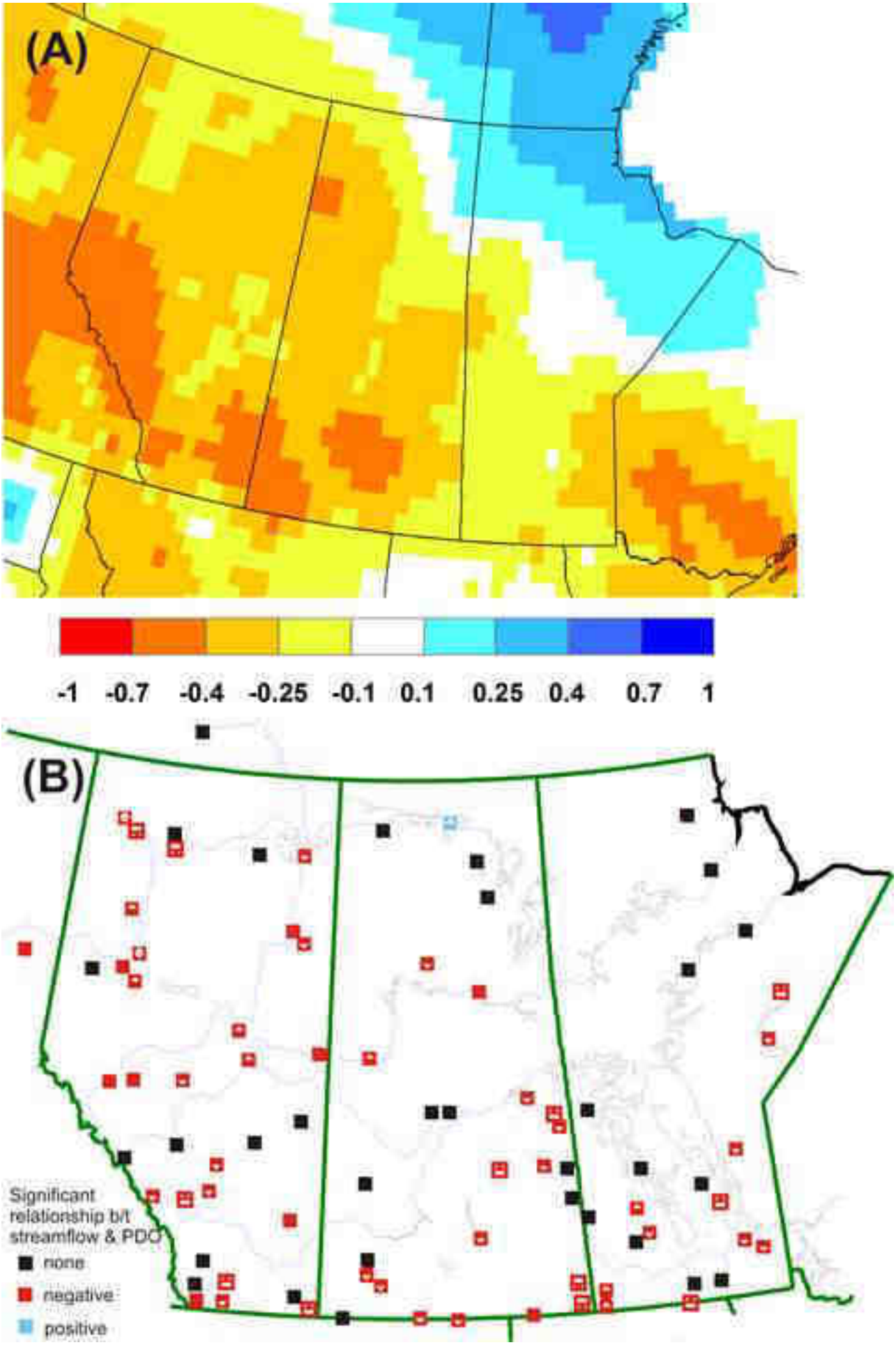

Figure5

Click here to download high resolution image

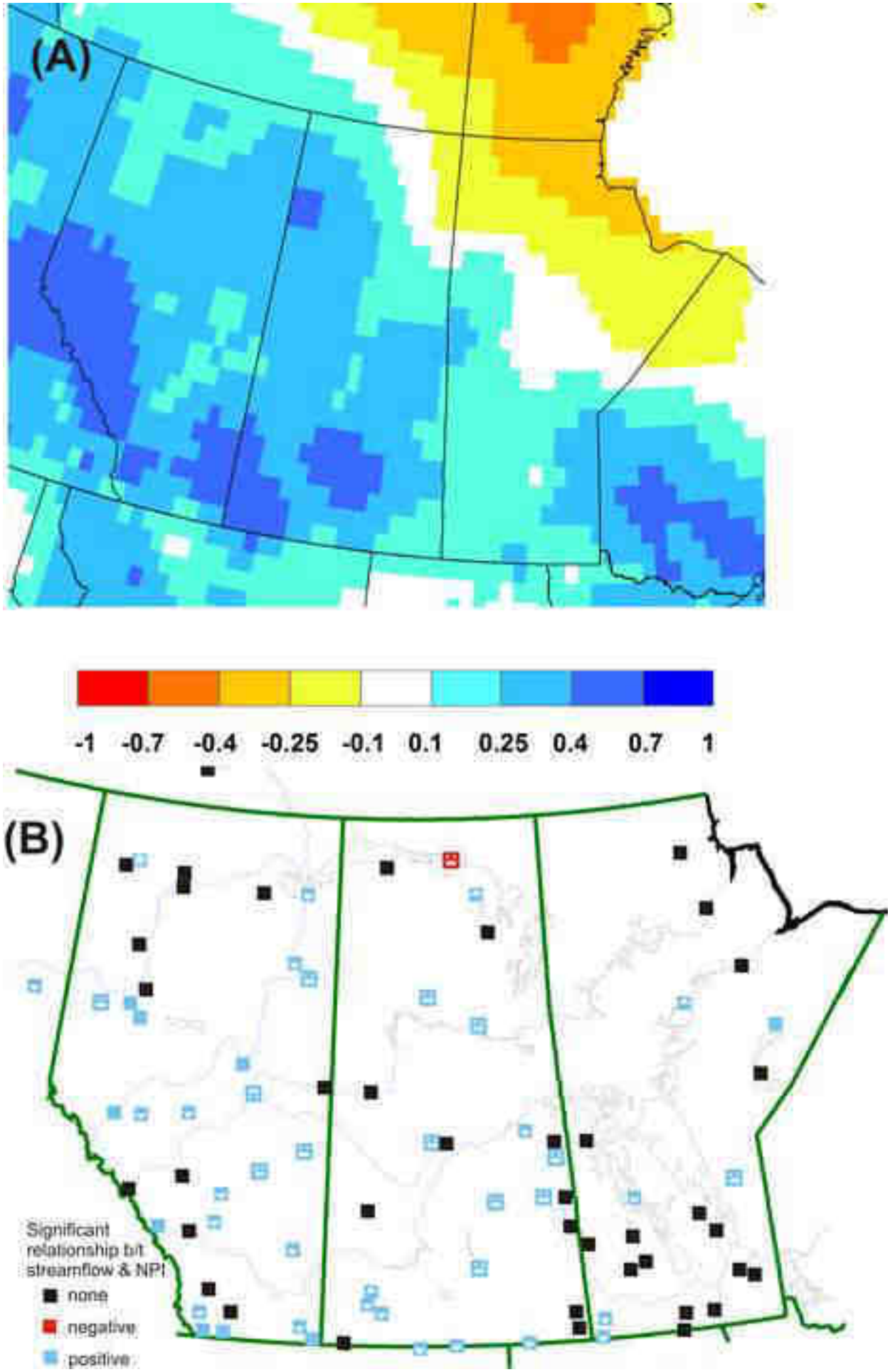

Figure6

Click here to download high resolution image

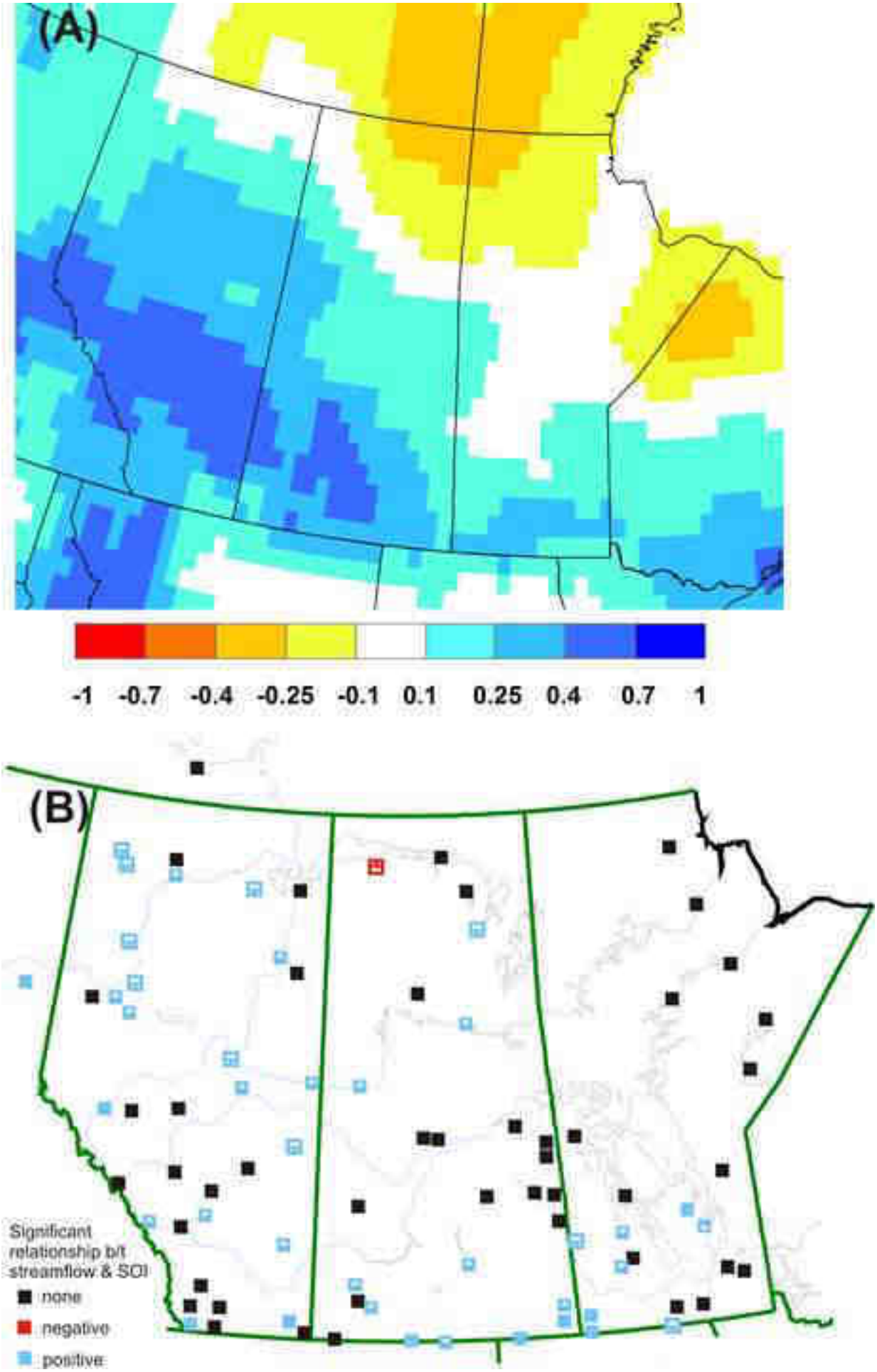

Figure7

Click here to download high resolution image

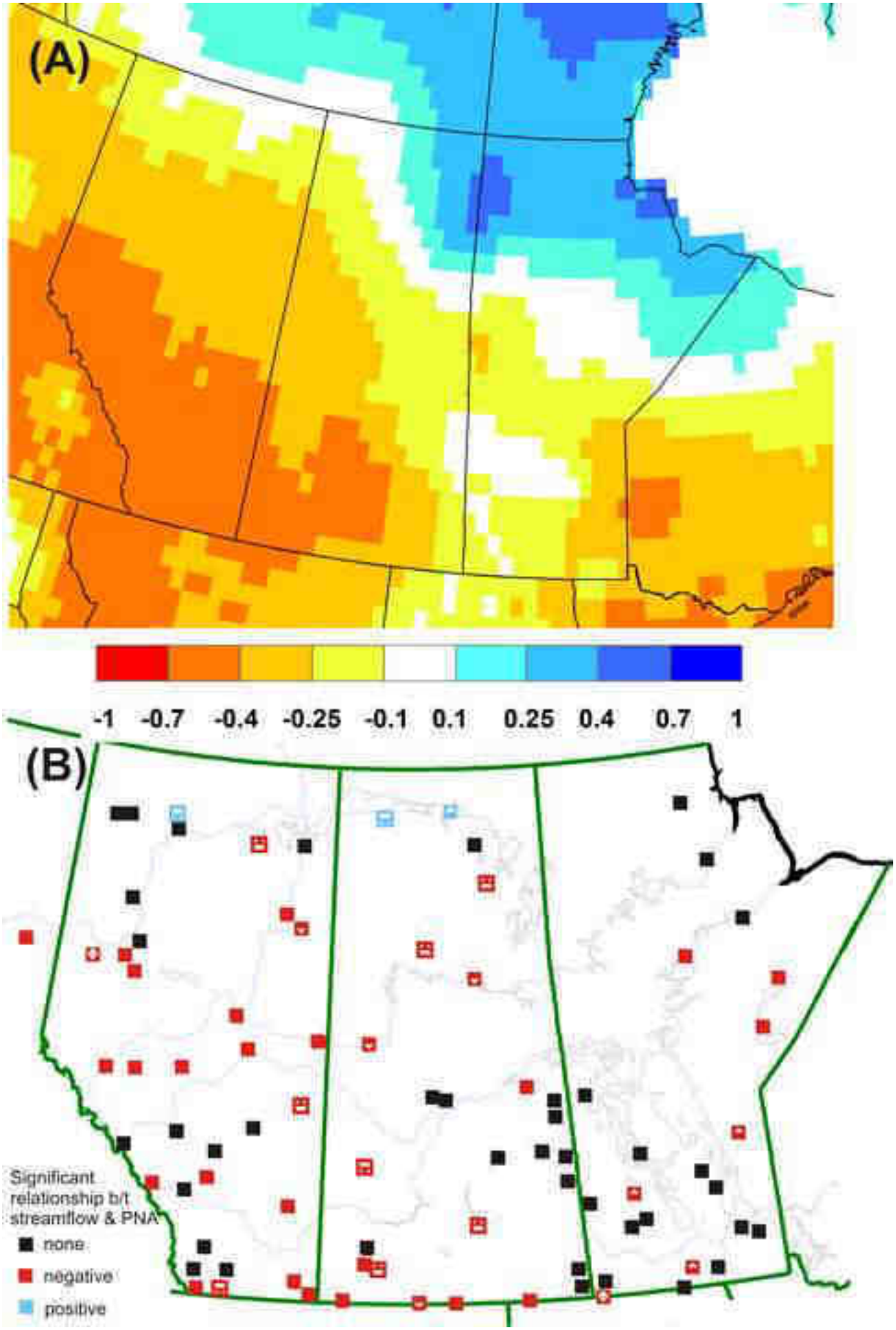

Figure8

Click here to download high resolution image

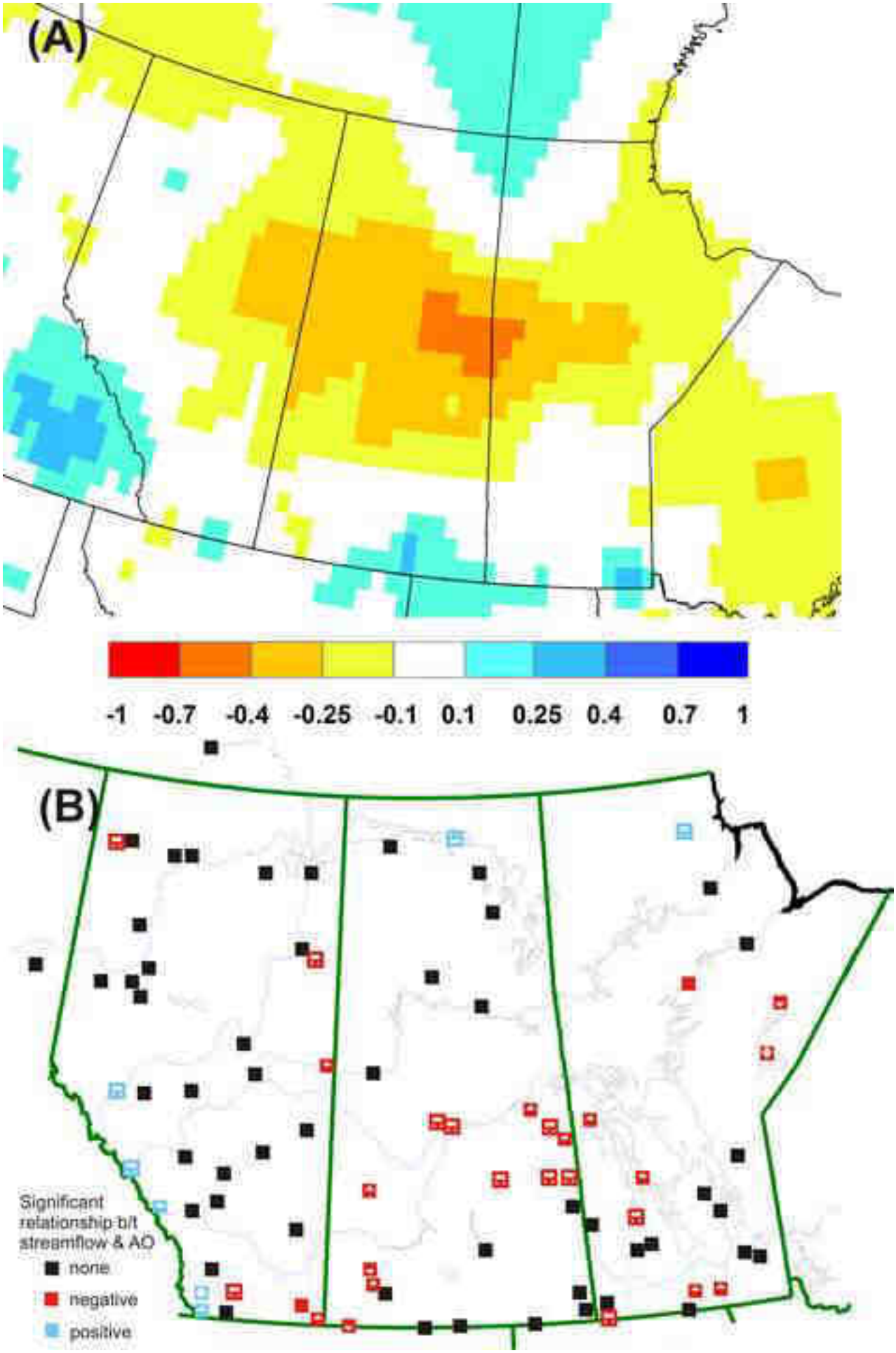

Figure9

Click here to download high resolution image

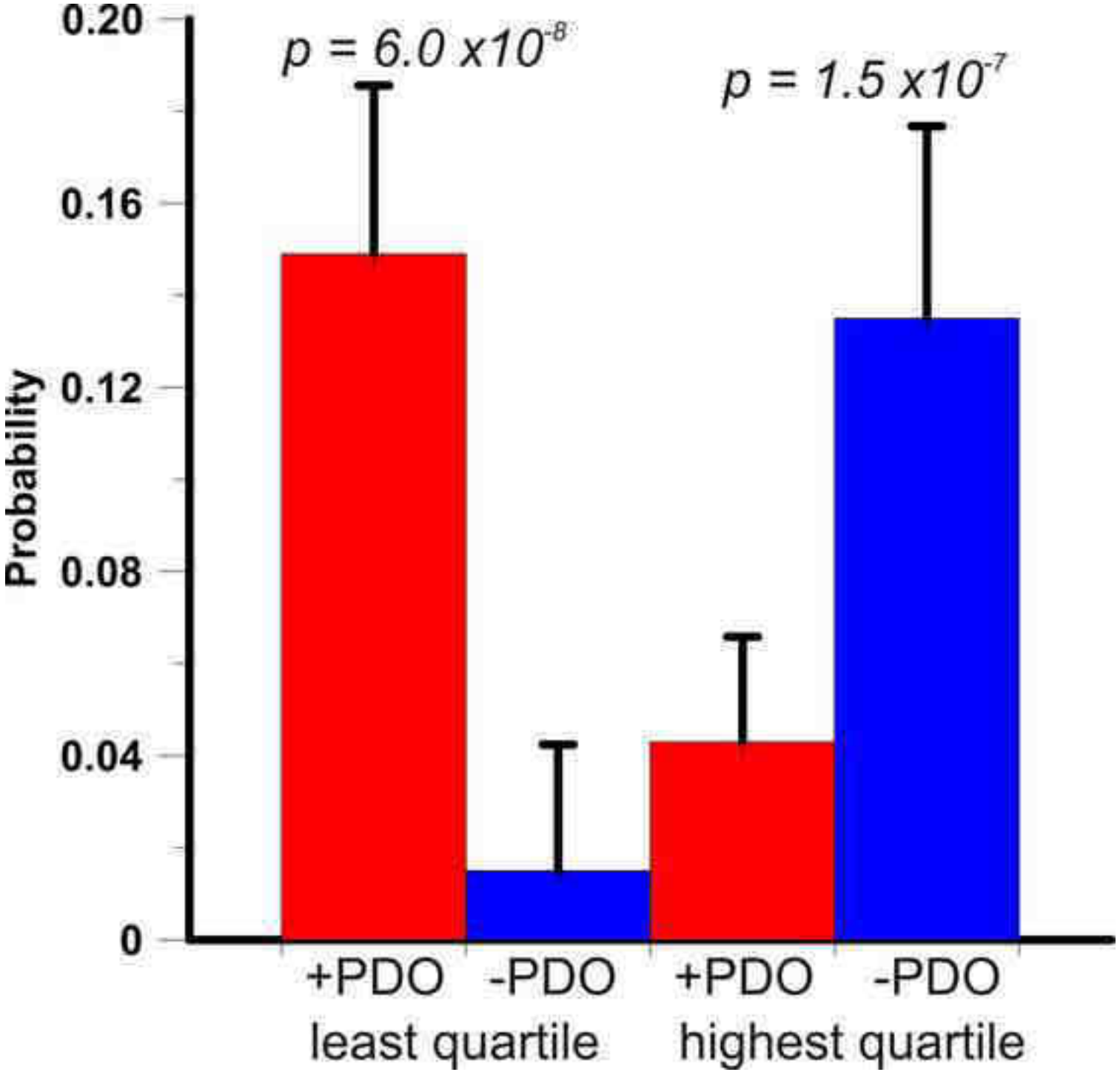

Figure10

Click here to download high resolution image

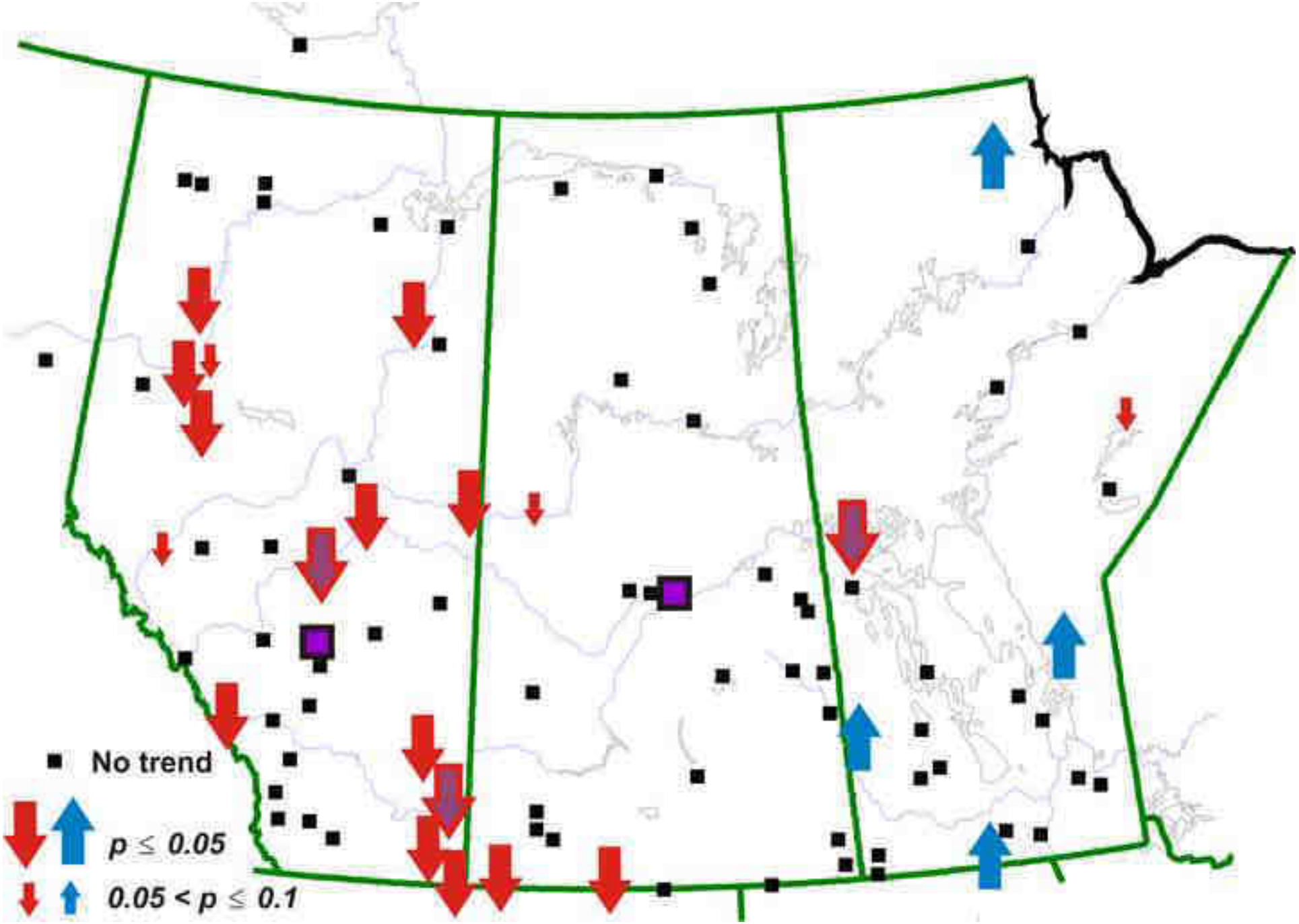

Groundwater levels and teleconnection patterns in the Canadian Prairies

Cesar Perez-Valdivia[*,1], Dave Sauchyn[1,] and Jessica Vanstone[1]

[*] Corresponding author; email: perezvac@uregina.ca; phone: (306) 337-2294
[1] Prairie Adaptation Research Collaborative, University of Regina.
Suite 120-2 Research Dr. Regina, Saskatchewan S4S 7H9

ABSTRACT

ABSTRACT

Thirty one hydrological time series of shallow groundwater levels, precipitation, and moisture-sensitive tree-ring chronologies were analyzed and related to two climate indices: Nino 3.4 and PDO. Spearman rank correlation and spectral analyses (Multi Taper Method, Continuous Wavelet Transform, and Wavelet Coherence) were used to document the influence of El Niño Southern Oscillation (ENSO), and the Pacific Decadal Oscillation (PDO), on shallow (depth < 20 m) groundwater levels records from the Canadian Prairies. Modes of variability in the 2-7, 7-10, and 18-22 year bands were detected and reconstructed. Correlations and wavelet coherence between these oscillation modes and the climate indices suggest that variability in the 2-7 and 7-10 year bands is highly influenced by ENSO. The oscillation modes in the 18-22 year band reflect a strong negative correlation with the PDO index. When either of these teleconnections, (ENSO/PDO), is in their respective positive phases, groundwater levels depict the effect of

associated warmer and drier winters experienced over much of interior Canada and the US, affecting important resource inputs of the hydrological cycle and groundwater recharge.

Keywords: groundwater levels, oscillation modes, correlations, ENSO, PDO,

INTRODUCTION

Global climate variability at interannual to interdecadal scales has been linked to oceanic and atmospheric teleconnection patterns such as the El Niño-Southern Oscillation (ENSO) and the Pacific Decadal Oscillation (PDO)(Rubio-Alvarez and McPhee 2010; Wang et al., 2008 among others). In North America, these large-scale climate oscillations are major drivers of hydroclimate variability, and therefore the understanding of how these teleconnection patterns affect hydroclimatic variables has been a major research focus for the past two decades (Hurrell and van Loon 1997; Bonsal et al. 2001; Enfield et al., 2001; McCabe et al., 2004; and others).

Some coupled sea-surface temperature (SST) and atmospheric teleconnection anomaly patterns recur on a regular basis. ENSO and the PDO (Rasmusson and Carpenter 1982; Shabar *et al.* 1997; Mantua *et al.* 1997; Minobe 1997; Bonsal *et al.* 2001; Coulibaly and Burn 2004; MacDonald and Case 2005; Fleming and Quilty 2006; Gan *et al.* 2007; Gobena and Gan 2006, 2009) are two of the more important SST phenomena that affect climate in the Northern Hemisphere (Speer 2010). ENSO is a cyclical but irregular 2-7 year SST oscillation in the tropical Pacific Ocean, consisting of a warm (El Niño) phase, during which SSTs in the tropical eastern Pacific are anomalously warm, and a cool (La Niña) phase associated with cool SSTs in the eastern Pacific (Case 2000; Rasmusson and Carpenter 1982). Prairie precipitation is less affected by ENSO than temperature; however, winter precipitation during El Niño (La Niña)

events is significantly lower (higher) than normal (Shabbar *et al.,* 1997). The Pacific Decadal Oscillation (PDO) is a large scale pattern of SST variability characterized by a gradient between anomalously cool SSTs in the east-central North Pacific and anomalously warm SSTs off the central west coast of North America recurring every 15-25 and 50-70 years (Case 2000; Mantua *et al.* 1997; Minobe 1997). North Pacific SSTs affect precipitation amounts on the Prairies through links with 500 mb height anomalies in the mid-troposphere. During a positive phase of the PDO, this teleconnection occurs more frequently, resulting in long-term persistence of the negative precipitation anomaly (Knox and Lawford 1990). The PDO has positive (warm) and negative (cool) phases that appear to persist for two-three decades. Positive PDO (warm) phases occurred between 1925-46 and 1977-1998. These periods have been associated with warm winter and spring time temperatures in northwest North America, and dry conditions in the west to central North America (Fagre *et al.* 2003). Negative (cool) PDO phases occurred between 1900-1924 and 1947-1976, bringing with them cool winter and spring temperatures over western North America, as well as wet conditions in the Pacific Northwest, northern Rockies and central Prairies.

Climatic fluctuations in precipitation and temperature, and their effect on amounts of evapotranspiration and snow cover, are key determinants in linkages of large-scale climatic patterns to groundwater recharge (Tramblay *et al.* 2011). Precipitation and temperature drive infiltration and are indirect components of the groundwater reservoir budget, thereby suggesting that the influence of climatic patterns on aquifer reservoirs should be visible through groundwater levels. Despite the importance of groundwater resources, few studies have documented natural variability in Canadian groundwater systems. Fleming and Quilty

(2006) examined the influence of ENSO on water levels in shallow aquifers in British Columbia. They showed that during La Niña years water levels are above average and below average during El Niño years reflecting variability in winter and spring precipitation that recharges the aquifer systems. Perez-Valdivia and Sauchyn (2011) found strong correlations between groundwater levels in southwestern Canada and moisture-sensitive tree-ring records and were able to reconstruct historical groundwater levels for the past 300 years at two wells in southern and central Alberta, Canada. They analyze the natural variability in groundwater systems by spectral analysis, main findings of this study suggest the existence oscillation modes in groundwater levels at 2-8 and 8-16 year bands. A most recent study by Tremblay *et al.* (2011) analyze the variability of groundwater systems for three different regions across Canada and their linkage to climate indices such as North Atlantic Oscillation (NAO), the Artic Oscillation (AO), the Pacific-North American pattern (PNA) and El Niño Southern Oscillation (ENSO). The regions represented by this study are Prince Edward Island, southern Manitoba, and Vancouver Island and only one groundwater time series per region was analyzed. Results of this study suggest that groundwater at different regions have different patterns of variability. They found that groundwater variability in the Prince Edward region is mostly influenced by the NAO and AO, groundwater variability in Manitoba are influenced by the PNA and in groundwater variability in the Vancouver Island are influenced by NAO, AO, and ENSO.

Groundwater is the source of domestic fresh water for almost nine million Canadians (30.3% of the population); with 67 percent or six million living in rural areas. It is estimated that 23.1, 42.8, and 30.2 percent of the population in Alberta, Saskatchewan, and Manitoba, respectively, relies on groundwater (Statistic Canada, 1996). Global groundwater withdrawals have increased

86 by ten percent since 1950, being close to 1000 km^3 per year (Shah et al., 2007) and are
87 expected to continue to increase in response to economic and population growth. Increments
88 in groundwater demand can reflect climatic conditions such as droughts which rapidly limit
89 surficial water resources.

90 Over the historical period of instrumental records, repeated droughts have highlighted the
91 Canadian Prairies' vulnerability to even small deviations from normal moisture conditions.
92 Widespread drought throughout the region "has disrupted farming and caused economic
93 hardship several times in the last 100 years, most notably during the 1890s, 1930s, and 1950s
94 (Stockton and Meko 1983, 17). The 'dustbowl' of the 1930s is one of the worst drought periods
95 in memory in western North America, and caused much hardship both environmentally and
96 economically. "During 1961 (the worst single year drought on the Prairies, with approximately
97 50% of normal growing season precipitation), total net farm income dropped by 48% ($300
98 million) from the previous year" (Bonsal *et al.* 1999, 191). The drought of 1988 had many
99 impacts on the agricultural sectors of Canada "(with emphasis on Manitoba and Saskatchewan),
100 including wind erosion, production, grain quality, inventories, marketing, livestock, incomes,
101 farm management, global production and prices" (Wheaton *et al.* 1992, 192). The sparse snow
102 cover and high spring temperatures resulted in little or no spring runoff from prairie
103 watersheds in 1988, such that the mean volume was 60 to 70% of normal volume. The lack of
104 precipitation caused an agricultural output decrease of 12% resulting in a direct production loss
105 of $1.8 billion in 1981 dollars (Wheaton *et al.,* 1992). The drought of 2001 "resulted in an
106 economic shortfall of $4 billion or more and required supportive measures from various

governments. Grain yield data reveal a similar shortfall in total yields during 1961 and 1977, both also being severe drought years" (Khandekar 2004, 12).

With the prediction that droughts are likely to become more frequent under global warming (Kharin and Zwiers, 2000) understanding the natural variability in groundwater levels and its drivers is fundamental in order to manage water resources under extreme climatic conditions (droughts). Thus this study aims to identify the influence of major teleconnection patterns such as El Niño Southern Oscillation and Pacific Decadal Oscillation on shallow aquifers through the Canadian Prairies.

STUDY AREA, DATA, AND METHODS

Study Area

The Canadian Prairie Provinces of Alberta, Saskatchewan, and Manitoba (Figure 1) extend from the eastern slopes of the Rocky Mountains to the Hudson Bay. The climate varies from cold winters to sub-humid summers. In Calgary, Regina and Winnipeg the mean winter temperatures (1971-2000) are -7.5°C, -13.8°C, and -15.6°C respectively. Mean summer temperatures reach over 15°C, increasing to the east (15.2°C; 17.7°C; 17.9°C), with maximum means of 17.3°C in Calgary, 20.3°C in Regina, and 20.6°C in Winnipeg. On the contrary, mean annual temperatures increase towards the southwest (Southern Alberta) where it is 5.0°C to 6.0°C., while Calgary, Regina, and Winnipeg exhibit mean annual temperatures of 4.0°C, 2.8°C and 2.2°C.

The annual precipitation in the Prairies varies from just below 300 mm in southeastern Alberta and southwestern Saskatchewan to over 900 mm in the Rocky Mountains. Mean annual

precipitation for the period 1971-2000 at Calgary, Regina, and Winnipeg was 457 mm, 444 mm, and 574 mm respectively. Spring and summer register over 60% of the annual precipitation; however, much is lost to evapotranspiration, mostly from the unsaturated soil water zone where it is available for annual plant growth (Perez-Valdivia and Sauchyn 2011). Winter precipitation (snow) is an important source of water to recharge surface and groundwater systems. Approximately 25% of the annual precipitation occurs as snow fall during the months of November to March where mean temperatures are below zero. Given the distribution of precipitation and temperature through the Prairies, south central areas are under moisture stressed conditions and are supplied with water from the surrounding Rocky Mountains and foothills.

DATA

Groundwater, Precipitation, and Climate indices

Twenty one monthly groundwater level time series were obtained from Alberta Environment, Saskatchewan Watershed Authority, and Manitoba Water. These records are part of a larger monitoring network that extends throughout the Prairie Provinces. The selection of the twenty one wells was based on length and continuity of the records (at least 20 years), percentage of missing data (less than 20%), anthropogenic effects (no pumping) and depth of the aquifer (shallow < 20 meters depth). Missing values were estimated using correlations with nearby water level records and median values were used when correlation was not possible. The continuous time series were plotted to check that the process of replacing missing data did not create outliers. The selected groundwater levels respond mostly to spring snowmelt and spring

149 and summer precipitation period in which maximum levels are observed. Table 1 summarizes
150 the groundwater records used in this study.
151 Seven time series of monthly precipitation, from stations relatively close to the groundwater
152 wells (Figure 1, Table 2), were obtained from the Adjusted Historical Canadian Climate Data
153 (Mekis and Hogg, 1999). These data have been homogenized and adjusted and are suitable for
154 studies of climate variability and change. Monthly climate indices of ENSO 3.4, and PDO were
155 obtained from the Earth Systems Research Laboratory (National Oceanic and Atmospheric
156 Administration, available at http://www.esrl.noaa.gov/psd/data/climateindices).

157 ***Tree-ring Chronologies***

158 As climate records often predate ground water monitoring by several decades, these data can
159 potentially be used to estimate changes within an aquifer prior to the establishment of direct
160 measurement (Ferguson and St. George 2003). Although tree-rings have most often been used
161 to reconstruct precipitation and streamflow and to study the low-frequency variability in these
162 hydroclimate variables (Watson and Luckman, 2001; Axelson *et al.,* 2009), the direct
163 relationship between tree growth and factors important to recharge suggests that
164 dendrochronological data may also be useful in historical ground water model studies
165 (Ferguson and St. George 2003). Albeit many reconstructions of precipitation and streamflow
166 exist, only a few have successfully investigated the relationship between tree-rings and
167 groundwater within the Canadian Prairies (Ferguson and St. George 2003; Perez-Valdivia and
168 Sauchyn 2011), recognizing the common response of tree growth and groundwater levels to
169 effective precipitation, and the often lagged response times (Perez-Valdivia and Sauchyn 2011).

In this study, tree-ring indices are used as a surrogate for long-term instrumental records (Hanson *et al.* 2004), in order to identify relationships with significant periodicities (found common amongst groundwater, precipitation and tree-ring records), such as the low frequency of the PDO which exceeds the length of all but a few of the instrumental hydroclimatic records from the Canadian Prairies. Three tree-ring chronologies, from *Pinus flexilis* (Limber pine; Oldman River and Whirpool Point) in the foothills of central and southern Alberta, and *Quercus Macrocarpa* (Burr Oak; Davon Fram) in southeastern Saskatchewan were analyzed to identify coherent low frequency climate signals across the Prairie Provinces (Table 2). These tree-ring chronologies contain annual moisture signals spanning more than 150 years in Saskatchewan and more than 900 years in Alberta. The tree ring chronologies have annual resolution, thus they are not directly comparable temporally with our monthly groundwater time series if not are used as verification tool of the hydroclimatic variability affecting the Canadian Prairies and groundwater levels. The wood and tree-ring data were processed in the Tree-ring Laboratory at the Prairie Adaptation Research Collaborative, University of Regina using standard dendrochronological methods (Stokes and Smiley, 1968; Fritts, 1976; Cook, 1985; Cook and Kairiukstis 1990) and the semi-automated tree-ring analysis software WinDendro Density (version 2009a). Tree growth trends were removed using a negative exponential curve or a cubic spline with 67% length of the time series. This detrending is considered conservative because it preserves most of the low frequency signals recorded in the tree-rings. Crossdating, which assigns the correct calendar year to individual tree-rings, was verified with COFECHA (Holmes, 1983). The lengths of the chronologies are 946, 805, and 152 years for Whirlpool Point (WPP), Old Man River (OMR), and Devon Farm (DEV) respectively.

METHODS

The methodology used in this study is similar to that proposed by Hanson *et al.* (2004) and Tremblay *et al.* (2011), to assess the relationship between hydrologic time series and climatic variability. It consists of detrending hydrological time series by fitting a low order polynomial. This detrending removes part of the low frequency (signals that are longer than half of the period of record) and anthropogenic effects. The groundwater wells are not directly affected by pumping; their implementation was only to monitor groundwater levels in different aquifers. However, these groundwater records might be influenced by pumping through other wells in the same aquifer. The residual time series, the difference between the observed data and the values calculated with the polynomial, are standardized to a zero mean and unit variance for inter-comparison. Spearman's rank correlation for non-parametric time series was used to calculate lagged correlations for up to 36 months were calculated for monthly groundwater levels, precipitation, temperatures, and indices of ENSO 3.4 and PDO. A lag of up to 36 months was considered to be enough for groundwater time series to reflect the influence of teleconnection patters and precipitation because all the wells in this study are shallow and located in material of high hydraulic conductivity. The Multi Taper Method (MTM; Ghil et al., 2002) of spectral analysis was used to identify dominant oscillation modes in the groundwater (residuals), precipitation, and residual tree-ring time series and to extract and reconstruct significant quasi-periodic signals. MTM is non-parametric and uses a series of tapers that reduce the variance of spectral estimates which is an advantage over other spectral window methods (Percival and Walden, 1993). We applied the SSA-MTM toolkit (Ghil et al, 2002), with

213 robust background estimation, to the residual time series. The bandwidth parameter *p* was set
214 at two and the numbers of tapers was set at three which has been suggested for the analysis of
215 climate records consisting of a few hundred observations (Mann and Park, 1993).

216 Continuous wavelet transform (CWT; Torrence and Compo, 1998; Grinsted et al., 2004) was
217 also used to identify the main oscillatory modes of variability in groundwater levels and the
218 tree-ring chronologies. The CWT complements the MTM method by identifying periods of
219 dominant oscillation modes, with the added feature of the time-frequency domain, which
220 depicts when these dominant frequencies occur throughout the time series (Torrence and
221 Compo, 1998; Jevrejeva *et al.* 2003). Among all the wavelet families, Morlet wavelet (w_0=6) was
222 used since it provides a good balance between time and frequency domains and is
223 recommended when the purpose is to extract dominant signals (Grinsted et al. 2004). The
224 statistical significance was assessed against a red noise background at a 95% confidence level.
225 The CWT function creates a cone of influence (COI) that delimits a region of the wavelet
226 spectrum in which edge effects become important and the power could be suppressed
227 (Torrence and Compo 1998; Jevrejeva *et al.* 2003; Grinsted *et al.* 2004; Gobena and Gan 2009).
228 The spectral power outside the cone of influence should be interpreted with caution.

229 Oscillation modes detected using MTM and wavelet analyses were reconstructed and
230 correlated with the respective frequencies of known oscillation modes of atmospheric and sea-
231 surface temperature (SST) forcings thought to be primary drivers of hydroclimatic variability
232 affecting groundwater recharge (ENSO and PDO indices). Areas in the time-frequency plane
233 where two time series exhibit common power (coherence) or consistent phase behaviour

indicate a relationship between the signals. Coherence is a measure of the intensity of the covariance of the two series in time-frequency space, unlike the cross-wavelet power which is a measure of the common power (Jevrejeva *et al.* 2003). Wavelet transform coherence (WTC) analysis greatly facilitates the detection of the quasi-periodic component indicative of a system anomaly (MathWorks 2011). Following Torrence and Webster (1999) coherence is defined as:

$$R_n^2(s) = \frac{\left|S\left(s^{-1}W_n^{XY}(s)\right)\right|^2}{S\left(s^{-1}\left|W_n^X(s)\right|^2\right) * S\left(s^{-1}\left|W_n^Y(s)\right|^2\right)}$$

where *S* is a smoothing operator. $R_n^2(s)$ gives a quantity between 0 and 1, and measures the cross-correlation between two time series as a function of frequency. The equation above, represents the normalized covariance between two time series because the wavelet transform conserves variance (Gobena and Gan 2009). The statistical significance level ($p < 0.05$) of the wavelet coherence is estimated using Monte Carlo methods with red noise background resulting in significant periodicities of coherence delineated by significance contours. As in the CWT, regions outside of the COI should be interpreted with caution.

RESULTS AND DISCUSSION

Correlations

The results of correlation analyses (Table 3) suggest that most of the residual groundwater time series have significant correlations with precipitation at lags of 9 to 24 months. Significant correlations suggest that these aquifers are recharged primarily by precipitation that infiltrates the soil.

253 Correlations between groundwater levels and mean temperature indicate that groundwater
254 records are significantly correlated ($p < 0.05$) with temperature over a five month period (lags 3
255 to 8; Table 3). As expected, temperature correlates negatively with most groundwater time
256 series, suggesting that increased temperatures, primarily during the warmer months of May to
257 October, causes increased amounts of evapotranspiration, resulting in decreased amounts of
258 groundwater levels.

259 Wells Atto, Banb, C500, Ob005, Melf, and Rice did not show significant correlations at any lag,
260 for either precipitation or temperature. These results indicate that although these six wells are
261 in sand; they may be influenced more by nearby streamflow recharge, or by beds of lower
262 hydraulic conductivity or a degree of confinement, than by precipitation as their primary
263 sources of recharge. Further research should be focused on determining the recharge
264 mechanisms for these aquifers.

265 Thirteen of the twenty one groundwater records show significant negative correlations with
266 both the ENSO 3.4 and PDO indices, suggesting that large scale SST and atmospheric
267 teleconnections may be drivers influencing fluctuations in groundwater levels. Most of these
268 correlations occur around lags of 13-20 months, however, correlations with PDO occur at
269 slightly longer lags than for ENSO. The most significant correlations were for wells Sten (-0.28
270 lag 13) and W108 (-0.32 lag 33) with ENSO and PDO respectively.

271 Few wells (Si13, Sten, and W159) with significant correlations to precipitation, ENSO, and PDO,
272 exhibit shorter lag times with ENSO and PDO than with precipitation. These findings suggest
273 that precipitation may not be the main source of groundwater recharge for these wells; rather,

relationships with streamflow or subsurface flows may exist, having stronger influences than precipitation as primary sources of groundwater renewal, resulting in longer lags in the effects of precipitation on groundwater recharge. Future analyses are suggested and required to investigate this further.

Spectral Analyses

Multi Taper Method (MTM)

Results of the MTM suggest that there are significant modes of high-, interdecadal and low-frequency variability in groundwater levels in the Canadian Prairies at frequencies of 2-7 years, 7-10 years, and 18-22 years (Table 4). Similar findings were reported by Perez-Valdivia and Sauchyn (2011) identifying coincident periodicities of high and interdecadal frequencies, in their tree-ring reconstructions of groundwater levels in Alberta, Canada. MTM applications to annual precipitation records show similar results, highlighting significant oscillations also found within the 2-7 and 7-12 year frequencies (Table 5). MTM analysis of the moisture-sensitive tree-ring chronologies show that they register oscillation modes in the 2-7, 9-15, 22-25, 64, and 85 year frequency ranges (Table 5; Figures 2, 3, and 4). The interannual, interdecadal and multi-decadal variability found within the tree-rings provides evidence that both the tree-ring chronologies and groundwater wells, may be responding to the same climatic drivers affecting available resources (*i.e.* precipitation) for both tree growth and aquifer recharge.

295 ***Continuous Wavelet transform (CWT)***

296 Wavelet results (Table 4) mirror those of the MTM analysis, suggesting natural variability, at
297 high- and interdecadal frequencies, exists the in groundwater level time series. Lower
298 frequency activity, greater than 20 years, is not identified in the groundwater levels by wavelet
299 analysis, likely given the short length of the time series. Significant interannual variability
300 coinciding with 2-6 year frequencies, usually related to the El Niño-Southern Oscillation (ENSO;
301 Shabbar and Skinner 2004; Gobena and Gan 2006), is evident throughout much of the entire
302 lengths of the groundwater time series, however, is concentrated most heavily during the late
303 1960s-early 70s, mid 1980s, early 1990s and 2000s (Figures 2, 3, and 4). Interdecadal
304 oscillations (coinciding with frequencies at 7-12 years) are also depicted in the groundwater
305 time series, most notably during the 1980s and 1990s.

306 Precipitation records yield similar results to their MTM analysis, identifying significant
307 oscillations within the 2-6 and 7-10 year bands, but also identify the presence of low frequency
308 oscillations within the 20-30 year bands (Table 5). All accounts of the high and low frequencies
309 detected previously via MTM analysis, are also identified by wavelet analysis for the tree-ring
310 chronologies (Table 5; Figures 2, 3, and 4), and coincide to periods of occurrence found within
311 both groundwater and precipitation time series, but also provide the advantage of long record
312 length and thus the identification of low frequency signals, in this case in the bands of 16-32,
313 32-64 and 64-128 years. In Alberta, the low frequency in the WPP and OMR chronologies
314 (Figures 2 and 3)concur with the oscillation modes detected in precipitation records at Calgary,
315 and Lethbridge and also identifies a significant periodicity of lower frequency variability around

316 the 64 year band, documented previously by Axelson et al. (2009). The DEV chronology in
317 southeastern Saskatchewan (Figure 4) shows significant activity within the high-frequency
318 bands (2-7 years) and also at periodicities coinciding with the ~20 and ~50 year oscillation
319 modes detected in groundwater levels and precipitation at Calgary, Lethbridge, Regina and
320 Estevan (Table 5, Fig. 4). Frequencies within the 20-30 year bands have been associated with
321 ocean-atmosphere teleconnection forcings, such as the PDO (Mantua *et al.* 1997; Minobe
322 1997), where shifts in oscillation patterns, 'warm' or 'cool' phases, are marked by widespread
323 variations in Pacific Basin and North American climate. PDO-related temperature and
324 precipitation patterns have been strongly linked to regional hydrologic variable (*i.e.* snow pack
325 and streamflow) anomalies, especially in western North America (Cayan 1995; Manuta *et al.*
326 1997; Bitz and Battisti 1999; Nigam *et al.* 1999).The commonality in results of both MTM and
327 wavelet spectral analyses, amongst groundwater, precipitation and tree-ring time series,
328 suggests that all three are responding to a common coherent signal, being driven by the same
329 mechanism or forcings (*i.e.* large scale atmospheric teleconnections).

330 ***Reconstruction of oscillation modes***

331 To associate plausible drivers of groundwater level variability, modes at significant frequencies
332 were extracted from groundwater time series and correlated with oscillations associated with
333 sea surface temperature and atmospheric forcings, specifically ENSO and PDO (Table 6). The
334 high-frequency reconstructed mode (2-7 year) has mostly a strong negative correlation with
335 ENSO (Table 6), but it also seems to be related to the high frequency component of the PDO,
336 causing much of the interannual variability found within the groundwater level time series.

337 Correlation coefficients range from -0.02 to -0.33, however, stronger correlations are reached
338 at lags longer than 10 months. The high-frequency variability corresponding to ENSO was
339 previously identified in other analyses of prairie hydrologic time series (e.g. Coulibaly and Burn,
340 2004; Gan *et al*. 2007).

341 The reconstructed modes in the 7-10 year band show mainly stronger correlations with ENSO
342 than for PDO (Table 6). Correlation coefficients range from 0.00 to -0.30 with the strongest
343 correlations having lags of 0 to 7 months, which suggest that at this periodicity there is a lag
344 response of groundwater levels to ENSO events. Similar results are reported by Fleming and
345 Quilty (2006) in their investigation of ENSO signals in precipitation, streamflow and shallow
346 groundwater levels in southwester British Columbia. Even though ENSO events lead to changes
347 in the annual hydrometeorological cycle, they do not appreciably impact their timing with peak
348 streamflows, lagging precipitation by one to two months, with groundwater having further lags
349 by two to four months, or longer (Bonsal and Shabbar 2008). Since aquifers are relatively slow
350 responding systems, winter precipitation anomalies associated with ENSO strongly control
351 water levels for the remainder of the year (Bonsal and Shabbar 2008).

352 The PDO seems to have a strong negative influence on the low-frequency variability in
353 groundwater levels (Table 6). From the 16 groundwater time series with significant low-
354 frequency variability, 12 show strong correlations with the PDO indices, ranging from -0.17 to -
355 0.52 for the reconstructed 18-22 year band. This multidecadal (~20 year) oscillation mode was
356 also very apparent in the moisture-sensitive tree-ring chronologies in southwest Alberta and
357 southeast Saskatchewan, suggesting that due to the limitation of short groundwater time

series, the low frequency variability affecting the Prairie region, is likely able to be inferred from the tree-ring chronologies, which ultimately serve as proxies of hydroclimatic variability.

Links to oscillatory indices

Links between climate indices, groundwater level, and tree-ring time series, were further examined by plotting the extracted significant frequencies and their respective climate indices to visually depict when these cycles were in their respective negative or positive phases, and by computing wavelet transform coherence (WTC) between groundwater and tree-ring chronology time series, and the climate indices (ENSO and PDO) (Figures 5 and 6). WTC was used to identify both frequency bands and time intervals within which groundwater and tree-ring time series and climate indices are covarying (Torrence and Webster 1999). Significant coherence is shown in each run of the WTC analysis, where contours enclose statistically significant periods ($p \leq 0.05$), based on a red-noise process as determined by a Monte Carlo experiment (Jevrejeva *et al.* 2003). Another important feature of the WTC analysis is the ability to investigate the phase difference between components of the two time series during periods of significant coherence. The vectors plotted in each of the WTC analyses (Figures 5 and 6) indicate the phase differences between significant spectral oscillations identified for the groundwater level time series and the climate indices at each respective frequency, and at each time and period. Vectors pointing to the right indicate that the two signals are in phase, whereas a left-pointing arrow indicates an anti-phase relationship. Arrows deviating from the horizontal are indicative of lead-lag relationships between the two signals (Gobena and Gan 2009). If a link exists between two

379 time series, a consistent or slowly varying phase lag would be expected, and the phenomena
380 would be considered to be phase-locked (*i.e.* phase-arrows point only in one direction for a
381 given wavelength; Grinsted *et al.* 2004). Because the lead/(lag) relationships can be difficult to
382 interpret, (*i.e.* a lead of 90° can also be interpreted as a lag of 270° or a lag of 90° relative to the
383 anti-phase – opposite sign; Grinsted *et al.* 2004), for this study, phase angle associations were
384 noted strictly as either being in-phase/anti-phase locked, or if a lead/lag relationship exists.

385 For simplicity and to limit the length of the manuscript, only results for reconstructed
386 frequencies of groundwater levels having the strongest correlations with climatic indices are
387 shown. Results discussed describe findings common to reconstructed significant frequencies
388 and WTC analyses for all groundwater wells, suggesting a common coherent response of the
389 groundwater levels to common drivers of variability, however, are discussed in more detail for
390 the time series selected for illustration.

391 Groundwater level time series show common coherence with high frequencies of the ENSO
392 indices at periodicities corresponding to 2-3 years (Figure 5a), most predominantly in the early
393 1970s and throughout much of the 1980s, early 1990s.

394 Investigations at the interdecadal timescale (7-10 years; Figure 5b) indicate a very distinct anti-
395 phase locked relationship between the groundwater time series and ENSO indices as depicted
396 by the WTC analysis. This anti-phase relationship is first evident in the plotted graphs of phase
397 relationships, during the early 1990s, and is more evident throughout much of the late 20th and
398 early 21st centuries, These results indicate the negative effect of ENSO in its positive (El Niño)
399 phase, bringing warmer and drier winters affecting the hydrological cycle and groundwater

400 recharge, over much of the Canadian Prairies, as is evident in the decreased amounts of
401 groundwater levels during these periods; a finding similar to results of investigations of
402 streamflow and the Niño-3 index in Southern Alberta (Gobena and Gan 2009).

403 As wavelet analyses were unable to depict the low frequency variability (≥ 20 years) in
404 groundwater level time series, due to their limited in record lengths, (although evident in the
405 MTM analyses) coherency analyses were carried out between tree-ring indices and
406 precipitation indices with the PDO indices. Based on previous correlation analyses, and the
407 coherence indicating a strong significant relationship between the DEV chronology and
408 precipitation time series, and ultimately the precipitation time series with the PDO index
409 (Figure 6), validates the assumption that all three variables are responding to similar drivers of
410 variability, therefore, using the tree-ring indices as surrogates for longer term instrumental
411 records to depict variability at low-frequencies was deemed valid. As depicted in Figure 5c,
412 both the graphed extracted frequencies of groundwater time series and WTC between the DEV
413 chronology and the PDO index, indicate a very significant anti-phased locked relationship,
414 supporting a physical mechanism of signal propagation from the PDO to precipitation indices,
415 which ultimately is reflected in tree growth and groundwater recharge (Grinsted *et al.* 2004).
416 From the graph in Figure 5c, we can see that when the PDO index switches from its extreme
417 cool phase to warm phase during the mid 1970s, we can see a temporal response in decreased
418 amounts of groundwater levels. We can also see that when either of these teleconnections,
419 (ENSO/PDO), is in their respective positive phases (Figure 5), groundwater levels depict the
420 effect of associated warmer and drier winters experienced over much of interior Canada and

421 the US, affecting important resource inputs of the hydrological cycle and groundwater
422 recharge.

423 **CONCLUSIONS**

424 Twenty-one groundwater level time series, seven precipitation records and three moisture-
425 sensitive tree-ring chronologies, were investigated with the objective of analyzing the effects of
426 climate variability on groundwater levels in the Canadian Prairies. Correlation analyses suggest
427 that all the shallow aquifers show significant positive and negative relationships to both
428 precipitation and temperature, respectively, indicating that groundwater levels are significantly
429 influenced by hydroclimatic variability. Strong significant negative correlations were also
430 indentified for relationships between groundwater levels and ENSO and PDO indices,
431 suggesting that these ocean-atmosphere oscillation patterns may be possible drivers of
432 hydrologic variability affecting groundwater levels and aquifer recharge.
433 Results of spectral analyses (MTM and CWT) agree that there is significant variability in
434 groundwater levels at frequencies of 2-7, and 7-10 years. Oscillation modes in these two bands
435 were also detected in precipitation records throughout the Prairie Provinces. MTM results also
436 suggest a multi-decadal oscillation mode in groundwater levels, with periodicities of 18-22
437 years. This 18-22 year frequency was also identified in precipitation records, and detected in
438 the moisture sensitive tree-ring chronologies, which record available soil moisture, a
439 hydroclimate variable with more persistence than precipitation.
440 Significant spectral peaks determined by MTM and wavelet analyses were investigated further
441 via extracting reconstructions of significant frequencies, and examining for periods of common

coherence between the groundwater level time series and the coupled ocean-atmosphere teleconnections, ENSO and PDO.

The extracted significant high-frequency oscillation modes (2-7 and 7-10 years) in groundwater levels were found to exhibit a strong negative correlation to the ENSO index. Strong relationships were also determined to exist between the 18-22 yr oscillation mode in precipitation and tree-ring indices and the PDO index. The linkage between groundwater levels and tree-growth in their responses to precipitation, serves to reinforce that both respond to a common coherent signal (*i.e.* precipitation) and are limited by moisture availability. Thus, the relationship that exists between variability in precipitation driven by the influence of the PDO index, serves to support that the same relationship, and significant oscillations of variability found within the groundwater level time series, can be associated with variability driven by the PDO index.

Therefore we conclude that the ENSO and PDO indices show significant relationships with high and low-frequency variability depicted in the groundwater levels. The results of spectral analyses coincide with the conclusions of other previous studies which have detected the influence of ENSO and PDO on hydrologic variables in western Canada. Despite that a similar study has partially investigated this question with coincident tools, our study is the first to investigate the influence of these climate drivers on the variability of groundwater levels over such a large scale and number of wells in the Canadian Prairies.

Further investigation is recommended to examine the interactive effects of climate drivers on groundwater levels. The spatial variability of teleconnection patterns represented by the

464 different oscillation modes detected in the tree-ring chronologies also needs to be considered.
465 Special attention to the stationary, but not consistently significant signals, detected in the DEV
466 chronology in south eastern Saskatchewan is recommended for the study of long-term
467 hydrologic variability. Finally, moisture-sensitive tree-ring chronologies capture similar climate
468 signals to groundwater level records which may prove them useful for reconstructing historical
469 levels of groundwater levels in shallow aquifers in southern Saskatchewan as previously
470 demonstrated for southern Alberta.

471 **ACKNOWLEDGMENTS**

472 This research was funded by the Drought Research Initiative, the Inter-American Institute for
473 Global Change Studies (CRN2047) and the Prairie Adaptation Research Collaborative. We thank
474 Dr. Garth van der Kamp of the Northern Hydrological Research Centre for his support and
475 advice.

476

477

478

479

480

481

482

483

REFERENCES

Axelson, J. N., D. J. Sauchyn, and J. Barichivich (2009), New reconstructions of streamflow variability in the South Saskatchewan River Basin from a network of tree ring chronologies, Alberta, Canada, *Water Resour. Res., 45*, doi:10.1029/2008WR007639.

Bitz, C.C., and D.S. Battisti, (1999), Interannual to decadal variability in climate and the glacier mass balance in Washington, Western Canada, and Alaska, *Journal of Climate, 12*, 3181-3196.

Bonsal, B., and E. Wheaton (2005), Atmospheric circulation comparisons between the 2001 and 2002 and the 1961 and 1988 Canadian Prairie droughts, *Atmosphere-Ocean*, 43(2), 163-172.

Bonsal, A., and A. Shabbar (2008), Impacts of large-scale circulation variability on low streamflows over Canada: a review, *Canadian Water Resources Association,* 33(2), 137-154.

Bonsal, B., A . Shabbar, and K. Higuchi (2001), Impacts of low frequency variability modes on Canadian winter temperature, *Int. J. Climatol.*, *21*, 95-108.

Bonsal, B.R., X. Zhang, and W.D Hogg (1999), Canadian Prairie growing season precipitation variability and associated atmospheric circulation. *Climate Research, 11*, 191-208.

Case, R.A. (2000) *Dendrochronological investigations of precipitation and streamflow for the Canadian Prairies,* PhD dissertation, University of California, Los Angeles, CA.

Cayan, D.R. (1996), Interannual climate variability and snowpack in the western United States, *Journal of Climate, 9*, 928-948.

Cook, E.R. (1985), A time series analysis approach to tree-ring standardization. Ph.D. Thesis, Univ. of Arizona, Tucson, USA.

Cook, E.R., and L. A. Kairiukstis (1990), Methods of dendrochronology: applications in the environmental sciences. Kluwer, Dordrecht.

Coulibaly, P., and D.H. Burn (2004), Wavelet analysis of the variability in Canadian streamflows, Water *Resour. Res., 40*, doi:10.1029/2003WR002667.

Enfield, D. B., A. M. Mestas-Nuñez, and P. J. Trimble (2001), The Atlantic Multidecadal Oscillation and its relation to rainfall and river flows in the continental U.S., *Geophys. Res. Lett., 28,* 2077– 2080.

Fagre, D.B., D.L. Peterson, A.E. and Hessl (2003), Taking the pulse of mountains: Ecosystem responses to climatic variability, *Climatic Change, 59*(1-2), 263-282.

Ferguson, G., and S. St. George, (2003), Historical and estimated ground water levels near Winnipeg, Canada, and their sensitivity to climatic variability, *Journal of the American Water Resources Association, 39*(5), 1249-1259.

Fleming, S.W., and E. J. Quilty (2006). Aquifer responses to El Niño-Southern Oscillation, southwest British Columbia, *Ground Water,* 44(4), 595-599.

Fritts, H.C. (1976), *Tree rings and climate*. Academic Press, London.

Gan, T.Y., A.K. Gobena, and Q. Wang (2007), Precipitation of southwestern Canada: Wavelet, scaling, multifractal analysis, and teleconnection to climate anomalies. *Journal of Geophysical Research*, 112, D10110.

Ghil, M., R.M. Allen, M.D. Dettinger,K. Ide, D. Kondrashov, M.E. Mann, A. Robertson, A. Saunders, Y. Tian, F. Varadi, P. Yiou (2002), Advanced spectral methods for climatic time series, *Rev. Geophys. 40* (1), 1.1–1.41.

Gobena, A. K., and T. Y. Gan (2006), Low-frequency variability in southwestern Canadian streamflow: Links with large-scale climate anomalies, *Int. J. Climatol., 26,* 1843–1869.

Gobena, A. K., T. Y. Gan (2009), The role of pacific climate on low frequency hydroclimatic variability and predictability in Southern Alberta, Canada, *J. Hydrometeor, 10,* 1465-1478.

Grinsted, A., J.C. Moore, and S. Jevrejeva (2004), Application of the cross wavelet transform and wavelet coherence to geophysical time series, *Nonlinear Processes in Geophys., 11,* 561-566.

Hanson R.T., M.W. Newhouse, M.D. Dettinger (2004), A methodology to assess relations between climatic variability and variations in hydrologic time series in the southwestern United States, *Journal of Hydrology 287,* 253-270.

Holmes, R.L. (1983), Computer-assisted quality control in tree-ring dating and measurements, *Tree-Ring Bull, 43*, 69–75.

Hurrell, J.W., and H. Van Loon (1997), Decadal variations in climate associated with the North Atlantic Oscillation, *Climatic Change 36,* 301–326.

Jevrejeva, S., J.C. Moore, and A. Grinsted (2003), Influence of the Arctic Oscillation and El Niño-Southern Oscillation (ENSO) on ice conditions in the Baltic Sea: The wavelet approach, *J. Geophys. Res.*, 108(D21), 4677, doi:10.1029/2003JD003417.

565 Khandekar, M.L. (2004), *Canadian Prairie drought: a climatological assessment,* Alberta
566 Environment. pp. 37.
567
568 Kharin, V.V., and F.W. Zwiers (2000), Changes in extreme in an ensemble of transient climate
569 simulations with a coupled atmosphere-ocean GCM, *Journal of Climate 13,* 3760-3788.
570
571 Knox, J.L., and R.G. Lawford (1990), The relationship between Canadian Prairie dry and wet
572 months and circulation anomalies in the mid-troposphere, *Atmosphere-Ocean 28,* 189-215.
573
574 MacDonald, G.M., and R.A. Case (2005), Variations in the Pacific Decadal Oscillation over the
575 past millennium, *Geophys. Res. Lett*, 32(8), L08703, doi:10.1029/2005GL022478.
576
577
578 Mann, M. E., and J. Park (1993), Spatial correlations of interdecadal variation in global surface
579 temperatures, *Geophys. Res. Lett., 20,* 1055–1058
580
581 Mantua, N. J., S. R. Hare, Y. Zhang, J. M. Wallace, and R. C. Francis (1997), A Pacific interdecadal
582 climate oscillation with impacts on salmon production, *Bull. Amer. Meteor. Soc.,* 78, 1069–1079.
583
584 Mantua, N.J., and S.R. Hare (2002), The Pacific Decadal Oscillation, *J. Oceanography, 58,* 35-44.
585
586 MathWorks. (2011), Wavelet coherence. The MathWorks, Inc. http://www.mathworks.com.
587
588 McCabe, G., M. Palecki, and J. L. Betancourt (2004), Pacific and Atlantic Ocean influences on
589 multi-decadal drought frequency in the United States, *Proc. Natl. Acad. Sci*., 101, 4136–4141.
590
591 Mekis, É., and W.D. Hogg (1999) Rehabilitation and analysis of Canadian daily precipitation time
592 series, *Atmosphere-Ocean 37*(1), 53-85.
593
594 Minobe, S. (1997) A 50-70 year climatic oscillation over the North Pacific and North America.,
595 *Geophys. Res. Lett, 24*, 683-686.
596
597
598 Minobe, S., (2000), Spatio-temporal structure of the pentadecadal variability over the North
599 Pacific*, Prog. Oceanogr., 47,* 381– 408.
600
601 Nigam, S., Barlow, M., and E.H., Berbery, (1999) Analysis links Pacific decadal variability to
602 drought and streamflow in the United States, EOS, Transactions, American Geophysical Union
603 80(51) December 21.
604
605
606 Percival D. B., and A.T. Walden (1993), *Spectral Analysis for Physical Applications*. Cambridge
607 University Press, Cambridge UK, 583 pp

Perez-Valdivia, C., and D. Sauchyn (2011), Tree-ring reconstruction of groundwater levels in Alberta, Canada: long term hydroclimatic variability, *Dendrochronologia 29,* 41-47.

Rasmussen, E.M., and T.H. Carpenter, (1982) Variations in tropical sea surface temperature and surface wind fields associated with the Southern Oscillation/El Nino, *Monthly Weather Review, 110*, 354-384.

Rubio-Alvarez, E., and, J. McPhee J. (2010) Patterns of spatial and temporal variability in streamflow records in south central Chile in the period 1952-2003, Water Resour. Res. 46, 16.

Shabbar, A., B. Bonsal, M. Khandekar (1997), Canadian precipitation patterns associated with the Southern Oscillation, *Journal of Climate, 10,* 3016-3027.

Shabbar, A., and W. Skinner. (2004), Summer drought patterns in Canada and the relationship to global sea surface temperatures, *Journal of Climate, 17*, 2866-2880.

Shah, T., J. Burke, K. Villholth (2007), Groundwater: a global assessment of scale and significance, in: *Water for Food, Water for Life* (ed. by D. Molden), 395–423

Speer, J.H. (2010) *Fundamentals of tree-ring research.* The University of Arizona Press. pp. 333.

Statistics Canada (1996), Quaterly Estimates of the Population of Canada, the Provinces and the Territories, 11-3, *Catalogue 91-001*, Ottawa.

Stokes M.A., and T.L Smiley (1968), An introduction to tree-ring dating. University of Chicago Press, Chicago.

Torrence, C., and G. P. Compo (1998), A practical guide towavelet analysis. *Bull. Am. Meteorol. Soc. 79*, 61–78.

Torrence, C., and P. Webster (1999), Interdecadal changes in the ENSO-Monsoon system, *Journal of Climatology, 12,* 2679-2690.

Tremblay, L., Larocque, M., Anctil, F., and C. Rivard. (2011), Teleconnections and interannual variability in Canadian groundwater levels, *Journal of Hydrology, 410,* 178-188.

Wang, L., W. Chen, and R. Huang (2008), Interdecadal modulation of PDO on the impact of ENSO on the East Asian winter monsoon, *Geophys. Res. Lett., 35,* L20702,doi:10.1029/2008GL035287.

649 Watson, E., and B.H. Luckman, (2001), Dendroclimatic reconstruction of precipitation for sites
650 in the southern Canadian Rockies, *The Holocene 11,* 203– 213.
651

652 Wheaton, E.E., Arthur, L.M., Chorney, B., Shewchuk, S., Thorpe, J., Whiting, J., and Wittrock, V.
653 (1992), The prairie drought of 1988, *Climatological Bulletin, 26*(3), 188-205.
654

655
656
657
658
659
660
661
662
663
664
665
666
667
668
669
670
671
672
673
674
675
676
677
678
679
680
681
682
683
684
685
686
687

688 **Table 1:** Groundwater wells. Bedrock aquifers are typically composed of sandstone and in some other
689 cases by fractured shale or coal. Surficial aquifers are composed of sand, gravel, silt, and clay. Intertill
690 aquifers have glacial gravels, sands and silts between layers of till.

Well name	Well ID	Prov.	Depth of Water table	Latitude	Longitude	Elevation (m)	Period		Aquifer type	Lithology
Barons 615E	W117	AB	19.8	49.993	-113.077	964.5	Jul-71	Dec-07	Bedrock	Sandstone
Elkwater 2294E	W108	AB	33.5	49.661	-110.288	1220.0	Sep-85	Jul-05	Surficial	Sand/gravel
Conq 500	C500	SK	19.2	51.574	-107.174	555.2	Dec-71	Dec-08	Intertill	Sand
Swanson	Swan	SK	9.2	51.650	-107.066	534.9	Jan-72	Dec-08	Surficial	Sand
Verlo	Verl	SK	12.8	50.373	-108.897	737.6	Feb-65	Apr-09	Surficial	Clay/silt
Atton	Atto	SK	16.2	52.816	-108.869	536.4	Feb-66	Dec-08	Surficial	Sand
Devon #2	W159	AB	7.6	53.388	-113.691	693.3	Apr-67	Jul-05	Surficial	Sand
Duvernay 2489E	W270	AB	20.7	53.773	-111.700	580.0	Jun-88	Jul-07	Bedrock	Sandstone
Bangor B	Ban B	SK	15.3	50.899	-102.287	527.6	Nov-70	Oct-08	Intertill	Sand
Simpson 13-04	SI13	SK	7.2	51.457	-105.193	496.6	Jul-68	Dec-08	Surficial	Sand
Riceton	Rice	SK	22.4	50.164	-104.317	579.1	Jul-68	Dec-07	Intertill	Sand
Forger	Forg	SK	5.9	49.705	-102.863	606.5	Apr-66	Dec-08	Surficial	Sand
Stenen	Sten	SK	14.6	51.821	-102.410	na	Sep-65	Dec-08	Suficial	Gavel/sand
Winkler #5	Ob005	MB	6.7	50.875	-97.855	278.7	Jun-69	Jun-09	Surficial	Sand/gravel
Beauval	Beau	SK	16.2	55.117	-107.745	434.3	Nov-74	Apr-09	Intertill	Sand
Conq 501	C501	SK	8.2	51.579	-107.315	572.6	Feb-72	Apr-09	Surficial	Sand/silt
Conq 502	C502	SK	19.2	51.570	-107.315	572.0	Jan-72	Apr-09	Intertill	Sand/gravel
M0-5	Og003	MB	9.1	49.768	-97.300	236.9	May-67	Apr-09	Carbonate-rock	Limestone Dolomite
Melfort	Melf	SK	10.6	52.950	-104.448	451.1	Nov-67	Apr-09	Surficial	Sand/silt
Waterton Dam	W105	AB	12.2	49.320	-113.634	1176.0	May-65	Oct-93	Surficial	Sand
Elnora	W129	AB	13.7	51.967	-113.552	894.3	Jul-62	Jul-08	Surficial	Clay

691

692

693

694

695

696

Table 2. Weather stations and tree-ring chronologies

	Name	*Latitude*	*Longitude*	*Elevation (m)*	*Period*
Weather stations	Estevan	49.070	-103.000	568	1945-2004
	Lethbridge	49.700	-112.780	894	1909-1986
	Calgary	51.117	-114.017	1071	1895-2005
	Edmonton	53.570	-113.520	668	1929-2004
	Regina	50.433	-104.667	574	1904-2003
	Saskatoon	52.233	-106.617	491	1906-2004
	Winnipeg	49.900	-97.233	237	1895-2005
Tree-ring chronologies	Devon Farm (DEV)	50.470	-101.820	440	1862-2005
	Oldman River (OMR)	49.900	-114.200	1427	1203-2007
	Whirlpool Point (WPP)	52.000	-116.450	1356	1062-2007

Table 3. Correlation coefficients for monthly standardized groundwater levels and monthly standardized climate indices, precipitation, and mean temperature. Bold coefficients are significant at 99% and the subscript number denotes the lag in months at which maximum negative or positive correlation was reached.

Well	*ENSO*	*PDO*	*Precipitation*	*Temperature*
Atto (n=515)	**-0.24** $_{\mathbf{17}}$	**-0.20** $_{\mathbf{17}}$	0.10 $_{12}$	-0.05 $_{5}$
Banb (n=456)	**-0.20** $_{\mathbf{15}}$	-0.10 $_{19}$	0.07 $_{12}$	-0.02 $_{7}$
Beau (n=366)	**-0.23** $_{15}$	**-0.19** $_{11}$	**0.19** $_{14}$	**-0.48** $_{\mathbf{7}}$
C500 (n=455)	**-0.15** $_{26}$	**0.05** $_{36}$	0.05 $_{26}$	0.00 $_{8}$
C501 (n=415)	-0.08 $_{14}$	-0.08 $_{21}$	**0.22** $_{14}$	**-0.25** $_{\mathbf{8}}$
C502 (n=510)	-0.08 $_{12}$	-0.04 $_{19}$	**0.26** $_{12}$	**-0.30** $_{\mathbf{6}}$
Forg (n=513)	**-0.20** $_{15}$	**-0.15** $_{19}$	**0.27** $_{12}$	**-0.29** $_{\mathbf{6}}$
Ob005 (n=475)	**-0.25** $_{14}$	**-0.20** $_{14}$	0.0 $_{12}$	-0.10 $_{6}$
Og003 (n=453)	-0.08 $_{9}$	**-0.19** $_{\mathbf{17}}$	**0.32** $_{9}$	**-0.37** $_{\mathbf{3}}$
Melf (n=440)	**-0.20** $_{3}$	**-0.14** $_{36}$	0.08 $_{12}$	-0.03 $_{7}$
Rice (n=478)	-0.08 $_{20}$	**-0.26** $_{34}$	0.08 $_{0}$	-0.04 $_{9}$
Si13 (n=486)	**-0.18** $_{2}$	**-0.13** $_{\mathbf{36}}$	**0.18** $_{12}$	**-0.15** $_{\mathbf{6}}$
Sten (n=520)	**-0.28** $_{13}$	**-0.17** $_{9}$	**0.19** $_{24}$	**-0.22** $_{\mathbf{7}}$
Swan (n=444)	**-0.36** $_{12}$	-0.10 $_{18}$	**0.22** $_{11}$	**-0.24** $_{\mathbf{4}}$
Verl (n=504)	**-0.15** $_{15}$	**-0.22** $_{6}$	**0.13** $_{11}$	-0.09 $_{16}$
W105 (n=322)	-0.09 $_{25}$	-0.02 $_{19}$	**0.41** $_{\mathbf{13}}$	**-0.62** $_{\mathbf{6}}$
W108 (n=239)	-0.04 $_{36}$	**-0.32** $_{33}$	**0.22** $_{12}$	**-0.34** $_{\mathbf{6}}$
W117 (n=445)	+0.04 $_{34}$	-0.08 $_{36}$	**0.18** $_{12}$	**-0.28** $_{\mathbf{6}}$
W129 (n=441)	-0.03 $_{7}$	-0.12 $_{8}$	**0.43** $_{12}$	**-0.50** $_{\mathbf{6}}$
W159 (n=476)	**-0.16** $_{6}$	-0.11 $_{20}$	**0.35** $_{11}$	**-0.47** $_{\mathbf{6}}$
W270 (n=230)	**-0.42** $_{11}$	+0.08 $_{7}$	**0.22** $_{11}$	**-0.24** $_{\mathbf{5}}$

Table4. MTM and wavelets analyses summarized for each well. Note there was no spectral analyses for w129 because the record had more than three consecutive years with missing data. Hp: high power detected but not significant at $p < 0.05$; ooci: significant periodicity but out of the cone of influence.

Well name	Well ID	MTM	Wavelets periodicities		
			32-64 months (2.6-5.3 yr)	64-128 months (5.3-10.6 yr)	>128 months (> 10.6 yr)
Atton	Atto	2.3, 4.5, 9.5, 21.4	yes	hp	-
Bangor B	Ban B	2.4, 5.3, 19	yes	yes	yes
Beauval	Beau	7.8, 17.2	-	hp	hp
Conq 500	C500	2.0, 3.2, 5.0, 18	-	yes	ooci
Conq 501	C501	2.9, 7.8, 18.6	-	hp	hp
Conq 502	C502	2.9, 7.8, 18.7	-	hp	hp
Forger	Forg	3.4, 5.7, 21.4	-	-	-
Melfort	Melf	4.1, 8.5, 20.8	yes	yes	yes
Winkler #5	Ob005	6.5, 20.0	-	-	-
M0-5	Og003	20.9	hp	hp	hp
Riceton	Rice	2.7, 7.1, 19.8	yes	ooci	-
Simpson 13-04	SI13	1.7, 2.1, 3.6, 20.5	yes	yes	Yes
Stenen	Sten	1.8, 2.2, 4.3, 21.9	-	hp	yes
Swanson	Swan	2.1, 3.2, 7.8	yes	yes	hp
Verlo	Verl	4.1, 8.5, 21.2	hp	yes	hp
Waterton Dam	W105	-	-	-	-
Elkwater 2294E	W108	10	yes	hp	-
Barons 615E	W117	3.4, 18.3	-	yes	Yes
Devon #2 (North)	W159	2.9, 19	-	-	-
Duvernay 2489E	W270	9.6	yes	-	-

Table 5. Multi Taper and wavelets analyses summarized for precipitation and tree-ring chronologies. Hp: high power detected but not significant at $p < 0.05$; ooci: significant periodicity but out of the cone of influence.

Well name	MTM (yrs)	Wavelets periodicities		
		32-64 months (2.6-5.3 yr)	64-128 months (5.3-10.6 yr)	128-256 months (10.6-21.3 yr)
Edmonton	2.3, 9.0	hp	yes	hp
Calgary	3.1, 4.0, 6.1, 12.2	yes	hp	yes
Lethbridge	12.2	yes	hp	yes
Saskatoon	3.8	yes	ooci	hp
Regina	2.3, 4.6, 10.7	yes	yes	yes
Estevan	4.5	yes	yes	yes
Winnipeg	3.0	yes	yes	hp
Tree-ring Chronologies				
Oldman River	2.5, 2.9, 7.3, 14, 24, 64	yes	yes	yes
Whirlpool Pool	2.7, 4.7, 6.2, 9.2, 85	yes	yes	yes
Devon Farm	2.4, 22.7	yes	yes	yes

Table 6. Correlation coefficients between reconstructed oscillation modes and ENSO and PDO indices. The subscript number denotes the lag at which maximum negative correlation was reached. The significance of these correlations needs to be evaluated considering the reduction of the degrees of freedom through the signal reconstruction.

	2 - 7 yr		*7 - 10 yr*		*~ 20 yr*
Well	***ENSO***	***PDO***	***ENSO***	***PDO***	***PDO***
Atto (n=515)	-0.29 $_{18}$	-0.14 $_{15}$	-0.30 $_{7}$	-0.10 $_{0}$	-0.24 $_{29}$
Banb (n=456)	-0.33 $_{18}$	-0.19 $_{18}$	-	-	-0.33 $_{17}$
Beau (n=366)	-	-	-0.11 $_{0}$	-0.14 $_{0}$	-0.17 $_{19}$
C500 (n=455)	-0.17 $_{26}$	-0.19 $_{23}$	-	-	-0.05 $_{34}$
C501 (n=415)	-0.13 $_{12}$	-0.13 $_{19}$	-0.09 $_{19}$	-0.05 $_{36}$	-0.05 $_{1}$
C502 (n=510)	-0.16 $_{9}$	-0.16 $_{12}$	-0.17 $_{0}$	-0.04 $_{0}$	0.01 $_{1}$
Forg (n=513)	-0.10 $_{15}$	-0.05 $_{8}$	-	-	-0.42 $_{9}$
Ob005 (n=475)	-	-	-	-	-0.17 $_{29}$
Og003 (n=453)	-	-	-	-	-0.37 $_{1}$
Melf (n=440)	-0.32 $_{30}$	-0.20 $_{26}$	-0.28 $_{2}$	-0.07 $_{0}$	-0.12 $_{28}$
Rice (n=478)	-0.02 $_{16}$	-0.04 $_{21}$	-0.04 $_{2}$	0.00 $_{35}$	-0.37 $_{36}$
Si13 (n=486)	-0.17 $_{6}$	-0.15 $_{15}$	-	-	-0.34 $_{0}$
Sten (n=520)	-0.24 $_{16}$	-0.21 $_{14}$	-	-	-0.41 $_{14}$
Swan (n=444)	-0.12 $_{7}$	-0.01 $_{0}$	-0.12 $_{5}$	-0.07 $_{0}$	-
Verl (n=504)	-0.31 $_{5}$	-0.14 $_{0}$	-0.11 $_{0}$	0.10 $_{0}$	-0.43 $_{1}$
W105 (n=322)	-	-	-	-	-
W108 (n=239)	-	-	-0.02 $_{0}$	0.05 $_{0}$	-
W117 (n=445)	-0.09 $_{5}$	-0.15 $_{5}$	-	-	-0.32 $_{12}$
W129 (n=441)	-	-	-	-	-
W159 (n=476)	-	-	-	-	-0.52 $_{11}$
W270 (n=230)	-	-	-0.24 $_{0}$	0.02 $_{0}$	-

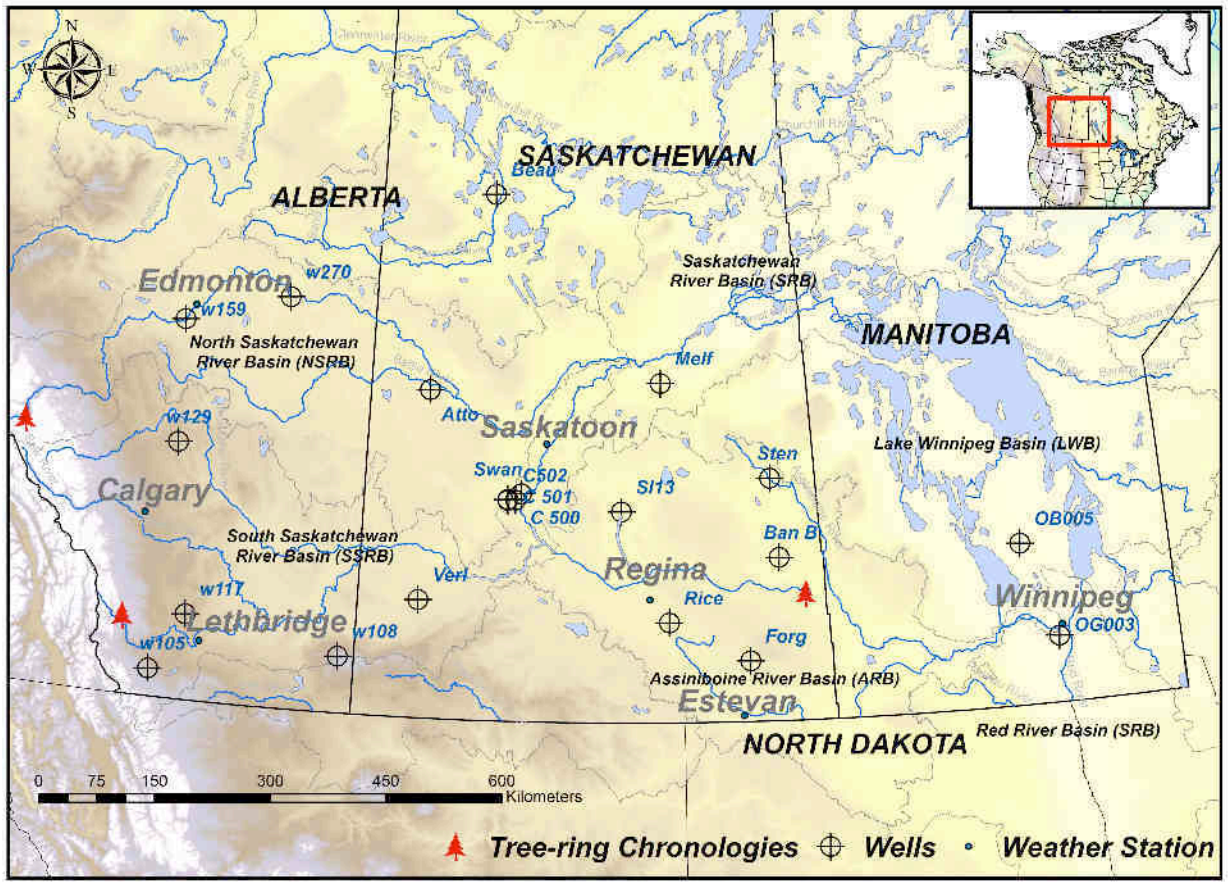

794

795 **Figure 1:** Study area map giving the locations of the groundwater observation wells and tree-
796 ring sites, and cities with long precipitation records.
797

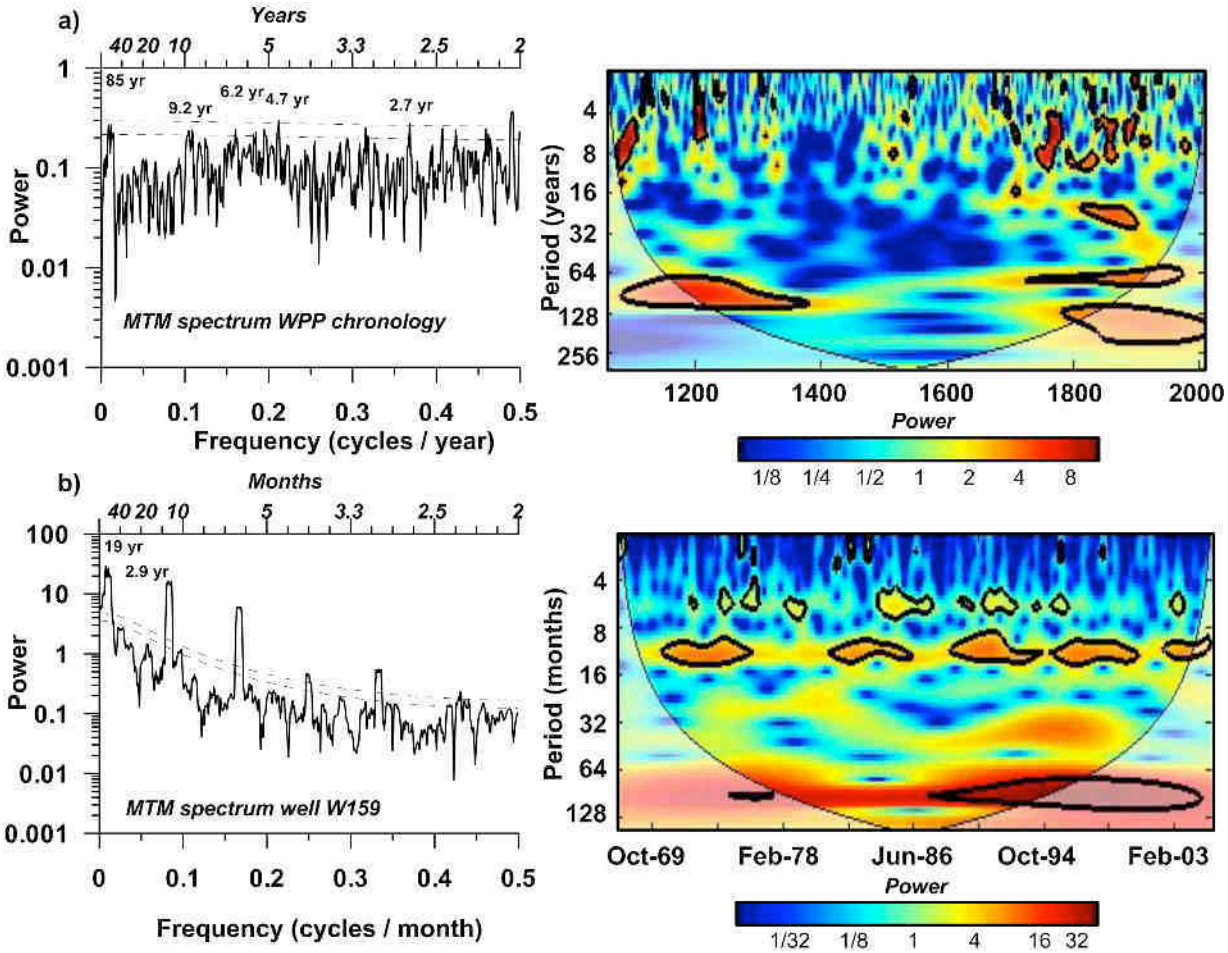

Figure 2: Multi taper and wavelet analysis for the tree ring chronology WPP (a) and the residual time series for well W159 (b). Both records are from the upper North Saskatchewan River Basin.

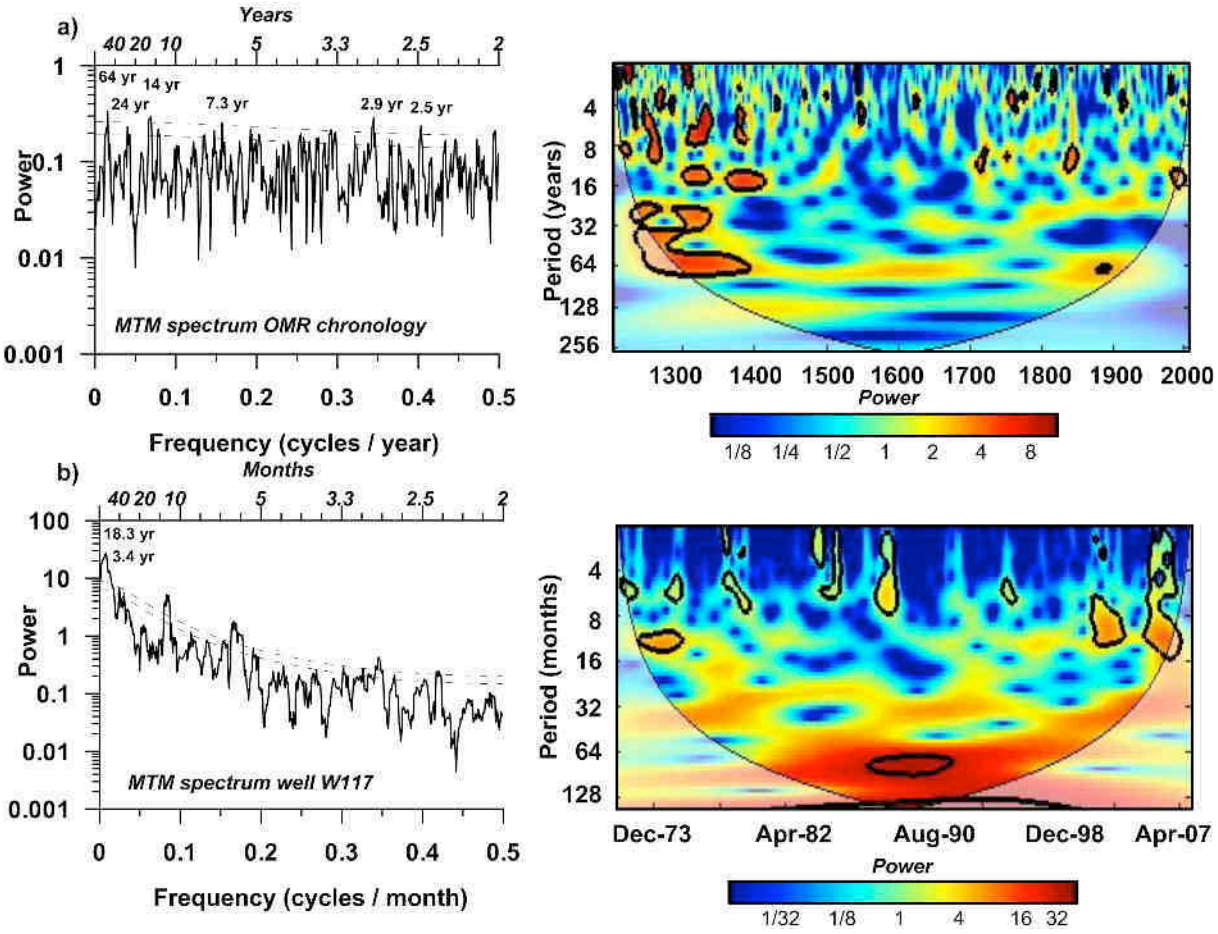

Figure 3: Multi taper and wavelet analysis for the tree ring chronology OMR (a) and the residual time series for well W117 (b). Both records are from the upper South Saskatchewan River Basin.

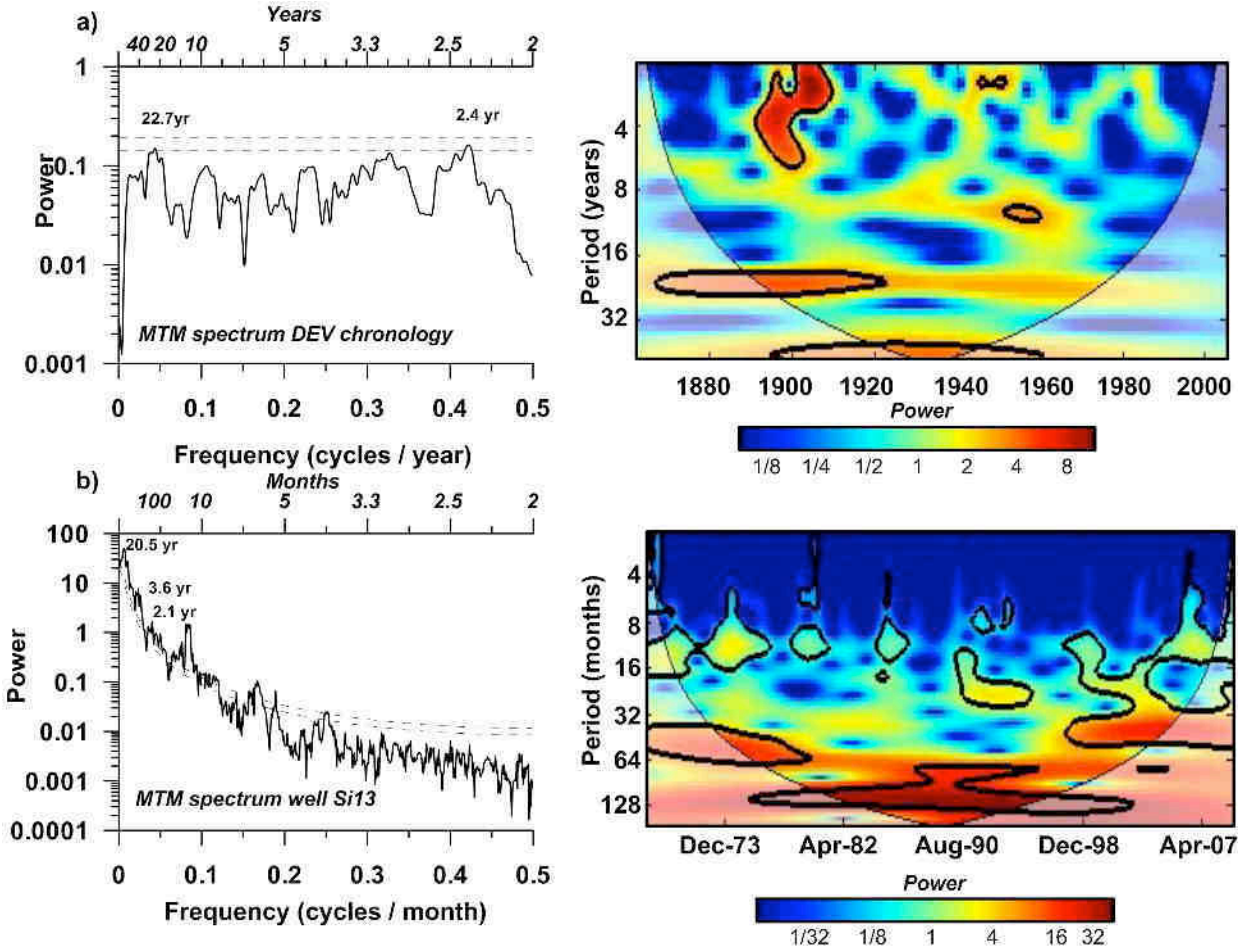

Figure 4: : Multi taper and wavelet analysis for the tree ring chronology DEV (a) and the residual time series for well Si13 (b). Both records are from the Assiniboine River Basin.

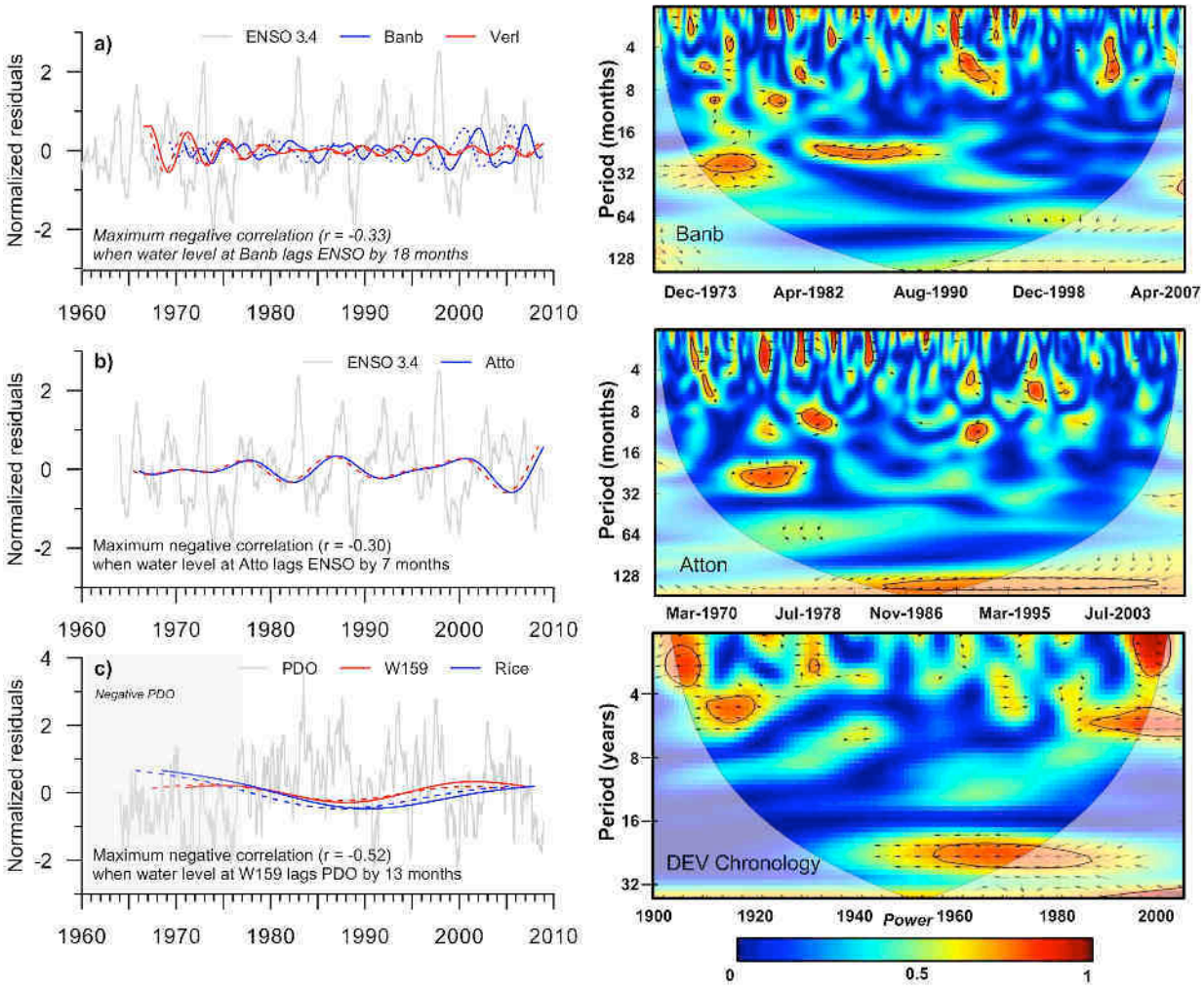

Figure 5: Plots showing the correlations between the reconstructed oscillation modes and the climate indices (left) and wavelet coherence between selected groundwater time series and climate indices (right). a) Correlation between ENSO index and reconstructed groundwater time series at 2-7 year band for wells BanB and Verl and wavelet coherence between groundwater levels at Banb and ENSO. b) Correlation between ENSO index and reconstructed groundwater time series at 7-10 year band for well Atto and wavelet coherence between groundwater levels at Atto and ENSO. c) Correlation between PDO index and reconstructed groundwater time series at ~20 year band for wells W159 and Rice and wavelet coherence between the DEV tree ring chronology and PDO. The dotted line represents the lagged time series by n months.

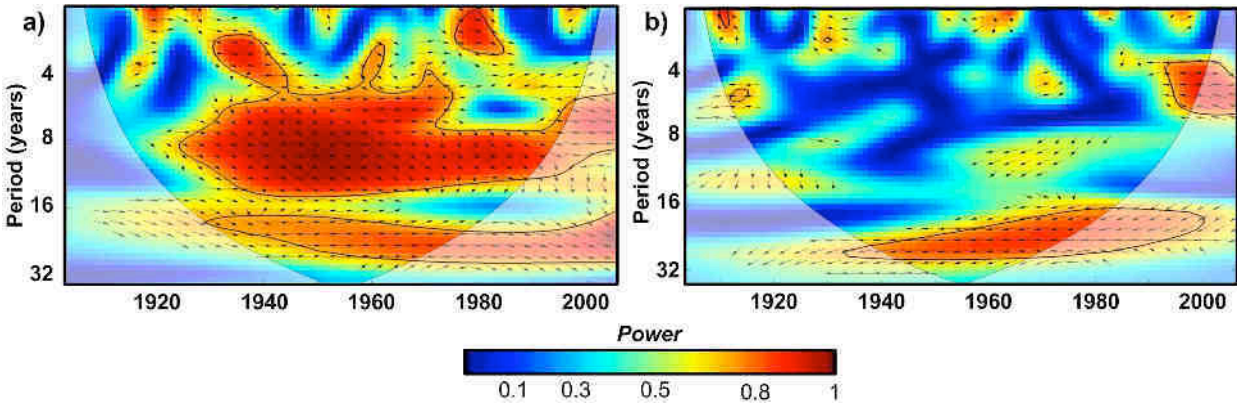

Figure 6. a) Wavelet coherence between precipitation at Regina and the DEV chronology. b) Wavelet coherence between the DEV chronology and the PDO index.